The Synthesis and Development of Novel Quinolone Antimalarials Targeting the bc_1 Protein Complex of *Plasmodium falciparum*

Thesis submitted in accordance with the requirements of the

University of Liverpool for the degree of Doctor of Philosophy

By

Robin Neil Cowley

June 2012

Abstract

In recent years investigation of the biological mode of action of the antimalarial compound atovaquone has validated the *Plasmodium falciparum* bc_1 protein complex as a target for the development of novel antimalarials. This project is concerned with the design, synthesis and development of quinolone based antimalarial compounds targeting the Q_o site of the *Plasmodium falciparum* bc_1 protein complex.

A small array of quinolone-based compounds, substituted at the 3 and 7 positions, has been developed utilising the Gould-Jacobs methodology. The synthesised compounds express activity as low as 0.46 nM *versus Plasmodium falciparum* malaria parasites *in vitro*. Activity at the bc_1 protein complex has been confirmed and selectivity for the parasite protein over the mammalian equivalent has been demonstrated. Poor solubility has been highlighted as a potential issue; however steps have been taken towards the development of carbamate prodrugs with encouraging results.

Docking studies performed *in silico,* using the crystallised structure of yeast bc_1 protein, demonstrate a key role for residues His181 and Glu272 in the recognition of high potency inhibitors and have aided in the rationalisation of the observed biological activities. The orientation of the quinolone group in the active site and interaction of the inhibitors with the hydrophobic channel leading to the active site have both been shown to be of significance for biological potency.

Computer lead design of a new chemotype has resulted in the development of a second array of quinolone based compounds synthesised by a divergent method based on the Huisgen 1,3-dipolar cycloaddition. Docking studies predicted the synthesised compounds to be potent inhibitors of *Plasmodium falciparum* bc_1. However, *in vitro* results for the array proved disappointing, an outcome attributed to a failure to account for membrane permeability and the physical location of the targeted bc_1 protein complex.

Contents

Acknowledgements

Here it is then, the culmination of four years of research, I can't quite believe it. First and foremost I must thank Prof. Paul O'Neill, not only for offering me the opportunity to carry out this piece of research but also for his help and support during the project. So Paul for one last time, I have good news and I have bad news...

Every member of the O'Neill group has my gratitude as I'm sure I've picked the brains of each of them more than once over the years. Some deserve special thanks however, Drs Peter Gibbons and Ian Hale in particular, for proof reading various sections of this thesis, Shirley Leung and Walid Abd El Magid for their parts in the synthesis of some of the compounds covered and Lee Taylor for also not caring about football in a city where its ever present.

Special thanks as well to Alex Lawrenson, Dr Raman Sharma and Dr Neil Berry, as without their help the modelling portion of this project would never have happened, although there have been numerous occasions when that would have made me quite happy. I also owe huge debts of gratitude to Miss Moya McCarron for remaining patient with me as I brought a steady stream of what appeared to be samples of sand down for mass spec. analysis and to my colleagues in the Liverpool School of Tropical Medicine, in particular Dr Alison Shone, for carrying out the biological assays on my compounds.

I can't express how much the friends I've made here, chemists and non-chemists, mean to me, Emma, Matt, Neil, Ev, Maia, Tania, James, Carol, Ralph, Inder, Lee, Rachel, Katie and Vicky thank you all so much for your friendship, the tea break conversations and in some cases managing to live with me for over four years.

My family I have to thank for inspiring me to become a scientist in the first place by nurturing my curiosity and pushing me to always try and achieve my best. For that, their unending support and always asking me how things were going, even though they rarely understood the answers, I love them all.

Finally but most importantly, my future wife Michelle, thank you so much for putting up with me. I don't know how or why you do it but I do know that I couldn't have done this without you; I love you more than I can ever say.

ACT	Artemisinin-based combination therapy
ATP	Adenosine triphosphate
DAPCy	*trans*-diacetylpalladium (II) bis(dicyclohexylamine)
DFT	Density functional theory
DMF	Dimethylformamide
DMSO	Dimethylsulphoxide
DNA	Deoxyribose Nucleic Acid
EC_{50}	Half maximal effective concentration
EPR	Electron Paramagnetic Resonance
Eq.	equivalents
EtOAc	Ethyl acetate
EtOH	Ethanol
Glu	Glutamate
His	Histidine
HIV	Human Immunodeficiency Virus
HRMS	High resolution mass spectrometry
IC_{50}	Half maximal inhibitory concentration *versus* a blank
Ile	Isoleucine
ISP	Iron-Sulphur Protein
KO^tBu	Potassium tertiary butoxide
Leu	Leucine
MAP	Malaria Atlas Program
MeCN	Acetonitrile
MeOH	Methanol
Met	Methionine
mmol	millimole
P.	*Plasmodium*
$Pd(PPh_3)_4$	Palladium tetrakistriphenylphosphine
PDB	Protein Data Bank
*Pf*CRT	*Plasmodium falciparum* Chloroquine Resistance Transporter

Phe	Phenylalanine
ppm	Parts per million
RMSD	Root mean square deviation
TB	Tuberculosis
THF	Tetrahydrofuran
$Ti(O^iPr)_4$	Titanium (IV) isopropoxide
TLC	Thin layer chromatography
Tyr	Tyrosine
UHDBT	5-*n*-undecyl-6-hydroxy-4,7-dioxobenzothiazole
Val	Valine
WHO	World Health Organisation

The development of quinolone esters as novel antimalarial agents targeting the Plasmodium falciparum bc_1 protein complex

Robin Cowley, Suet Leung, Nicholas Fisher, Mohammed Al-Helal, Neil G. Berry, Alexandre S. Lawrenson, Raman Sharma, Alison E. Shone, Stephen A. Ward, Giancarlo A. Biagini and Paul M. O'Neill

Med. Chem. Commun., 2012, **3**, 39-44

DOI: 10.1039/C1MD00183C

Chapter 1

Introduction

1.1 Malaria

Malaria is potentially the oldest infectious, parasitic disease known to man and it continues to be one of the most prevalent and deadly even today. Evidence suggests that malaria existed as far back as 50,000 years ago and that the parasites have evolved alongside mankind.[1]

Although once far more widespread than it currently is, malaria is still a global issue, with almost 50% of the world population living in regions considered high risk for the disease.[2] The most recent figures from the World Health Organisation (WHO) show that it is responsible for 500 million cases of severe illness each year, at least 3 million of which will be fatal.[3]

The burden of malaria is not simply a medical one; it is also an economic problem. Areas with intense transmission rates show an average loss of 1.3% of their annual economic growth compared to regions with lower levels of infection [4] resulting in a stark correlation between malaria and poverty. The disease distribution centres firmly on the tropical and sub-tropical regions of the globe which includes some of the poorest nations on the planet and they are likely to remain that way for as long as malaria remains prevalent.[4]

In the early 20th century malaria was even more widespread than at present; however a concentrated effort following the Second World War and extending in to the 1960's saw the disease eradicated from most of the world's temperate zones. Unfortunately the incidence of malaria has increased dramatically in recent years and malaria is returning to regions from which it had previously been eliminated.[5]

This is largely due to the spread of resistance to current therapies both in the parasites themselves and the *Anopheles* mosquitoes that spread the parasites from host to host. It is also the result of a symbiosis between malaria and other infections such as tuberculosis (TB) and human immunodeficiency virus (HIV) which have similar global distributions and inhibit an individual's ability to fight the malaria parasite.[2]

There are four separate species of the malaria parasite that infect humans, *Plasmodium malariae, P.ovale,* which are milder, *P.vivax and P.falciparum*, each with different distributions and subtly different biology giving rise to differences in lifecycles and disease mechanisms.[6] There is also a fifth species, *P.knowlesi,* a monkey form of malaria common in macaques. However it is a zoonosis, an infection capable of crossing to humans, this species is potentially fatal and infection rates in south-east Asia have recently increased dramatically.[7]

Plasmodium vivax is the most widespread of the species, occurs in a number of drug resistant strains and causes a more severe infection than *P.ovale* and *P.malariae*, but still only infrequently results in death of the patient, usually when their immune system is compromised in some way.[8] *P.vivax* also has the most complex biology of the five species with a peculiarity of the lifecycle leading to the condition known as chronic malaria, in which symptoms can reoccur for years after the original infection.[9] This is due to the ability of *P.vivax* parasites to enter a dormant liver stage called hypnozoites, where they are hidden and protected from the host's immune system in vesicles contained within the host's hepatocytes. If not treated with one of the 8-aminoquinolines, e.g. primaquine, these dormant parasites sporadically become active, reinfecting the blood cells leading to the characteristic debilitating bouts of fever.[9]

Plasmodium falciparum, the focus of this work, is by far the deadliest form of the disease, causing severe acute infections responsible for over 90% of malaria attributed fatalities.[8] In the most severe cases *P.falciparum* parasites can cross an individual's blood brain barrier resulting in a condition called cerebral malaria, invariably fatal if not identified and treated rapidly. *P.falciparum* is notoriously difficult to treat effectively as its biology allows it to mutate rapidly resulting in multiple resistant forms. WHO estimates that 85% of *P.falciparum* cases are now chloroquine resistant, with multi-drug resistance rising rapidly.[3]

The majority of the deaths due to *P.falciparum* infection occur in sub-Saharan Africa where it is estimated to kill a child every 30 seconds[3, 5],

however *P.falciparum* is endemic in 87 countries [10] and it is the resistant forms of this species in particular that are responsible for the re-emergence of malaria in areas cleared of the disease in the mid 20th century. In 2007 the Malaria Atlas Program (MAP) at Oxford University published the results of the first global survey of *P.falciparum* incidence and distribution in over 4 decades (Figure 1.1).[10] The results of the MAP survey state that 2.4 billion people live in regions considered high risk for *P.falciparum*, with a further 1 billion living in regions with unstable or spreading risk, that's a combined total of 40% of the world population.[10]

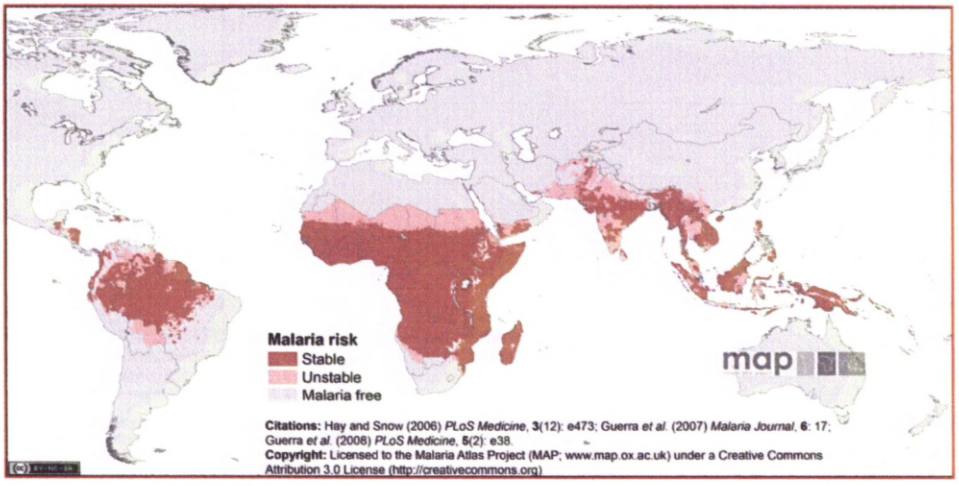

Figure 1.1: The results of the MAP survey showing the 2006 global distribution of Plasmodium falciparum.[10]

1.1.2 Parasite Lifecycle

As has already been alluded to, part of the difficulty with the effective treatment of malaria is the complex parasite lifecycle (Figure 1.2). In the course of a complete lifecycle malaria parasites go through eight separate parasitic forms, not including hypnozoites in *P.vivax*.[6] Each of these forms have different intra and extracellular structures, metabolic processes and lifespan, meaning that drug therapies can rarely target more than one parasite form effectively.

A bite from an infected female *Anopheles* mosquito results in transmission of parasite sporozoites as the mosquito injects its salivary cocktail of anticoagulants and begins feeding. These sporozoites travel rapidly through the host bloodstream and within half an hour of the bite taking

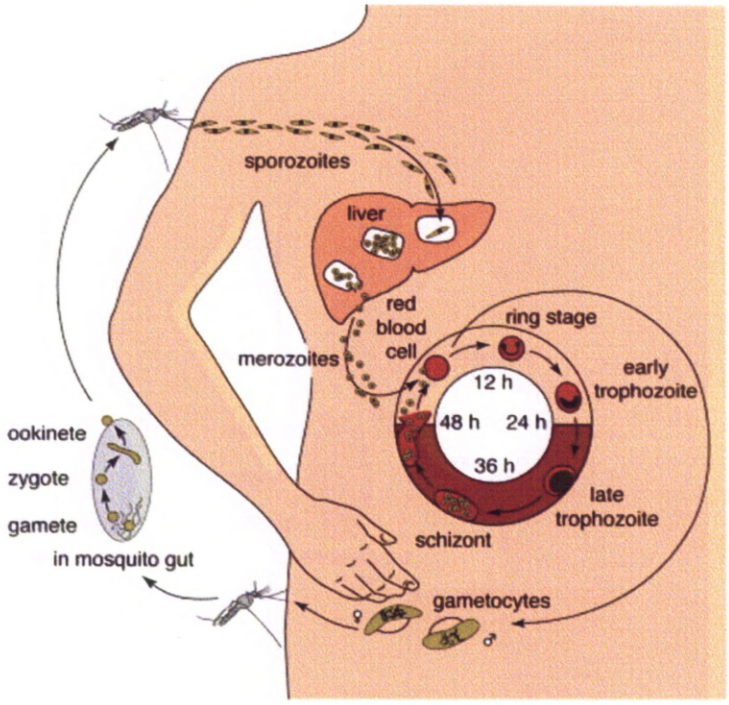

Figure 1.2: A general schematic showing the lifecycle of malaria parasites.[11]

place are hidden in the hepatocytes of the liver where they enter the primary exo-erythrocytic division cycle.[12]This stage of the lifecycle is difficult to study and little is known about the precise changes that occur to the parasites while they are in the liver. Until recently it was believed that sporozoites settled in the first liver cell that they entered, however extensive studies published in 2001 by Dr. Rodríguez and her colleagues at the New York University School of Medicine have now established that sporozoites may penetrate as many as five hepatocytes before settling on one in which to develop further.[13] This is the longest single stage of the parasite lifecycle and varies in length according to species, in *P.falciparum* it lasts around 5 and a half days.[12]

The primary exo-erythrocytic phase ends with the infected hepatocytes rupturing and flooding the host bloodstream with the second parasitic form, merozoites. It was only in 2006 that work by Dr. Sturm *et al.* first established the method by which merozoites escape the liver into the blood stream without triggering the host immune system.[14] The merozoites directly manipulate the biology of the hepatocyte they inhabit inducing the first stage of apoptosis in which the cell detaches from its neighbours allowing it to move freely within the liver. Once the hepatocyte has detached however the merozoites subvert the usual cell death processes and prevent apoptosis

from progressing by blocking the release of Ca^{2+} ions that would normally act as a signal to phagocytes to engulf the dead cell. This means that the host immune system does not recognise the detached cell as being dead and it is allowed to drift undetected through the liver, giving the occupying merozoites a safe, secure ride to the bloodstream.[14] To access the red blood cells required for the next stage of their lifecycle the parasites must enter the small blood vessels of liver (sinusoids) which are separated from the hepatocytes by a layer of extracellular matrix, called the space of Disse and single layer of endothelial cells. This is achieved by the formation of parasite filled vesicles dubbed merosomes, which are extruded through the endothelium into the bloodstream (Figure 1.3).[14]

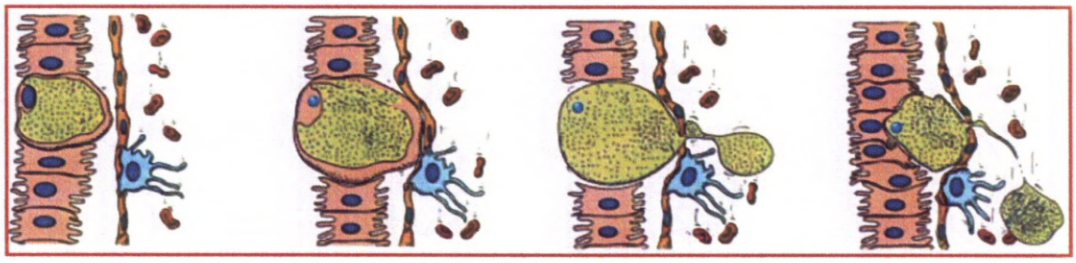

Figure 1.3: Cartoon of the current hypothesis for merosome formation; hepatocytes (pink) infected with merozoites (green) bud through the space of Disse and sinusoidal endothelium (orange), forming a parasite filled vesicle eventually breaking away into the bloodstream avoiding detection by the phagocytic Kupffer cells (blue).[14]

The released merosomes can contain just a few or many thousands of merozoites and drift through the cardiovascular system for up to 72 hours before rupturing. Upon release the merozoites instantly begin to invade the red blood cells and begin the next stage of development, the asexual erythrocytic division cycle.[6]

The blood borne stage of the parasite lifecycle is the most extensively studied, particularly in *P.falciparum*, and it is at this point that the majority of drug therapies and prophylactic compounds have their action. As merozoites invade erythrocytes (red blood cells) their structure changes, first becoming immature trophozoites, also referred to as a ring form parasites (Figure 1.4a), then mature trophozoites (Figure 1.4b) before dividing into between 8 and 32 merozoites within a self contained vacuole called a schizont (Figure 1.4c) which can occupy up to two thirds of the infected erythrocyte.[15] This progression is fuelled by the digestion of the protein portion of haemoglobin,

a process which releases haem which when in solution is toxic to the parasite.[6] The parasite counteracts this by polymerising the haem to form hemozoin, also called malaria pigment, which is crystalline and precipitates out of solution.[16] Once the new merozoites are fully matured, after around 48 hours, the schizont ruptures releasing them into the bloodstream to repeat the cycle.

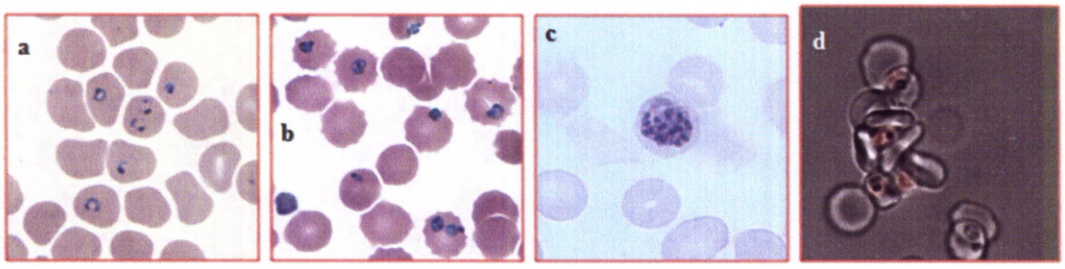

Figure 1.4: Thin blood smears showing P.falciparum as a) ring form parasites, b) mature trophozoites c) a schizont and d) a light microscopy image showing a rosette of infected cells.[15, 17]

The rupturing of the erythrocytes releases various toxins and waste products into the host's bloodstream causing the characteristic fever associated with the disease. As with the liver stages, because the parasites are hidden within host cells they are rarely detected by the immune system and the only threat to the parasite is the body's natural periodic destruction of erythrocytes in the spleen. To reduce the risk of this occurring before the parasites are fully matured they again manipulate the biology of the cell they occupy causing the infected erythrocytes to express adhesive surface proteins on their exterior membranes. This results in infected red blood cells adhering to each other, forming rosettes (Figure 1.4d)[17] and the endothelial linings of smaller blood vessels where the flow of blood is slower. The narrow, slow flowing blood vessels of the alveoli are particularly susceptible and pulmonary emboli are a common result of infection with malaria.

1.2 Antimalarial Chemotherapy

Herbal remedies for malaria have existed for millennia, but many consider the discovery of quinine (Figure 1.5) in the 17th century as the advent of antimalarial chemotherapy.[18] Not successfully synthesised until 1918, [19, 20] the natural source of quinine is the bark of the *cinchona* tree native to Peru. Quinine was the first effective treatment for malaria and continued to be of

great importance up until the development of its fully synthetic derivatives in the 1940's, since that time it continues to be an important alternative to more recently developed drugs in resistant malaria infections.

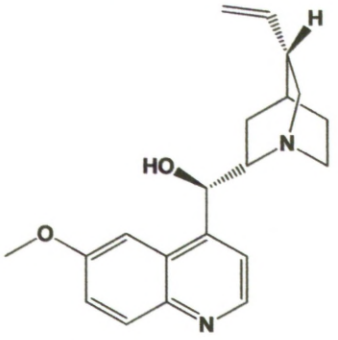

Figure 1.5: The structure of quinine.

1.2.1 Chloroquine and the 4-aminoquinolines

The first class of fully synthetic antimalarials, chloroquine and its related compounds such as amodiaquine, all have the same core structure based on a quinoline ring system (Figure 1.6).

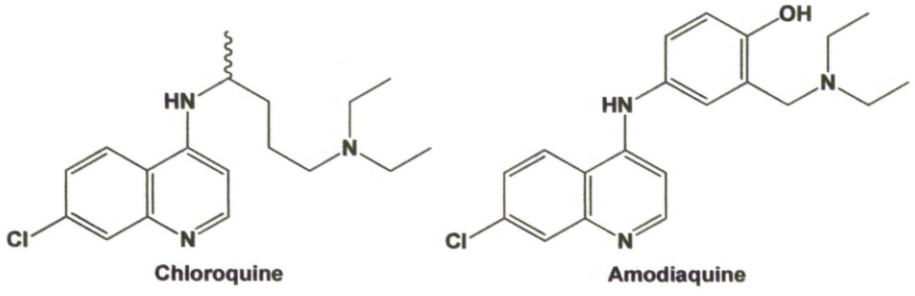

Figure 1.6: The structures of 4-aminoquinoline compounds chloroquine and amodiaquine.

Antimalarials of this structure have two key features; the quinoline ring itself and the secondary amine at the 4 position of the quinoline ring paired with the tertiary amine with four carbon atoms in between. The presence of this pair of nitrogens is the key to the mechanism of action for this class of compounds. They are blood schizonticidal agents,[6] meaning they kill the parasite in its blood borne form. During development of the trophozoite parasite form, host haemoglobin is broken down in acidic vacuoles within the parasites and haem is crystallized into hemozoin. The 4-aminoquinolines are absorbed into the acidic vacuoles and the nitrogens in their side chains are protonated preventing them from passing back out of the vacuole and allowing them to accumulate in high concentrations. The quinoline ring portion of their structure then comes into play as they chelate with the

porphyrin ring system of haem and prevent its conversion into hemozoin, poisoning the parasite with its own feeding mechanism.[21]

Chloroquine was originally called Resochin when it was developed in Germany by Bayer in 1934. It was initially considered too toxic for use in humans and it wasn't until 1946 that British and American scientists searching for an alternative to quinine following the Second World War rediscovered the compound and it was licensed for use. As a class, the 4-aminoquinolines have very few severe side-effects, though chloroquine has a narrow therapeutic index in children.[22] The most common side-effects are itching and disturbed sleep although long term use at high doses can result in damage to the eye.[6] More problematic than the side-effects for this class is the emergence of resistance.

Overuse of chloroquine, and in particular improper use, have led to resistant strains of parasite that have rendered the class as a whole almost completely obsolete.[6] Resistant forms of the parasite express a mutated form of "*Plasmodium falciparum* Chloroquine Resistance Transporter" (PfCRT) protein in the membranes of their digestive vacuoles. Under normal circumstances this protein is believed to be involved in the passive transport of amino acids and short chain peptides out of the digestive vacuole. In its "wild-type" form the opening of the protein has a lining of basic residues that would repulse the active, doubly protonated form of chloroquine maintaining a high concentration within the digestive vacuole. In the mutant forms of PfCRT these basic residues are absent meaning that protonated chloroquine can leak rapidly out of the digestive vacuole down a steep electrochemical gradient dramatically reducing the concentration of chloroquine at its point of activity and consequently conferring resistance to the parasite.[23]

With few alternative therapies available when the 4-aminoquinolines were first compromised the resistant strains have spread rapidly and the need for novel antimalarials grows ever greater.

1.2.2 Artemisinin based therapies

In the mid 1960's a Chinese army study of over 200 traditional herbal remedies for malaria identified a breakthrough for malaria chemotherapy.[24] That compound was artemisinin and it remained a closely guarded secret for

many years. When the structure (Figure 1.7) was eventually released to the wider world in the late 1970's[25] the proposed sesquiterpene lactone and particularly the endoperoxide bridge, were met with scepticism by western scientists who claimed that the structure would be too reactive and fragile to be useful as a drug.

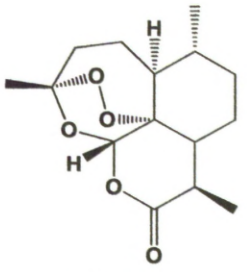

Artemisinin

Figure 1.7: The structure of artemisinin.

It was not until 1984, when the compound was reisolated by a team in Washington D.C.[26] that interest in the compound really began to mount. However it still took a further 17 years for the compound to be internationally licensed as a treatment by the World Health Organisation (WHO). This was in part because the WHO were desperate to avoid a repeat of chloroquine's story with indiscriminate overuse of the drugs leading to resistance and loss of efficacy. It was, in part, this issue which led WHO to ban the use of artemisinin derivatives as monotherapies.

The other reason that artemisinins are not used a monotherapies is their rapid metabolism. Artemisinin itself has very poor bioavailability, therefore a range of semi-synthetic derivatives, such as artemether and artesunate (Figure 1.8), have been developed. These compounds are still metabolised relatively rapidly however and so are used in combination with traditional antimalarials such as amodiaquine (+ artesunate = Coarsucam™) or other antimalarials not ordinarily used on their own such as lumefantrine (+ artemether = Coartem®) (Figure 1.8). These mixtures are referred to as artemisinin-based combination therapies (ACTs) and are only licensed for treatment and not for use as prophylaxis.

Despite these efforts resistance is still being seen to emerge in south-east Asia in cases of *P.falciparum*.[27] The necessity for dual therapies and the difficulty inherent in obtaining large quantities of artemisinin also means that

ACTs are very expensive compared to the 4-aminoquinoline class, limiting their use where they are needed most.

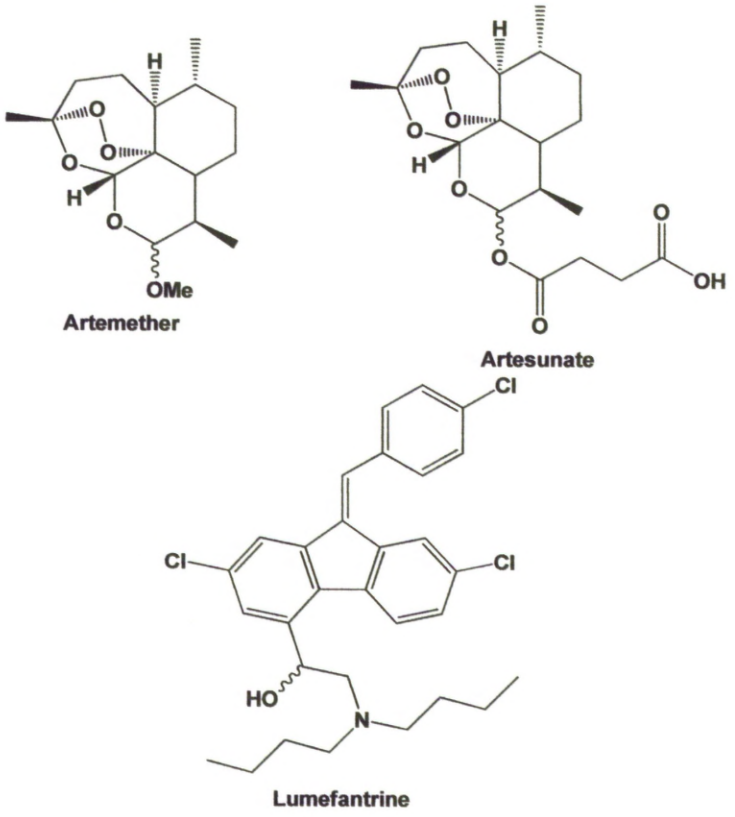

Figure 1.8: Structures of the semi-synthetic artemisinin derivatives artemether and artesunate and of lumefantrine an antimalarial agent used in combination with artemether to form the ACT Coartem®.

Like the 4-aminoquinolines, artemisinins are blood schizonticidal agents acting on the developing trophozoites. The exact mechanism of the artemisinins' therapeutic effect has been a matter of debate for the past decade. What is known is that the endoperoxide ring system is the active pharmacophore, both in artemisinin and the related synthetic compounds in development, as analogues lacking this structural motif are inactive.[28] It is generally accepted that the key step in activation of the artemisinins is iron-mediated cleavage of the endoperoxide bridge resulting in carbon-centred radicals that go on to damage key parasite targets.[28]

The issues of debate are both the iron source, haem bound or free iron, and the key target of the generated radicals.[29] There is compelling evidence that an important target is the porphyrin ring system of haem,[30, 31] but evidence also exists for attack of key proteins[32] and parasite DNA.[33] The

development of fully synthetic endoperoxide based drugs such as OZ277 and OZ439 (Figure 1.9) has further complicated the issue.[29, 34]

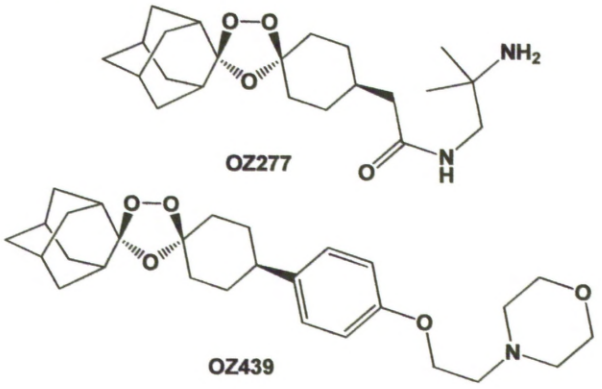

Figure 1.9: Structures of OZ277 and OZ439, examples of the fully synthetic trioxolane compounds currently in development.

It may be that the compounds have a multi-target mode of action and that it is this that has staved off the development of widespread resistance thus far.[29]

1.2.3 Atovaquone

In 2000 the drug preparation Malarone® was released by GlaxoSmithKline for the treatment and prevention of uncomplicated, multidrug resistant malaria. The active ingredient of Malarone® (Figure 1.10) is atovaquone but it is administered in combination with the dihydrofolate reductase inhibitor proguanil, to slow the development of resistance.

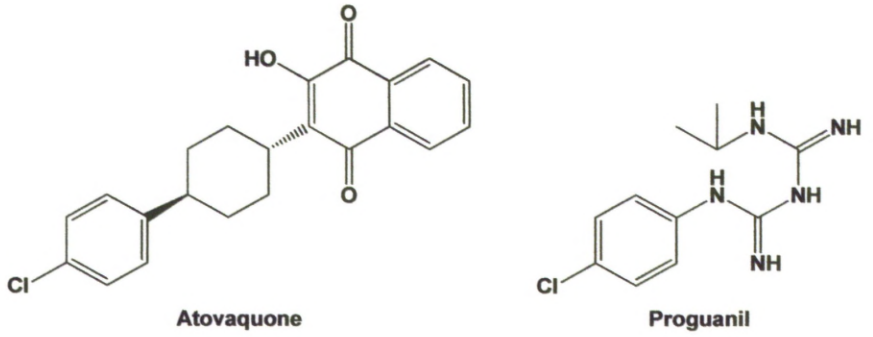

Figure 1.10: The structures of atovaquone and proguanil, the ingredients of the antimalarial preparation Malarone®.

Atovaquone is a hydroxynapthoquinone that acts as a selective mitochondrial poison, competitively inhibiting the cytochrome bc_1 protein complex in the parasite mitochondria disrupting the membrane potential that provides energy for mitochondrial function.[35] It is the first drug of any kind in

clinical use to do this and represents a completely new drug class. Proguanil has does not kill *P.falciparum* parasites but prevents their proliferation at the schizont stage and is synergistic in use with atovaquone as the combination completely prevents the biosynthesis of pyrimidines required for nucleic acid replication.[36] The inhibition of mitochondria by atovaquone is of critical importance as these organelles are present at every stage of the parasite lifecycle, meaning that atovaquone is the only currently licensed drug proven to act on the parasite during both the erythrocytic and exo-erythrocytic stages of its lifecycle.[36-38]

However, atovaquone is far from perfect; as with the ACTs, Malarone® is relatively expensive and its widespread use in the resource-poor, disease-endemic areas where it is needed most is limited.[39] The relationship of the groups on the central cyclohexane ring of the compound must be *trans* or activity is lost, raising the complexity and therefore the cost of preparation. The necessity for proguanil to be included in the therapeutic dose also raises the cost but when used as a monotherapy, resistance to atovaquone develops within days and once present renders even the combined therapy ineffective.[40, 41] The factors governing resistance to atovaquone will be covered in more detail later, but it is important to note that cheaper alternatives that overcome the resistance issues identified are desperately needed.[42]

1.3 The Cytochrome bc_1 Protein Complex

At first it would seem that cytochrome bc_1 is an unusual choice as a drug target as the protein complex exists in some form in all mitochondria, meaning that it is present in all respiring eurkaryotic cells, including those of humans. This target therefore presents a selectivity issue for the design of new therapeutic agents. However the determination that bc_1 is the site of action for atovaquone has definitively validated this target for exploitation by a new generation of antimalarial therapies for use against *P.falciparum*.[35]

1.3.1 General Structure of the bc_1 Complex

Although it catalyses a chemical process cytochrome bc_1 should not be referred to as an enzyme as it is not a single protein. Instead it is, as its name

suggests, a homodimeric complex each identical half of which is composed of ten interwoven polypeptide chains embedded with a number of haem units. The catalytic core of each consists of three separate subunits; cytochrome *b*, cytochrome c_1 and the Rieske iron-sulphur protein (ISP).[43] The function of the other seven subunits is not well understood and they are currently presumed to be largely structural in nature[44] anchoring the complex in the inner membrane of mitochondria.

The catalytic core contains two binding sites for the endogenous compounds involved in the catalytic processes through which the complex functions. These are termed alternatively Q_o or *P* on the outer, electropositive portion of the complex and Q_i or *N* on the inner, electronegative portion. Q_o is the site of action for atovaquone and the target of this study. It is known in *P.falciparum* to consist of a hydrophobic channel roughly 15 Å in length with a polar pocket at the end containing glutamic acid and histidine residues essential for its function.[45, 46]

1.3.2 The Protonmotive Q-Cycle

Normal function of the complex requires the cofactors ubiquinol and ubiquinone; these cofactors interact with the Q_i and Q_o sites on cytochrome *b* in a sequence of redox reactions to "pump" protons out of the inner matrix of mitochondria and into the intermembrane space (Figure 1.11). This generates a membrane potential that in turn provides the energy for a number of downstream processes including enzymes involved in ATP production and active transport processes.[46, 47] This process has been studied in great detail over the years and is best described by Mitchell's Q-cycle hypothesis (Figure 1.12).[48]

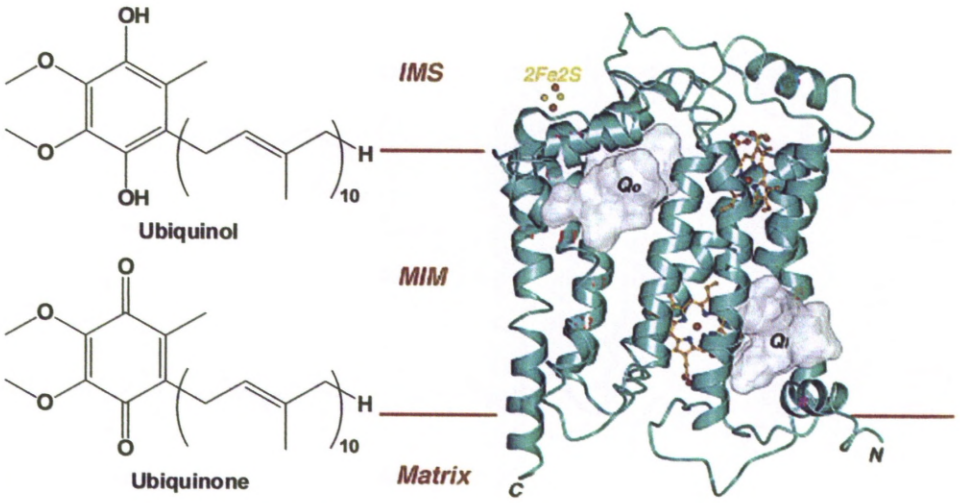

Figure 1.11: Showing the structures of the endogenous bc_1 ligands, ubiquinol and ubiquinone and a ribbon model of cytochrome b subunit of the bc_1 complex showing key binding regions and the 2Fe2S cluster of the Rieske (ISP) protein (IMS = intermembrane space, MIM = mitochondrial inner membrane).[47]

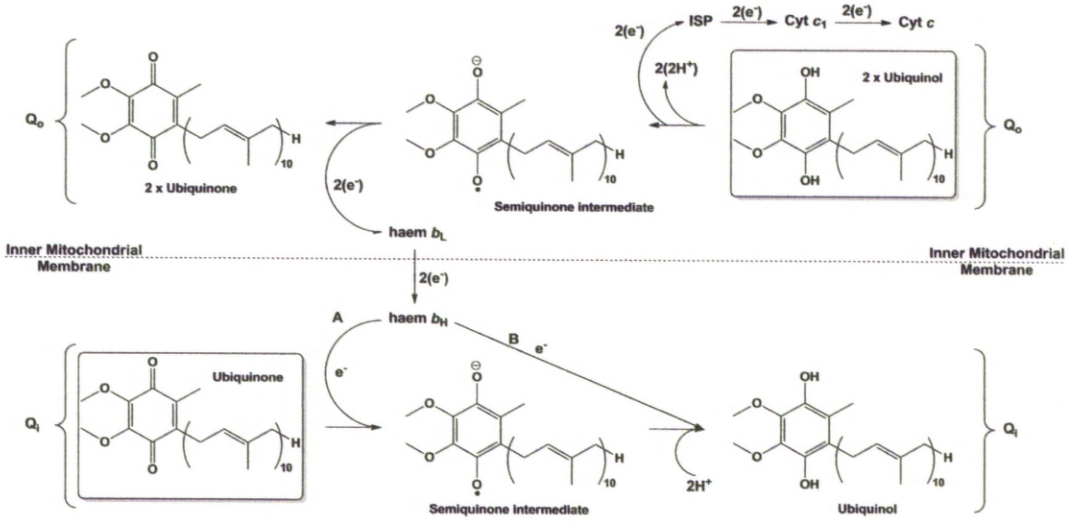

Figure 1.12: Showing a schematic of the protonmotive Q cycle across the inner membrane of the mitochondria.

The Q_i and Q_o sites are both part of cytochrome *b* but are distinct in that they are on opposing sides of the mitochondrial inner membrane. The sites are connected by a transmembrane electron transport pathway formed by two haem groups, b_L and b_H (Figure 1.12).[42] In each bifurcated reaction cycle a molecule of ubiquinol is oxidised at Q_o releasing two protons (H^+) and 2 electrons (e^-). One of these electrons passes across the electron transport pathway to reduce one of the carbonyl groups of a molecule of ubiquinone bound at Q_i, the other electron passes to the 2Fe-2S cluster of the ISP, reducing it. The reduction of the ISP causes a conformational change in the

cytoplasmic region of the protein, which brings the 2Fe-2S cluster in close proximity to the haem group bound in cytochrome c_1, the electron then passes from the 2Fe-2S cluster to reduce the haem group. Reduced cytochrome c_1 is reoxidised by soluble cytochrome *c* and from there the electron goes on to power cellular processes. In each complete cycle this process happens twice, therefore two molecules of ubiquinol are oxidised for every one molecule of ubiquinone reduced, a net translocation of four protons out of the mitochondrial matrix into the cytoplasm. This proton transfer results in a relative charge being maintained across the mitochondrial membrane and it is this charge that powers the cell.[49-51]

1.3.3 Inhibition of the Cytochrome bc_1 Protein Complex

Although only recently validated as an antimalarial target by the studies on atovaquone's mechanism of action, the bc_1 protein complex has been known to be the site of action for a number of fungicides and antibiotics for several years, including the natural inhibitors stigmatellin, myxothiazol and antimycin A_1 (Figure 1.13). There have been numerous studies carried out on the various inhibitors available for research by crystallography, spectroscopy and kinetic studies meaning that their mechanisms of action are generally well known with respect to their particular targets.[45, 46, 52, 53] Though the toxophores identified across the existing range of bc_1 inhibitors show great variation (Figure 1.13), the compounds can be broadly classified according to their binding site and effect on the protein complex.

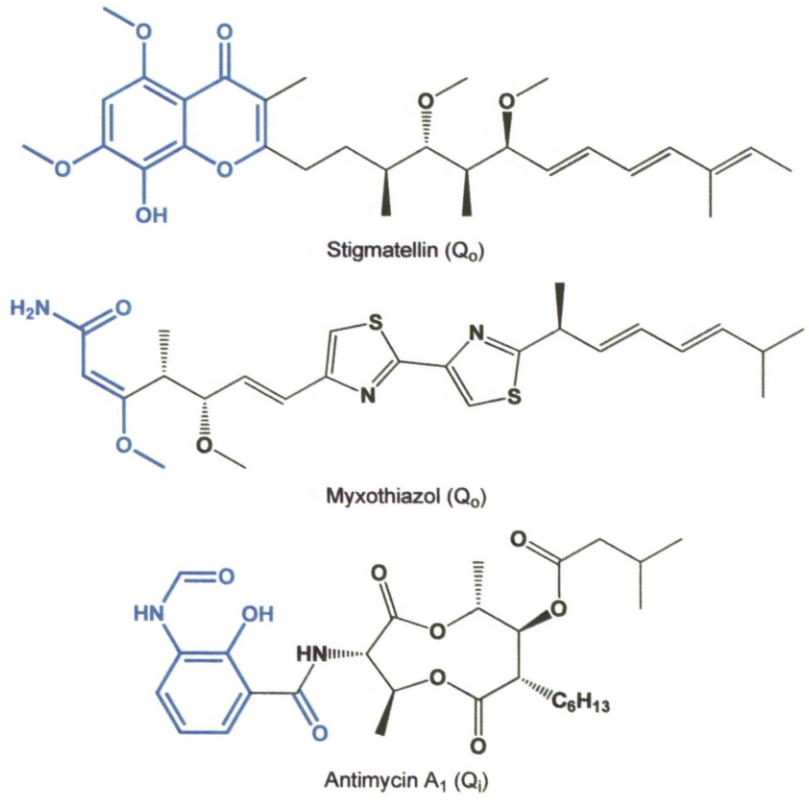

Figure 1.13: Showing the structures of a selection of natural bc_1 inhibitors with their identified toxocophores highlighted in blue.[46]

Class I compounds are Q_o site inhibitors and historically have been further subdivided into 3 subclasses, Ia - Ic, according to their chemical characteristics. However recent literature has sought to reclassify the Q_o inhibitors into just 2 subclasses according to their structural effects on the protein target and in particular their effect on ISP region mobility rather than by their chemical class.[54]

Class Ia compounds include myxothiazol (Figure 1.13) and are characterised as those that bind at the Q_o site and are believed to hinder electron transfer from the endogenous quinol to the ISP.[46] The new Xia classification identifies these compounds as P_m type; P indicating positive region, i.e. Q_o binders, and 'm' indicating that the ISP remains mobile while the inhibitors are bound.[54] As their toxocophore these compounds typically contain an E-β-methoxyacrylate moiety or close structural relative. Synthetic examples of the class include commercial fungicides azoxystrobin, kresoxim-methyl and the new potential antimalarials in development by Ridley *et al.* (Figure 1.14).[55]

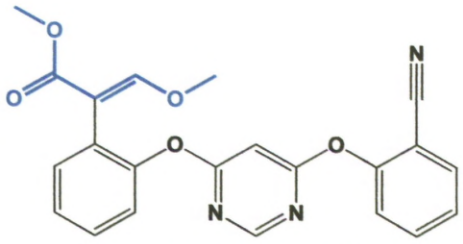

Azoxystrobin (Syngenta)[45]

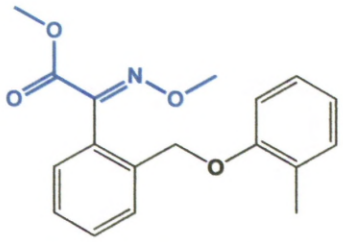

Kresoxim-methyl (BASF)[45]

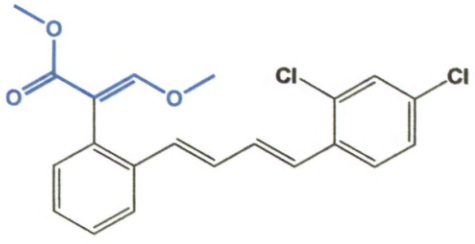

Ridley Compound 15j[54]

Figure 1.14: Class P_m bc_1 inhibitors with their toxocophores highlighted in blue.

Class Ib and Ic inhibitors under the traditional system were considered to be separate due to their differing core structures. Class Ib structures possess a chromone ring system like stigmatellin (Figure 1.13) whereas Ic inhibitors are generally 2-hydroxy quinone analogues such as UHDBT (Figure 1.15). However the DuPont agrochemical famoxadone (Figure 1.15) is structurally different to both classes but has been shown to work in the same way.[46] Under the new system famoxadone and compounds from both Ib and Ic classes are all considered to be P_f inhibitors; P again indicating Q_o binding and 'f' indicating that when bound these compounds fix the ISP region in a set position.[54]

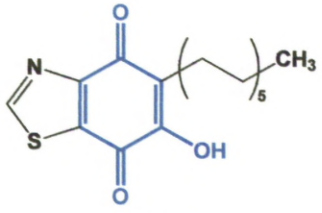

UHDBT

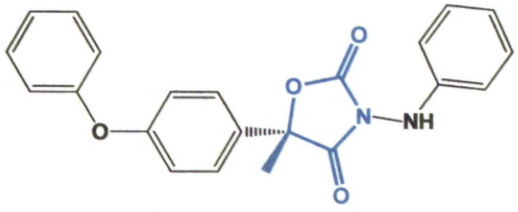

Famoxadone (DuPont)

Figure 1.15: Class P_f bc_1 inhibitors with their toxocophores highlighted in blue.

Finally there are the class II inhibitors; these are compounds that bind at the alternative Q_i site. In terms of resistance Q_i is a more desirable target than Q_o in that it suffers less from the point mutation issues that can present a problem for Q_o binders.[56] However the fact that it is situated on the inner face of the inner mitochondrial membrane makes it relatively inaccessible

and to date only antimycin A_1 (Figure 1.13) and its analogues are known to be Q_i specific. The amino acid sequence of the Q_i active site is also well conserved between species potentially making selectivity a challenge.[46]

1.3.4 Inhibition by Atovaquone

Atovaquone is a class Ib inhibitor, like stigmatellin it binds reversibly at Q_o competitively interfering with ubiquinol oxidation and temporarily locking the ISP region in place. A number of studies have been carried out to ascertain the exact binding position of atovaquone to try and better understand the factors controlling its selectivity and resistance mechanisms. To date the bc_1 complex of *P.falciparum* has not been successfully isolated and crystallised for analysis therefore these studies have been carried out in bacterial[35] and yeast based systems.[43, 57, 58] Of particular note are the studies by Trumpower *et al.* using the crystal structure coordinates of stigmatellin-bound *Saccharomyces cerevisiae* yeast bc_1 in combination with biological and spectroscopic data to model the interactions of atovaquone with the Q_o pocket (Figure 1.16).[58]

Electron paramagnetic resonance (EPR) spectroscopy indicates that like stigmatellin and UHDBT, atovaquone binds tightly with the Q_o pocket when the water-soluble mobile region of the ISP is closest to cytochrome *b* allowing the compound to interact directly with both protein chains. It was observed that the inter-atomic distances in the head group of atovaquone (Figure 1.10) were a match with those of UHDBT (Figure 1.15) and that the hydroxyl groups in the two compounds have the same pKa.[58] Studies using optical spectra have shown that the hydroxyl group of UHDBT is ionised when bound with bc_1 resulting in the formation of a hydrogen bond between the His181 residue and the ionised oxygen.[59] Crystallisation studies using UHDBT have shown that a second, water mediated hydrogen bond is formed between the Glu272 residues of cytochrome *b* and the carbonyl group of the quinone ring.[59]

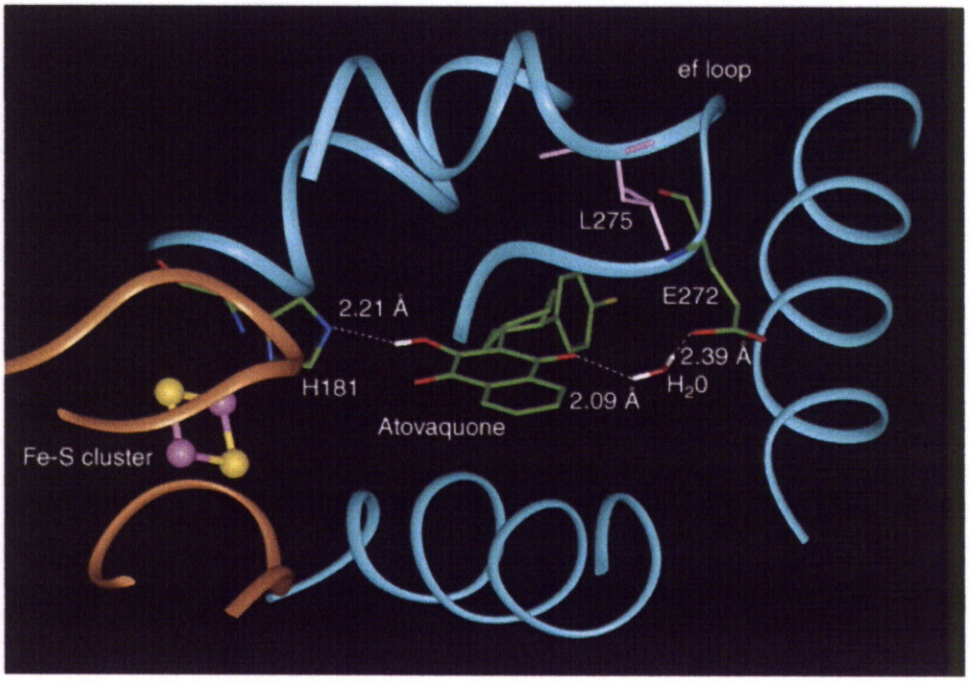

Figure 1.16: In silico docking results from the Trumpower study. Cytochrome b is shown as cyan ribbons and a section of the ISP is shown in orange. The [2Fe-2S] Rieske cluster is shown as yellow and purple balls; docked atovaquone is shown in green. Key amino acids His181, Glu272 and Leu275 are highlighted.[58]

The Trumpower study uses this as a guide to manually dock atovaquone overlaid on the ring structure of stigmatellin, orientated such that the carbonyl and hydroxyl groups form hydrogen bond interactions analogous to those of UHDBT.[58] The manually docked structure was then energy minimised *in silico* to predict the precise binding position of atovaquone in Q_o (Figure 1.16). The results indicate that this orientation would promote strong binding between atovaquone and both cytochrome *b* and the ISP accounting for the observed fixture of the mobile protein region during binding.[58]

The study also used comparison of the protein sequence between protozoan bc_1 and mammalian bc_1 to explain the selectivity of atovaquone. In the mammalian sequence the leucine at 275 found in yeast is replaced by phenylalanine. Modelling of this change showed that it directly effects the region of the hydrophobic channel leading to Q_o that is occupied by the chlorine substituted aromatic ring of atovaquone. In the yeast protein the channel is relatively open at this point, where as in mammalian bc_1 the increased van der Waals radius of the phenylalanine residue results in a bulge in the wall of the channel giving rise to unfavourable steric interactions

(Figure 1.17). This alteration is responsible for the reduced sensitivity of mammalian bc_1 proteins to atovaquone compared to protozoan proteins. Site directed mutagenesis of yeast bc_1 to create L275F mutants have confirmed this with the mutated proteins showing similar levels of insensitivity to atovaquone.[58]

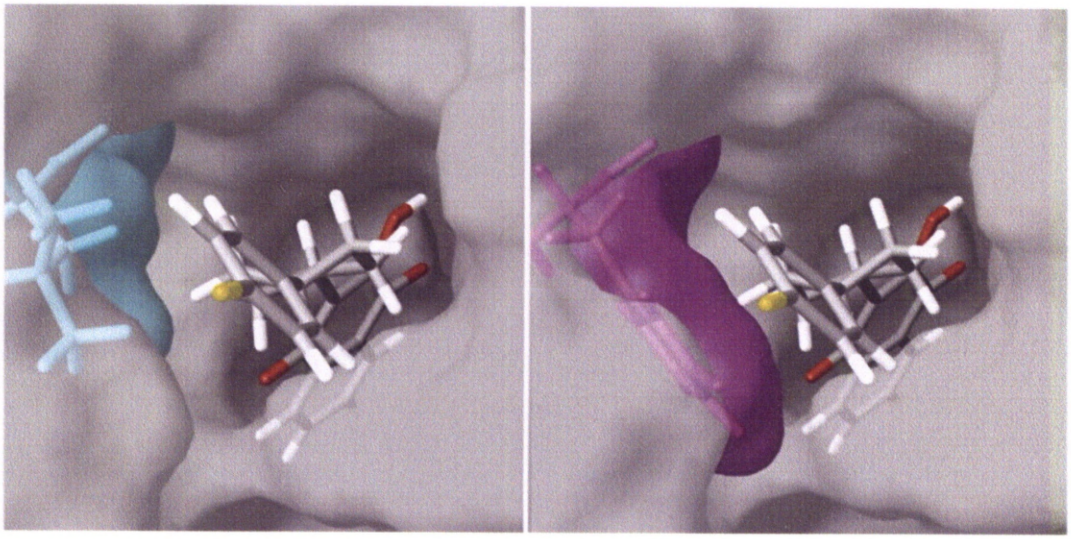

Figure 1.17: Left atovaquone docked in yeast bc_1 with the region occupied by Leu275 highlighted in cyan. Right atovaquone docked in bovine bc1 with the region occupied by Phe275 highlighted in purple.[58]

1.3.5 Atovaquone Resistance

In sensitive parasites atovaquone is highly potent, with an average IC_{50} of ~6 nM, and has a reasonable therapeutic index; the parasite protein is inhibited at concentrations ~200-fold lower than those required to have any noticeable affect on human bc_1.[35] However single point mutations in the gene's coding for the Q_o binding site have been shown to confer up to a 760-fold drop in potency, rendering the drug effectively inactive at safe therapeutic doses.[60]

The majority of resistance-conferring mutations cause alterations in the amino acids forming the hydrophobic channel leading to Q_o rather than altering the structure of Q_o itself as alterations here tend to render the protein complex inactive themselves.[40, 41, 57, 60-62] The most common mutation in parasite isolates leading to Malarone® treatment failure are those that alter the amino acid at position 268 in the cytochrome *b* structure, usually a tyrosine (Y268) this residue is often exchanged for serine in resistant strains

(Y268S).[63, 64] Indeed site directed mutagenesis studies mimicking this single alteration at the equivalent residue (Y279S) in yeast bc_1 have shown drops in atovaquone sensitivity from 60 nM in the parent strain, to >4000 nM in the mutated strains.[65] Research appears to indicate that this residue is involved in a hydrophobic stabilising interaction with ubiquinol and it is likely that the mutation results in a significant respiratory penalty for the parasite.[58]

Other mutations have been identified and as with the Y268 mutation most appear to significantly alter the structure of the hydrophobic region of the Q_o site. A side-effect of this is that atovaquone resistance tends to confer cross resistance to other Q_o inhibitors. For example in strains of *P.yoelli* in which atovaquone resistance was induced by sub-optimal dosing, myxothiazol resistance was also observed in all the mutated strains although at lower levels than that towards atovaquone.[40] This cross resistance highlights a critical drug design challenge for the development of novel bc_1 inhibitors that we hope to overcome.

1.4 Antimalarials in Development Targeting the Cytochrome bc_1 Protein Complex

While atovaquone is the first inhibitor to be licensed for the treatment of malaria, other compounds acting at the same site in organisms such as fungi and some insects, have been in existence for the best part of five decades. Since the elucidation of atovaquone's mode of action led to the validation of the bc_1 complex as an antimalarial target, work on bc_1 inhibition as a therapy for malaria has intensified. The β-methoxyacrylate compounds in development by Ridley *et al.* (Figure 1.14) have already been briefly discussed but these are in their infancy.[55] The more established areas of antimalarial bc_1 inhibition research tend to be based on aromatic ring systems and can be broadly divided into four classes based on their core chemical structure.

1.4.1 Atovaquone analogues –1,4-Naphthoquinones

This class of compounds have the same basic core as atovaquone (Figure 1.18) but seek to improve on atovaquone's relatively poor bioavailability[66] and other pharmaceutical properties. The structurally related

1,2-naphthoquinones have also been investigated but were not confirmed to be bc_1 inhibitors.[67]

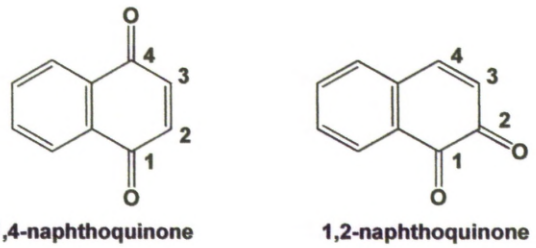

Figure 1.18: Core structures of the naphthoquinone class of compounds

The antimalarial activity of 1,4-naphthoquinones was identified in the 1940's when a study at Harvard in conjunction with Abbott Laboratories recognised hydrolapachol (Figure 1.19) as a potential antimalarial and developed a number of synthetic derivatives with high levels of potency in bird models.[68] The majority of the compounds identified during the course of this work possessed long aliphatic or cycloalkane-based side-chains (Figure 1.19) and suffered from rapid metabolic degradation. One compound from the study, termed M-2350 (Figure 1.19) did reach early stage clinical trials in man, but was found to be poorly absorbed when administered orally or intramuscularly.[69]

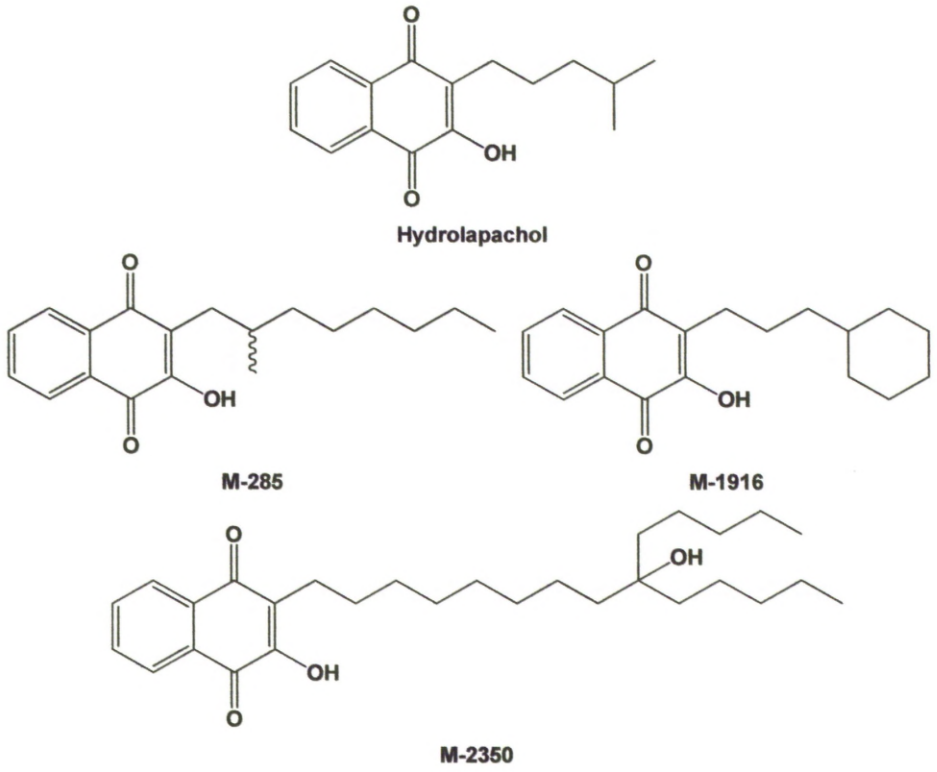

Figure 1.19: Structures of naphthoquinone antimalarials identified by Fieser et al in 1948.[68]

In recent years the Trumpower group of Dartmouth Medical School have revisited this work focusing on analogues of M-285 (Figure 1.19), specifically the *S*-enantiomer (S-10576) which they have determined is significantly more parasite selective than the corresponding *R*-enantiomer.[70] The group sought to increase the compound's metabolic stability through the use of perflourinated side-chains and substitution at the 8-position of the naphthoquinone head group (Figure 1.20).[70-72]

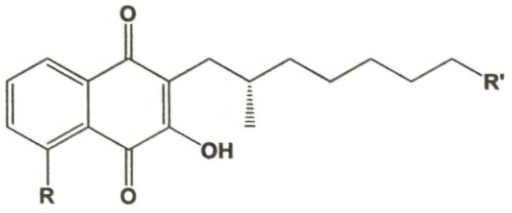

S-10576: R = H, R' = CH_3
NQ1: R = H, R' = CF_3
NQ2: R = CH_3, R' = CH_3
NQ3: R = CH_3, R' = CF_3

Figure 1.20: The general structure of 2-hydroxy-naphthoquinones developed and investigated by the Trumpower group.

While these alterations did indeed improve the metabolic profile of the compounds, their species selectivity was dramatically reduced compared to the parent compound[71] and the inclusion of a methyl group at the 8-position significantly reduced potency (Table 1.1).[72]

Table 1.1: Activity of naphthoquinone compounds against liver stage P.berghei sporozoites in vitro.[72]

Inhibitor Compound	IC_{50} *versus P.berghei* (nM)
Atovaquone	19.7
S-10576	96.2
NQ1	17.1
NQ2	246.5
NQ3	4451.8

In summary 1,4-naphthoquinone-based compounds continue to show promise as bc_1 inhibitors, however the continuing need for chiral purity to ensure good levels of parasite selectivity is an issue and the current leads require considerable further development to increase their drug-like character.

1.4.2 Pyridones

Clopidol (Figure 1.21) has been known as a potent antimalarial since the 1960's and recent collaborative efforts by GlaxoSmithKline and various research groups have produced a number of pyridone based compounds (Figure 1.21).[73]

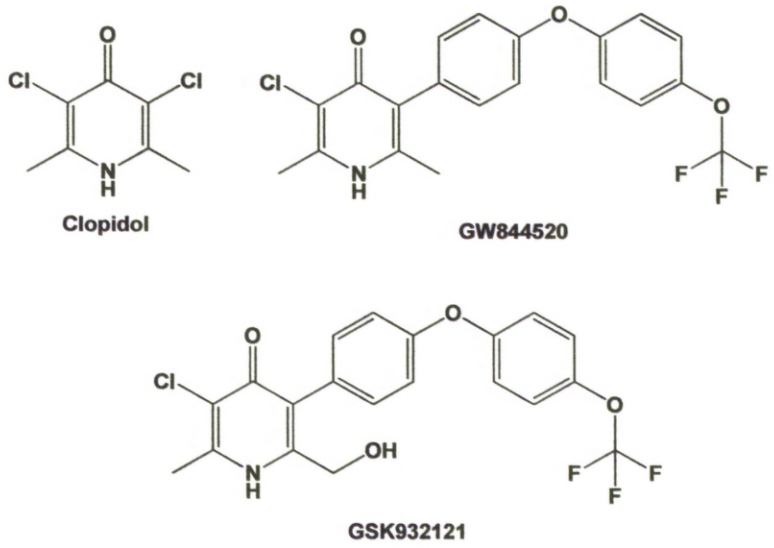

Figure 1.21: Showing the structures of clopidol and recently developed pyridone based antimalarials.

Many of these compounds exhibit impressive antimalarial potency, GW844520 (Figure 1.21) has a recorded IC_{50} of 2 nM, and importantly they maintain activity against atovaquone resistant strains of parasite.[42] The solubility issues so often encountered with these compounds have been overcome by the introduction of a hydroxyl moiety as in GSK932121 (Figure 1.21), allowing the formulation of the compounds as phosphate prodrugs.[74] A selection of lead compounds of this type reached early stage clinical trials but were withdrawn after toxicity issues were identified that have yet to be resolved.[75]

1.4.3 Acridinediones and Acridones

These classes have very similar core structures and so are discussed together here (Figure 1.22). Acridinediones are well known in the antimalarial literature as they are established haem binders, one of the best known being the experimental drug floxacrine (Figure 1.22). Floxacrine was developed

during the late 1970's and initially showed promise for use as a prophylactic agent but limited solubility, rapid resistance development and unacceptable side-effects led to its development being temporarily abandoned.[76]

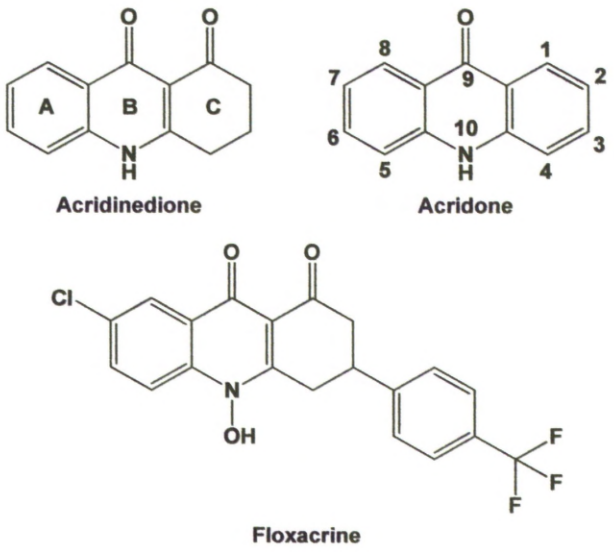

Figure 1.22: The structures of acridinedione and acridone ring systems and of floxacrine, an acridinedione based antimalarial first developed in the 1970's.

More recently acridinediones have garnered increased attention following the discovery that they can have a dual mode of action. Developed in 2001 in an attempt to overcome the drawbacks of floxacrine, WR 243251 (Figure 1.23) is an inhibitor of hematin polymerisation with comparable haem binding to that of chloroquine. However WR 243251 has higher overall potency against *P.falciparum* than chloroquine and maintains activity against chloroquine resistant parasite strains, indicating that a second mechanism of action may be present.[76] This hypothesis is supported by the fact that the ketone hydrolysis product WR 243246 (Figure 1.23) has a similar level of potency against *P.falciparum* as its parent compound, but does not inhibit hematin polymerisation to any appreciable level.[76]

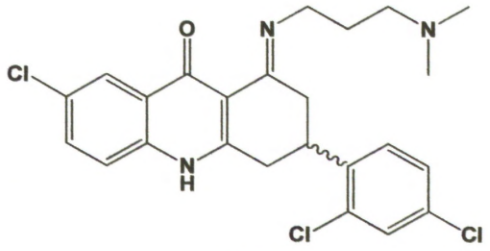

WR 243251

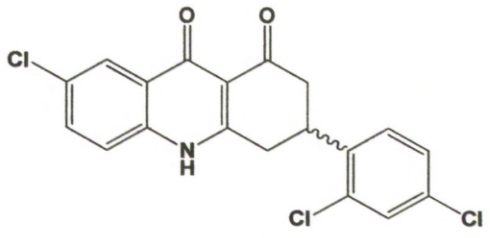

WR 243246

Figure 1.23: Structures of some recently developed floxacrine derivatives.

It was observed that acridinediones similar to WR 243251 and WR 243246 (Figure 1.23) exhibited cross resistance with atovaquone resistant parasite strains[77] and further investigation led to the discovery that these compounds are potent and highly parasite selective bc_1 inhibitors; in particular WR 249685, the *S*-enantiomer of WR 243246 (Figure 1.23), is more than 4600 times more potent against *P.falciparum* bc_1 protein than it is against the mammalian protein.[78] Interestingly, despite being structurally very similar to the active derivatives, floxacrine (Figure 1.22) has only negligible activity against bc_1 with no measurable degree of selectivity.[42, 78] This suggests that while the acridinedione core clearly has some exciting properties the further development of analogues for clinical use could be hampered by restricted substitution options.

The structurally related acridones benefit over the acridinediones by being fully aromatic and therefore avoiding the issue of chiral isomers that can arise from substitution of the alkyl C ring of acridinediones (Figure 1.22). Interest in the acridones arose following the observation by the Riscoe group that an intermediate in their work on haem binding acridones (Figure 1.24) was active as an antimalarial at 45 nM against *P.falciparum*, but did not interfere with hematin polymerisation.[79]

Development of their initial hit allowed the group to develop a small library of highly potent compounds, with their lead compound having activity of around 1 pM against *P.falciparum in vitro* (Figure 1.24).

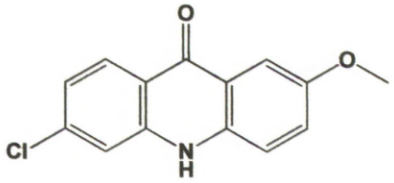

6-chloro-2-methoxyacridin-9(10*H*)-one

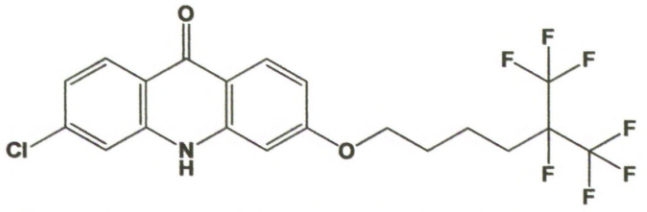

3-chloro-6-((5,6,6,6-tetrafluoro-5-(trifluoromethyl)hexyl)oxy)acridin-9(10*H*)-one

Figure 1.24: The structure of the intermediate indentified by Riscoe et al. during their work on haem binders (top) and the lead compound that developed from it (bottom).[79]

The group found that activity was increased if substitution was moved from the 2-position to the 3-position on the C ring and that perfluorinated alkyl chains comprising at least one CF_3 group gave the highest levels of potency. While it has not yet been proven that these compounds are bc_1 inhibitors their structural similarity to compounds that are, observed cross-resistance with atovaquone[80] and other evidence from outside the field of antimalarial research would certainly seem to support this hypothesis.[79] A potential concern with the acridone structures currently published is that the flexibility of the side-chains currently utilised may result in issues with selectivity although no toxicity problems were reported following *in vivo* tests.[79] At present, little further development appears to have been carried out on these compounds with the majority of work on acridones instead focusing on the nitrogen substituted haem binding variants that have been demonstrated to reverse chloroquine resistance.[81, 82]

1.4.4 Quinolone based compounds

In the late 1940's work at Bayer resulted in the synthesis of endochin (Figure 1.25).[83] The compound was extremely active in bird models both as a prophylactic agent and as a treatment, however in mammal models activity all but disappeared and the compound was dropped.

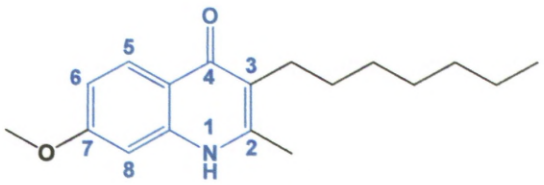

Endochin

Figure 1.25: The structure of the Bayer compound endochin with the quinolone core structure highlighted.[83]

The quinolone core (Figure 1.25) however has continued to reappear in antimalarial studies. In the late 1960's during a combined study by ICI and the Liverpool School of Tropical Medicine searching for anticoccididial compounds it was noted that a number of the quinolone esters (Figure 1.26) developed were active against malaria in rodent and monkey models.[84] The compounds showed high potency, up to 50 times that of chloroquine against *P.berghei*, and were successful both as treatments and as prophylactics. Of particular interest was the observation that the compounds appear to have been effective against all stages of the parasite life cycle and chloroquine resistant strains, suggesting that they were probably inhibiting a respiratory target such as bc_1.[84] However there were issues with the development of resistance in rodent models and there appears to have been little further development of the compounds.

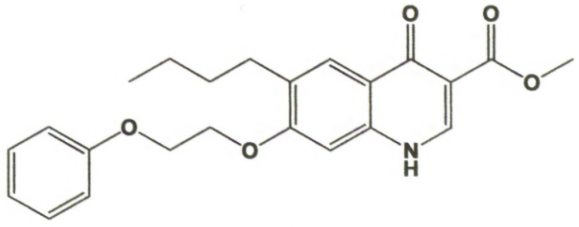

ICI 56780

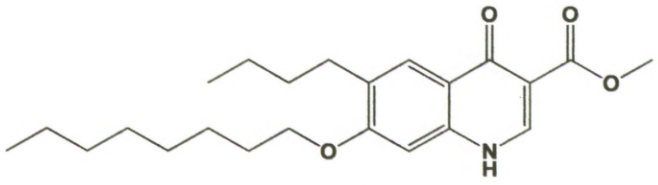

ICI 60128

Figure 1.26: Quinolone esters identified by ICI as potent antimalarials in animal models.[84]

Fluoroquinolone antibiotics, such as ciprofloxacin (Figure 1.27), were shown to have antimalarial activity during the 1980's[85] and during the drive for new antimalarials in the 1990's fluoroquinolones were studied extensively as potential replacements for the failing aminoquinolines despite being

markedly less potent.[86-94] However, severe side effects,[95-97] resistance issues[88, 89] and the advent of artemisinin eventually caused enthusiasm for the compounds to wane.

More recently the observation that some fluoroquinolones, including grepafloxacin and trovafloxacin (Figure 1.27), have limited activity against hepatic stage parasites as well as the erythrocytic stage resulted in interest being rekindled for a time with the belief that a dual mode of action could be established.[98, 99] However activities against *P.falciparum* were still too low for the compounds to be considered promising drug leads, even against chloroquine resistant parasite strains.[98] More potent fluoroquinolones have been recently developed in Japan by substitution at the quinolone nitrogen with side-chains containing pyridyl rings but these compounds have yet to be investigated beyond a simple initial screening.[100]

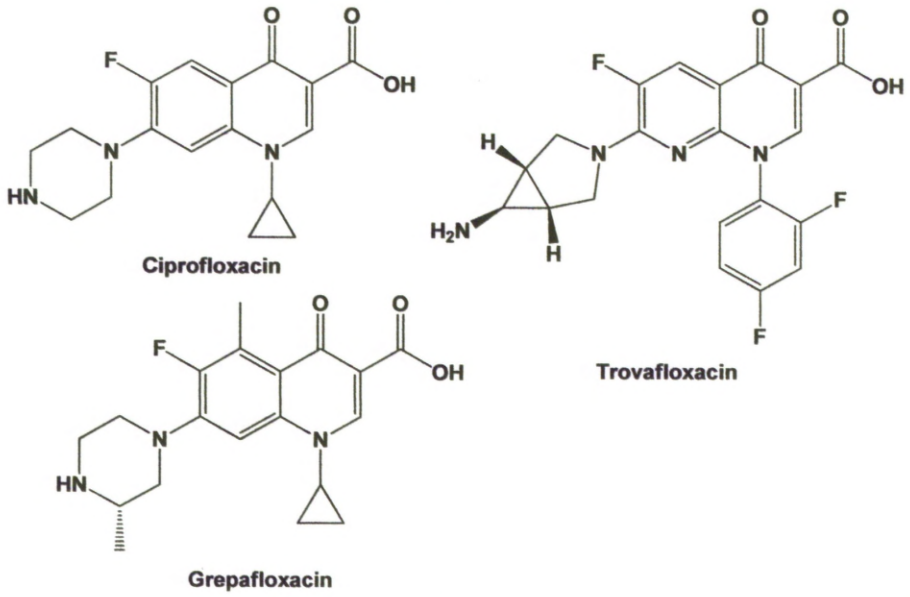

Figure 1.27: Fluoroquinolone-based antibacterials with multi-stage activity against P.falciparum malaria.[98]

Recent work by R. K. Guy *et al.* on quinolone 3-esters substituted at the 2-position with short aromatic side-chains (Figure 1.28) have shown promise with a lead compound achieving a 50% parasite clearance of both chloroquine-sensitive and chloroquine-resistant strains of *P.falciparum* at around 100 nM *in vitro*. Whether or not these compounds target parasite bc_1 has yet to be determined, but evidence from the study certainly suggests that it is a possibility.[101]

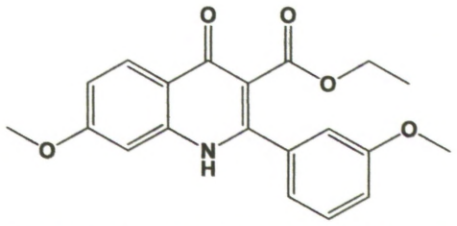

ethyl 7-methoxy-2-(3-methoxyphenyl)-4-oxo-1,4-dihydroquinoline-3-carboxylate

Figure 1.28: Structure of the lead compound identified by R. K. Guy et al.[101]

The most promising studies on antimalarial quinolones in recent years have been on endochin-type structures.[80, 102, 103] Endochin (Figure 1.25) was developed by Bayer in the 1940's and showed promise in avian models but is rapidly metabolised in mammals leading to poor bioavailability.[83] Cross-resistance of endochin-based compounds with atovaquone has been noted on a number of occasions in recent years and indicates that agents of this structure are almost certainly targeting the bc_1 protein complex.[80, 102]

In 2008 a study was published by Riscoe and Winter in which they applied findings from their work on antimalarial acridones[79] to a quinolone core structure by substitution with perfluorinated alkyl chains (Figure 1.29).[80] They found that by extending the 3-heptyl chain of endochin to an undecyl chain (11 carbons) and terminating with a trifluoromethyl moiety activity against *P.falciparum* was doubled *in vitro*, (IC_{50} = 1.4 nM *versus* 2.8 nM for endochin against chloroquine resistant parasite strains) and cross-resistance in atovaquone resistant parasite strains was significantly diminished (IC_{50} = 4.7 nM *versus* 17.4 nM for endochin against multidrug resistant parasite strains). A synergistic relationship with clopidol (Figure 1.21) was also determined, but the solubility of the lead compounds was very poor.[80]

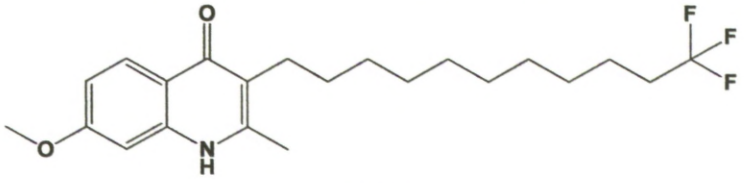

ELQ-103

Figure 1.29: The structure of the lead compound identified by Riscoe et al in 2008.[80]

In a continuation of this study published in 2011 the group sought to optimise the structure of their initial hit, ELQ-103 (Figure 1.29) by changing the substitution pattern of the quinolone ring, introducing novel functionality in an effort to increase solubility and reduce metabolic instability. Their resulting

library of around 30 compounds established a new lead in the form of ELQ-121 (Figure 1.30) which exhibited 10-fold higher potency than ELQ-103 against 4-aminoquinoline resistant parasite strains. While ELQ-121 does exhibit marginally increased cross-resistance with atovaquone compared to ELQ-103, more importantly *in vitro* metabolic studies showed that ELQ-121 exhibits enhanced metabolic stability.[103] Solubility of the compounds was still an issue for *in vivo* use but the successful synthesis of a poly(ethylene) glycol prodrug, ELQ-125 (Figure 1.30) has improved on this, with successful cure achieved in mouse models infected with multi-drug resistant parasites.[103]

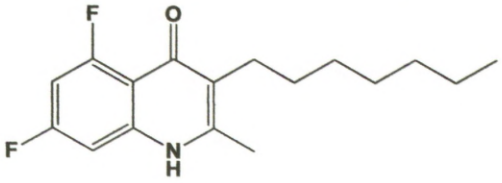

ELQ-121

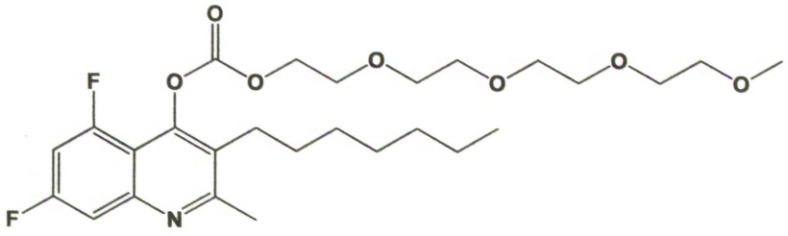

ELQ-125

Figure 1.30: The lead compound, ELQ-121, and related prodrug, ELQ-125, from the most recent study by Riscoe et al.[103]

In parallel to the Riscoe et al studies the Manetsch group of the University of South Florida in partnership with the Medicines for Malaria Venture designed and synthesised a library of over 60 endochin-type quinolones in an effort to establish a comprehensive structure-activity relationship for this class of compounds against *P.falciparum* parasites.[102]

As with the Riscoe studies they found that altering the alkyl chain length at the 3-position modulated activity and that the carbonyl at the 4-position, as well as the lack of substitution at N-1 are key factors for this chemotype. It was also established that only limited changes to the 5, 6, 7 and 8 positions are well tolerated but the presence of a halogen atom, particularly chlorine, at the 6-position does enhance activity and reduces cross-resistance. Increasing solubility by shortening the 3-alkyl chain length resulted in a dramatic reduction in parasite selectivity and attempts to increase solubility

utilising various alkenyl side chains were found to severely hamper activity against both sensitive and multidrug resistant parasite strains. While 3-aryl substituted analogues also exhibited a drop in potency it was less severe and both solubility and metabolic stability *versus* human liver microsomes were much improved.[102]

In summary it was determined that the most potent endochin derivatives had structures in which there was an alkyl chain of at least 7 carbons in length at the 3-position, positions 5 and 8 were unsubstituted, there was a methoxy group at the 7-position and a chlorine atom at the 6-position (Figure 1.31). However it was suggested that, while less potent, an aryl group at the 3-position offers better scope for further development.[102]

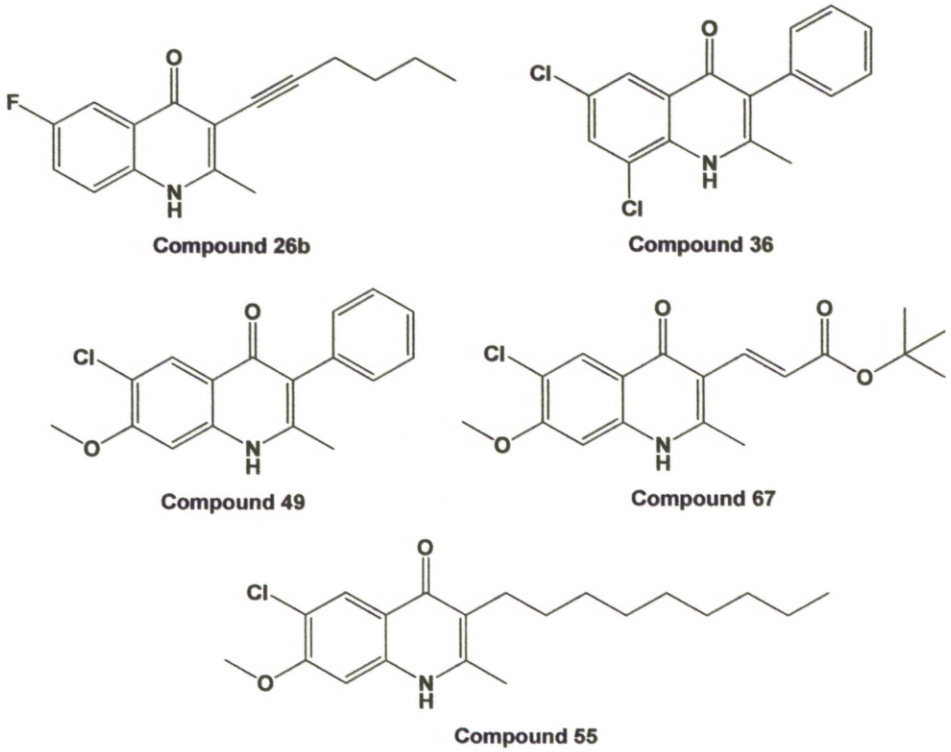

Figure 1.31: Examples from the Manetsch et al. study of endochin derivatives including their most potent analogue, compound 55, and their suggested scaffold for further development, compound 49.[102]

1.5 Project Aims

For this project we decided to focus on a quinolone core similar to those identified by ICI in the 1960's (Figure 1.26). We hope that by varying the functional groups at the 3 and 7-positions of the quinolone ring we will be able to design analogues with high levels of potency against the *P.falciparum*

bc_1 protein and achieve good levels of selectivity over mammalian proteins. It is also hoped that through the use of *in silico* modelling of the compounds synthesised we will be able to determine the factors governing atovaquone cross-resistance for this class of compounds and so develop antimalarial agents that maintain activity against multidrug resistant parasite strains.

Chapter 2

Results and Discussion 1: Building a Structure–Activity Relationship for 4-Quinolone based Inhibitors of the P.falciparum bc_1 Complex

2. Results and Discussion 1: Building a Structure–Activity Relationship for the *P.falciparum* bc_1 Complex

2.1 Quinolone Synthesis

As noted in the introduction, we have selected the 4-quinolone ring system as the core of our target compounds. In the literature, 4-quinolones are commonly presented as their tautomers, 4-hydroxyquinolines (Figure 2.1). However, studies have demonstrated that for the majority of examples, the preferred tautomer both in solution and the solid state is the 4-quinolone.[104] This finding has also been borne out by our own analysis, which will be shown later. Therefore, compounds will be presented as their 4-quinolone tautomer for the remainder of this discussion.

The quinolone system has found use in a range of pharmaceutical applications and forms the core of a well established class of antibiotics. Consequently, many different synthetic pathways have been developed for their formation from a variety of starting points.

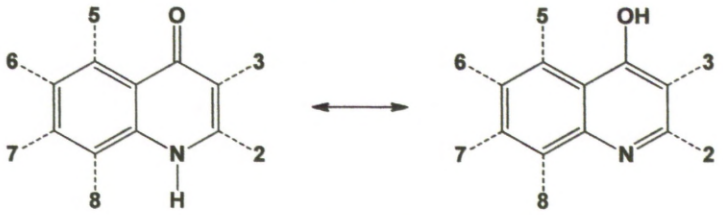

Figure 2.1: Showing the numbering system used for 4-quinolone/4-hydroxyquinoline based ring substitutions.

There are a number of notable named examples for the synthesis of quinolones. The Conrad-Limpach synthesis can be used to synthesise 4-quinolones substituted at the C2 and C3 positions from anilines and β-ketoesters (Scheme 2.1).[105]

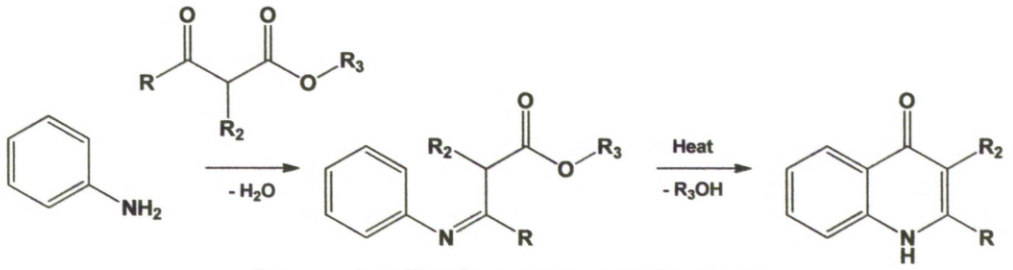

Scheme 2.1: The Conrad-Limpach Synthesis

The Camps cyclisation is a base-catalysed method which, dependent on choice of conditions and starting material, can be used to give either C2 substituted 4-quinolones or 2-hydroxyquinolines from *ortho*-acylaminoacetophenones (Scheme 2.2).[106]

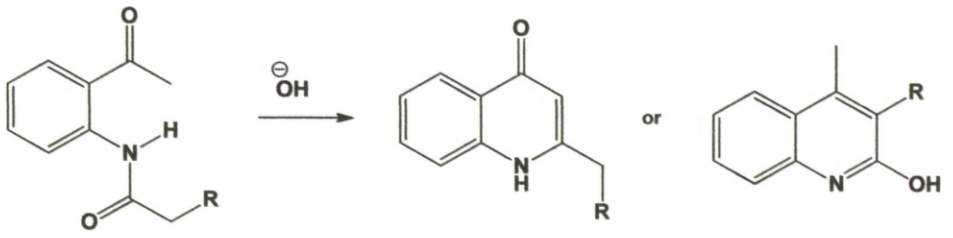

Scheme 2.2: The Camps Cyclisation

The Niementowski quinoline synthesis uses anthranilic acid derivatives and ketones or aldehydes to yield 4-hydroxyquinolines disubstituted at both C2 and C3 positions, or monosubstituted at C3, respectively (Scheme 2.3).[107]

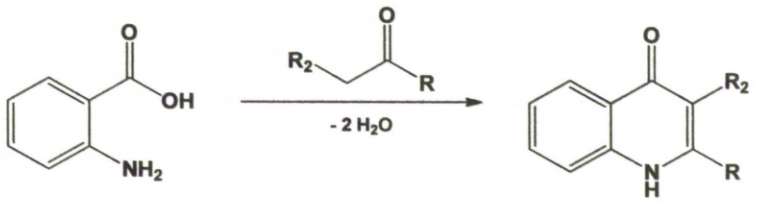

Scheme 2.3: The Niementowski Quinoline Synthesis

For the development of our initial library, we chose to utilise the Gould-Jacobs reaction. First published in 1939 by R. Gordon Gould and Walter A. Jacobs, this method is a two stage process which proceeds *via* the reaction of an α,β-unsaturated ester (usually a malonate derivative) with an aniline. This is followed by a thermally driven cyclisation in which the phenyl ring of the aniline acts as a nucleophile, attacking the carbon of the ester carbonyl group (Scheme 2.4).[108] This allows functionalities such as esters and nitriles to be easily incorporated at the 3-position, which we believe should interact favourably with the hydrophilic amino acid residues in the Q_o target site.[52, 53, 109]

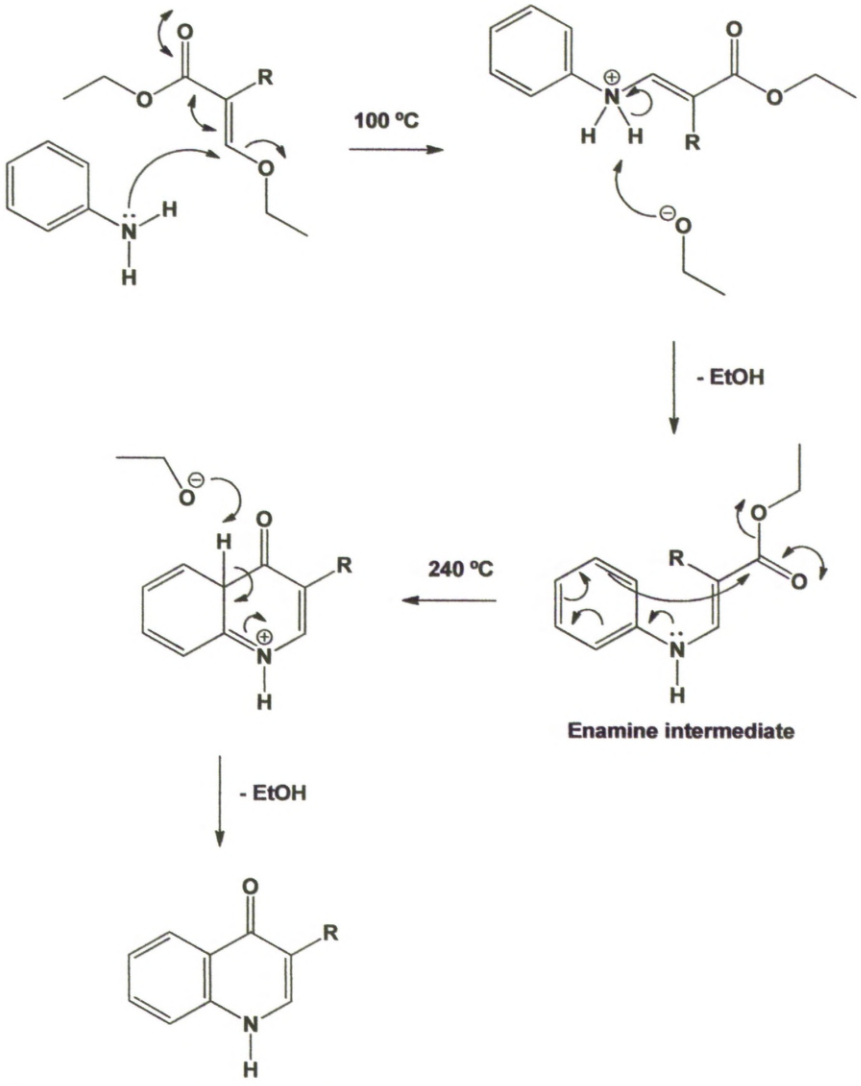

Scheme 2.4: The mechanism by which the Gould-Jacobs Quinolone Synthesis proceeds.

2.2 Validating the Template – Synthesis of 1st Generation Inhibitors

Choosing to utilise the Gould-Jacobs methodology for the synthesis of our quinolone targets ensured that we could use commercially available anilines to rapidly synthesise a small number of compounds to test the validity of our design.

The particular process followed was that used by Stern *et al.* in 2006 to develop a series of CB_2 cannabinoid agonists with similar core structures to our targets,[110] but there is little variation across the literature.[110-114] The first stage of the reaction is solvent free, with an aniline dissolved directly in one equivalent of malonic ester. This is then heated to 100 °C overnight, before cooling to give the enamine intermediate as a crude solid (Figure 2.4). The

crude enamine is then added directly to refluxing Dowtherm A (Fluka) at 240 °C and further heated for 1 – 2 hours, followed by cooling and precipitation of the product using hexane. Following reprecipitation from a suitable solvent (usually dimethylformamide), the products are obtained in moderate to good yields as off-white powders. To obtain our first two targets, this was accomplished by reaction of diethyl 2-(ethoxymethylene) malonate **1** with 3-phenoxyaniline **2** and 3-benzyloxyaniline **3**, to give compounds **4** (Scheme 2.5) and **5** (Scheme 2.6) respectively.

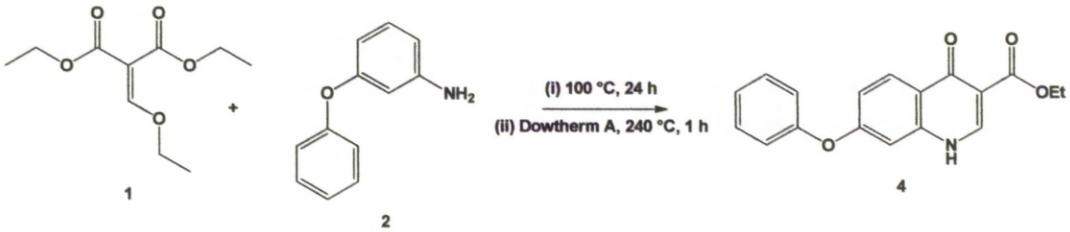

*Scheme 2.5: Synthesis of compound **4**.*

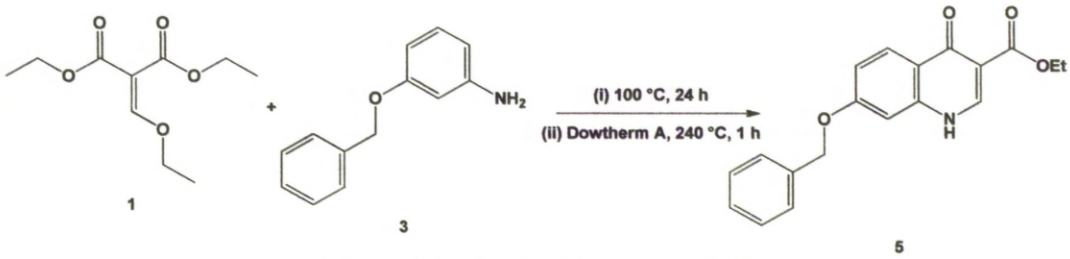

*Scheme 2.6: Synthesis of compound **5**.*

2.2.1 Synthesis of ethyl 7-(4-(trifluoromethoxy)phenoxy)-quinolin-4-one-3-carboxylate

Following the work of Riscoe *et al.* on the effect of perfluorinated side-chains on the antimalarial activity of acridones,[79] we also wanted to include an analogue with a trifluoromethoxy moiety on the aryl ring. As no commercially affordable anilines were available with this structure, it was necessary to synthesise this intermediate.

The most common method for the synthesis of diphenyl ethers is the Ullmann coupling process, which can be either palladium-[115] or copper-catalysed.[116, 117] In terms of affordability, the copper-catalysed options were more desirable to us. After experimenting with a number of methods, a glycine mediated process developed by Ma and Cai in 2003 was selected.[116] The Ullmann reaction cannot be carried out using anilines as this would result in a side reaction at the nitrogen, in addition to the desired coupling

through oxygen. Therefore, 3-nitrophenol **7** was used as the starting material and reacted with 4-(trifluoromethoxy)iodobenzene **8** to give 1-nitro-3-(4-(trifluoromethoxy)phenoxy)benzene **9** (Scheme 2.7) in yields of approximately 60% following purification by chromatography.

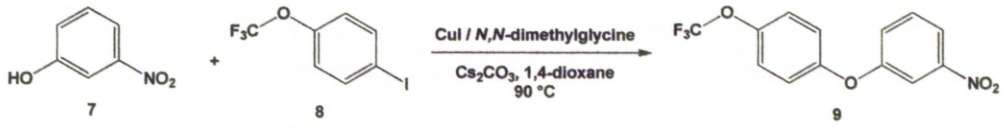

*Scheme 2.7: Ullmann coupling reaction to synthesise **8**.*

The mirror reaction of 4-(trifluoromethoxy)phenol and 3-iodonitrobenzene was also attempted, in the hope that yields could be increased. However, it was quickly discovered that the R_f of 4-(trifluoromethoxy)phenol was essentially identical to that of **9**, making efficient purification of the product impractical.

Synthesis of **9** was followed by reduction of the nitro group to the primary amine, giving 3-(4-(trifluoromethoxy)phenoxy)aniline **10**, by a zinc-mediated process used previously in the group for the same transformation (Scheme 2.8).[118] The process consistently gives greater than 90% yields after purification, and while not being the most elegant method available, it benefits from not requiring the use of hydrogen gas as palladium-catalysed alternatives would.

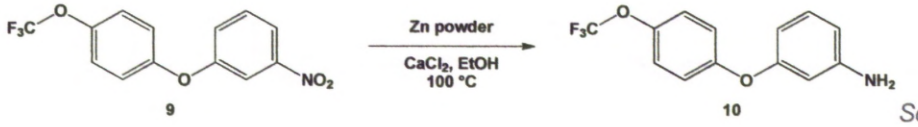

*Scheme 2.8: Zinc mediated reduction of **8** to **9**.*

Reaction of **10** with **1** *via* the Gould-Jacobs protocol gave ethyl 7-(4-(trifluoromethoxy)phenoxy)-quinolin-4-one-3-carboxylate **6** in good yield (Scheme 2.9). The first three compounds synthesised in this manner were submitted for biological testing.

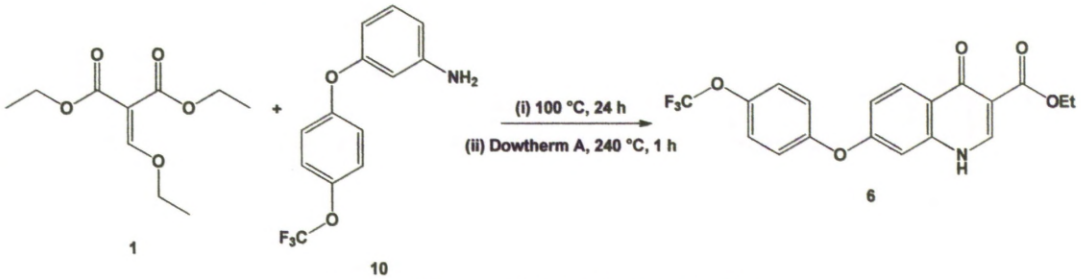

*Scheme 2.9: Synthesis of compound **6**.*

2.2.2 Initial Test Results

Pure samples of **4**, **5** and **6** were assessed *in vitro* in a growth inhibition assay against erythrocytic stage, "wild-type" *P.falciparum* 3D7 strain parasite cultures. The results (Table 2.1) indicated two things; our chosen template was certainly active against *P.falciparum*. Also, solubility was an inherent problem, with compound **5** proving impossible to test biologically.

Table 2.1: Results for the 1st generation compounds

Code	IC_{50} *versus* 3D7 parasites (nM)[a]	Isolated Yield (%)	CLogP by ALog PS2.1[c]
4	19.3	61.7	3.07 ± 0.40
5	No Data[b]	66.7	3.02 ± 0.45
6	5.3	79.8	4.07 ± 0.84

[a] *Average value from at least 3 independent experiments.* [b] *Insufficient solubility for testing.*
[c] *http://www.vcclab.org/lab/alogps/*

While the inability to test compound **5** was disappointing, the potency of compounds **4** and **6** was very exciting, compound **6** in particular as it demonstrated similar potency to atovaquone.

2.3 Improving Solubility – Synthesis of 2nd Generation Inhibitors

While the *in vitro* results for **4** and **6** clearly demonstrated that the 3,7-substituted quinolone template is active against *P.falciparum*, the poor solubility exhibited by all three compounds (particularly **5**) indicated that absorption *in vivo* was likely to be a problem. As the Medicines for Malaria Venture profile for the development of novel antimalarials specifies that new candidates must be orally bioavailable, this was a problem of some urgency.[119] Our first attempt at tackling this issue was to lower the CLogP of the compounds by replacement of the 3-ester group of the lead compounds with a variety of amides.

This was achieved by heating the ester in an excess of the appropriate amine for 1 hour at 120 °C using Dowtherm A as a solvent (Scheme 2.10). The resulting amides were then purified by column chromatography to remove any residual ester compound before submission for biological screening. This method of synthesis was not compatible with all the amines

attempted. Morpholine, for example, evaporated from the reaction mixture faster than it reacted. However, a number of amides were successfully produced and tested (Table 2.2).

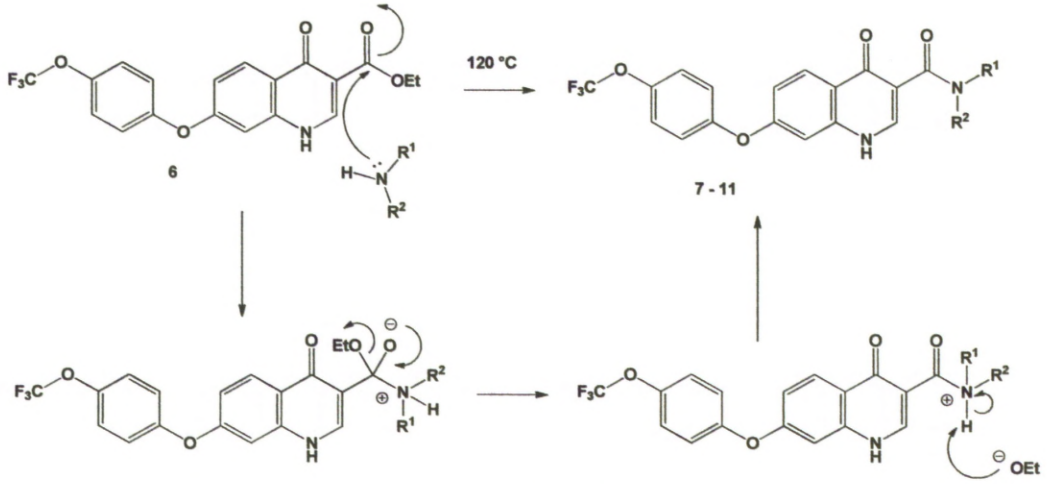

Scheme 2.10: Synthetic route to the amide series.

Table 2.2: Results for the amide series compounds

Code	Structure	Isolated Yield (%)	IC_{50} *versus* 3D7 parasites (nM)[a]	CLogP by ALog PS2.1[b]
7	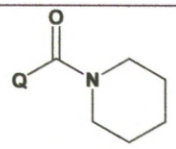	45.1	Not Tested	4.14 ± 0.68
8	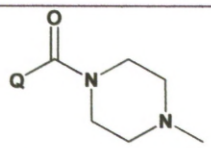	55.4	2728	3.08 ± 0.79
9	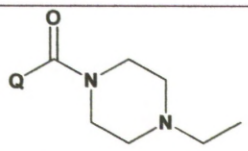	87.8	3511	3.57 ± 0.87
10	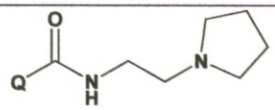	39.5	350	3.70 ± 0.79
11	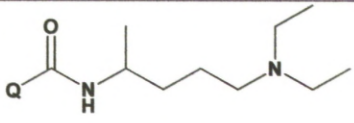	30.0[c]	1120	4.21 ± 0.78

[a] *Average value from at least 3 independent experiments.*

[b] *http://www.vcclab.org/lab/alogps/.* [c] *Synthesised from* ***4****.*

Although not reflected in the CLogP values calculated for the compounds (Table 2.2), the solubility of the amide series was an improvement over the original esters. However when tested *in vitro* they demonstrated vastly reduced activity, with the most potent amide **10** over 60-fold less potent than compound **6** (Table 2.2). This observation implied that the nature of the functional group at the 3-position was critical for good activity against *P.falciparum*. The electron distribution pattern for esters and amides differs significantly, (Figure 2.2) leading to speculation that this has an effect on the binding of the compounds with the target protein. In esters, the electronegative ether oxygen draws electron density away from the carbon atom of the carbonyl group, in turn drawing electron density away from the carbonyl oxygen making it less available for hydrogen bond formation. In amides, donation of the nitrogen lone pair into the carbonyl carbon ensures that the reverse occurs with the carbonyl oxygen consequently relatively electron rich.

This is offset, however, by the resulting partial double bond character of the carbon nitrogen bond (Figure 2.2) reducing amide flexibility. This may compromise the ability of the group to orientate itself for optimal binding within a target protein.[120]

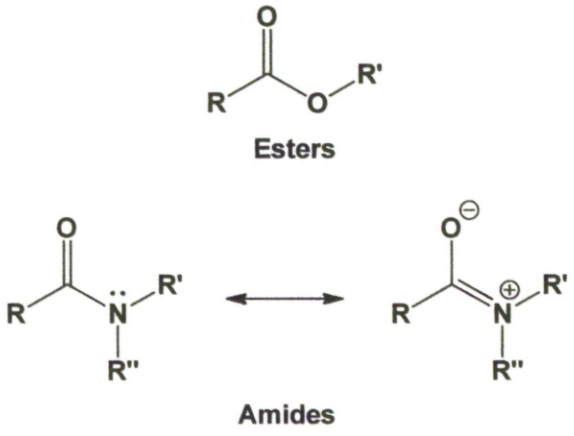

Figure 2.2: Displaying the difference in electron distribution between esters and amides.

In order to further our understanding of the structure-activity relationship, it was decided to test the tolerances of the 3-position by synthesising a number of analogues based on compound **4**.

2.4 Exploring the 3-position: Synthesis of 3rd Generation Inhibitors

In order to test the importance of the group at the 3-position, the obvious first step was to remove the functionality from that point on the ring altogether. A procedure was found in the literature to hydrolyse the ethyl ester of **4**, followed by decarboxylation of the resulting carboxylic acid to give **12** (Scheme 2.11).[114] This method worked well, generating the target compound in a greater than 85% yield following purification by chromatography.

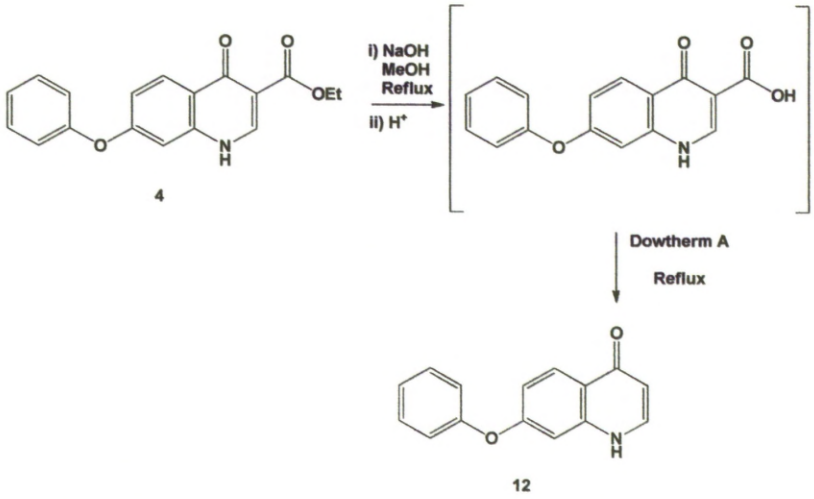

*Scheme 2.11: Reduction and decarboxylation of **4** to remove functionality from the 3-position.*[114]

2.4.1 Synthesis of a 3-Nitrile Analogue

It was postulated that simply by exchanging diethyl ethoxymethylenemalonate **1** with ethyl(ethoxymethylene)cyanoacetate **13** in the Gould-Jacobs procedure, a 3-nitrile analogue could be easily produced. This proved to be less simple in practice, with **13** being much slower to react with 3-phenoxyaniline **2** and giving a far less clean reaction than had previously been observed for the solvent free reactions carried out during the synthesis of the esters. A search of the literature and a certain amount of trial and error eventually led to the discovery that using a small amount of ethanol (~1 mL/mmol) to dissolve the reactants, rather than carrying out the reaction solvent free, and using a slightly elevated reaction temperature (120 °C *versus* 100 °C) gave the ethyl 2-cyano-3-((3-phenoxyphenyl)amino)acrylate product **14** (Scheme 2.12) in near quantitative yields as a mixture of *E* and *Z*

isomers (Figure 2.3).[112] Unlike the previous analogues, it was not possible to take the intermediate through to the thermal cyclization step crude; instead it was properly isolated, washed and dried.

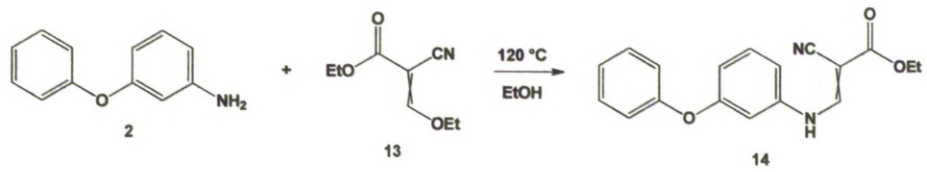

*Scheme 2.12: Synthesis of ethyl 2-cyano-3-((3-phenoxyphenyl)amino)acrylate **14**.*

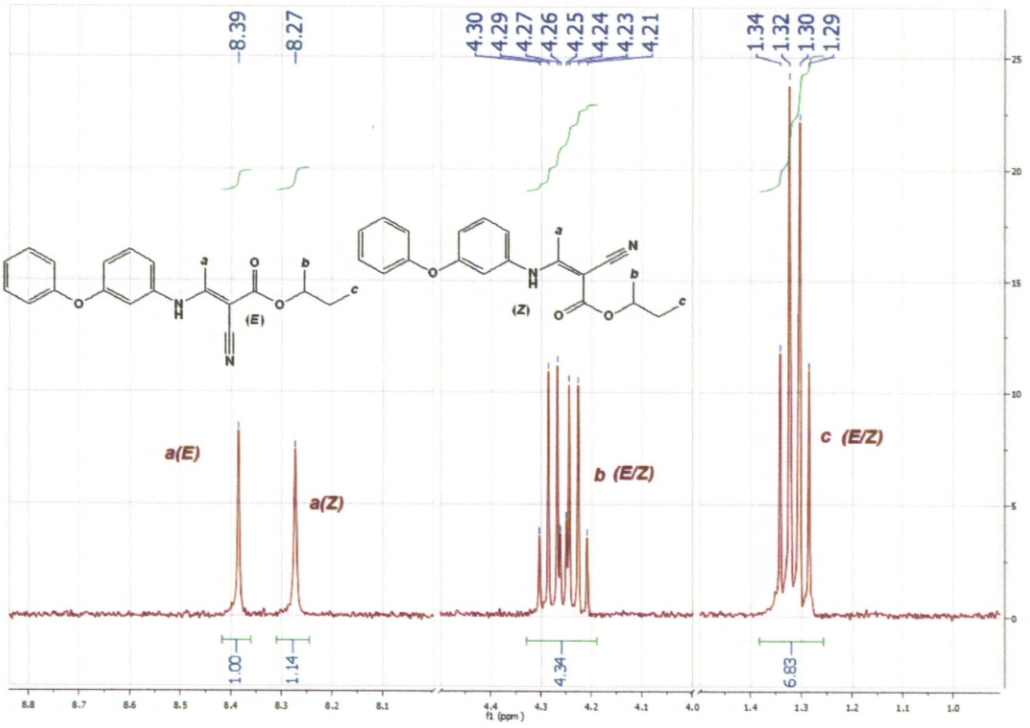

*Figure 2.3 – ^{1}H NMR expansion of **14** showing E/Z isomerism of the enamine proton **a** and the ethyl ester protons **b** and **c**.*

Cyclisation of **14** also proved more difficult compared with the previous ester syntheses. Rather than the 1 – 2 hour reaction times found to be adequate for the ester analogues, it was necessary to maintain temperatures of 240 °C overnight to obtain reasonable yields of the desired product. This reduced reaction rate is presumably due to the requirement of the *E*-isomer of **14** to rearrange before it can successfully ring close to give **15** (Scheme 2.13). Attempts to increase the reaction rate by further elevating the temperature resulted in the formation of degradation products.

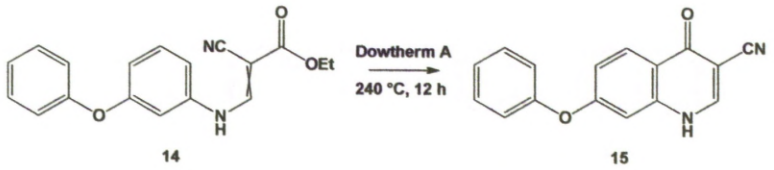

14 15

*Scheme 2.13: Cyclisation to give 4-oxo-7-phenoxy-1,4-dihydroquinoline-3-carbonitrile **15**.*

2.4.2 Pyrazoloquinolinone Derivative

The discovery of a paper by A. Carotti *et al.* while investigating potential bioisosteres, inspired the synthesis of a tricyclic derivative, 7-phenoxy-2*H*-pyrazolo[4,3-*c*]quinolin-3(5*H*)-one **16**.[121] Bioisosteres are defined as chemical groups that maintain or enhance the biological properties of a compound, such as their metabolic profile, without making significant changes to the physiochemical properties.[122] A classic example is the replacement of hydrogen with fluorine on aromatic rings to reduce metabolism by cytochrome P450 enzymes.

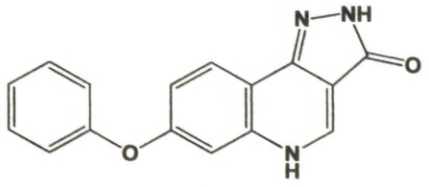

16

The pyrazoloquinolone structure was of interest because the pyrazole ring is a bioisostere of the β-ketoester structure of the initial hit molecules. The pyrazole introduces an additional hydrogen bond donor without much increase in steric bulk. We were also interested to see the effect of the extension of the conjugation system and the reduced flexibility at the 3-position. **16** Was synthesised from **4** in two straightforward steps.[121] Reflux conditions in phosphoryl chloride displaced the carbonyl oxygen of the quinolone to give ethyl 4-chloro-7-phenoxy-1,4-dihydroquinoline-3-carboxylate **17** in high yields (Scheme 2.14).

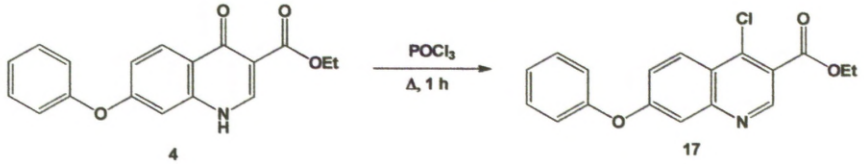

4 17

*Scheme 2.14: Reaction of **4** with phosphoryl chloride to give ethyl 4-chloro-7-phenoxy-1,4-dihydroquinoline-3-carboxylate **17**.*

The 4-chloro compound **17** was then reacted with hydrazine, which displaces the chloride before attacking the ester to ring close forming a pyrazolone ring (Scheme 2.15). Provided the reaction conditions were kept reasonably anhydrous, using dry solvents and an N_2 atmosphere, both reaction steps were almost quantitative, with yields of 91.6% and 97.4% respectively.

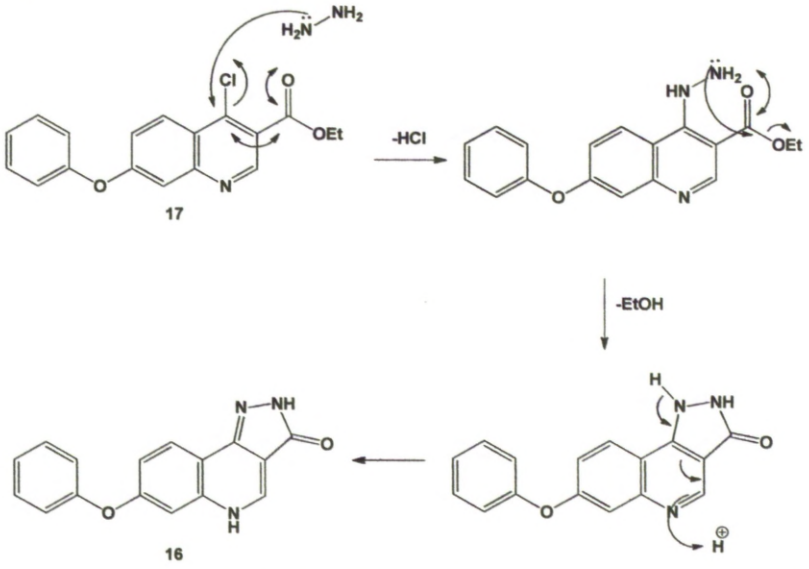

*Scheme 2.15: Reaction of **17** with hydrazine to give the tricyclic target **16** in high yield.*[121]

2.4.3 Transesterification

In addition to generating new functionalities at the 3-position, we also experimented with different esters to determine whether steric bulk at the 3-position was of significance in the binding conformation. Using a titanium (IV) isopropoxide catalysed transesterification procedure found in the literature, a number different alcohols were reacted with **4**, with varying degrees of success.[123] Isopropanol, cyclopentanol and cyclohexanol were all used successfully to give compounds **18** to **20** respectively (Scheme 2.16). However, yields for the synthesis of compound **18** were reduced by the difficulty inherent in distinguishing it from the starting material **4** when purifying by column chromatography.

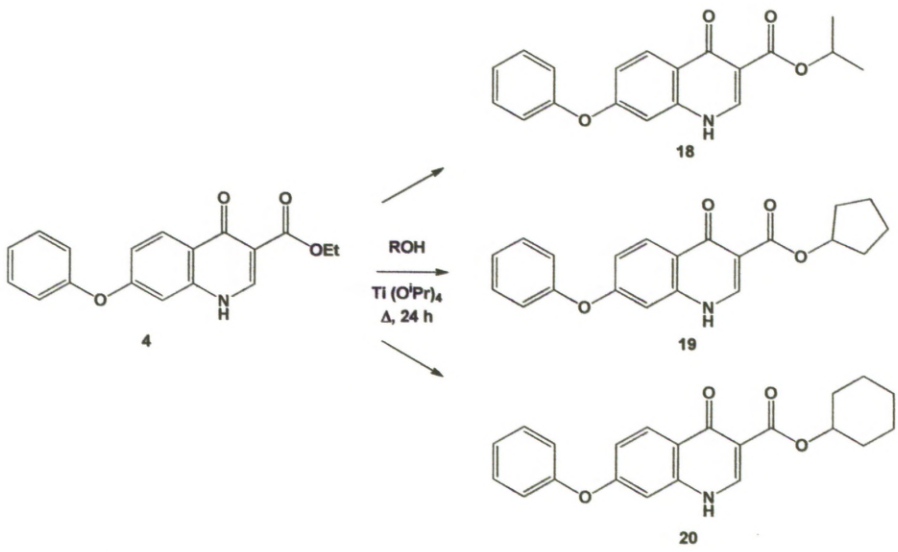

*Scheme 2.16: Successful transesterification reactions of **4** with secondary alcohols.*[123]

Attempts to carry out the same reaction with a number of other alcohols were less successful. In particular, the reaction of **4** with 2-(pyrrolidin-1-yl)ethanol, (intended to give an ester analogue of the most potent amide **10**), proved unsuccessful despite a number of attempts with various reaction conditions. We postulate that this was due to destruction of the product by the titanium derived Lewis acid present in the reaction mixture through an elimination pathway (Scheme 2.17), but have no evidence to support this hypothesis beyond the continued failure to obtain the desired product.

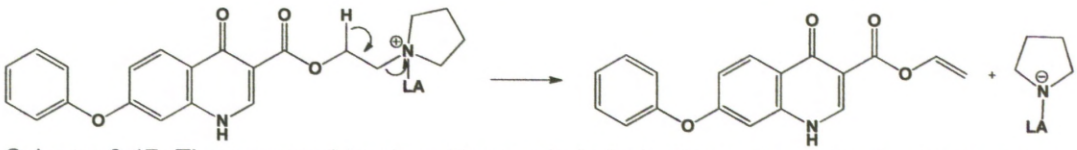

Scheme 2.17: The proposed Lewis acid promoted elimination pathway leading to the failure to isolate the desired 2-(pyrrolidin-1-yl)ethyl target.

2.4.4 Analysing the 3rd Generation Inhibitors

Once synthesised, a selection of the novel quinolones were tested *in vitro* against 3D7 *P.falciparum* parasites for comparison with the original hits (Table 2.3).

Table 2.3: Results for the 3rd generation compounds

Compound	IC_{50} *versus* 3D7 parasites (nM)[a]	Isolated Yield (%)	CLogP by ALog PS2.1[c]
4	19.3	-	3.07 ± 0.40
6	5.30	-	4.07 ± 0.84
12	6725	88.4	2.72 ± 0.42
15	8103	87.9	2.84 ± 0.80
16	No activity at 1 μM	97.4	2.85 ± 0.73
18	8.45	32.4	3.42 ± 0.45
19	Not Tested[b]	68.6	3.77 ± 0.62
20	29.6	31.3	4.36 ± 0.67

[a] *Average value from at least 3 independent experiments.* [b] *Purity of isolated compound insufficient for biological testing.* [c] *http://www.vcclab.org/lab/alogps/*

The results from the 3rd generation of compounds support the observation that esters are the superior group in the 3-position, with both the decarboxylated compound **12** and nitrile analogue **15** demonstrating much reduced potency *in vitro*. Perhaps more significantly, the result for **18** reveals that a slight increase in the size of the ester group (ethyl to isopropyl) increases biological activity. Further increases in size are not well tolerated, with a drop in potency observed for the cyclohexyl ester **20**. However, this compound maintains higher potency than any of the amides of similar size, suggesting that the other properties of the functional group are also important.

2.5 Exploring the 7-position - Modifying the Linker

Having established that the preferred group in the 3-position is an ethyl or isopropyl ester, we turned our attention to the "tail" section of the compounds at the 7-position on the quinolone ring. As the channel leading to the Q_o active site is known to be lined with hydrophobic residues, we surmised that substitution of the phenoxy linker with a methylene group to give the corresponding benzyl compounds might improve activity. 3-Benzylaniline **21**

is commercially available and reacted easily with diethyl ethoxymethylenemalonate **1** to give ethyl 7-benzyl-4-oxo-1,4-dihydroquinoline-3-carboxylate **22** in good yield.

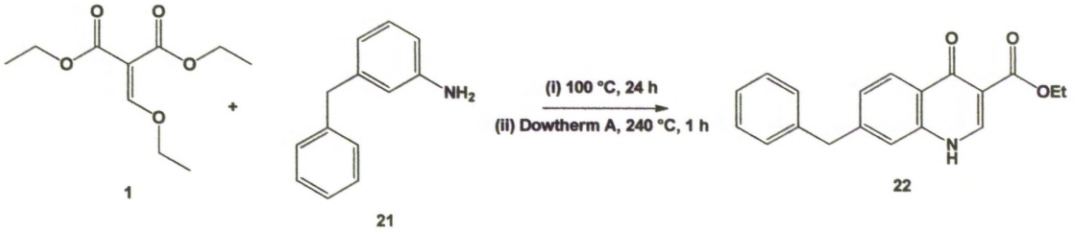

*Scheme2.18: Synthesis of **22** by the Gould-Jacobs method.*

2.5.1 Revisiting the Benzyloxy Linker

It had been observed during the biological testing that compound **6** is marginally more soluble than **4**, suggesting that in addition to increasing potency, the trifluoromethoxy group also improved solubility, despite raising the the ClogP of the compound. Therefore, an analogue of **5** with a trifluoromethoxy moiety on the aryl ring was synthesised in order to test the potency of the benzyloxy linker system. As with the synthesis of **6**, the desired aniline starting material was not commercially available. This compound was synthesised from 3-nitrophenol **7**, which was reacted with 4-trifluoromethoxy benzyl bromide **23** in the presence of base to yield 1-nitro-3-((4-(trifluoromethoxy)benzyl)oxy)benzene **24** (Scheme 2.19).

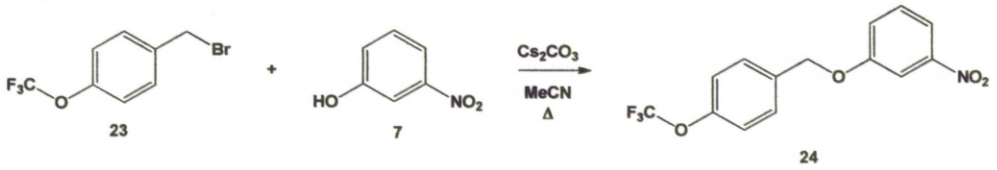

*Scheme 2.19: Synthesis of intermediate **24** from 3-nitrophenol **7**.*

The nitro group was then reduced to the primary amine using the same zinc-mediated method previously employed to give aniline compound **25** (Scheme 2.20).[118]

*Scheme 2.20: Zinc mediated reduction of nitro compound **24** to prepare aniline **25**.*

Reaction of **25** with **1** via the Gould-Jacobs protocol to give the desired product **26** (Scheme 2.21) was found to be lower yielding than for the earlier analogues, but gave a sufficient quantity of product for *in vitro* testing. Consequently, no further attempts were made at optimising the reaction.

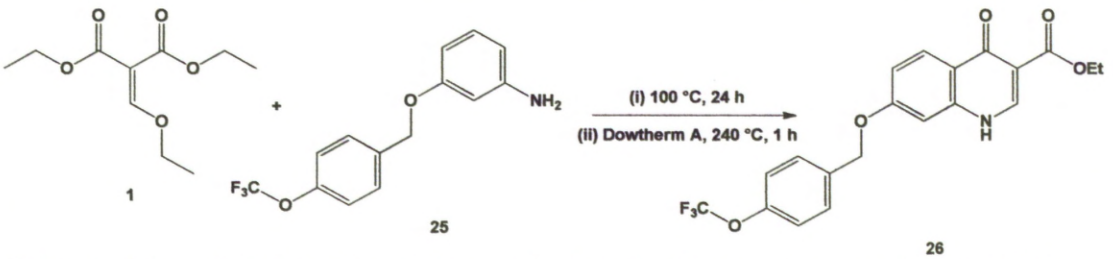

Scheme 2.21: Gould-Jacobs reaction of ***1*** *with* ***25*** *to give ethyl 4-oxo-7-((4-(trifluoromethoxy)benzyl)oxy)-1,4-dihydroquinoline-3-carboxylate* ***26****.*

2.5.2 Incorporating Heterocycles

Following the disappointing results from attempts to increase solubility *via* the use of amides at the 3-position, it was decided to try and increase solubility by incorporation of heterocycles into the "tail" portion of the compounds, allowing us to formulate salts. Unfortunately, this proved problematic and only two of the analogues attempted survived the harsh conditions of the Gould-Jacobs thermal cyclisation. The first analogue that was successfully produced was a piperazine containing compound, ethyl 7-(4-benzylpiperazin-1-yl)-4-oxo-1,4-dihydroquinoline-3-carboxylate **27**.

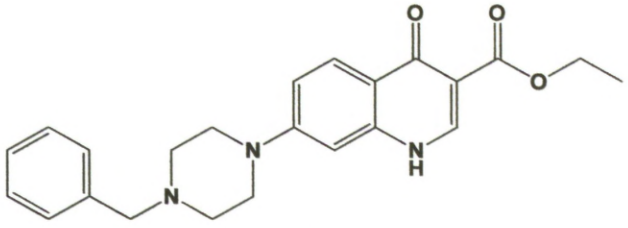

27

Synthesis began with reaction of 3-fluoronitrobenzene **28** with *N*-benzylpiperazine **29** in the presence of base, displacing fluoride to give 1-benzyl-4-(3-nitrophenyl)piperazine **30** (Scheme 2.22).[124]

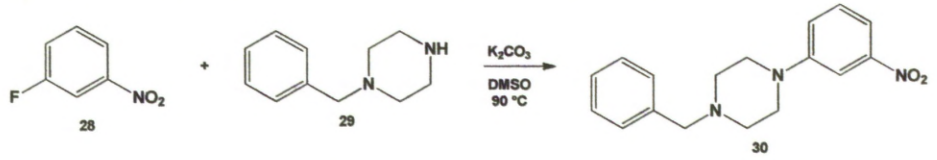

Scheme 2.22: Reaction of ***28*** *and* ***29*** *to give 1-benzyl-4-(3-nitrophenyl)piperazine* ***30****.*

This was followed by tin (II) chloride mediated reduction of the nitro group to the amine **31** (Scheme 2.23).[125] The tin procedure was utilised following the discovery that the zinc mediated method (employed in the synthesis of earlier analogues) was resulting in a partial cleavage of the benzyl group from the piperazine ring, resulting in a reduced yield and a difficult purification.

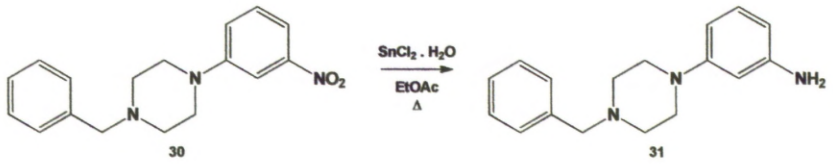

*Scheme 2.23: Tin (II) chloride mediated reduction of nitro compound **30** to yield aniline intermediate **31**.*

Reaction of **31** with diethyl ethoxymethylenemalonate **1** *via* the Gould-Jacobs procedure generated **27** in a moderate yield (Scheme 2.24). It was surprising to find that the solubility of the product was quite poor, and we were unable to successfully formulate either hydrochloride or citric acid salts of the compound that was stable in solution.

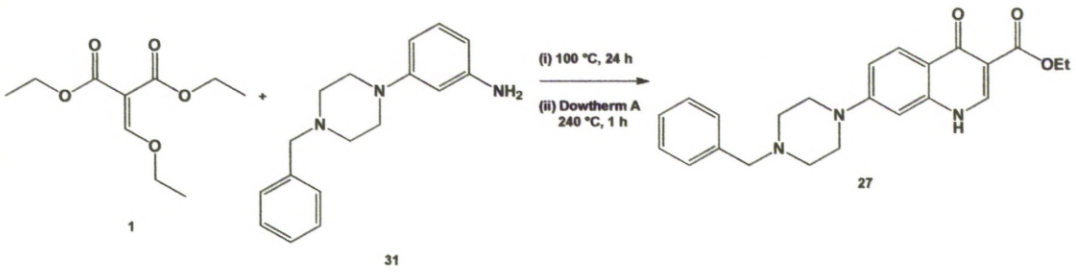

*Scheme 2.24: Using the Gould-Jacobs reaction of **1** with **31** to give quinolone target **27**.*

An analogue with a chlorine at the 4-position of the terminal phenyl ring was also attempted but decomposed during cyclisation. Resynthesis was not attempted as having found that incorporating heterocycles directly into the "tail" part of the compounds did not improve solubility, we instead targeted analogues with terminal heterocycles on flexible alkyl linkers, such as ethyl 7-(4-(2-morpholinoethoxy)phenyl)-4-oxo-1,4-dihydroquinoline-3-carboxylate (Figure 2.3).

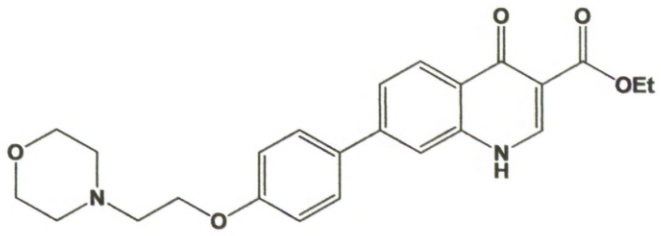

Figure 2.3: Terminal heterocyclic target ethyl 7-(4-(2-morpholinoethoxy)phenyl)-4-oxo-1,4-dihydroquinoline-3-carboxylate.

However, we were only partially successful in this aim, as the thermal cyclisation conditions again proved to be problematic. Instead of obtaining the desired 3-ethyl ester, only 7-(4-(2-morpholinoethoxy)phenyl)quinoline-4(1*H*)-one **32** was recovered in sufficient quantities for biological evaluation.

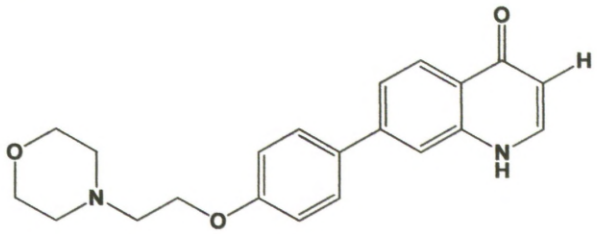

32

A key step in the synthesis was the Suzuki coupling of 3-bromonitrobenzene **33** with 4-methoxybenzene boronic acid **34**,[126] followed by boron tribromide demethylation of the methoxy group to give 3'-nitro-[1,1'-biphenyl]-4-ol **35** (Scheme 2.25).[127]

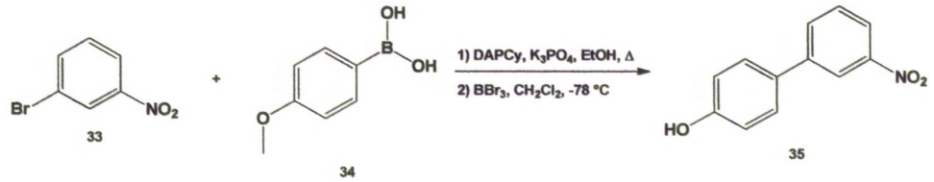

*Scheme 2.25: Synthesis of biphenyl intermediate **35**.*

Reaction of **35** with *N*-(2-chloroethyl)morpholine hydrochloride **36** gave 4-(2-((3'-nitro-[1,1'-biphenyl]-4-yl)oxy)ethyl)morpholine **37**. The nitro group was then successfully reduced by the tin (II) chloride-mediated procedure employed previously, to give the desired aniline compound 4'-(2-morpholinoethoxy)-[1,1'-biphenyl]-3-amine **38** (Scheme 2.26).

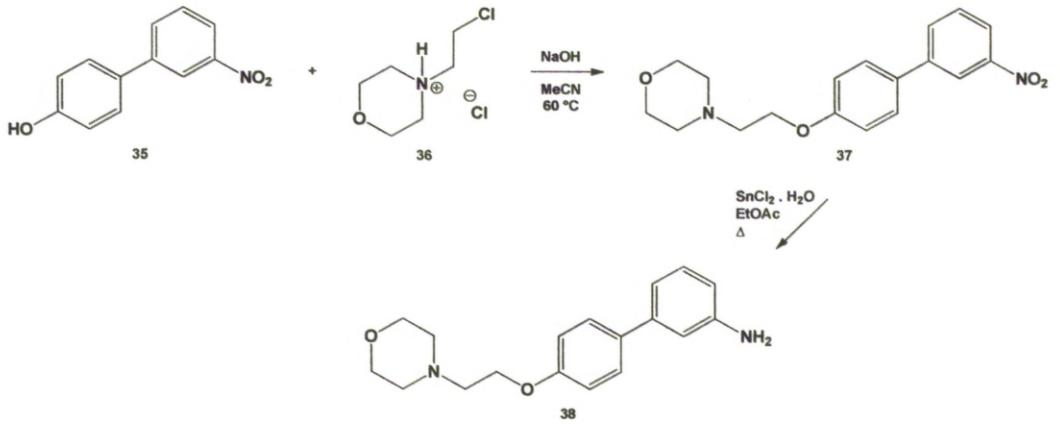

*Scheme 2.26: Synthesis of **38** from **35**.*

The Gould-Jacobs reaction of this compound with **1** failed to yield the desired ethyl ester in isolatable quantities over several attempts, although HPLC purification of the product mixture from one attempt did yield sufficient quantity of compound **32** for an *in vitro* test. It would appear that the target ester is unstable under the Gould-Jacobs conditions and the bulk of the isolated product had undergone decarboxylation. Additional analogues incorporating *N*-methyl and *N*-ethyl substituted piperazine in place of morpholine were attempted but repeatedly decomposed during the cyclisation step and so were abandoned.

2.5.3 Evaluation of 4th Generation Inhibitors

The four new compounds were submitted for testing and evaluated according to their performance *in vitro* compared to the initial hit compound (Table 2.4).

Table 2.4: Results for the 4th generation compounds;

Compound	IC_{50} *versus* 3D7 parasites (nM)[a]	Isolated Yield (%)	CLogP by ALog PS2.1[c]
22	4.57	57.4	3.36 ± 0.43
26	5.00	16.0	4.05 ± 0.82
27	No Data [b]	36.1	3.14 ± 0.77
32	1368	3.9	2.69 ± 0.75

[a] *Average value from at least 3 independent experiments.* [b] *Insufficient solubility for testing.*
[c] *http://www.vcclab.org/lab/alogps/*

Interestingly, the switch from an oxygen to a methylene linker between the aromatic rings of the "tail" (**22** *versus* **4**) resulted in a 4-fold increase in potency, presumably as a result of more favourable interactions between the

hydrophobic regions of the target protein and the carbon than for the more polar oxygen linker.

With the trifluoromethoxy group present, the benzyloxy linked compound **26** displayed similar levels of potency to the corresponding phenoxy compound **6**. However, solubility was still extremely poor, and the additional difficulty involved in the synthesis of compound **26** led us to discard this particular chemotype.

As mentioned previously, piperazine compound **27** proved surprisingly insoluble. In a similar manner to compound **5**, it was unable to be tested *in vitro*. Although salts were formulated, they were unstable and often precipitated out of solution unpredictably.

Compound **32** was more active than anticipated, considering it lacked the all important ester group functionality at the 3-position, suggesting that if a more reliable route to the intended target had been developed, the compound may have had potential.

2.6 Identification of the Lead?

From the initial synthesis of the hit compounds through the development of the subsequent generations, two observations stood out. The inclusion of a trifluoromethoxy moiety on the aryl "tail" resulted in an approximate 4-fold increase in potency (compound **4** *versus* **6**); and the switch from an oxygen linker to a methylene linker produced a similar 4-fold increase in potency (compound **4** *versus* **22**). The question therefore was, were these effects additive? If both these modifications were included in a single compound, ethyl 4-oxo-7-(4-(trifluoromethoxy)benzyl)-1,4-dihydroquinoline-3-carboxylate **39**, would we get a molecule with an even better profile?

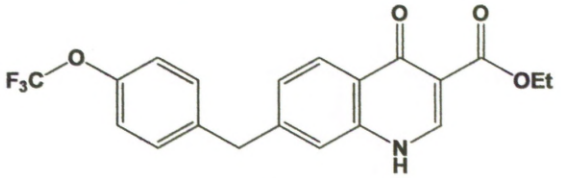

39

2.6.1 Synthesis of 3-(4-(trifluoromethoxy)benzyl)aniline

Synthesising 3-(4-(trifluoromethoxy)benzyl)aniline **40** was a relatively simple process, involving the palladium tetrakis(triphenylphosphine)-

catalysed Suzuki coupling of 4-(trifluoromethoxy) benzyl bromide **41** with 3-nitrophenylboronic acid **42**. This consistently gave 1-nitro-3-(4-(trifluoromethoxy)benzyl)benzene **43** in 76 – 89 % yields, following purification by column chromatography.(Scheme 2.27).

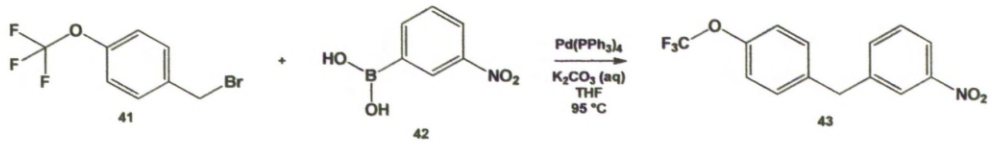

*Scheme 2.27: Suzuki coupling synthesis of 1-nitro-3-(4-(trifluoromethoxy)benzyl)benzene **43**.*

The nitro compound **43** was then reduced to give the desired aniline intermediate **40** in high yields(> 96%), using the same tin (II) chloride-mediated procedure previously used in the synthesis of the heterocycle containing compounds **27** and **32** (Scheme 2.28).

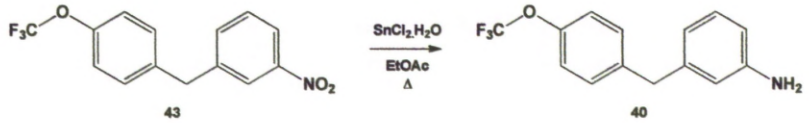

*Scheme 2.28: Tin (II) chloride-mediated reduction of **43** to key aniline intermediate **40**.*

2.6.2 Lead Compound Synthesis

For reasons that we have been unable to satisfactorily explain, difficulties became apparent in the latter stages of the synthesis. While the aniline compound **40** had been synthesised with relative ease, using it in the Gould-Jacobs quinolone synthesis proved surprisingly problematic. In the first attempt at carrying out the synthesis of **39**, the enamine intermediate **44** was taken through to the cyclisation step without purification, following evaporation of the volatile by-products (as had been done for most previous instances of this reaction step). However, instead of the solid product expected, the thermal cyclisation reaction of **44** returned a dark brown oil, which was comprised of an inseparable mixture of multiple components.

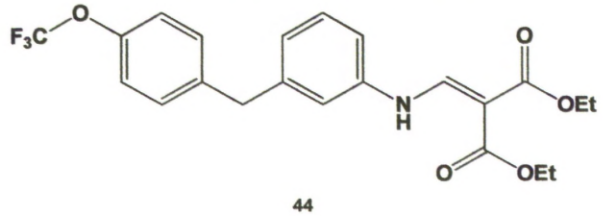

At the second attempt, diethyl 2-(((3-(4-(trifluoromethoxy) benzyl)phenyl)amino)methylene)malonate **44** was isolated and purified.

However, after the usual solvent free, overnight reaction, just 8% of the desired compound was isolated from the reaction mixture. Eventually, after small scale optimisation of various conditions, including longer reaction times, higher temperatures, dilution and a variety of work-up procedures, a method was found that consistently gave satisfactory yields. Dilution of the aniline **40** in ethanol, followed by overnight reaction at 100 °C and isolation of the product by reduced pressure removal of the volatile components rather than the precipitation from non-polar solvents employed previously, generated **44** in yields of up to 97%.

Further problems were encountered when the first attempt at cyclising the isolated, pure intermediate **44**, gave just a 6% yield of **39**. However, this was a sufficient quantity for an *in vitro* test, which gave promising results (Table 2.5). In subsequent synthetic runs, the yield of ethyl 4-oxo-7-(4-(trifluoromethoxy)benzyl)-1,4-dihydroquinoline-3-carboxylate **39** has been improved to just over 50% by careful monitoring of the reaction temperature. It has been found that while earlier analogues could tolerate a certain amount of variation in temperature between 240 – 250 °C with little consequence, **39** has a much smaller margin for error, degrading rapidly if reaction temperatures rose much above 240 °C.

*Table 2.5: In vitro results for compound **39** and the previous analogues contributing to its design.*

Compound	IC_{50} *versus* 3D7 parasites (nM)[a]	CLogP by ALog PS2.1[b]
4	19.3	3.07 ± 0.40
6	5.30	4.07 ± 0.84
22	4.57	3.36 ± 0.43
39	**0.46**	4.41 ± 0.79

[a] *Average value from at least 3 independent experiments.* [b] *http://www.vcclab.org/lab/alogps/*

2.7 Further Development of the Lead - Prodrugs

At 0.46 nM, compound **39** is the most potent quinolone antimalarial developed by the O'Neill group to date. However, despite its *in vitro* potency when the compound was tested orally, *in vivo* testing using mouse models infected with *P.berghei* revealed that the compound was much less active, with only a slight reduction of parasitaemia observed. This was attributed to

its poor solubility, leading to low absorption and consequently insufficient bioavailability to exert a curative effect on the parasites.

As our previous attempts to increase the solubility of these compounds by modification of the functional groups had led to the loss of biological activity, an alternative approach was attempted, namely the synthesis of prodrugs. Prodrugs are compounds which have additional functionality designed to increase the solubility of the active species, promoting increased absorption of the compound. Once absorbed, they can be easily metabolised to generate the active species in sufficient concentration to exert the desired effect.

Esterases are one of the most common enzyme classes and work by hydrolysing ester bonds to give an alcohol and a carboxylic acid.[6] It was surmised that the substitution of the quinolone carbonyl with a group that would be metabolised to give the 4-hydroxyquinoline (in turn tautomerising to give the active compound **39**), (Scheme 2.28), would increase *in vivo* activity.

Our initial attempts to synthesise a simple ethyl carbonate prodrug by reaction of **39** with ethyl chloroformate (following deprotonation with potassium *t*-butoxide) were frustrated by poor yields. Examination of the literature revealed a possible explanation; in 2007, while working on quinolone based antibacterial agents, Hammerschmidt *et al.* observed that at room temperature, ethyl and *t*-butyl carbonates of quinolone *N*-oxides would rearrange to their *N*-substituted isomers.[128] While our compounds are not *N*-oxides, and so are unable to rearrange in this fashion, this does suggest that the prodrug targets we were aiming for could be unstable enough to hydrolyse rapidly back to the starting material during isolation explaining the apparent lack of reaction we were observing. During the same study in which they observed the rearrangement of carbonate quinolones, Hammerschmidt *et al.* also noted that the related carbamates were more stable, and did not rearrange in this fashion.[128]

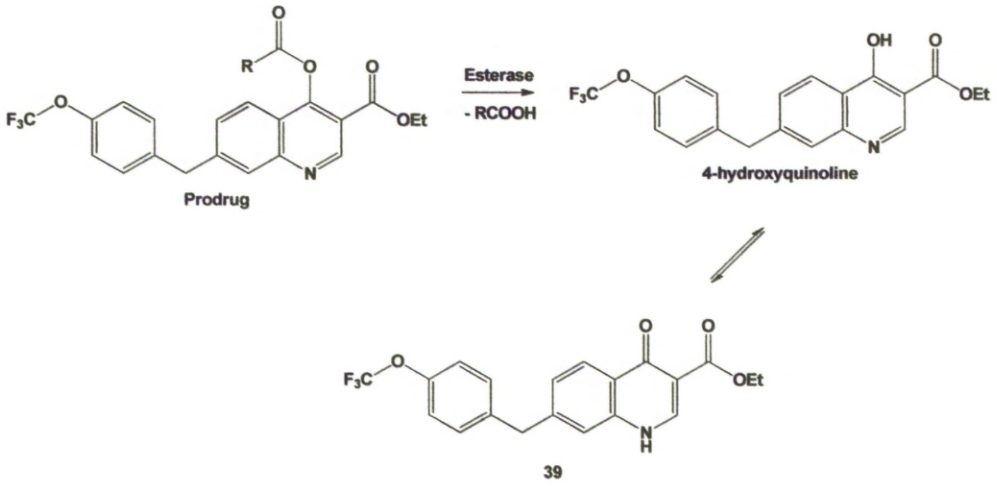

*Scheme 2.28: Esterase activation of a compound **39** based prodrug.*

Therefore, compounds **6** and **39** were reacted with *N*-morpholine carbonyl chloride **45** according to the literature conditions to yield prodrugs **46** and **47** respectively, in modest but adequate yields (Scheme 2.29). *In vivo* testing of both prodrugs has given very promising results for further development, with a parasite clearance of 45.8% at 30 mg/kg oral dose for **46** and **47** achieving a rate of 57.7% from a daily 20 mg/kg oral dose.

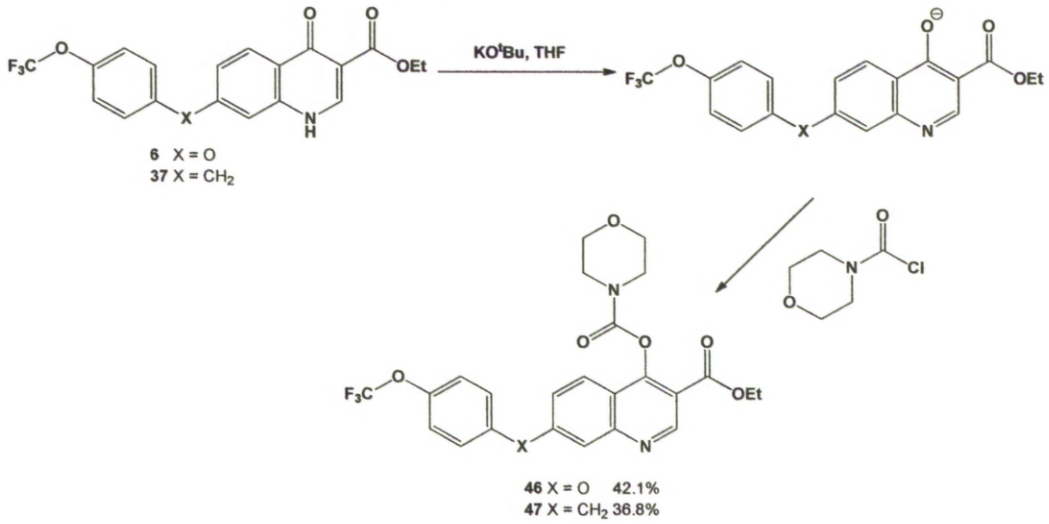

*Scheme 2.29: Synthesis of N-morpholine carbamate prodrugs of compounds **6** and **39**.*

2.8 Confirmation of bc_1 Activity: Cross-Resistance and Selectivity Testing

In addition to testing against 3D7 "wild-type" parasite strains of *P.falciparum*, which are not resistant to any current antimalarial agents, a number of the synthesised compounds were also tested *in vitro* against the atovaquone-resistant TM90C2B parasite strain to assess the compounds for the presence of any cross resistance (Table 2.6).[42]

Table 2.6: Atovaquone cross resistance results for a cross section of the synthesised library.

Compound	IC_{50} *versus* 3D7 parasites (nM)[a]	IC_{50} *versus* TM90C2B parasites (nM)[a]
6	5.30	488
10	350	442
15	8103	No activity at 1 μM
18	8.45	No activity at 1 μM
20	29.6	No activity at 1 μM
26	5.00	No activity at 1 μM

[a] *Average value from at least 3 independent experiments.*

While these results were discouraging in that the tested compounds clearly have not avoided the issues that result in atovaquone resistance, the very fact that the library demonstrates cross resistance with atovaquone indicates that the compounds produced are indeed bc_1 inhibitors. The result for the trifluoromethoxy substituted ethyl ester compound **6** is encouraging. Although a 92 fold drop in potency is observed, this is a distinct improvement over the 6000-fold drop in potency observed for atovaquone in the same parasite strain. The result for compound **10**, the ethyl-*N*-pyrollidine amide is unusual and may indicate that this compound has a mode of action other than the intended bc_1 inhibition.

To further confirm that the compounds were indeed targeting the intended active site, a selected group of compounds were tested against isolated samples of *P.falciparum* bc_1 protein in enzyme inhibition studies (in addition to the whole cell parasite growth inhibition assays used to generate the *in vitro* test data for all the synthesised compounds) (Table 2.7).

Table 2.7: Enzyme inhibition results confirming bc_1 activity.

Code	IC_{50} *versus* 3D7 parasites (nM)[a]	EC_{50} *versus* parasite bc_1 isolates (nM)[a]
6	5.30	141
22	4.57	227
39	0.46	1.3

[a] *Average value from at least 3 independent experiments.*

These results clearly show that we have been successful in designing bc_1 inhibitors with good activity against the desired target. Having confirmed this, it was important to establish that the developed compounds were selective

for parasite bc_1 over the equivalent mammalian protein. The standard check for bc_1 selectivity is testing against bc_1 protein isolated from bovine cardiac tissue. Although it differs very slightly from human bc_1 protein, the amino acid sequence for the Q_o binding region of both cytochrome *b* and the ISP segment are near identical.[78] Therefore, a selection of analogues with the highest *in vitro* potencies were tested against isolated bovine bc_1 protein samples (Table 2.8).

Table 2.8: Results of selectivity testing against bovine bc_1 for the most potent analogues versus P.falciparum in vitro.

Compound	EC_{50} *versus* 3D7 isolates (nM)[a]	EC_{50} *versus* bovine bc_1 isolates (nM)[a]	Selectivity Factor
6	141	200	1.4
22	227	483	2.1
39	1.3	17.7	13.6

[a] *Average value from at least 3 independent experiments.*

Unfortunately, as the results show, the compounds demonstrate only a low degree of selectivity for the parasite protein over mammalian bc_1. The lead compound **39** demonstrated the highest selectivity of the tested compounds with a selectivity factor of over 10-fold, however this level of selectivity is nearly half that of atovaquone, which has a therapeutic index of 24-fold.[78]

In addition to the test results shown above, two other analogues were tested *in vitro* against bovine bc_1 protein isolates but not against the parasite protein as the *P.falciparum* protein is difficult to isolate and its availability consequently highly limited.

Table 2.9: Results of testing against bovine bc_1 protein isolates in vitro.

Compound	EC_{50} *versus* bovine bc_1 isolates (nM)[a]	IC_{50} *versus* 3D7 parasites (nM)[a]
18	3220	8.45
26	6470	5.00

[a] *Average value from at least 3 independent experiments.*

EC_{50} and IC_{50} values are not strictly comparable due to the different ways in which they are recorded; EC_{50} values are tested for against isolated proteins where as IC_{50} data indicates activity against whole cell parasites. However when it is considered that they are structurally very similar and have

comparable IC_{50} values to compound **6**, the high EC_{50} values *versus* mammalian bc_1 recorded for compounds **18** and **26** are significant and may indicate an increase in parasite selectivity. The result for the benzyloxy derivative **26** was of limited interest, as we had previously discounted this structure for further development due to its very poor solubility. The result for the isopropyl ester **18** was of much more interest however, as it appears to indicate that a very slight change in the ester group at the 3-position may be sufficient to significantly increase selectivity.

2.9 Increasing the Selectivity of the Lead

Following the result for compound **18** an additional analogue was designed. Using the same titanium (IV) isopropoxide mediated method as employed previously for the synthesis of esters **18**, **19**, and **20**, a small quantity of the lead compound **39** was reacted with isopropanol to give the isopropyl ester analogue **48** (Scheme 2.30).[123]

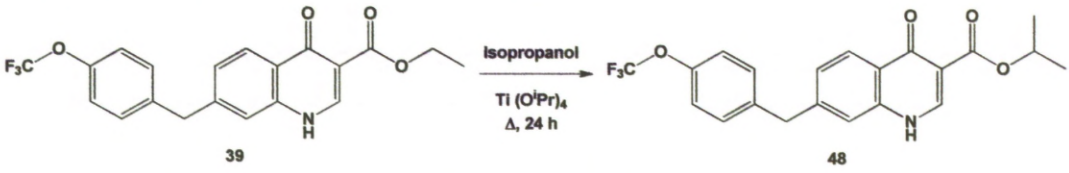

*Scheme 2.30: Lewis acid-catalysed transesterification of **39** to yield **48**.*

At the time of writing, selectivity analysis has not been carried out for compound **48**, however preliminary *in vitro* results *versus* 3D7 parasites appear promising, with an IC_{50} reported at 0.98 nM.

2.10 Summary

A small but significant library of quinolone-based compounds have been developed and demonstrated to have activity at the bc_1 protein of *P.falciparum* malaria parasites.[129] It has been shown that while the most active compounds are compromised by poor solubility, it is possible to formulate carbamate prodrugs with good activity *in vivo*. While selectivity over mammalian bc_1 is currently relatively low, progress has been made towards potentially increasing selectivity for the parasite target. At present the problem of atovaquone cross resistance has not been completely resolved, but resistance is reduced relative to atovaquone itself.

In order to better understand the observed structure-activity relationships, and to guide any further development of these compounds, the synthesised library has been modelled by *in silico* docking with the crystal structure of yeast bc_1.

2.11 Experimental

Commercially available starting materials were sourced from Sigma-Aldrich, Alfa Aesar, Acros Organics or Apollo Scientific Ltd. and used without additional purification. Solvents were obtained from either Fisher Scientific or VWR and used without purification unless otherwise stated.

Flash column chromatography purification was carried out using silica gel (particle size 40-63 μm), sourced from Sigma-Aldrich and thin layer chromatography (TLC) was carried out using Merck aluminium backed sheets 20 x 20 cm Silica gel 60 F_{254}. TLC plates were visualised using an ultraviolet lamp (254 nm).

Analysis

^{1}H NMR spectra were recorded using a Bruker Avance 400 (400 MHz) machine; ^{13}C spectra were recorded on the same machine (100 MHz). Chemical shifts (δ) are recorded in ppm relative to an internal tetramethylsilane standard. Deuterated solvents were supplied by Sigma-Aldrich and Cambridge Isotope Laboratories and were used without additional purification. ^{1}H spectra multiplicities are recorded as singlet (s), broad singlet (bs), doublet (d), triplet (t), quartet (q), doublet of doublets (dd), doublet of triplets (dt) or multiplet (m), coupling constant *J* values are given in Hz where appropriate.

High resolution mass spectroscopy (HRMS) was carried out by Dr. A. Mills and Miss M. McCarron via electrospray ionisation (EI) using a Micromass LCT Mass Spectrometer. Samples were injected as methanol solutions using a direct infusion syringe pump.

Elemental analysis (CHN) was performed by Mr. S. Apter and Mrs. J. Ellis of this department. Melting points and decomposition temperatures, where reported, were identified using a Gallenkamp melting point apparatus and are reported uncorrected in °C.

General Method A: Synthesis of enamine intermediates

The appropriate aniline (1 eq.) was dissolved in diethyl ethoxymethylenemalonate **1** (1 eq.). The mixture was heated to 100 °C and stirred overnight. The still warm solution was poured into petroleum ether (50 mL) and cooled in an ice/acetone bath resulting in a precipitate that was collected by filtration, washed with cold petroleum ether and dried under vacuum.

Diethyl 2-(((3-phenoxyphenyl)amino)methylene)malonate

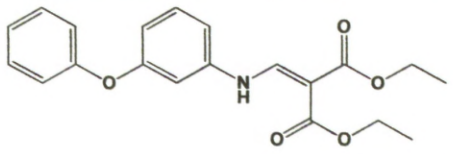

Synthesised according to general method A to give an off-white solid.

(4.82 g, yield 99.0%)

Melting point: 50 – 53 °C

^{1}H NMR (MeOH-d4) δ 8.48 (s, 1H), 7.39 – 7.33 (m, 3H), 7.18 – 7.14 (m, 1H), 7.06 – 7.03 (m, 2H), 6.99 – 6.97 (dd, 1H, *J* = 8.1, 2.1), 6.88 –6.87 (t, 1H, *J* = 2.2), 6.77 – 6.74 (dd, 1H, *J* = 8.2, 2.2), 4.30 – 4.25 (q, $OC\underline{H}_2CH_3$, *J* = 7.1), 4.22 – 4.17 (q, $OC\underline{H}_2CH_3$, *J* = 7.0), 1.34 – 1.30 (t, $OCH_2C\underline{H}_3$, *J* = 7.0), 1.32 – 1.28 (t, $OCH_2C\underline{H}_3$, *J* = 7.1);

^{13}C NMR δ 170 (C=O), 168 (C=O), 161, 158, 153, 143, 133, 131 (2C), 125, 121 (2C), 116, 113, 109, 95, 62 (2C), 15 (2C);

HRMS: $[M+H]^+$ $C_{20}H_{22}NO_5$ requires 356.15 found 356.15;

CHN for $C_{20}H_{21}NO_5$ requires C 67.59 H 5.96 N 3.94 found C 67.68 H 5.99 N 3.88

Diethyl 2-(((3-(benzyloxy)phenyl)amino)methylene)malonate

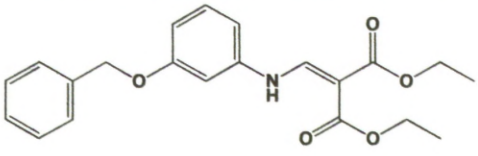

Synthesised according to general method A to give an off-white solid.

(4.39 g, yield 92.2%)

^{1}H NMR (MeOH-d4) δ 8.50 (s, 1H), 7.46 – 7.27 (m, 5H), 6.86 – 6.85 (t, 1H, *J* = 2.2), 6.83 – 6.79 (m, 2H), 4.88 (s, 2H), 4.31 – 4.25 (q, $OC\underline{H}_2CH_3$, *J* = 7.1), 4.23 – 4.18 (q, $OC\underline{H}_2CH_3$, *J* = 7.1), 1.36 – 1.32 (t, $OCH_2C\underline{H}_3$, *J* = 7.1), 1.35 – 1.31 (t, $OCH_2C\underline{H}_3$, *J* = 7.1);

HRMS: $[M+H]^+$ $C_{21}H_{24}NO_5$ requires 369.16 found 440.13;

CHN for $C_{21}H_{23}NO_5$ requires C 68.28 H 6.28 N 3.79 found C 56.05 H 4.62 N 3.14.

General Method B: Thermal cyclisation of quinolones

The appropriate diethyl malonate enamine intermediate (10 mmol) was added to boiling Dowtherm A® (50 mL) and refluxed for 1 hour. The solution was cooled to room temperature and diluted with n-hexane (20 mL). The resulting precipitate was collected by filtration, washed with ethyl acetate and pulled dry. Reprecipitation from dimethylformamide using n-hexane gave the final compounds.

Ethyl 4-oxo-7-phenoxy-1,4-dihydroquinoline-3-carboxylate ***(4)***

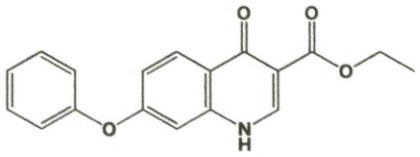

Synthesised according to general method B to yield a cream powder.

(2.61 g, yield 61.7%)

Melting point: > 250 °C

^{1}H NMR (DMSO-d6) δ 8.50 (s, 1H), 8.15 – 8.13 (d, 1H, *J* = 8.9), 7.51 – 7.48 ($^{app.}$t, 2H), 7.31 – 7.27 (t, 1H, *J* = 7.4), 7.21 – 7.19 (d, 2H, *J* = 7.7), 7.08 – 7.05 (dd, 1H, *J* = 8.9, 2.4), 6.97 (d, 1H, *J* = 2.4), 4.22 – 4.17 (q, $OC\underline{H}_2CH_3$, *J* = 7.0), 1.29 – 1.25 (t, $OCH_2C\underline{H}_3$, *J* = 7.0);

^{13}C NMR δ 168 (C=O), 160 (C=O), 154, 145, 140, 136, 131 (2C), 128, 125,123, 121 (2C), 116, 104, 60, 15;

HRMS: $[M+H]^+$ $C_{18}H_{16}NO_4$ requires 310.10 found 310.11;

CHN for $C_{18}H_{15}NO_4$ requires C 69.89 H 4.89 N 4.53 found C 69.74 H 4.75 N 4.44.

Ethyl 7-(benzyloxy)-4-oxo-1,4-dihydroquinoline-3-carboxylate ***(5)***

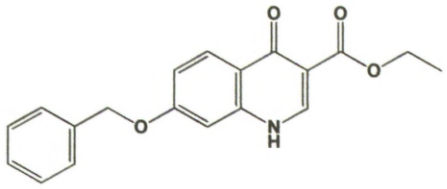

Synthesised according to general method B to yield a white solid.

(2.56 g, yield 66.7%)

Melting point: > 250 °C

^{1}H and ^{13}C NMR data not obtained due to insolubility of compound in all available solvents;

HRMS $[M+H]^{+}$ $C_{19}H_{18}NO_4$ requires 324.1236, found 324.1238;

CHN for $C_{19}H_{17}F_3NO_4$ requires C 70.58 H 5.30 N 4.33 found C 70.34 H 5.35 N 4.29.

Synthesis of 1-nitro-3-(4-(trifluoromethoxy)phenoxy)benzene ***(9)***

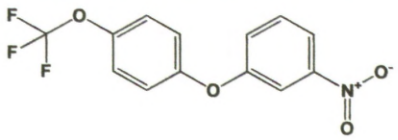

3-Nitrophenol **7** (1.393 g, 10.01 mmol), caesium carbonate (1.639 g, 5.03 mmol) and *N,N*-dimethylglycine (308 mg, 2.99 mmol) were dissolved in 1,4-dioxane (4 mL). Copper (I) iodide (208 mg, 1.09 mmol) and 4-(trifluoromethoxy)iodobenzene **8** (0.31 mL, 2.0 mmol) were added and the reaction mixture heated to ~100 °C with vigorous stirring under nitrogen. When no iodobenzene was visible by TLC (10% ethyl acetate/*n*-hexane) the reaction mixture was cooled and poured into aqueous sodium hydroxide (2 M, 25 mL). The aqueous mixture extracted with dichloromethane (3 x 25 mL) and ethyl acetate (2 x 30 mL). The combined organic extracts were dried over sodium sulphate and concentrated under reduced pressure. Purification by flash column chromatography (Silica gel, 2% Ethyl acetate/petroleum ether) gave **9** as a yellow oil.

(348 mg, yield 58.1%)

^{1}H NMR (Acetone-d6) δ 8.05 – 8.03 (dd, 1H, J = 7.7, 1.6), 7.83 – 7.82 (t, 1H, J = 2.3), 7.74 – 7.70 (t, 1H, J = 8.2), 7.53 – 7.50 (dd, 1H, J = 8.2, 2.4), 7.46 – 7.43 (m, 2H), 7.29 – 7.26 (dt, 2H, J = 9.1, 2.4);

^{13}C NMR δ 159, 156, 151, 147, 132, 126, 124, 123, 122, 121, 119, 118, 114;

HRMS: $[M+Na]^+$ $C_{13}H_8F_3NO_4Na$ requires 322.03 found 322.03;
CHN for $C_{13}H_8F_3NO_4$ requires C 52.19 H 2.70 N 4.68 found C 52.06 H 2.69 N 4.71.

*Synthesis of 3-(4-(trifluoromethoxy)phenoxy)aniline **(10)***

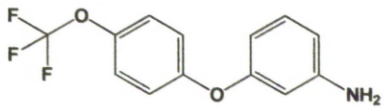

9 (2.80 g, 9.36 mmol) and zinc powder (20.2 g, 0.3 mol) were suspended in ethanol (50 mL). A solution of calcium chloride (760 mg, 6.85 mmol) in water (1.0 mL) was added and the mixture heated to reflux with vigorous stirring. When TLC (10% ethyl acetate/petroleum ether) showed complete conversion the reaction mixture was cooled and filtered to remove the zinc. Solvents were evaporated and the residue purified by flash column chromatography (2% ethyl acetate/petroleum ether) to give **10** as an orange oil.

(2.31 g, yield 91.8%)

^{1}H NMR (Acetone-d6) δ 7.32 – 7.31 (m, 2H), 7.09 – 7.05 (m, 3H), 6.50 – 6.47 (m, 1H), 6.36 – 6.34 (t, 1H, *J* = 2.3), 6.26 – 6.23 (m, 1H), 4.87 (bs, NH_2);
^{13}C NMR δ 159, 158, 151, 145, 132 (2C), 124 (2C), 121 (2C), 112, 110, 107;
HRMS: $[M+H]^+$ $C_{13}H_{11}F_3NO_2$ requires 270.07 found 270.07;
CHN for $C_{13}H_{10}F_3NO_2$ requires C 58.00 H 3.74 N 5.20 found C 58.05 H 3.76 N 5.18.

Diethyl 2-(((3-(4-(trifluoromethoxy)phenoxy)phenyl)amino)methylene) malonate

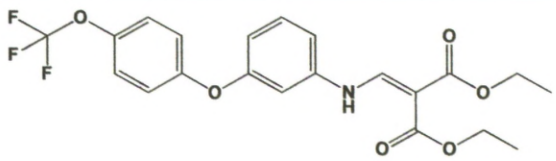

Synthesised from **10** according to general method A to yield off-white crystals.

(4.79 g, yield 89.9%)

^{1}H NMR (MeOH-d4) δ 8.47 (s, 1H), 7.41 – 7.37 (t, 1H, *J* = 8.2), 7.31 – 7.28 (m, 2H), 7.13 – 7.10 (dt, 2H, *J* = 9.1, 2.2), 7.04 – 7.01 (dd, 1H, *J* = 8.0, 2.2), 6.95 – 6.94 (t, 1H, *J* = 2.2), 6.80 – 6.77 (dd, 1H, *J* = 8.2, 2.2), 4.30 – 4.24 (q,

OCH_2CH_3, J = 7.2), 4.23 – 4.17 (q, OCH_2CH_3, J = 7.1), 1.34 – 1.30 (t, OCH_2CH_3, J = 7.1), 1.32 – 1.28 (t, OCH_2CH_3, J = 7.2);

^{13}C NMR δ 170 (C=O), 168 (C=O), 160, 157, 153, 143, 133, 124 (2C), 122 (2C), 116, 114, 109, 101, 95, 62 (2C), 15 (2C);

HRMS: $[M+H]^+$ $C_{21}H_{21}F_3NO_6$ requires 440.13 found 440.13;

CHN for $C_{21}H_{20}F_3NO_6$ requires C 57.40 H 4.59 N 3.19 found C 56.05 H 4.62 N 3.14.

Ethyl 4-oxo-7-(4-(trifluoromethoxy)phenoxy)-1,4-dihydroquinoline-3-carboxylate ***(6)***

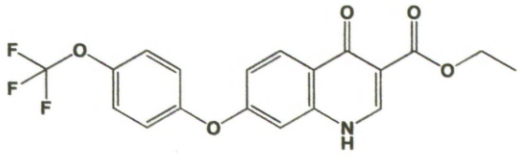

Synthesised according to general method B to yield a beige solid.

(3.39 g, yield 79.8%)

Melting point: > 250 °C

^1H NMR (DMSO-d6) δ 12.13 (bs, NH), 8.73 (s, 1H), 8.36 (d, 1H, J = 8.9), 7.72 – 7.69 (d, 2H, J = 8.8), 7.57 – 7.52 (dt, 2H, J = 9.0, 3.6), 7.35 – 7.31 (dd, 1H, J = 8.9, 2.4), 7.22 (d, 1H, J = 2.3), 4.45 – 4.36 (q, OCH_2CH_3, J = 7.1), 1.50 – 1.38 (t, OCH_2CH_3, J = 7.1);

^{13}C NMR δ 176 (C=O), 164, 151, 147, 145, 142, 137, 133 (2C), 129, 127,122, 119 (2C), 113, 107, 64, 13;

HRMS: $[M+H]^+$ $C_{19}H_{15}F_3NO_5$ requires 394.09 found 394.09;

CHN for $C_{19}H_{14}F_3NO_5$ requires C 58.02 H 3.59 N 3.56 found C 58.29 H 3.69 N 3.34.

General Method C: Amide Synthesis

Dowtherm A® (25 mL) was heated to boiling point. **6** (1 g, 2.5 mmol) was added followed by the appropriate amine (5 mmol). The temperature was reduced to ~ 120 °C and the reaction mixture left for 1 hour. Cooling to room temperature and dilution with n-hexane (20 mL) resulted in a precipitate that was collected by filtration. Purification by column chromatography (methanol/dichloromethane) gave the pure amides in moderate yields.

3-(Piperidine-1-carbonyl)-7-(4-(trifluoromethoxy)phenoxy)quinolin-4(1H)-one (7)

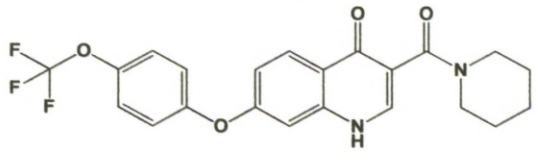

Synthesised according to general method C to yield an off-white powder.

Melting point: > 250 °C

(100 mg, yield 45.1%)

^{1}H NMR (DMSO-d6) δ 8.16 (d, 1H, *J* = 8.9), 8.04 (s, 1H), 7.51 – 7.49 (d, 2H, *J* = 8.8), 7.33 – 7.31 (dt, 2H, *J* = 9.0, 2.3), 7.11 – 7.08 (dd, 1H, *J* = 8.9, 2.4), 7.02 (d, 1H, *J* = 2.4), 3.56 (bs, 2H), 3.23 (bs, 2H), 1.60 (bs, 2H), 1.50 (bs, 4H);

^{13}C NMR δ 172 (C=O), 165, 160, 154, 141, 140, 128, 123 (2C), 122 (2C), 119, 115, 105, 48 (2C), 42 (2C), 26, 25, 24;

HRMS: $[M+Na]^+$ $C_{22}H_{19}F_3N_2O_4Na$ requires 455.1195, found 455.1196;

CHN for $C_{22}H_{19}F_3N_2O_4$ requires C 61.11 H 4.43 N 6.48 found C 60.64 H 4.22 N 6.21.

3-(4-Methylpiperazine-1-carbonyl)-7-(4-(trifluoromethoxy)phenoxy) quinolin-4(1H)-one ***(8)***

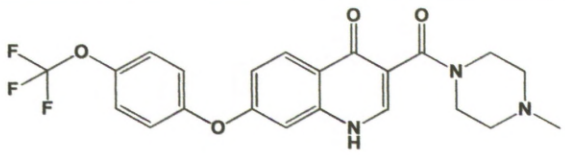

Synthesised according to general method C to yield a.

(309 mg, yield 55.4%)

Melting point: > 250 °C

^{1}H NMR (MeOH-d4) δ 8.27 (d, 1H, *J* = 9.0), 8.05 (s, 1H), 7.41 – 7.38 (d, 2H, *J* = 8.7), 7.27 – 7.24 (dt, 2H, *J* = 9.0, 2.1), 7.17 – 7.14 (dd, 1H, *J* = 9.0, 2.3), 6.97 (d, 1H, *J* = 2.3), 3.78 (bs, C$\underline{H_2}$), 3.44 (bs, C$\underline{H_2}$), 2.54 (bs, C$\underline{H_2}$), 2.49 (bs, C$\underline{H_2}$), 2.32 (s, NC$\underline{H_3}$);

^{13}C NMR δ 176, 169, 163, 156, 147, 143, 142, 130, 125 (2H), 123 (2H), 119, 118 (2H), 106 (2H), 101, 57, 55, 46;

HRMS: $[M+H]^+$ $C_{22}H_{21}F_3N_3O_4$ requires 448.1484, found 448.1474;

CHN for $C_{22}H_{20}F_3N_3O_4$ requires C 59.06 H 4.51 N 9.34 found C 58.81 H 4.45 N 9.35.

3-(4-Ethylpiperazine-1-carbonyl)-7-(4-(trifluoromethoxy)phenoxy) quinolin-4(1H)-one ***(9)***

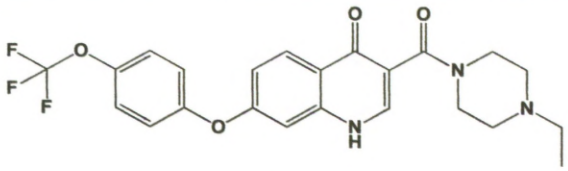

Synthesised according to general method C to yield a beige powder.

(201 mg, yield 87.8%)

Melting point: 246 - 248 °C (decomp.)

^{1}H NMR (DMSO-d6) δ 8.27 (d, 1H, *J* = 9.0), 8.05 (s, 1H), 7.40 – 7.38 (d, 2H, *J* = 8.8), 7.26 – 7.24 (dt, 2H, *J* = 9.1, 2.3), 7.17 – 7.14 (dd, 1H, *J* = 9.1, 2.3), 6.97 (d, 1H, *J* = 2.3), 3.79 (bs, C$\underline{H}_2$), 3.45 (bs, C$\underline{H}_2$), 2.58 (bs, C$\underline{H}_2$), 2.53 (bs, C$\underline{H}_2$), 2.51 – 2.46 (q, NC$\underline{H}_2$CH$_3$, *J* = 7.2), 1.14 – 1.10 (t, NCH$_2$C$\underline{H}_3$, *J* = 7.2);

^{13}C NMR δ 221, 176, 168, 163, 156, 142, 129, 125 (2C), 123 (2C), 119, 118, 106, 54, 53, 12;

HRMS: $[M+Na]^+$ $C_{23}H_{22}F_3N_3O_4Na$ requires 484.1460 found 484.1472;

CHN for $C_{23}H_{22}F_3N_3O_4$ requires C 59.87 H 4.81 N 9.11 found C 59.70 H 4.84 N 9.14.

4-Oxo-N-(2-(pyrrolidin-1-yl)ethyl)-7-(4-(trifluoromethoxy)phenoxy)-1,4-dihydroquinoline-3-carboxamide ***(10)***

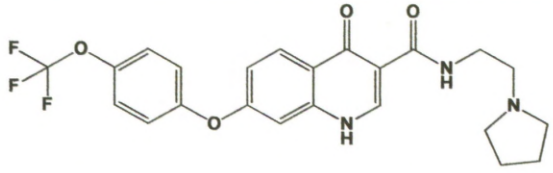

Synthesised according to general method C to yield a pale yellow solid.

(460 mg, yield 39.5%)

Melting point: 188 - 192 °C

^{1}H NMR (DMSO-d6) δ 8.69 (s, 1H), 8.34 (d, 1H, *J* = 9.0), 7.39 (d, 2H, *J* = 8.5), 7.38 – 7.25 (m, 2H), 7.19 – 7.17 (dd, 1H, *J* = 9.0, 2.4), 6.99 (d, 1H, *J* = 2.3), 3.64 – 3.61 (t, CH$_2$C$\underline{H}_2$, *J* = 6.7), 2.82 – 2.79 (t, CH$_2$C$\underline{H}_2$, *J* = 6.7), 2.73 – 2.69 (t, 4H, *J* = 6.6), 1.87 – 1.83 (m, 4H);

^{13}C NMR δ 175, 146, 133, 130, 125 (2C), 123 (2C), 118, 106, 101 (2C), 57, 55 (2C), 39, 24 (2C);

HRMS: $[M+H]^+$ $C_{23}H_{23}F_3N_3O_4$ requires 462.1641 found 462.1656;

CHN for $C_{23}H_{22}F_3N_3O_4$ requires C 59.87 H 4.81 N 9.11 found C 59.69 H 4.87 N 9.07.

*Synthesis of N-(5-(diethylamino)pentan-2-yl)-4-oxo-7-phenoxy-1,4-dihydroquinoline-3-carboxamide **(11)***

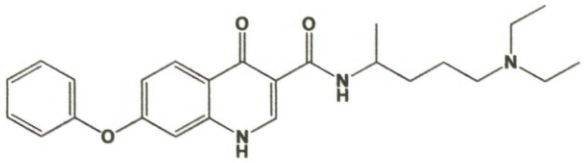

4 (252 mg, 0.82 mmol) was suspended in Dowtherm A (10 mL). 4-amino-1-diethylaminopentane (0.8 mL, 4.1 mmol) was added and the mixture heated to 200 °C for 2 hours. Resulting orange solution concentrated under reduced pressure to give an orange oil. Residue taken up in dichloromethane (30 mL) and extracted with aqueous HCl (2N, 2 x 40 mL). Aqueous extracts neutralised with saturated aqueous NaOH and extracted with ethyl acetate (2 x 70 mL). Organic extracts dried over magnesium sulphate and concentrated. Purification by flash column chromatography (1% methanol/dichloromethane) gave a hygroscopic yellow waxy solid.

(103 mg, yield 30.0%)

^1H NMR ($CDCl_3$) δ 10.24 – 10.22 (d, NH, J = 8.4), 8.66 (s, 1H), 8.29 – 8.27 (d, 1H, J = 9.0), 7.41 – 7.37 ($^{app.}$t, 2H), 7.22 – 7.18 (t, 1H, J = 7.5), 7.12 – 7.10 (d, 2H, J = 8.3), 7.07 – 7.05 (dd, 1H, J = 9.0, 2.2), 6.92 – 6.91 (d, 1H, J = 2.1), 4.20 – 4.07 (m, NC<u>H</u>CH_3), 2.55 – 2.50 (q, 2 NC<u>H</u>$_2$$CH_3$, J = 6.9), 2.45 – 2.36 (m, 2H), 1.52 (bs, 4H), 1.22 – 1.20 (d, NCHC<u>H</u>$_3$, J = 6.6), 0.98 – 0.95 (t, 2 NCH_2C<u>H</u>$_3$, J = 7.1);

^{13}C NMR δ 177 (C=O), 165, 162 (C=O), 155, 144, 141, 130 (2C), 129, 125, 122, 121 (2C), 117, 112, 105, 53, 47 (2C), 45, 35, 32, 22, 11 (2C);

HRMS: $[M+H]^+$ $C_{25}H_{32}N_3O_3$ requires 422.2444, found 422.2442;

CHN for $C_{25}H_{31}N_3O_3$ requires C 71.23 H 7.41 N 9.97, found C 68.67 H 7.38 N 8.17 (5% H_2O present).

*Synthesis of 7-phenoxyquinolin-4(1H)-one **(12)***

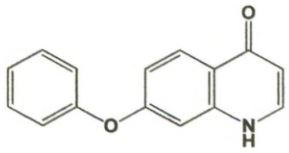

4 (299 mg, 0.97 mmol) was suspended in methanol (5 mL). NaOH soln. (10% aq., 7.5 mL) was added and the mixture heated at 100 °C for 1 hour. The resulting solution was cooled to room temperature and acidified by addition of HCl soln. (10% aq.) until a precipitate was observed. The solid was collected by filtration, washed with chloroform (30 mL) and methanol (10 mL) and pulled dry to yield crude 4-oxo-7-phenoxy-1,4-dihydroquinoline-3-carboxylic acid (260 mg).

The crude carboxylic acid was added to boiling Dowtherm A (20 mL) and reflux was maintained for 1 hour. The reaction mixture was cooled to room temperature and purified by flash column chromatography (Silica gel, 3% methanol/chloroform) to yield **12** as a cream powder.

(203 mg, yield 88.4%)

Melting point: 178 - 181 °C

^{1}H NMR (MeOD-d^{4}) δ 8.23 – 8.20 (d, 1H, *J* = 9.1), 7.87 – 7.85 (d, 1H, *J* = 7.3), 7.48 – 7.44 (t, 2H, *J* = 7.8), 7.28 – 7.24 ($^{app.}$t, 2H), 7.15 – 7.13 (d, 2H, *J* = 7.7), 7.11 – 7.08 (dd, 1H, *J* = 9.1, 2.3), 6.90 (d, 1H, *J* = 2.3), 6.27 – 6.25 (d, 1H, *J* = 7.3);

^{13}C NMR δ 180 (C=O), 164, 157, 144, 142, 132 (2C), 129, 127, 123, 122 (2C), 117, 110, 105;

HRMS: $[M+H]^{+}$ $C_{15}H_{12}NO_2$ requires 238.0868, found 238.0872;

CHN for $C_{15}H_{11}NO_2$ requires C 75.94 H 4.67 N 5.90, found C 75.74 H 4.64 N 5.88.

*Synthesis of ethyl 2-cyano-3-((3-phenoxyphenyl)amino)acrylate **(14)***

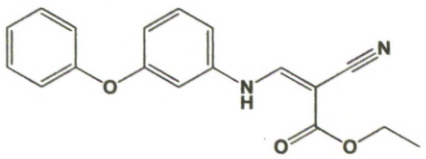

3-phenoxyaniline **2** (2.05 g, 11.05 mmol) and ethyl(ethoxymethylene)cyanoacetate **13** (1.87 g, 11.05 mmol) were mixed in

ethanol (10 mL) and heated to 100 °C overnight. The resulting brown soln. was cooled and the product precipitated by addition of petroleum ether (40 mL). The solid was recovered by filtration, pulled dry and dried in a vacuum desiccator for 24 hours to yield ethyl 2-cyano-3-((3-phenoxyphenyl)amino)acrylate **14** as a mixture of *E* and *Z* isomers, as a pale brown solid.

(3.23 g, yield 94.6%)

^{1}H NMR (MeOD-d^{4}) δ 8.39 (s, 1H, *E*), 8.27 (s, 1H, *Z*), 7.4 – 7.35 (m, 3H), 7.17 – 7.14 (t, 1H, *J* = 7.3), 7.04 – 7.02 (m, 3H), 6.98 – 6.93 (dt, 1H, *J* = 13.5, 2.2), 6.78 – 6.74 (m, 1H), 4.30 – 4.25 (q, $C\underline{H}_2CH_3$, *E*, *J* = 7.1), 4.26 – 4.21 (q, $OC\underline{H}_2CH_3$, *Z*, *J* = 7.1), 1.34 – 1.30 (t, $OCH_2C\underline{H}_3$, *E*, *J* = 7.1), 1.32 – 1.29 (t, $CH_2C\underline{H}_3$, *Z*, *J* = 7.1);

^{13}C δ 169/167 (*E/Z* C=O), 161, 158, 154/153 (*E/Z*), 143/142 (*E/Z*), 134, 132 (2C), 125, 121 (2C), 119, 117, 116, 113, 110, 109, 77, 59/58 (*E/Z*), 15;

HRMS: $[M+NH_4]^+$ $C_{18}H_{20}N_3O_3$ requires 326.1505, found 326.1509;

CHN for $C_{18}H_{16}N_2O_3$ requires C 70.12 H 5.23 N 9.09, found C 70.05 H 5.23 N 9.06.

Synthesis of 4-oxo-7-phenoxy-1,4-dihydroquinoline-3-carbonitrile ***(15)***

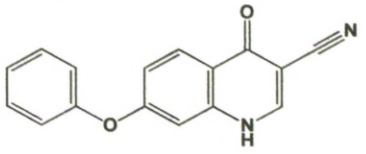

Ethyl 2-cyano-3-((3-phenoxyphenyl)amino)acrylate **14** (320 mg, 1.04 mmol) was dissolved in hot Dowtherm A (5 mL) and heated to reflux overnight. The resulting solution was cooled to room temperature and poured into n-hexane (50 mL) resulting in a brown precipitate. Solid recovered by vacuum filtration, washed with n-hexane and dried under suction to yield **15** as a dark tan solid.

(239 mg, yield 87.9%)

Melting point: 171 - 175 °C (decomp.)

^{1}H NMR (DMSO-d^{6}) δ 12.61 (bs, NH), 8.67 (s, 1H), 8.14 – 8.12 (d, 1H, *J* = 8.8), 7.53 – 7.49 ($^{app.}$t, 2H), 7.33 – 7.29 (t, 1H, *J* = 7.1), 7.22 – 7.20 (d, 2H, *J* = 8.3), 7.17 – 7.14 (dd, 1H, *J* = 8.8, 2.3), 6.98 (d, 1H, *J* = 2.3);

^{13}C NMR δ 174.1 (C=O), 161.7, 154.8, 147.3, 141.3, 130.9 (2C), 128.0, 125.7, 120.9 (2C), 117.2, 116.7, 105.0, 99.5, 94.0;

HRMS: $[M+H]^+$ $C_{16}H_{11}N_2O_2$ requires 263.0821, found 263.0817;

CHN for $C_{16}H_{10}N_2O_2$ requires C 73.27 H 3.84 N 10.68, found C 73.00 H 3.79 N 10.58.

*Synthesis of ethyl 4-chloro-7-phenoxyquinoline-3-carboxylate (**17**)*

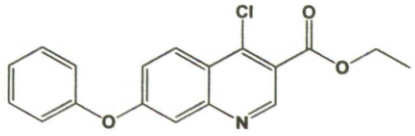

4 (0.76 g, 2.5 mmol) was dissolved in phosphoryl chloride (5 mL) under a nitrogen atmosphere. The resulting yellow solution was heated to reflux for 1½ hours before being poured onto ice (200 mL) and being left to stir overnight. The resulting aqueous solution was extracted with dichloromethane (2 x 250 mL) and the organic extracts dried over magnesium sulphate before evaporation to give **17** as a yellow solid.

(0.74 g, yield 91.6%)

Melting point: 105 - 108 °C (decomp.)

^1H NMR ($CDCl_3$) δ 9.15 (s, 1H), 8.41 – 8.39 (d, 1H, J = 9.3), 7.51 – 7.43 (m, 4H), 7.28 – 7.24 (m, 1H), 7.17 – 7.15 (d, 2H, J = 7.8), 4.51 – 4.46 (q, 2H, J = 7.1), 1.46 – 1.44 (t, 3H, J = 7.1);

^{13}C NMR δ 165 (C=O), 162, 155, 151, 127 (2C), 126, 123, 122, 121 (2C), 113, 62, 15;

HRMS: $[M+H]^+$ $C_{18}H_{15}{}^{35}ClNO_3$ requires 328.0740, found 328.0724;

CHN for $C_{18}H_{14}{}^{35}ClNO_3$ requires C 65.96 H 4.31 N 4.27, found C 65.37 H 4.32 N 5.10.

*Synthesis of 7-phenoxy-2H-pyrazolo[4,3-c]quinolin-3(5H)-one (**16**)*

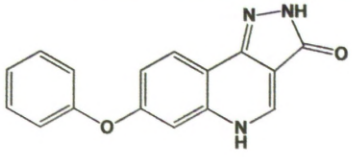

17 (0.50 g, 1.5 mmol) was dissolved in dry 1,4-dioxane (5 mL) under a nitrogen atmosphere. Hydrazine hydrate (0.50 mL, 3.1 mmol) was added slowly and the resulting solution heated to 80 °C. After ~ 30 minutes a yellow

precipitate was observed. Solid recovered by filtration, washed with petroleum ether and water and dried in a vacuum desiccator for 48 hours to yield a bright yellow powder.

(0.41 g, yield 97.4%)

Melting point: > 250 °C

^{1}H NMR (DMSO-d6) δ 12.29 (s, NH), 11.32 (s, NH), 8.48 – 8.47 (d, 1H, *J* = 5.9), 8.07 – 8.05 (d, 1H, *J* = 8.7), 7.50 – 7.46 ($^{app.}$t, 2H), 7.27 – 7.24 (t, 1H, *J* = 7.4), 7.18 – 7.13 (m, 4H);

^{13}C NMR δ 169.5, 163.4, 158.2, 141.5, 138.7, 136.9, 130.7 (2C), 124.9, 124.1, 120.1 (2C), 117.3, 112.3, 106.7, 94.7;

HRMS: $[M+H]^+$ $C_{16}H_{12}N_3O_2$ requires 278.0930, found 278.0916;

CHN for $C_{16}H_{11}N_3O_2$ requires C 69.31 H 4.00 N 15.15, found C 64.81 H 4.39 N 14.19.

*General Method D: Transesterification of **4***

4 (0.2 g, 0.65 mmol) was dissolved in an appropriate alcohol (10 mL). A catalytic quantity of titanium (IV) isopropoxide was added and the solution heated to reflux for 24 hours. Reaction mixture preabsorbed onto silica and purified by column chromatography eluting with ethanol in chloroform. The solid product was then washed with ethanol and dried in a desiccator.

*Isopropyl 4-oxo-7-phenoxy-1,4-dihydroquinoline-3-carboxylate **(18)***

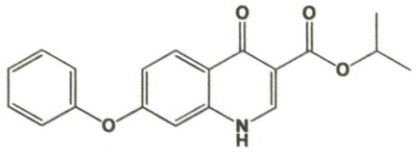

Synthesised from **4** according to general method D to yield a white solid.

(64.4 mg, yield 32.4%)

Melting point: > 250 °C

^{1}H NMR (DMSO-d6) δ 12.09 (bs, NH), 8.45 (s, 1H), 8.13 (d, 1H, *J* = 8.9), 7.52 – 7.48 ($^{app.}$t, 2H), 7.31 – 7.28 ($^{app.}$t, 1H), 7.22 – 7.19 (d, 2H, *J* = 8.1), 7.10 – 7.08 (dd, 1H, *J* = 8.9, 2.0), 6.97 (d, 1H, *J* = 1.9), 5.08 – 4.99 (m, C<u>H</u>$(CH_3)_2$, *J* = 6.2), 1.27 (d, CH$(C\underline{H}_3)_2$, *J* = 6.2);

^{13}C NMR δ 173 (C=O), 164, 161, 155, 145, 141, 131 (2C), 128, 125, 123, 121 (2C), 116, 110, 104, 67, 38, 22;

HRMS: $[M+H]^+$ $C_{19}H_{18}NO_4$ requires 324.1236, found 324.1232;

CHN for $C_{19}H_{17}NO_4$ requires C 70.58 H 5.30 N 4.33 found C 69.79 H 5.20 N 4.17.

Cyclopentyl 4-oxo-7-phenoxy-1,4-dihydroquinoline-3-carboxylate ***(19)***

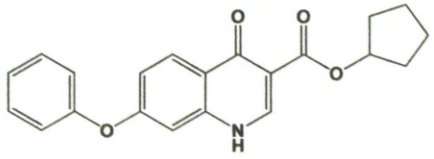

Synthesised from **4** according to general method D to yield a cream solid.

(116 mg, yield 68.6%)

Melting point: > 250 °C

^{1}H NMR (DMSO-d6) δ 12.12 (bs, NH), 8.49 (s, 1H), 8.19 (d, 1H, *J* = 8.9), 7.58 – 7.54 ($^{app.}$t, 2H), 7.37 – 7.33 ($^{app.}$t, 1H), 7.27 – 7.25 (d, 2H, *J* = 8.2), 7.15 – 7.12 (dd, 1H, *J* = 8.9, 2.2), 7.03 (d, 1H, *J* = 2.2), 5.28 – 5.25 (m, OC<u>H</u>), 1.94 – 1.63 (m, 8H);

^{13}C NMR δ 172, 161, 155, 145, 131 (2C), 128, 125, 122, 121 (2C), 116, 110, 105, 76, 32 (2C), 24 (2C);

HRMS: $[M+H]^+$ $C_{21}H_{20}NO_4$ requires 350.1392 found 350.1400;

CHN for $C_{21}H_{19}NO_4$ requires C 72.19 H 5.48 N 4.01 found C 70.05 H 5.35 N 3.59.

Cyclohexyl 4-oxo-7-phenoxy-1,4-dihydroquinoline-3-carboxylate ***(20)***

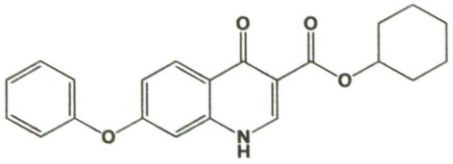

Synthesised from **4** according to general method D to yield a white powder.

(115 mg, yield 31.3%)

Melting point: > 250 °C

^{1}H NMR (DMSO-d6) δ 12.06 (bs, NH), 8.46 (s, 1H), 8.14 (d, 1H, *J* = 8.9), 7.52 – 7.48 (t, 2H, *J* = 7.9), 7.31 – 7.27 (t, 1H, *J* = 7.4), 7.21 – 7.19 (d, 2H, *J* = 7.9), 7.10 – 7.07 (dd, 1H, *J* = 8.9, 2.4), 6.97 (d, 1H, 2.4), 4.86 – 4.81 (m, OC<u>H</u>), 1.82 (bs, 2H), 1.74 (bs, 2H), 1.52 – 1.45 (m, 3H), 1.41 – 1.28 (m, 3H);

^{13}C NMR δ 207 (C=O), 173 (C=O), 161, 155, 145, 131 (2C), 128, 125, 123, 121 (2C), 116, 111, 104, 71, 31 (4C), 25, 23;

HRMS: $[M+Na]^+$ $C_{22}H_{21}NO_4Na$ requires 386.1368, found 386.1362;

CHN for $C_{22}H_{21}NO_4$ requires C 72.71 H 5.82 N 3.85 found C 72.29 H 5.77 N 3.75.

Synthesis of ethyl 7-benzyl-4-oxo-1,4-dihydroquinoline-3-carboxylate ***(22)***

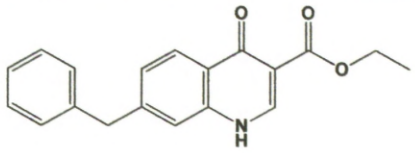

3-benzylaniline **21** (275 mg, 1.5 mmol) was stirred gently in diethyl ethoxymethylenemalonate **1** (0.30 mL, 1.5 mmol) and heated to 100 °C overnight. Dilution with petroleum ether (5 mL) and cooling in an ice/acetone bath resulted in a cream solid, recovered by filtration and pulled dry.

Crude diethyl 2-(((3-benzylphenyl)amino)methylene)malonate (519 mg) was added to boiling Dowtherm A (5 mL) and refluxed for 2.5 hours. The resulting solution was cooled to room temperature and poured in to *n*-hexane (25 mL). Solid collected by filtration, washed with diethyl ether, pulled dry and dried in a vacuum desiccator to yield **22** as a white powder.

(247 mg, yield 57.4 %)

Melting point: 242 - 246 °C (decomp.)

^{1}H NMR (DMSO-d6) δ 12.22 (bs, NH), 8.48 (s, 1H), 8.08 – 8.06 (d, 1H, J = 8.3), 7.37 – 7.21 (m, 7H), 4.22 – 4.17 (q, $OC\underline{H}_2CH_3$, J = 7.0), 4.09 (s, $ArC\underline{H}_2Ar$), 1.29 – 1.25 (t, $OCH_2C\underline{H}_3$, J = 7.1);

^{13}C NMR δ 178 (C=O), 174 (C=O), 165, 146, 145, 140, 139, 129 (2C), 128 (2C), 127, 126 (2C), 125, 118, 60, 41, 15;

HRMS: $[M+Na]^+$ $C_{19}H_{17}NO_3Na$ requires 330.1106 found 330.1111;

CHN for $C_{19}H_{17}NO_3$ requires C 74.25 H 5.58 N 4.56 found C 74.24 H 5.60 N 4.61.

*Synthesis of 1-nitro-3-((4-(trifluoromethoxy)benzyl)oxy)benzene **(24)***

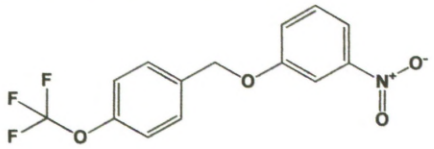

3-Nitrophenol **7** (4.09 g, 29.4 mmol) and cesium carbonate (9.84 g, 30.2 mmol) were dissolved in acetonitrile (25 mL). 4-(trifluoromethoxy)benzyl bromide **23** (2.0 mL, 12.5 mmol) was added and the mixture heated to reflux. Thin layer chromatography showed complete reaction after 2 hours. The reaction mixture was cooled to room temperature and the resulting inorganic precipitate screened off by filtration. The organic filtrate was concentrated directly onto silica gel and purified by column chromatography (0.5% methanol/3% ethyl acetate/96.5% petroleum ether). Product **24** was obtained as a yellow liquid.

(3.34 g, yield 85.9%)

^{1}H NMR (Acetone-d^6) δ 7.88 – 7.83 (m, 2H), 7.71 – 7.37 (m, 6H), 5.3 (s, OCH_2Ar);

HRMS: $[M+Na]^+$ $C_{14}H_{10}F_3NO_4Na$ requires 336.0460, found 336.0476.

*Synthesis of 3-((4-(trifluoromethoxy)benzyl)oxy)aniline **(25)***

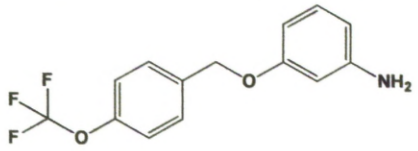

24 (3.32 g, 10.6 mmol) and zinc powder (21.53 g, 0.3 mol) were suspended in ethanol (50 mL). Calcium chloride (0.83 g, 7.48 mmol) and water (2 mL) were added and the mixture heated to reflux (90 °C) overnight. The cooled reaction mixture was filtered to remove inorganic solids and the filtrate concentrated under reduced pressure to yield an off-white solid with brown impurities. Recrystallisation from hot ethyl acetate gave **25** as beige flakes.

(2.72 g, yield 91.2 %)

^{1}H NMR (Acetone-d^6) δ 7.64 – 7.59 (m, 2H), 7.38 – 7.35 (m, 2H), 6.98 – 6.94 (t, 1H, J = 8.0), 6.37 – 6.36 (t, 1H, J = 2.2), 6.31 – 6.26 (m, 2H), 5.08 (s, OCH_2Ar);

^{13}C NMR δ 161, 151, 139, 131 (2C), 130 (2C), 122, 113, 109, 107, 104, 102, 69;

HRMS: $[M+H]^+$ $C_{14}H_{13}F_3NO_2$ requires 284.0898, found 284.0906;

CHN for $C_{14}H_{12}F_3NO_2$ requires C 59.37 H 4.27 N 4.95, found C 55.98 H 4.21 N 4.35.

Synthesis of ethyl 4-oxo-7-((4-(trifluoromethoxy)benzyl)oxy)-1,4-dihydroquinoline-3-carboxylate ***(26)***

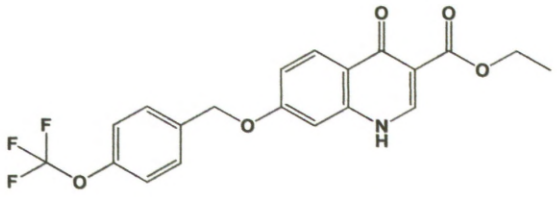

25 (2.65 g, 9.4 mmol) was dissolved in diethyl ethoxymethylenemalonate **1** (1.90 mL, 9.5 mmol) and ethanol (3 mL). The solution was heated to reflux overnight with vigorous stirring. Addition of the cooled solution to n-hexane (20 mL) resulted in an off-white precipitate, recovered by filtration and pulled dry to give crude diethyl 2-(((3-((4-(trifluoromethoxy)benzyl)oxy)phenyl) amino)methylene)malonate.

Crude intermediate was added to boiling Dowtherm A (15 mL) and refluxed for 2 hours. The resulting solution was cooled and poured into n-hexane (50 mL) to yield a fine brown powder. Recrystallisation from hot acetone gave **26** as fine beige crystals.

(0.609 g, yield 16.0%)

Melting point: > 250 °C

^1H NMR (DMSO-d6) δ 11.57 – 11.55 (bs, NH), 8.81 (s, 1H), 8.25 – 8.23 (d, 1H, J = 8.8), 7.29 – 7.21 (m, 3H), 7.00 – 6.99 (m, 2H), 6.76 – 6.74 (d, 1H, J = 7.1), 5.26 (s, 2H), 4.23 – 4.17 (q, $OC\underline{H}_2CH_3$, J = 7.0), 1.29 – 1.25 (t, $OCH_2C\underline{H}_3$, J = 7.1);

^{13}C NMR not obtained due to poor product solubility;

HRMS: $[M+H]^+$ $C_{20}H_{17}F_3NO_5$ requires 408.1059 found 408.1079;

CHN for $C_{20}H_{16}F_3NO_5$ requires C 58.97 H 3.96 N 3.44 found C 58.68 H 3.86 N 3.37.

*Synthesis of 1-benzyl-4-(3-nitrophenyl)piperazine **(30)***

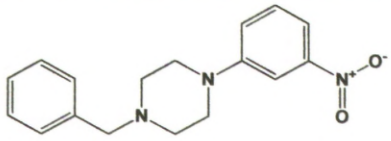

N-benzylpiperazine **29** (6.5 mL, 37.6 mmol) was added to a stirring mixture of 3-fluoronitrobenzene **28** (2.0 mL, 18.8 mmol) and potassium carbonate (3.94 g, 28.2 mmol) in dimethylsulphoxide under a nitrogen atmosphere. The mixture was heated to 90 °C and the reaction followed by TLC. After ~ 40 hours starting material was still evident however the reaction was quenched by cooling to room temperature and pouring in to ethyl acetate (50 mL). The resulting solution was washed with water (2 x 75 mL) and brine (75 mL) before being dried over sodium sulphate and being concentrated to give a viscous orange liquid. Column chromatography (10 % methanol/dichloromethane) gave the pure product **30** as an orange oil.

(3.49 g, yield 62.5%)

^{1}H NMR (Acetone-d6) δ 7.71 – 7.25 (m, 9H), 3.58 (s, NC$\underline{H_2}$Ar), 3.36 – 3.33 (t, 4H, *J* = 5.0), 2.62 – 2.60 (t, 4H, *J* = 5.1);

^{13}C NMR δ 153.5, 150, 139.8 131.2, 130.2 (2C), 129.5 (2C), 128.3, 122.3, 114.0, 110.1, 63.8, 53.9 (2C), 49.4 (2C);

HRMS: $[M+H]^+$ $C_{17}H_{20}N_3O_2$ requires 298.1556, found 298.1555;

CHN for $C_{17}H_{19}N_3O_2$ requires C 68.67 H 6.44 N 14.13, found C 68.66 H 6.48 N 14.18.

*Synthesis of 3-(4-benzylpiperazin-1-yl)aniline **(31)***

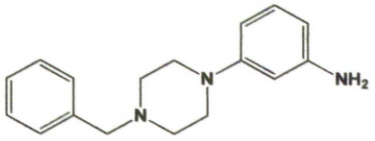

30 (3.30 g, 11.2 mmol) was dissolved in ethyl acetate (110 mL). Tin (II) chloride dihydrate (12.6 g, 55.8 mmol) was added and the resulting lemon yellow solution heated to 80 °C for 2 hours. Reaction mixture was then poured into water (200 mL) and basified with saturated $NaHCO_{3\,(aq.)}$ solution to pH 8. Inorganic precipitate removed by filtration and the aqueous filtrate extracted with ethyl acetate (4 x 50 mL). The combined organic layers were

dried over sodium sulphate and the solvents evaporated to yield the product as an off-white solid.

(1.92 g, yield 64.1%)

Melting point: 150 - 154 °C

^{1}H NMR (Acetone-d6) δ 7.38 – 7.25 (m, 5H), 6.91 – 6.87 (t, 1H, *J* = 8.0), 6.28 – 6.27 (t, 1H, *J* = 2.2), 6.22 – 6.19 (m, 2H), 4.4 (bs, NH_2), 3.53 (s, $ArC\underline{H}_2N$), 3.11 – 3.09 (t, 4H, *J* = 4.9), 2.54 – 2.52 (t, 4H, *J* = 5.0);

^{13}C NMR δ 154.5, 150.2, 139.8, 130.5, 130.2 (2C), 129.4 (2C), 128.2, 107.4, 106.4, 103.4, 63.9, 54.4 (2C), 50.3 (2C);

HRMS: $[M+H]^+$ $C_{17}H_{22}N_3$ requires 268.1814, found 268.1804;

CHN for $C_{17}H_{21}N_3$ requires C 76.37 H 7.92 N 15.72, found C 76.03 H 7.88 N 15.26.

Synthesis of ethyl 7-(4-benzylpiperazin-1-yl)-4-oxo-1,4-dihydroquinoline-3-carboxylate ***(27)***

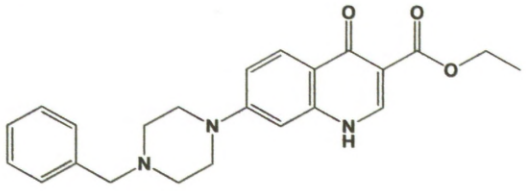

31 (1.09 g, 4.1 mmol) was dissolved in diethyl ethoxymethylenemalonate **1** (0.82 mL, 4.1 mmol) and ethanol (2.5 mL) and the solution was stirred at 90 °C overnight. Evaporation of the volatile components gave crude diethyl 2-(((3-(4-benzylpiperazin-1-yl)phenyl)amino)methylene)malonate as a brown oil. This was added Dowtherm A (7.5 mL) and heated to reflux for 30 minutes after which the temperature was reduced to 200 °C for 1 hour. The cooled reaction mixture formed a semi-solid brown gel. Filtration and extensive washing of the gel with diethyl ether yielded a beige powder.

(0.58 g, yield 36.1%)

Melting point: > 250 °C

^{1}H NMR (DMSO-d6) δ 11.86 (bs, NH), 8.40 (s, 1H), 7.94 – 7.92 (d, 1H, *J* = 9.1), 7.36 – 7.28 (m, 5H), 7.11 – 7.09 (d, 1H, *J* = 9.1), 6.80 (s, 1H), 4.21 – 4.16 (q, $OC\underline{H}_2CH_3$, *J* = 7.1), 3.54 (s, $NC\underline{H}_2Ar$), 3.31 (bs, 4H), 2.51 (bs, 4H), 1.28 – 1.25 (t, $OCH_2C\underline{H}_3$, *J* = 7.1);

^{13}C NMR not obtained due to poor product solubility;

HRMS: $[M+Na]^+$ $C_{23}H_{25}N_3O_3Na$ requires 414.1794, found 414.1807;
CHN for $C_{23}H_{25}N_3O_3$ requires C 70.57 H 6.44 N 10.73, found C 70.73 H 6.43 N 10.68.

*Synthesis of 3'-nitro-[1,1'-biphenyl]-4-ol **(35)***

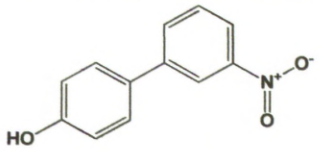

Palladium bis(dicyclohexylamine)diacetate (0.78 g, 0.13 mmol) was dissolved in ethanol (45 mL). Potassium phosphate (2.76 g, 13.0 mmol) was added followed by 1-bromo-3-nitrobenzene **33** (1.38 g, 6.83 mmol) and 4-methoxybenzeneboronic acid **34** (1.21 g, 7.96 mmol). Reaction mixture refluxed with vigorous stirring for 4 hours. Diluted with ethyl acetate (250 mL), washed with brine (2 x 100 mL) and dried over sodium sulphate. Column chromatography (5% ethyl acetate/petroleum ether) gave 4'-methoxy-3-nitro-1,1'-biphenyl (1.29 g, 82.1%). Dissolved in dry dichloromethane (45 mL) and saturated with N_2 gas at -78 °C. Tribromoboron solution (5 mL, 1M in dichloromethane) was added dropwise by syringe over the course of 5 minutes. Temperature maintained at -78 °C for 3 hours, before warming to room temperature and stirring overnight. Diluted with dichloromethane (30 mL) and washed with water (3 x 50 mL). Organic phase dried over magnesium sulphate and absorbed on to silica gel. Column chromatography (2 < 20% ethyl acetate/petroleum ether) furnished the product **35** as a crystalline yellow solid.

(1.04 g, yield 86.7%)

^{1}H NMR (Acetone-d6) δ 8.71 (s, 1H), 8.41 – 8.40 (t, 1H, J = 2.0), 8.17 – 8.14 (dd, 1H, J = 8.2, 2.2), 8.06 – 8.04 (d, 1H, J = 7.9), 7.74 – 7.70 (t, 1H, J = 8.0), 7.67 – 7.63 (m, 2H), 7.02 – 6.99 (m, 2H);

^{13}C NMR δ 159.5, 150.2, 143.9, 133.7, 131.4, 131.0, 129.6 (2C), 122.3, 121.8, 117.3 (2C);

HRMS: $[M+Na]^+$ $C_{12}H_9NO_3Na$ requires 238.0480, found 238.0474;
CHN for $C_{12}H_9NO_3$ requires C 66.97 H 4.22 N 6.51, found C 66.92 H4.20 N 6.49.

Synthesis of 4-(2-((3'-nitro-[1,1'-biphenyl]-4-yl)oxy)ethyl)morpholine ***(37)***

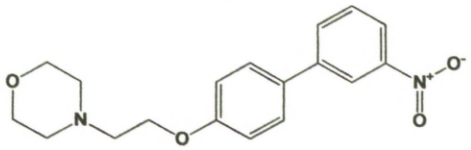

35 (0.28 g, 1.3 mmol) dissolved in anhydrous acetonitrile. Powdered sodium hydroxide (0.21 g, 5.2 mmol) and tetrabutylammonium hydrogen sulphate (0.92 g, 0.27 mmol) were added and the resulting orange mixture stirred at room temperature for 30 minutes during which time sodium chloride is observed to precipitate from the solution. *N*-(2-chloroethyl)morpholine (0.49 g, 2.6 mmol) added and the solution heated to 60 °C overnight. Filtered to remove inorganic precipitate, solid washed with dichloromethane (50 mL), washings combined with filtrate and concentrated under reduced pressure. Residue dissolved in ethyl acetate (50 mL) and washed with water (25 mL) and brine (25 mL) before drying over magnesium sulphate. Solvents removed and product crystallised under high vacuum to yield orange crystals.

(0.37 g, yield 86.1%)

^{1}H NMR (Acetone-d6) δ 8.43 – 8.42 (t, 1H, *J* = 2.0), 8.19 – 8.16 (dd, 1H, *J* = 8.2, 2.2), 8.10 – 8.08 (d, 1H, *J* = 7.8), 7.76 – 7.72 (m, 3H), 7.13 – 7.09 (m, 2H), 4.23 – 4.20 (t, 2H, *J* = 5.8), 3.64 – 3.61 (^{app}t, 4H), 2.80 – 2.77 (t, 2H, *J* = 5.8), 2.56 – 2.53 (^{app}t , 4H);

^{13}C NMR δ 150.2, 133.8, 132.3, 132.1, 131.4, 129.6 (2C), 122.5, 122.0, 116.5 (2C), 100.9, 67.9 (2C), 67.4, 58.7, 55.4 (2C);

HRMS: $[M+H]^+$ $C_{18}H_{21}N_2O_4$ requires 329.1501, found 329.1516.

Synthesis of 4'-(2-morpholinoethoxy)-[1,1'-biphenyl]-3-amine ***(38)***

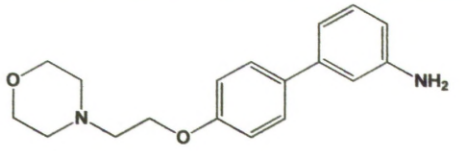

37 (0.59 g, 1.8 mmol) dissolved in ethyl acetate (18 mL). Tin (II) chloride dihydrate (2.1 g) added and the reaction mixture heated to reflux overnight. Diluted with water (50 mL) and saturated sodium hydrogencarbonate added until ~ pH 8. Inorganic precipitate filtered out and washed with ethyl acetate (100 mL), the aqueous filtrate extracted with ethyl acetate (2 x 50 mL).

Organic extracts and washings combined and washed with brine (50 mL) before drying over sodium sulphate. Solvents removed to yield **38** as a yellow oil.

(0.39 g, 72.0%)

^{1}H NMR (Acetone-d6) δ 7.52 – 7.50 (m, 2H), 7.12 – 7.08 (t, 1H, *J* = 7.8), 7.01 – 6.98 (m, 2H), 6.91 – 6.90 (t, 1H, *J* = 2.0), 6.83 – 6.81 (d, 1H, *J* = 7.7), 6.62 – 6.60 (dd, 1H, *J* = 7.9, 2.1), 4.68 (bs, $N\underline{H_2}$), 4.17 – 4.14 (t, 2H, *J* = 5.8), 3.63 – 3.61 (^{app}t, 4H), 2.78 – 2.75 (t, 2H, *J* = 5.8), 2.55 – 2.54 (m, 4H);

^{13}C NMR δ 154.5, 151.9, 150.2, 132.5, 130.6, 128.9 (2C), 116.3, 115.9 (2C), 114.1, 113.7, 67.9 (2C), 67.2, 58.8, 55.4 (2C);

HRMS: $[M+H]^+$ $C_{18}H_{23}N_2O_2$ requires 299.1760, found 299.1758;

CHN for $C_{18}H_{22}N_2O_2$ requires C 72.46 H 7.43 N 9.39, found C 70.38 H 7.37 N 10.25.

Synthesis and isolation of 7-(4-(2-morpholinoethoxy)phenyl)quinolin-4(1H)-one ***(32)***

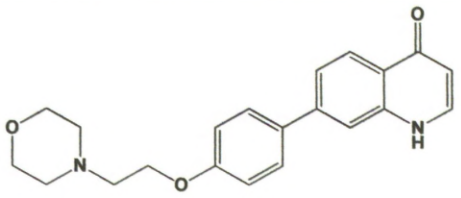

38 (0.39 g, 1.3 mmol) was dissolved in ethanol (1 mL) and diethyl ethoxymethylenemalonate **1** 0.26 mL, 1.3 mmol) added. Mixture heated to 100 °C overnight. Volatiles removed under reduced pressure to give diethyl 2-(((4'-(2-morpholinoethoxy)-[1,1'-biphenyl]-3-yl)amino)methylene)malonate as an orange oil. Dissolved in Dowtherm A (1 mL) and heated to 200 °C for 2 hours. Taken up in ethyl acetate and absorbed onto silica gel. Column chromatography (2% methanol/dichloromethane) gave a yellow oil. Reverse phase HPLC in acetonitrile gave pure **32** as a white solid.

(30.1 mg)

HPLC (100% MeCN) Retention time = 20.02 min;

^{1}H NMR (Acetone-d6) δ 10.98 – 10.94 (d, NH, *J* = 13.6), 8.63 – 8.60 (d, 1H, *J* = 13.7), 7.68 – 7.65 (dt, 2H, *J* = 9.7, 2.9), 7.58 (s, 1H), 7.49 – 7.41 (m, 2H), 7.30 – 7.28 (d, 1H, *J* = 7.6), 7.06 – 7.03 (dt, 2H, *J* = 9.7, 2.9), 4.20 – 4.15 (m, 4H), 3.63 – 3.61 (m, 4H), 2.78 – 2.75 (t, 2H, *J* = 5.8), 2.54 (m, 2H);

^{13}C NMR δ 169.7 (C=O), 160.3, 152.8, 152.5, 143.6, 141.5, 133.7, 131.5, 129.4 (2C), 124.0, 116.2 (2C), 67.9 (2C), 67.2, 58.8, 55.4 (2C);
HRMS: $[M+H]^+$ $C_{21}H_{23}N_2O_3$ requires 351.1709, found 351.1690.

*Synthesis of 1-nitro-3-(4-(trifluoromethoxy)benzyl)benzene **(43)***

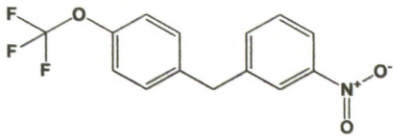

3-Nitrophenylboronic acid **42** (1.80 g, 10.8 mmol) and palladium tetrakistriphenyl-phosphine (0.27 g, 0.2 mmol) were stirred in degassed, anhydrous tetrahydrofuran (35 mL) under a nitrogen atmosphere. K_2CO_3 solution (15 mL, 2M aq.) was added followed by 4-(trifluoromethoxy)benzyl bromide **41** (2.09 g, 8.1 mmol). The resulting orange solution was heated to 95 °C overnight. TLC confirmed consumption of benzyl bromide **41**, the reaction was then quenched by cautious addition of aqueous HCl (50 mL, 2N). Mixture extracted with ethyl acetate (2 x 100 mL) and the combined organic extracts dried over magnesium sulphate. Preabsorbed onto silica gel and purified by column chromatography (4% ethyl acetate/petroleum ether) to give **43** as a yellow oil.

(1.99 g, yield 82.5%)

^1H NMR ($CDCl_3$) δ 8.11 – 8.06 (m, 2H), 7.52 – 7.46 (m, 2H), 7.22 – 7.11 (m, 4H), 4.09 (s, $ArC\underline{H_2}Ar$);
^{13}C NMR δ 148.9, 148.4, 142.8, 138.5, 135.4, 130.6 (2C), 129.9, 124.1, 122.0, 121.8 (2C), 121.4, 41.2.

*Synthesis of 3-(4-(trifluoromethoxy)benzyl)aniline **(40)***

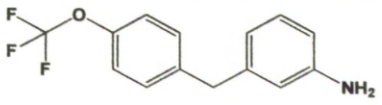

43 (1.99 g, 6.7 mmol) was dissolved in ethyl acetate (50 mL). Tin (II) chloride dihydrate (6.1 g, 27.0 mmol) was added and the resulting mixture heated to 90 °C overnight. TLC confirmed complete reaction. Diluted with water (75 mL) and basified to ~pH 8 using saturated aqueous $NaHCO_3$. Inorganic solid removed by filtration and washed with ethyl acetate (2 x 100 mL). Aqueous solution extracted with ethyl acetate (2 x 100 mL) and

combined organic extracts and washes were dried over magnesium sulphate. Evaporation gave the product as a yellow oil.

(1.50 g, yield 84.0%)

^{1}H NMR ($CDCl_3$) δ 7.21 – 7.19 (m, 2H), 7.13 – 7.07 (m, 3H), 6.60 – 6.58 (d, 1H, *J* = 7.6), 6.56 – 6.54 (dd, 1H, *J* = 7.9, 2.3), 6.48 (s, 1H), 3.88 (s, Ar$C\underline{H}_2$Ar), 3.65 (bs, NH_2);

^{13}C δ 147.0, 142.1, 140.3, 130.5, 129.9, 121.4, 119.7, 115.9, 113.6, 41.6;

HRMS: $[M+H]^+$ $C_{14}H_{13}F_3NO$ requires 268.0949, found 268.0947.

*Synthesis of diethyl 2-(((3-(4-(trifluoromethoxy)benzyl)phenyl)amino) methylene)malonate **(44)***

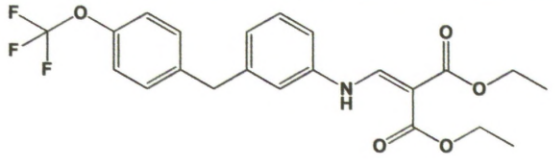

40 was dissolved in ethanol (15 mL/g) and diethyl ethoxymetylenemalonate **1** (1 eq.) was added. Reaction mixture was heated to 100 °C overnight. Once consumption of aniline **40** was confirmed by TLC volatile components were removed by at reduced pressure using a rotary evaporator to yield a red oil. Cooling under vacuum gave the desired product as an off-white crystalline solid.

(2.38 g, yield 97.4%)

^{1}H NMR ($CDCl_3$) δ 10.99 – 10.96 (d, NH, *J* = 13.7), 8.51 – 8.48 (d, 1H, *J* = 13.7), 7.33 – 7.29 (t, 1H, *J* = 7.8), 7.21 – 7.14 (m, 4H), 7.02 – 6.96 (m, 2H), 6.92 (s, 1H), 4.32 – 4.27 (q, $OC\underline{H}_2CH_3$, *J* = 7.1), 4.27 – 4.21 (q, $OC\underline{H}_2CH_3$, *J* = 7.1), 3.98 (s, Ar$C\underline{H}_2$Ar), 1.39 – 1.36 (t, $OCH_2C\underline{H}_3$, *J* = 7.1), 1.34 – 1.30 (t, $OCH_2C\underline{H}_3$, *J* = 7.1);

^{13}C NMR δ 169.5 (C=O), 166.2 (C=O), 152.2, 142.9, 139.9, 139.4, 130.5, 130.4, 125.9, 121.6, 118.2, 115.4, 94.0, 60.8, 60.5, 41.4, 14.8, 14.7;

HRMS: $[M+Na]^+$ $C_{22}H_{22}F_3NO_5Na$ requires 460.1348, found 460.1333.

*Synthesis of ethyl 4-oxo-7-(4-(trifluoromethoxy)benzyl)-1,4-dihydroquinoline-3-carboxylate **(39)***

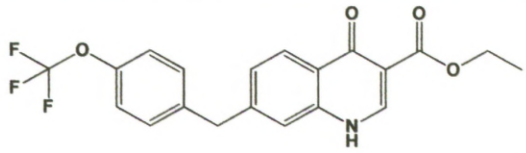

Synthesised from **44** according to general method B to yield a cream solid.

(1.18 g, yield 53.5%)

Melting point: > 250 °C

^{1}H NMR (DMSO-d6) δ 12.23 (s, NH), 8.49 (s, 1H), 8.09 – 8.07 (d, 1H, *J* = 8.6), 7.41 – 7.29 (m, 6H), 4.23 – 4.17 (q, $OC\underline{H_2}CH_3$, *J* = 7.1), 4.14 (s, $ArC\underline{H_2}Ar$), 1.29 – 1.25 (t, $OCH_2C\underline{H_3}$, *J* = 7.1);

^{13}C NMR δ 171.9 (C=O), 164.6 (C=O), 158.6, 150.5, 145.6, 144.7, 139.5, 139.0, 130.6 (2C), 130.2, 125.9, 125.7, 121.1 (2C), 117.9, 109.7, 59.4, 40.0, 14.2;

HRMS: $[M+Na]^+$ $C_{20}H_{16}F_3NO_4Na$ requires 414.0929, found 414.0919;

CHN for $C_{20}H_{16}F_3NO_4$ requires C 61.38 H 4.12 N 3.58, found C 61.46 H 4.11 N 3.56.

*Synthesis of 3-(ethoxycarbonyl)-7-(4-(trifluoromethoxy)benzyl)quinolin-4-yl morpholine-4-carboxylate, Prodrug **(46)***

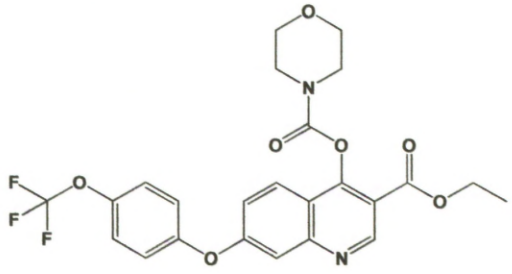

6 (0.18 g, 0.4 mmol) was suspended in freshly distilled anhydrous tetrahydrofuran (10 mL). Potassium *t*-butoxide (0.06 g, 0.6 mmol) was added and the mixture stirred at room temperature under nitrogen for 1 hour. *N*-morpholinecarbonyl chloride (0.10 mL, 0.9 mmol) was added by syringe and the resulting solution stirred at room temperature for 2 hours. *N*-morpholinecarbonyl chloride (0.10 mL, 0.9 mmol) was again added by syringe and the solution stirred for a further hour. Quenched with water (5

mL) and extracted with dichloromethane (3 x 10 mL). Organic extracts washed with water (10 mL) and brine (10 mL) before drying over magnesium sulphate and absorbing onto silica gel. Column chromatography (1% methanol/dichloromethane) gave a sticky yellow solid. Trituration with diethyl ether and drying under suction gave **46** as an off-white crystalline solid.

(0.094 g, yield 42.1%)

Melting Point: 168 – 172 °C

^{1}H NMR (DMSO-d6) δ 8.73 (s, 1H), 8.26 – 8.23 (d, 1H, *J* = 8.9), 7.52 – 7.50 (d, 2H, *J* = 8.3), 7.36 – 7.32 (dt, 2H, *J* = 9.1, 3.0), 7.21 – 7.18 (dd, 1H, *J* = 8.9, 2.3), 6.88 (d, 1H, *J* = 2.3), 4.27 – 4.21 (q, $OC\underline{H}_2CH_3$, *J* = 7.0), 3.57 – 3.54 (t, 4H, *J* = 4.8), 3.15 – 3.12 (t, 4H, *J* = 4.8), 1.31 – 1.27 (t, $OCH_2C\underline{H}_3$, *J* = 7.1);

^{13}C NMR δ 164.2 (C=O), 161.3 156.8, 153.9, 150.9 (C=O), 145.1, 138.8, 134.7, 129.6, 123.8 (2C), 122.9, 122.4 (2C), 116.6, 112.2, 104.2, 66.3 (2C), 60.5, 47.2 (2C), 14.6;

HRMS: $[M+H]^+$ $C_{24}H_{22}N_2O_7F_3$ requires 507.1379, found 507.1371.

3-(ethoxycarbonyl)-7-(4-(trifluoromethoxy)benzyl)quinolin-4-yl morpholine-4-carboxylate, Prodrug ***(47)***

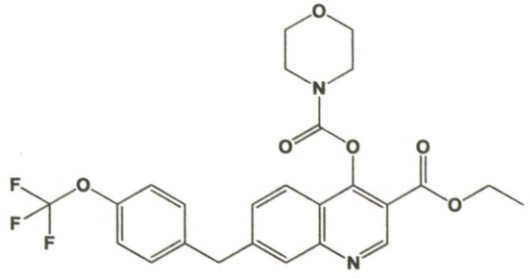

Synthesised from **39** according to the method used for **46**.

(0.18 g, yield 36.8%)

Melting Point: 175 – 178 °C

^{1}H NMR (DMSO-d6) δ 8.72 (s, 1H), 8.17 – 8.15 (d, 1H, *J* = 8.2), 7.44 – 7.31 (m, 6H), 4.26 – 4.20 (q, $OC\underline{H}_2CH_3$, *J* = 6.4), 4.20 (s, $ArC\underline{H}_2Ar$), 3.79 – 3.00 (m, 8H), 1.30 – 1.27 (t, $OCH_2C\underline{H}_3$, *J* = 7.1);

^{13}C NMR δ 173.1 (C=O), 164.3 (C=O), 151.0, 147.4, 144.9, 140.0, 137.5, 131.2 (2C), 127.2, 127.0, 125.6, 121.6 (2C), 116.6, 115.7, 111.8, 60.5 (2C), 55.08, 50.72, 47.2, 40.7, 14.6;

HRMS: $[M+Na]^+$ $C_{25}H_{23}N_2O_5F_3Na$ requires 527.1406, found 527.1425.

*Synthesis of isopropyl 4-oxo-7-(4-(trifluoromethoxy)benzyl)-1,4-dihydroquinoline-3-carboxylate **(48)***

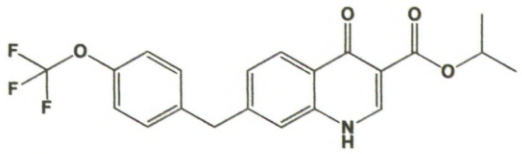

Synthesised from **39** according to general method D.

(0.11 g, yield 55.8%)

Melting point: > 250 °C

^{1}H NMR (DMSO-d6) δ 12.18 (s, NH), 8.44 (s, 1H), 8.08 – 8.06 (d, 1H, *J* = 8.2 Hz), 7.42 – 7.29 (m, 6H), 5.09 – 4.99 (sept, 1H, *J* = 6.3 Hz), 4.14 (s, 2H), 1.28 – 1.26 (d, 6H, *J* = 6.3 Hz);

^{13}C NMR δ 171.7 (C=O), 164.1(C=O), 151.3, 145.5, 144.5, 139.9, 139.6, 130.7 (2C), 125.9, 125.8, 125.6, 121.1 (2C), 120.6, 115.0, 110.5, 40.13, 30.59, 21.7 (2C);

HRMS: $[M+Na]^+$ $C_{21}H_{18}F_3NO_4Na$ requires 428.1086, found 428.1086.

Chapter 3

Results and Discussion 2: Docking Simulation

3. Results and Discussion 2: Docking Simulation

3.1 A Brief Introduction to Protein Ligand Docking Software

As computers have become increasingly powerful, computational chemistry has gained increased significance and computer-aided ligand docking is now a standard method for ascertaining the way in which small molecules bind with the active sites of proteins. The ability to predict the way in which a compound is likely to interact with a given target protein has two generic uses; either it can be used as a method to determine those compounds most likely to give good results when synthesised, referred to as virtual screening, or it is used to rationalise the observed results for compounds previously made and so inform further development, as in this study.

There are a number of different, highly regarded pieces of docking software including Glide,[130, 131] AutoDock[132] and GOLD[133-135] to name just a few, each of which evaluates ligands in a slightly different way and consequently have their own strengths and weaknesses. For the purposes of this study we have elected to use GOLD (**G**enetic **O**ptimization for **L**igand **D**ocking)[136] as it has been shown by a number of comparative reviews to give the best results for buried, hydrophobic binding sites such as the Q_o site of the bc_1 complex.[133, 137, 138]

GOLD performs molecular docking using a genetic algorithm in which the molecules to be docked are modelled using molecular mechanics and the strength of binding is predicted according to the non-covalent interactions observed between the ligand and the protein.[134] The predicted pose is then scored according to factors such as hydrogen bonding and van der Waals energies, ligand strain and steric clashes to generate a figure termed the GoldScore.[136]

3.2 The Protein

An atomic structure for *P. falciparum* bc_1 is not available and a homology model has yet to be published for use; due to the multi-subunit nature of the bc_1 protein complex and the many degrees of freedom involved in building, developing a homology model would be a far from trivial undertaking and it

was deemed impractical for this study, although work towards this is underway within the research group. Instead, in an effort to rationalise the observed biological trends the compounds were docked *in silico* using the high resolution (1.9 Å) crystal structure of yeast bc_1 protein from *Saccharomyces cerevisiae* (Protein Data Bank accession code 3CX5).[43] Although not identical to the parasite bc_1 complex the amino acid sequence of the yeast protein shares 40% homology and the Q_o region is well conserved between the two proteins.[78] The Q_o active site is the region of interest as this would appear to be the most probable site of action for the developed library; as evidenced by the cross-resistance with atovaquone resistant parasites discussed previously and the structural similarities with established Q_o binders.[42]

The yeast bc_1 complex was co-crystallised with stigmatellin (Figure 3.1) bound in the Q_o site (Figure 3.2).[43] Using the GOLD 5.0.1 protein-ligand docking suite,[136] stigmatellin can be removed and other compounds docked into the Q_o site.[135, 139]

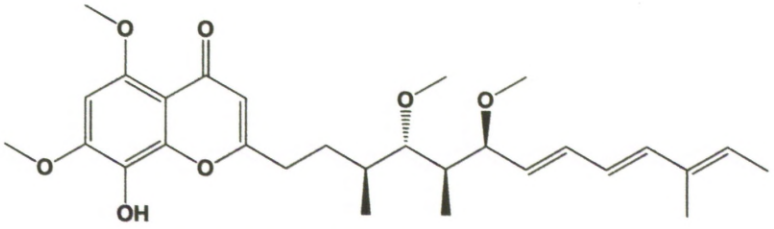

Figure 3.1: The structure of natural bc_1 Q_o inhibitor stigmatellin.

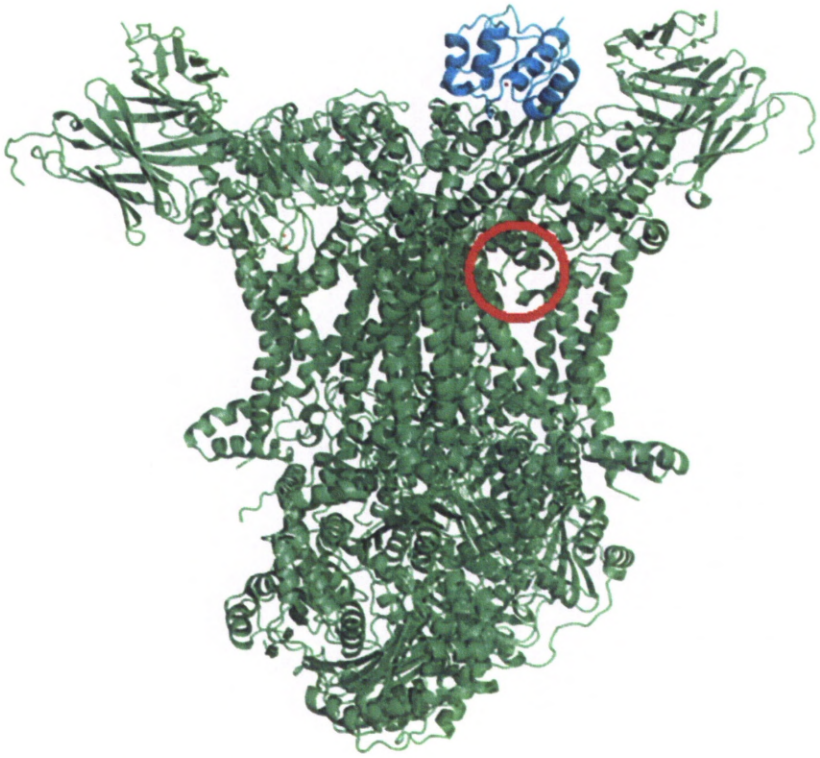

Figure 3.2: High resolution (1.9 Å) crystal structure of yeast bc1 protein from Saccharomyces cerevisiae (Protein Data Bank accession code 3CX5) displayed as a cartoon ribbon model (green) with cytochrome c (cyan) shown in the reduced position and the Q_o binding region indicated by a red circle.[43]

3.3 Docking Validation

In the docking simulation the receptor model of the protein is a rigid system with the amino acid fixed in the crystallised position. In a biological setting, however, a protein is a flexible structure that can adapt to it's environment. GOLD can allow for amino acid side-chain residues to be made flexible but cannot capture larger scale motions such as backbone motions. Crystallographic studies of bovine bc_1 co-crystallised with a variety of inhibitors, have shown the conformations of a number of Q_o site residues in cytochrome *b* to be particularly variable.[54] To ensure the most realistic protein environment for our docking study we selected flexibility in the analogous yeast bc_1 residues; Val146, Ile147 and Glu272. The water molecule HOH5607 is known to be involved in the binding of stigmatellin and the endogenous ligands[140] and so was retained in our docking model and it had the ability to rotate about the oxygen atom and translate to a limited degree ensuring the optimal docking position.

GOLD uses a molecular mechanics force field to evaluate the strength of non-covalent interactions between a given ligand, e.g. stigmatellin, and a designated active site, e.g. Q_o, producing a numerical value referred to as GoldScore. The GoldScore is used to guide a genetic algorithm to search for the optimal ligand-protein pose and thus demonstrate the most probable docking pose for a given protein-ligand complex. The reported pose with the highest GoldScore is considered to be the more favourable pose for the results of that search.

In cases where co-crystals are available, as with stigmatellin, the docking results can be validated by direct comparison with the crystallographically observed ligand pose using the root mean square deviation (RMSD) value. This value is generated by GOLD as a function of how different a given docking pose is compared to the original pose of the native ligand, with smaller RMSD values indicative of more similar docking poses, an RMSD value of 2 Å or less is considered the standard for a successful docking.[133, 134, 137, 141]

Therefore, in order to validate our chosen protein configuration stigmatellin was docked into the Q_o active site and the predicted docking poses compared to those of the co-crystallised ligand (Table 3.1 / Figure 3.2).

Table 3.1: Protein Validation Results

Pose	GoldScore	RMSD (Å)†
dock1	104.70	0.90
dock2	28.75	3.48
dock3	78.74	1.88
dock4	94.50	0.71
dock5	65.14	1.07
dock6	98.46	0.96
dock7	98.28	1.21
dock8	83.78	1.39
dock9	93.35	1.12
dock10	39.15	2.89

†*Root Mean Square Deviation.*

The program was configured such that a single docking run would consist of ten attempts producing ten distinct poses for comparison. These results show that the highest scoring docking pose for stigmatellin, dock1 (Table 3.1), has an RMSD of less than 1 Å compared to the observed pose from the PDB file and the average RMSD is 1.56 Å, well within the 2 Å standard for a successful docking.[133, 134, 141] In fact only two of the docking poses, dock 2 and dock 10, have RMSD values greater than 2 Å. As the resolution of the crystal structure is only 1.9 Å these results can be considered a validation of the protein configuration, meaning that any docking results produced for other ligands are likely to be accurate. The two outlying results can be attributed to the relatively large search space present in the docking simulation. As there is no reference crystal structure for the developed ligands, the number of attempts per docking run will be increased to twenty. This was to reduce the influence of any incongruous results when visually comparing the poses to establish if there was a relationship between GoldScore and observed interactions.

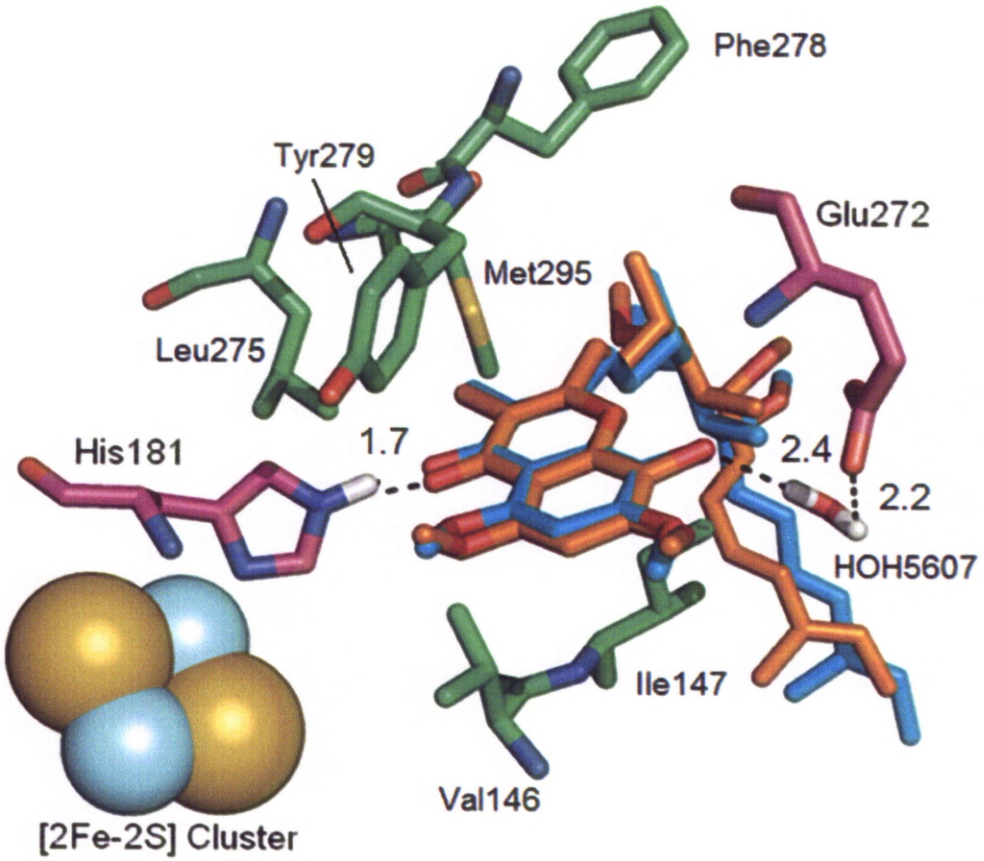

Figure 3.2: Image of the Q_o site with stigmatellin docked. Nitrogen atoms are shown in blue and oxygen atoms in red. The carbons of the key residues His181 and Glu272 are highlighted in pink and the residues forming the hydrophobic channel are shown in green. The [2Fe-2S] cluster of the ISP is shown as blue and yellow spacefilling atoms. The crystallographically observed ligand pose for stigmatellin is shown in cyan and the highest scoring result of the docking simulation (dock1) is displayed in orange with the predicted hydrogen bonding interactions indicated in black and labelled in Å.

3.4 Docking Atovaquone

Atovaquone (Figure 3.3) was also docked into the Q_o site using GOLD[136, 142] for the purpose of comparison with the synthesised quinolones and their docking poses. Results obtained were consistent with the literature, further validating the protein configuration and the docking protocol employed.[35, 78] The highest scoring poses (Table 3.2) consistently orientated atovaquone such that the polar hydroxynapthoquinone head group occupied the binding pocket, with the cyclohexane side chain lying in the hydrophobic channel. Differences in GoldScore mainly arose from the precise orientation of the tail relative to the hydrophobic residues. This orientation of the head group

promotes the formation of hydrogen bond interactions between the atovaquone carbonyl groups and the -NH of His181 and the carboxylate group of Glu272 through water HOH5607 (Figure 3.4).

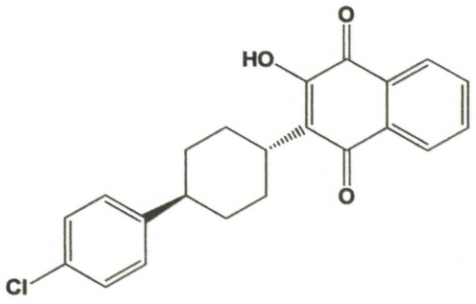

Figure 3.3: The structure of atovaquone, currently the only anti-malarial bc_1 inhibitor.

Table 3.2: Results from the docking of atovaquone in the Q_o site of yeast bc_1.

Docking Pose	GoldScore	Docking Pose	GoldScore
dock1	53.4704	dock11	59.6246
dock2	59.138	dock12	59.7703
dock3	59.8841	dock13	59.9727
dock4	59.7348	dock14	51.2095
dock5	59.6784	dock15	50.2908
dock6	51.6164	dock16	59.254
dock7	59.2893	dock17	59.024
dock8	59.5806	dock18	58.9632
dock9	59.6564	dock19	52.0205
dock10	50.3065	dock20	58.8999

Average GoldScore = 57.0692

Standard Deviation = 3.8115

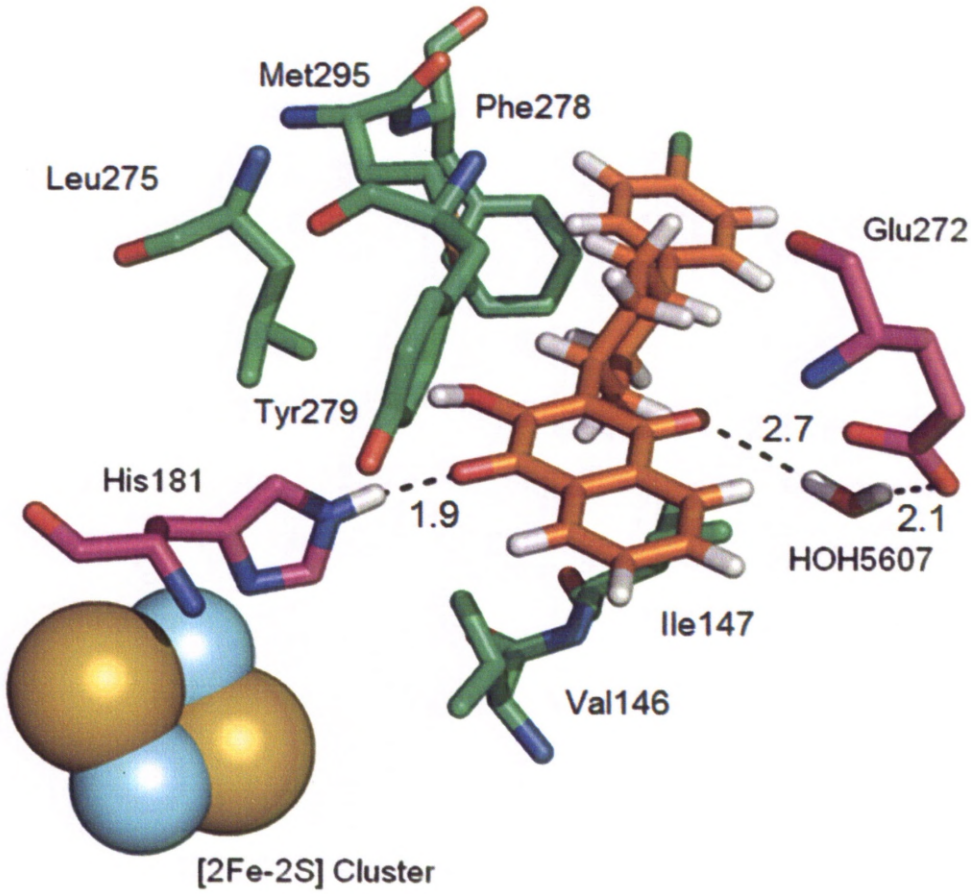

Figure 3.4: Image of the Q_o site with atovaquone docked. The key protein residues are highlighted and the [2Fe-2S] cluster is shown as blue and yellow spacefilling atoms. Atovaquone and water molecule HOH5607 are shown in their highest scoring orientation (dock13) as orange and red capped sticks respectively. Key hydrogen bonding interactions between atovaquone and the protein residues are shown in black and labelled in Å.

3.5 Preparing the Quinolone Ligands

In the earlier results and discussion section it was noted that 4-quinolones can adopt an alternative tautomer, 4-hydroxyquinolines. Before modelling the synthesised library it was important to establish which tautomeric form the compounds would adopt in a biological system, or the results of the docking simulation would be fundamentally flawed by inaccurate hydrogen bonding. This is of particular importance for the 3-ester compounds as it could be suggested that the potential for an intramolecular hydrogen bond system, between the 4-hydroxy moiety and the carbonyl of the 3-ester group, would favour the 4-hydroxyquinoline form (Figure 3.5).

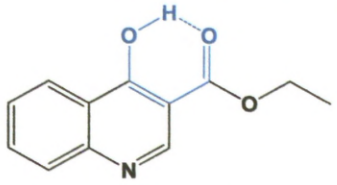

Figure 3.5: Showing the intramolecular hydrogen bond arrangement that could potentially favour the 4-hydroxyquinoline tautomer.

Close examination of the ^{1}H NMR spectra obtained for the compounds does not support this hypothesis however. The hydrogen atom on C2 of the quinolone ring has a characteristic chemical shift, appearing between 8 and 9 ppm, depending on the substitution at C3, allowing it to be easily identified. If the 4-hydroxyquinoline tautomer were the favoured configuration the peak corresponding to this hydrogen would be expected to be a singlet as the next nearest hydrogen atoms are 5 bonds distant, too far to result in the presence of any 2nd order splitting patterns (Figure 3.6).

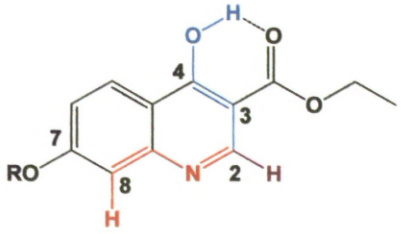

Figure 3.6: Showing the closest hydrogens to C2 in the 4-hydroxyquinoline tautomer.

Instead what is observed at around 8 ppm is a doublet with a coupling constant in the order of 8 Hz, indicating coupling with a proton on an adjacent atom. For many of the compounds this is accompanied by the presence of a broad peak, also occasionally observed as a doublet, at

approximately 12 ppm corresponding to a conjugated N-H, indicating that the compounds are present in the 4-quinolone configuration (Figure 3.7).

*Figure 3.7: Section of ^{1}H NMR for lead compound **39**, the presence of a doublet peak for enamine proton **b** indicating coupling to NH **a**, thereby confirming the quinolone conformer.*

3.6 Docking the Quinolone Ligands

Having established that the compounds are in the 4-quinolone tautomer, 3-dimensional representations for each of the seventeen synthesised quinolones tested *in vitro* (Table 3.3) were constructed and energy minimised using the *Spartan '08* molecular mechanics program.[143, 144] The files were then uploaded to the GOLD[136] protein-ligand docking suite and docked into the Q_o active site using the protein configuration previously validated by successful redocking of stigmatellin and atovaquone. As with the docking of atovaquone, the program was configured such that each quinolone structure produced twenty distinct docking poses for visual comparison and analysis.

Table 3.3: The structures and in vitro results for the synthesised quinolone inhibitors.

Compound	Structure	IC_{50} *versus* 3D7 (nM)[a]
4	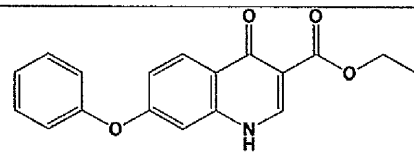	19.3
5	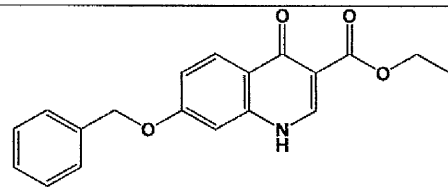	No Data[b]
6	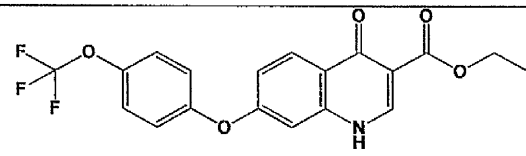	5.30
8	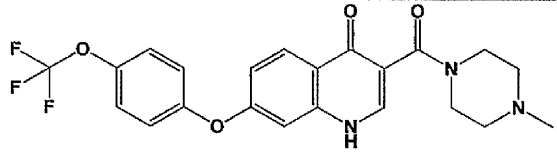	2728
9	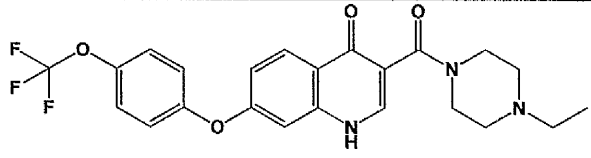	3511
10	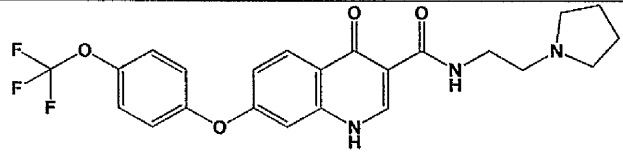	350
11	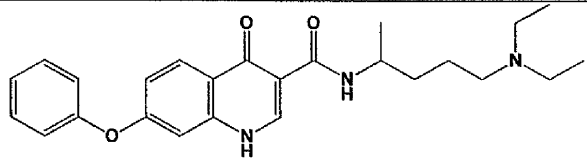	1120
12	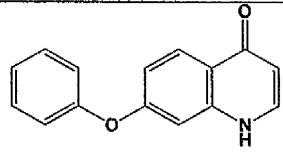	6725.0
15	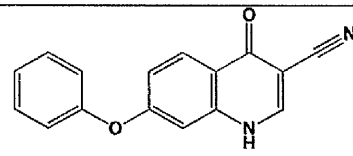	8102.5

[a] *Average value from at least 3 independent experiments.* [b] *Insufficient solubility for testing.*

Table 3.3 continued: The structures and in vitro results for the synthesised quinolone inhibitors.

Compound	Structure	IC_{50} *versus* 3D7 (nM)[a]
16	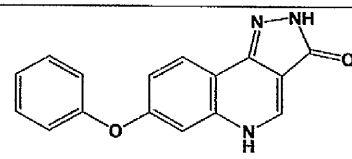	>1 μM
18	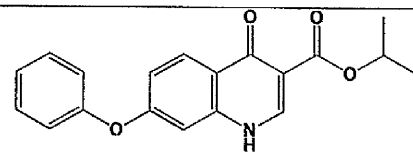	8.45
20	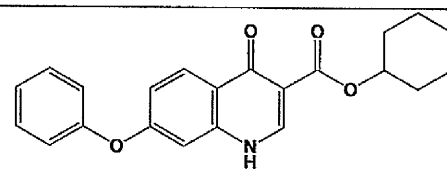	29.6
22	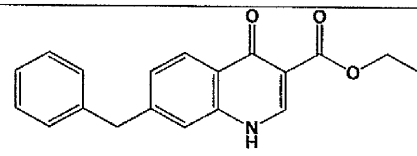	4.57
26	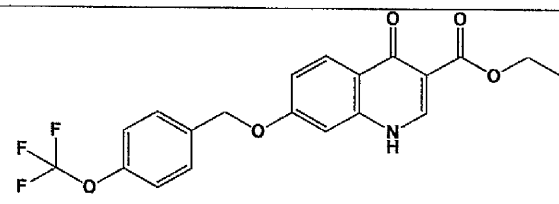	5.00
27	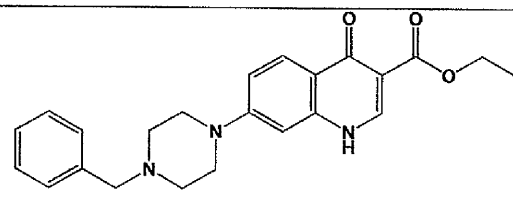	No Data[b]
32	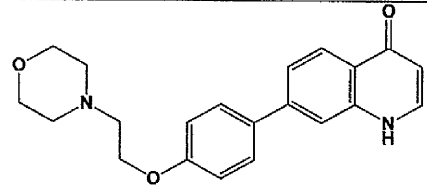	1368
39	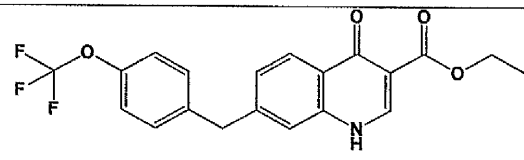	0.46

[a] *Average value from at least 3 independent experiments.* [b] *Insufficient solubility for testing.*

3.6.1 Docking of the Lead Compound

Compound **39** had the highest *in vitro* activity of the synthesised series, and therefore can be considered of most importance with regard to modelling interpretation. The compound did not score highest in the GoldScore evaluation; however it must be remembered that this figure is purely a descriptor of the strength of interaction between the protein and compound for a given docking pose, and does not account for any of the biological conditions influencing the activity of the compounds, such as membrane permeability.

The docking results for **39** are surprisingly consistent given the number of degrees of freedom afforded to the simulation. The GoldScores across the 20 distinct docking poses vary by less than 10 points (Table 3.4) and the key compound features are located in the same positions for each result, varying only in their precise alignment with the protein residues. As anticipated the compound is orientated such that the quinolone "head" occupies the Q_o binding pocket in a manner similar to that of stigmatellin (Figure 3.8).

*Table 4.4: Docking results for **39** in the Q_o site generated using GOLD 5.0.*

Docking Pose	GoldScore	Docking Pose	GoldScore
dock1	65.42	dock11	60.8198
dock2	64.4779	dock12	61.6874
dock3	64.8018	dock13	63.0822
dock4	64.8968	dock14	58.6105
dock5	57.8416	dock15	61.9741
dock6	64.3078	dock16	62.859
dock7	62.1144	dock17	60.4181
dock8	62.0518	dock18	62.6482
dock9	62.2712	dock19	62.013
dock10	64.4153	dock20	62.9725

Average GoldScore = 62.4842

Standard Deviation = 2.0090

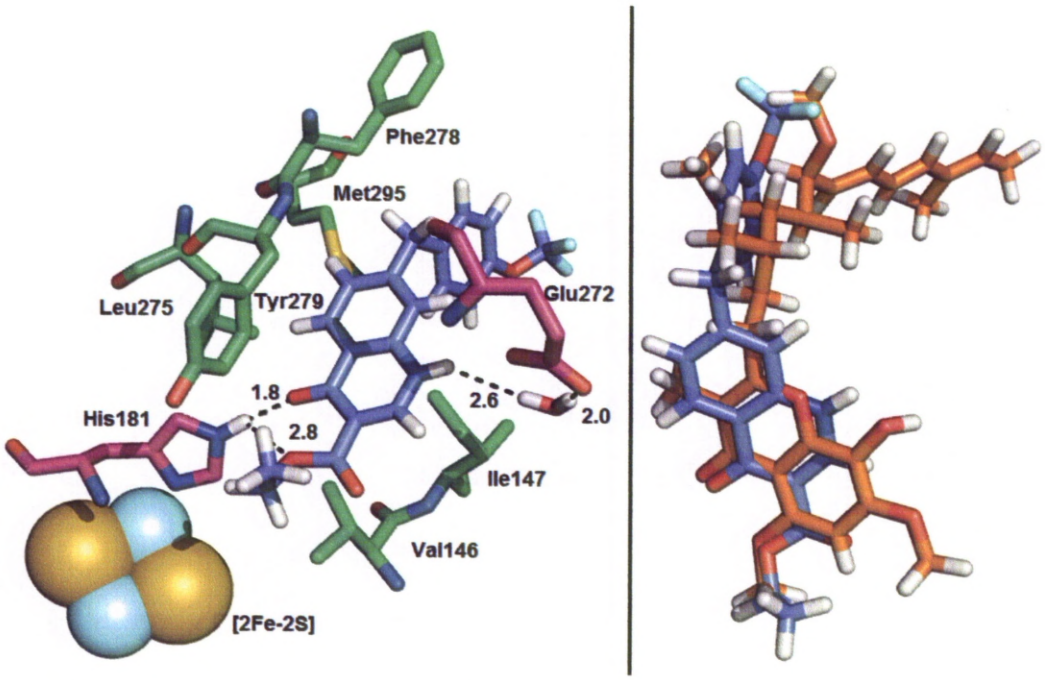

*Figure 3.8: Left; An image of the Q_o site with compound **39** docked. The key protein residues are highlighted and the [2Fe-2S] cluster is shown as blue and yellow spacefilling atoms. **39** and water molecule HOH5607 are shown in their highest scoring orientation (dock1) as blue and red capped sticks respectively. Key hydrogen bonding interactions between **39** and the protein residues are shown in black and labelled in Å. Right; an overlay of **39** (blue) on stigmatellin in its crystallised position (orange) showing the similarities in their orientations.*

The orientation of the quinolone promotes the formation of key hydrogen-bonds between the inhibitor compound and amino acid residues Glu272 and His181. The quinolone N1 hydrogen bonds through water HOH5607 to the glutamate while the C4 carbonyl and the alkoxy oxygen of the C3 ester group simultaneously interact with the protonated imidazole $^{\varepsilon}N$ atom of the ISP bound histidine (Figure 3.9). This provision of both H-bond donor and acceptor sites mimics the semiquinone transition state of the endogenous ligands during the bc_1 catalytic cycle[47, 49, 51, 145] and goes someway to explaining the efficacy of these quinolones as inhibitors. Additionally, the consistency of the results for compound **39** implies that the orientation of the compound is very stable and consequently the turnover of the compound in the Q_o site could be relatively slow, explaining the observed levels of potency.

3.6.2 The Effect of Different Linkers

Comparison of the docking results for **39** with those of **6** shows the influence of a phenoxy linker compared to the methylene linker of the lead compound. While the GoldScores again show only a small range (Table 3.5), the docking poses produced for **6** show much more variation. Fifteen of the produced poses, including dock 17 the highest scoring pose (Figure 3.9), have the same basic orientation as the docking poses produced for **39**.

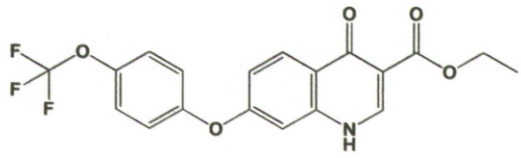

6

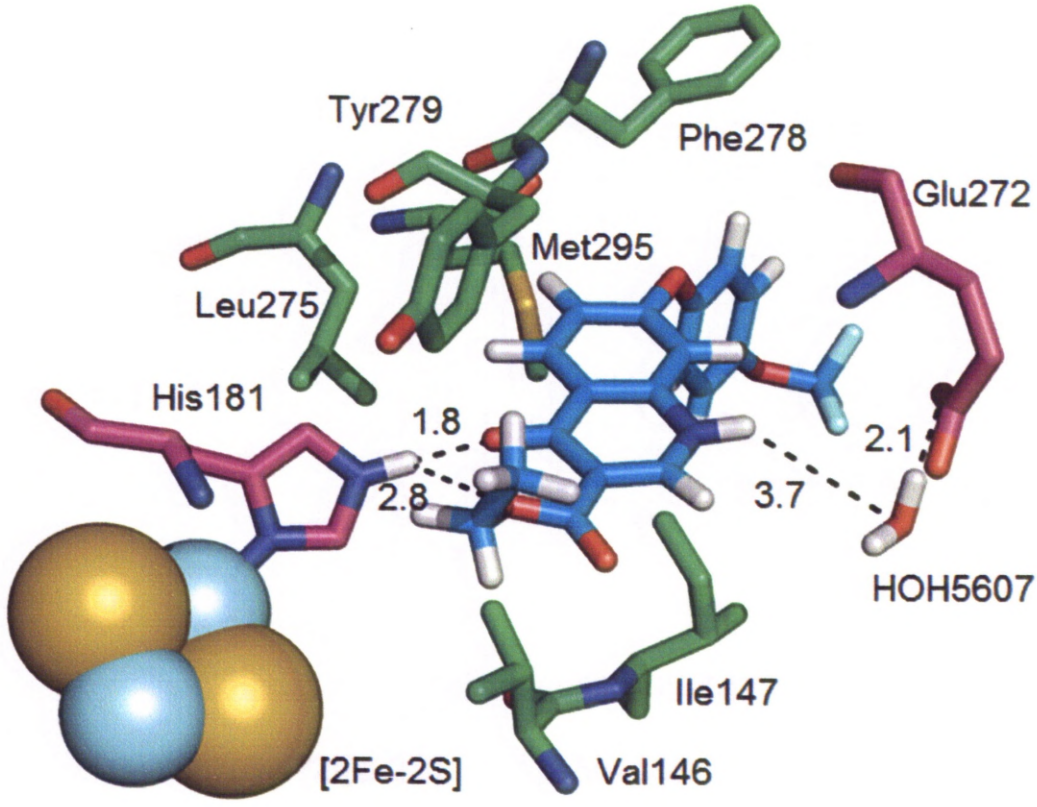

*Figure 3.9: Image of the Q_o site showing the highest scoring docking pose for **6** (dock17). The key protein residues are highlighted and the [2Fe-2S] cluster is shown as blue and yellow spacefilling atoms. Compound **6** and water molecule HOH5607 are shown as cyan and red capped sticks respectively. Key hydrogen bonding interactions between **6** and the protein residues are shown in black and labelled in Å.*

Table 3.5: Docking results for compound 6.

Docking Pose	GoldScore	Docking Pose	GoldScore
dock1	63.5541	dock11	63.6103
dock2	61.673	dock12	61.4812
dock3	61.9207	dock13	63.567
dock4	59.4241	dock14	60.084
dock5	62.1515	dock15	62.3768
dock6	62.8965	dock16	65.0524
dock7	58.9594	dock17	65.5616
dock8	61.258	dock18	60.375
dock9	63.2853	dock19	59.8731
dock10	59.8889	dock20	62.4021

Average GoldScore = 61.9698

Standard Deviation = 1.8401

While the orientation of the key chemical components may be the same, the position of the phenyl ring shows much more variation for **6** than was observed for **39**. This suggests that it is less well tolerated in the hydrophobic channel which would account for the observed drop in potency. A possible reason for this is visible in the modelled docking poses; when the inhibitors are docked with the quinolone head group in the active site, the bridging atoms are situated between leucine (Leu275), phenylalanine (Phe278) and tyrosine (Tyr279) residues in the hydrophobic channel (Figure 3.10). The methylene linker of **39** will be stable in this position; however, the proximity of these hydrophobic amino acid side-chains to the lone pairs of the phenoxy linker in compound **6** will have a destabilising effect on the binding of the inhibitor leading to reduced occupancy of the active site and consequently reduced potency compared to the lead compound.

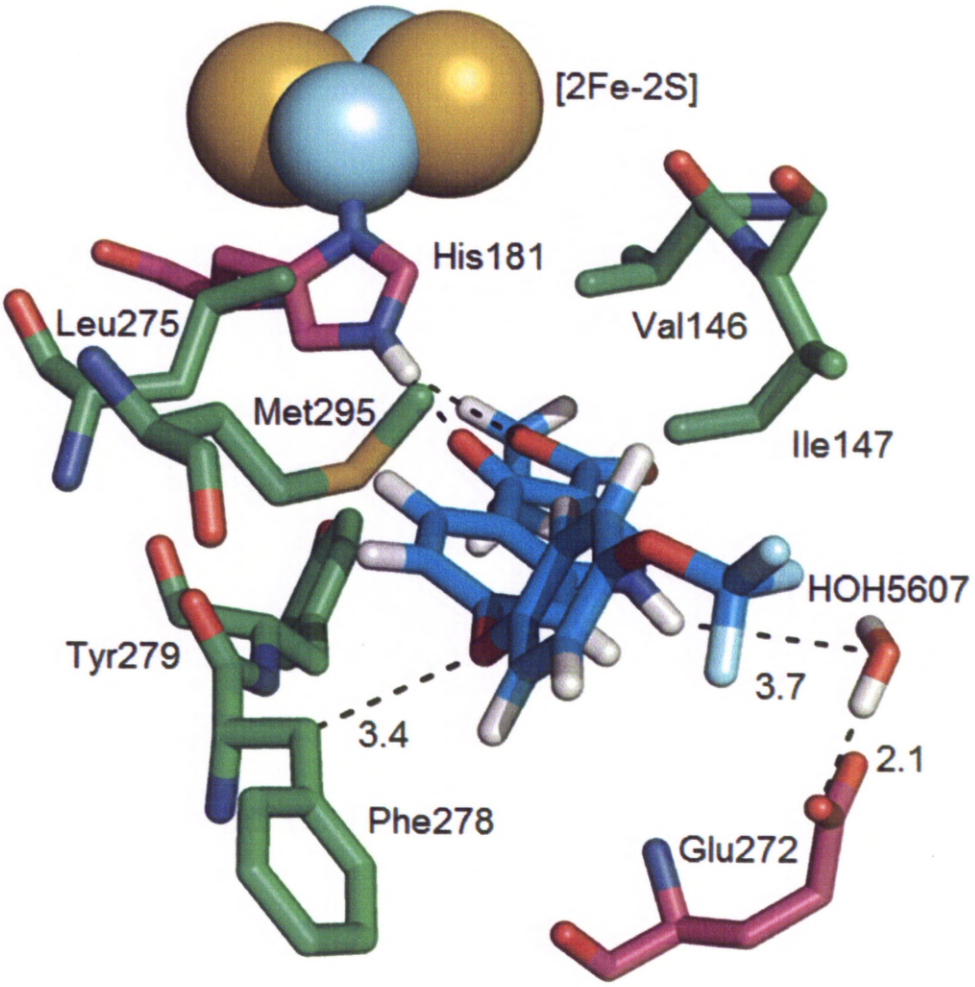

*Figure 3.10: View of compound **6** from the cytosolic end of the hydrophobic channel with the key residues forming the walls of the channel labeled, highlighting the proximity (3.4 Å) of the linker to Phe278.*

The same relationship is observed for the benzyloxy linked analogue **26**; in this case even more variation is seen in the docking poses and the GoldScores obtained cover a much wider range (Table 3.6).

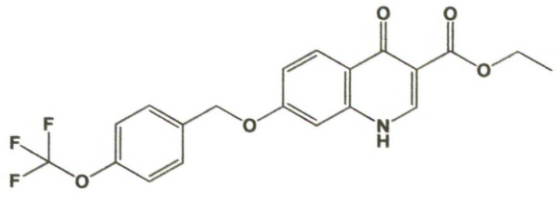

26

Table 3.6: Docking results for compound 26.

Docking Pose	GoldScore	Docking Pose	GoldScore
dock1	56.9194	dock11	62.19
dock2	54.9984	dock12	55.0078
dock3	55.6126	dock13	61.7178
dock4	53.678	dock14	64.4694
dock5	57.1042	dock15	56.7163
dock6	63.1699	dock16	51.7466
dock7	57.5033	dock17	57.5456
dock8	53.4713	dock18	57.6955
dock9	57.2041	dock19	54.8825
dock10	59.8253	dock20	54.0776

Average GoldScore = 57.2768

Standard Deviation = 3.4388

The highest scoring poses maintain the same position as the lead with the quinolone ester groups forming hydrogen bonds with amino acid residues Glu272 and His181 (Figure 3.11). However, the orientation of the "tail" in the hydrophobic channel shows great variation as the additional atom in the linker increases the flexibility of the system as the docking simulation seeks to accommodate the lone pairs of the benzyloxy oxygen atom between the hydrophobic residues lining the channel (Figure 3.12).

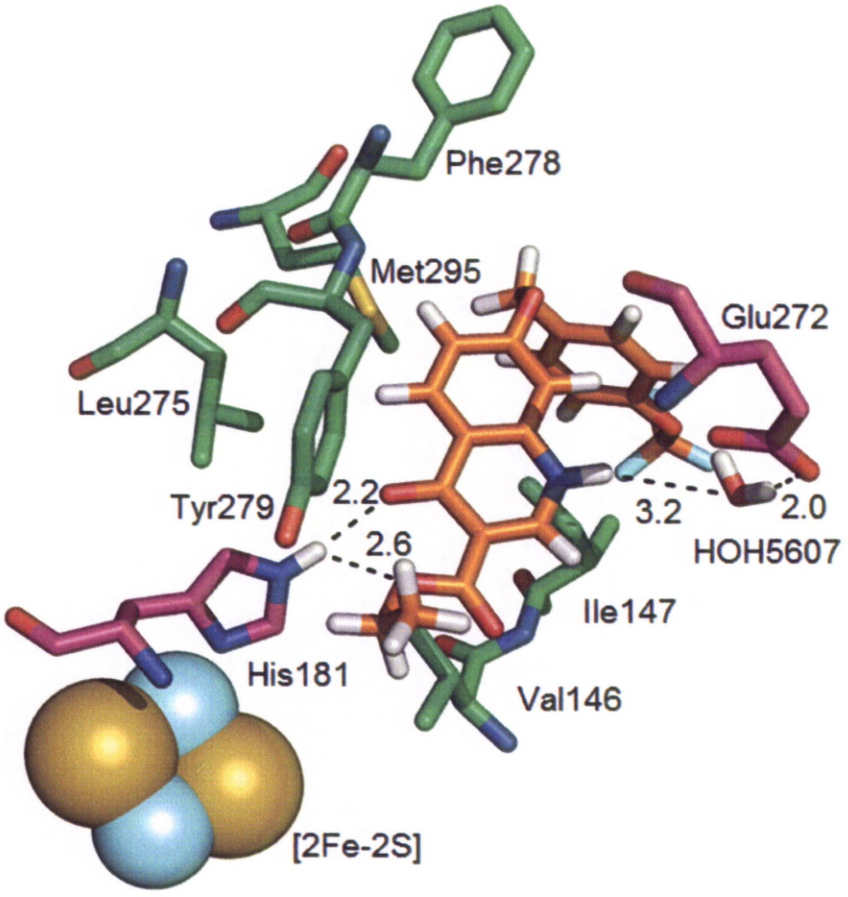

*Figure 3.11: The highest scoring pose for compound **26** (dock 14) in the Q_o active site. The key protein residues are highlighted and the [2Fe-2S] cluster is shown as blue and yellow spacefilling atoms. Compound **26** and water molecule HOH5607 are shown as orange and red capped sticks respectively with key H-bond interactions indicated in black and labeled in Å.*

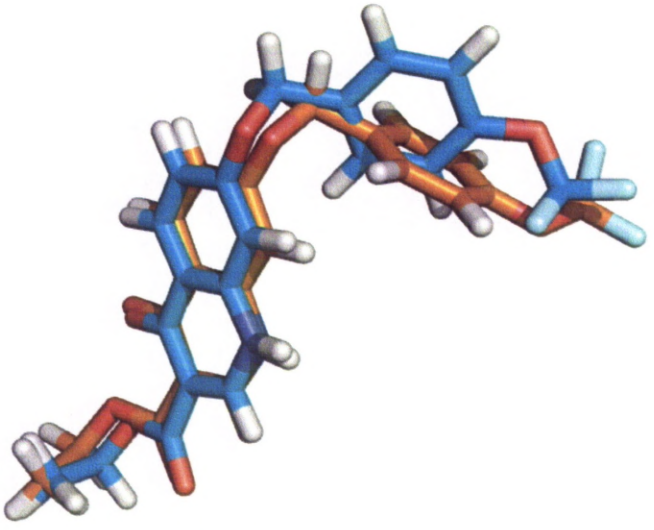

*Figure 3.12: Overlay of compound **26** dock 14 (orange) and dock 7 (cyan) showing variation in benzyloxy "tail" position arising from the increased linker flexibility.*

3.6.3 Heterocyclic "Tails"

While the piperazine containing compound **27** had proved too insoluble to test biologically, it was still interesting to dock the compound *in silico* in order to observe the interactions between the heterocyclic portion and the protein. As with the previous analogues the highest scoring docking pose positioned the quinolone head between His181 and Glu272. However, the curved shape of the hydrophobic channel and the relatively linear, inflexible structure of the compound, arising from the direct link between the quinolone C7 and the piperazine nitrogen, appears to force the quinolone head further into the active site than for the previously discussed compounds (Figure 3.13). This disrupts the hydrogen bonds with the amino acids, extending the distances and consequently weakening the interactions.

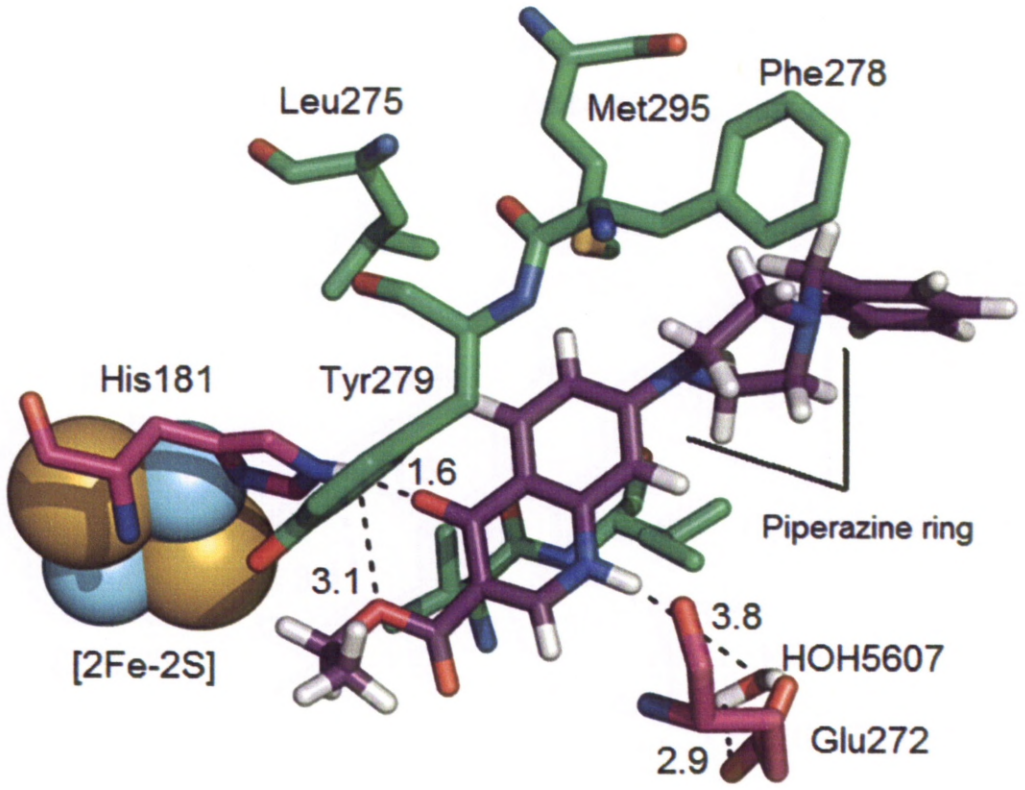

Figure 3.13: The highest scoring pose for compound **27** *(dock 6) in the Q_o active site. The key protein residues are highlighted and the [2Fe-2S] cluster is shown as blue and yellow spacefilling atoms. Compound* **27** *and water molecule HOH5607 are shown as purple and red capped sticks respectively with key H-bond interactions indicated in black and labeled in Å. Note the twist of the piperazine ring resulting from the proximity to Phe278.*

The piperazine ring also appears to be twisted out of the low energy boat conformer by the interactions with the hydrophobic residues forming the

walls of the channel leading to the active site, in particular Phe278. This weakening of the H-bonding system, in combination with the unfavourable interactions observed in the hydrophobic channel suggests that had **27** proved more soluble it is unlikely to have demonstrated potent activity.

The terminal morpholine compound **32** in contrast may well have proved a potent derivative had the desired ethyl ester been successfully isolated. Despite the lack of an ethyl ester group the highest scoring orientations for **32** correspond well with those of **39**, the lead. The quinolone head occupies the space between Glu272 and His181, although without the additional H-bond afforded by the ester group the position of **32** is much closer to Glu272 than is observed for the other analogues and may be hydrogen bonded directly to the glutamic acid residue rather than through a water mediated bond. This position may also be due in part to the rigidity of the biphenyl type structure at the quinolone C7 (Figure 3.14).

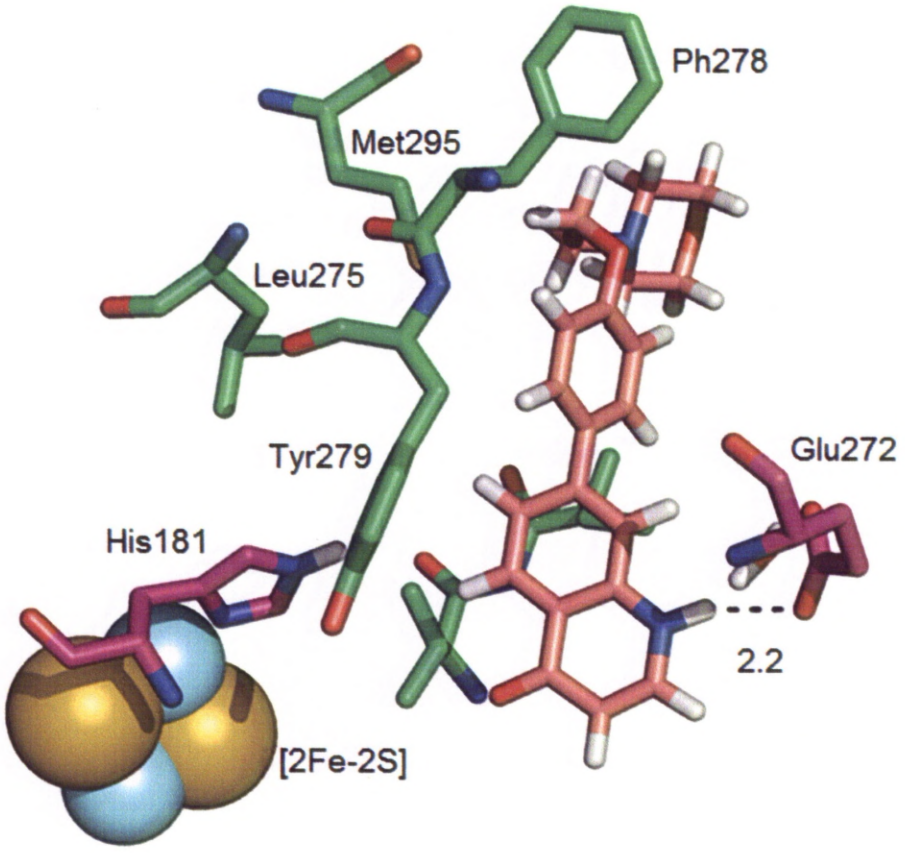

*Figure 3.14: The highest scoring pose for compound **32** (dock 11) in the Q_o active site. The key protein residues are highlighted and the [2Fe-2S] cluster is shown as blue and yellow spacefilling atoms. Compound **32** and water molecule HOH5607 are shown as pink and red capped sticks respectively with key H-bond interactions indicated in black and labeled in Å.*

Unlike the piperazine "tail" of **27,** the long flexible ethyloxy linker of **32** extends the terminal morpholine beyond the narrowest section of the hydrophobic channel formed by Phe278, Tyr279 and Leu275 that was the root cause of the unfavourable interactions identified for both **27** and analogues **6** and **26** discussed earlier (Figure 3.15). This may mean that compounds similar to **32** are better tolerated than some of the other analogues discussed, suggesting that compounds of this type may be worth further investigation in the future.

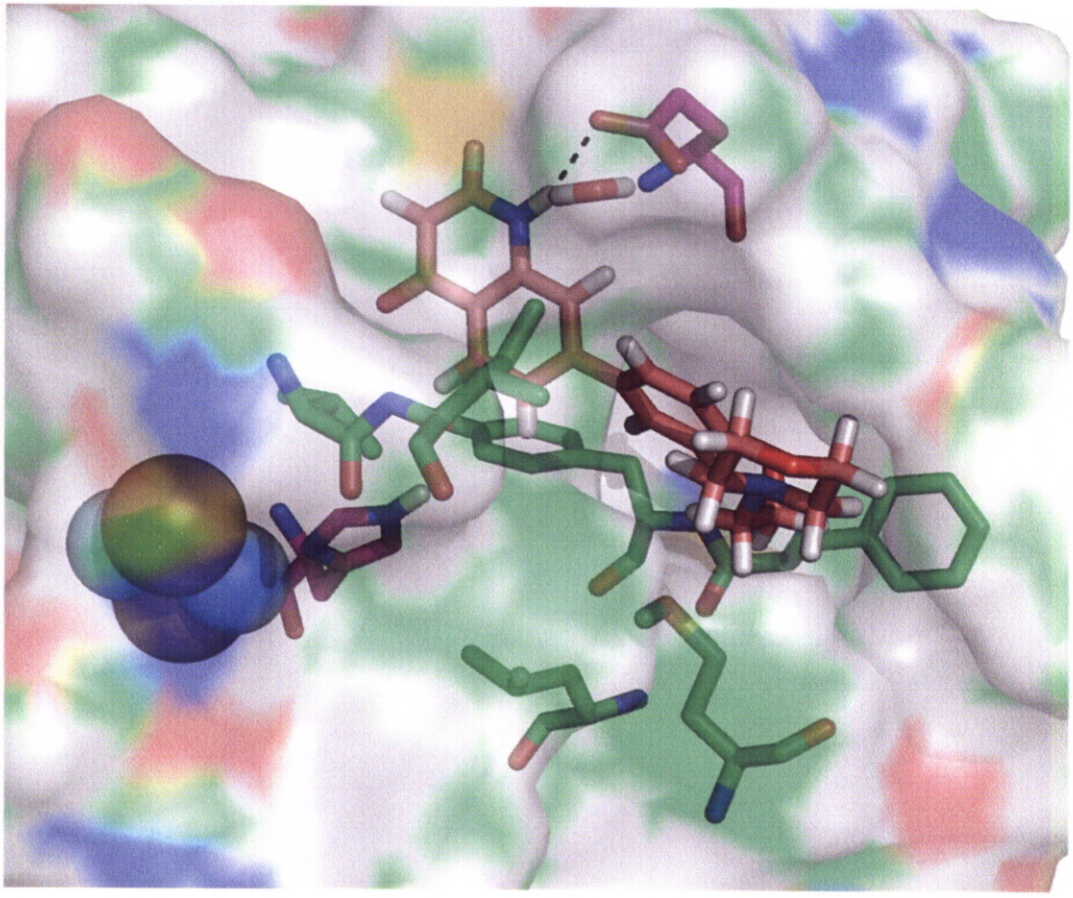

*Figure 3.15: Compound **32** viewed from the opening of the hydrophobic channel with the solvent accessible surface of the protein shown in order to highlight how the ethyloxy linker extends the morpholine tail beyond the hydrophobic region, the colours of the surface indicate the nature of the atom forming the surface at a given point, white indicates hydrogen, green = carbon, red = oxygen and blue = nitrogen.*

3.6.4 Increasing Potency with the Trifuoromethoxy Group

While the effects of the linker on potency have been relatively simple to explain by visual comparison of the docking poses for each compound, the increase in potency afforded by the inclusion of a trifluoromethoxy moiety is

harder to rationalise. This simple alteration leads to a 4-fold increase in potency for the phenoxy compounds **4** *versus* **6** and a 10-fold increase for the methylene linked compounds **22** *versus* **39** and yet the docking poses produced for the compounds by the simulation show only a slight variation in the position of the phenyl ring (Figure 3.16). The most logical explanation is that change in position brought about by the trifluoromethoxy group has a stabilising effect on the interactions between the phenyl ring and the residues of the hydrophobic channel leading to increased occupancy of the active site and consequently improved biological activity.

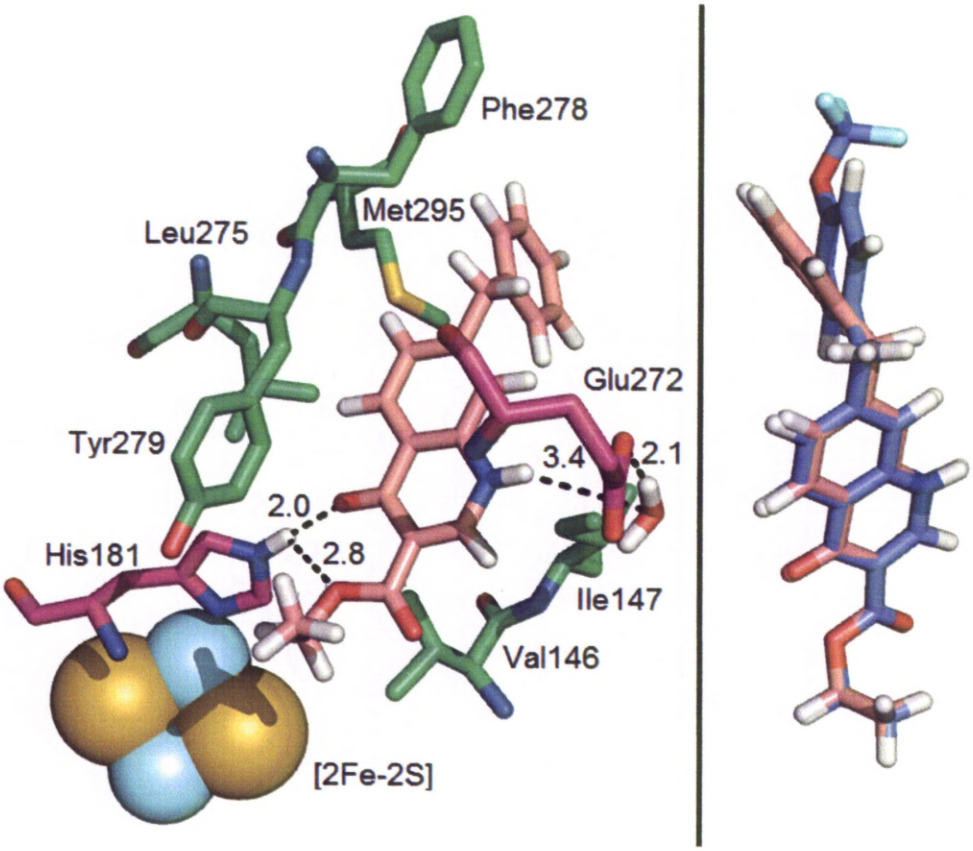

Figure 3.16: Left; An image of the Q_o site with compound **22** *docked. The key protein residues are highlighted and the [2Fe-2S] cluster is shown as blue and yellow spacefilling atoms.* **22** *and water molecule HOH5607 are shown in their highest scoring orientation as pink and red capped sticks respectively. Key hydrogen bonding interactions between* **22** *and the protein residues are shown in black and labelled in Å. Right; Comparing the highest scoring orientations for compounds* **22** *(pink) and* **39** *(blue), showing the change in the phenyl ring position arising from the presence of a trifluoromethoxy group.*

3.6.5 Explaining the Increased Parasite Activity of Isopropyl Esters

In addition to the ethyl ester of the lead compound and initial hits, a number of alternative esters were synthesised and two were tested biologically; an isopropyl ester **18** and a cyclohexyl ester **20**. Both compounds showed reasonable potency *in vitro* with the isopropyl analogue **18** showing a slight improvement in activity against 3D7, 8.45 nM, compared to the corresponding ethyl ester **4**, 19.3 nM.

When modelled **18** adopts the same basic binding position as the ethyl ester compounds, forming hydrogen bonds with Glu272 and His181 (Figure 3.17) and giving no immediate indication of why the activity should be any higher than that of compound **4**.

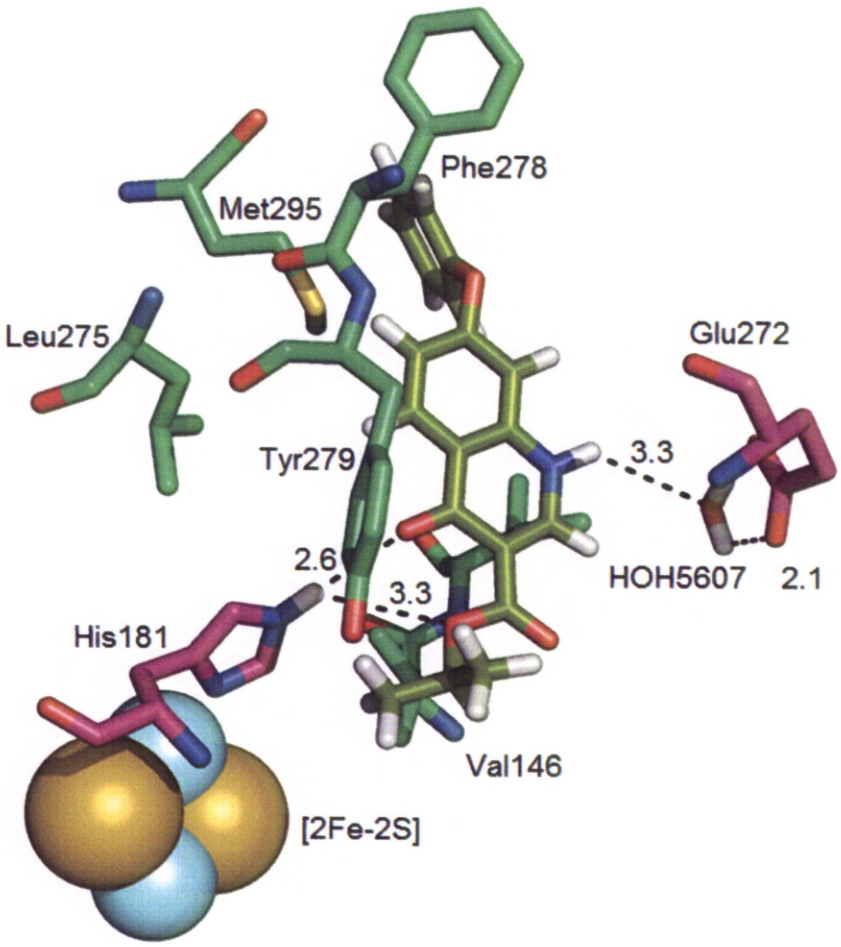

*Figure 3.17: Showing the predicted orientation of **18** in the Q_o active site. The key protein residues are highlighted and the [2Fe-2S] cluster is shown as blue and yellow spacefilling atoms. **18** and water molecule HOH5607 are shown in their highest scoring orientation as lime green and red capped sticks respectively. Key hydrogen bonding interactions between **18** and the protein residues are shown in black and labelled in Å.*

Showing the solvent accessible surface of the protein residues reveals a possible explanation however. With the surface visible it becomes clear that the isopropyl ester fits very neatly into the active site (Figure 3.18) holding the quinolone head equidistant from the key His181 and Glu272 residues, suggesting that the slight increase in activity may simply be the result of longer active site occupancy times.

The modelling also reveals why the isopropyl group may potentially increase selectivity for the parasite protein over the mammalian protein. While the valine and isoleucine residues that line that region of the Q_o pocket are conserved between the species, the residues close by in the sequence are not so well conserved, for example leucine (Leu149) in the yeast and parasite protein becomes phenylalanine (Phe149) in bovine bc_1. These alterations make the pocket in the bovine protein slightly more restrictive meaning the isopropyl ester of **18** is no longer as well tolerated and giving rise to the observed selectivity.

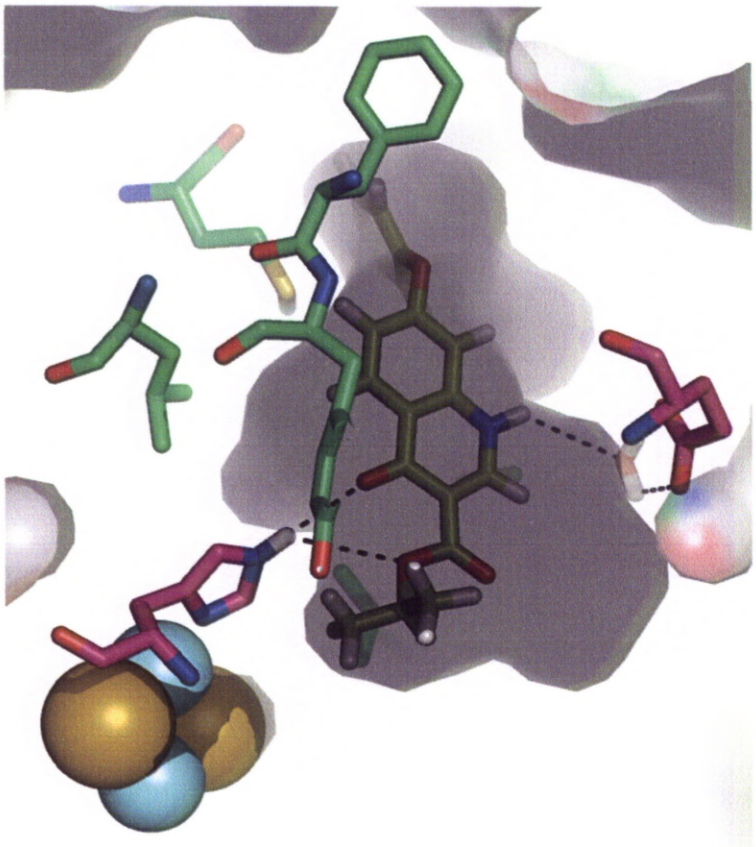

*Figure 3.18: Showing **18** docked in the Q_o active site; the shape of the Q_o region is indicated in grey using the solvent accessible surface of the constituent amino acids, revealing the tight fit of the inhibitor compound in the active site.*

3.6.6 Explaining the Poor Performance of the Amide Compounds

The GoldScores obtained for the amide compounds would, in isolation, suggest that the compounds were highly potent as several of them are considerably higher than the results for the lead (Table 3.7).

*Table 3.7: GoldScores and in vitro results for compound **39** and the amide compounds.*

Compound	IC_{50} *versus* 3D7 (nM)[a]	Highest GoldScore	Average GoldScore
39	0.46	65.42	62.48
8	2728	66.22	60.81
9	3511	69.50	63.91
10	350	70.46	62.51
11	1120	70.74	64.89

[a] *Average value from at least 3 independent experiments.*

However, GoldScore predicts the strength of binding, not how efficacious a compound is.[136] Examination of the binding poses revealed the reason for the low activity compared to the ester compounds. The bulky amides synthesised are not accommodated in the restrictive Q_o site and so the highest scoring poses have the compounds docked in a reversed configuration compared to the esters in which the phenyl ring portion of the compounds occupies the active site and the amide group extends out along the hydrophobic channel (Figure 3.19).

These docking poses are not conducive to good activity for a number of reasons; only one hydrogen bond interaction with the amino acids in the active site is possible (Figure 3.19) and the polar amide groups will not be well tolerated by the hydrophobic residues lining the channel. These factors mean that the amide analogues would be rapidly turned over by the enzyme resulting in no significant inhibition of the Q cycle.

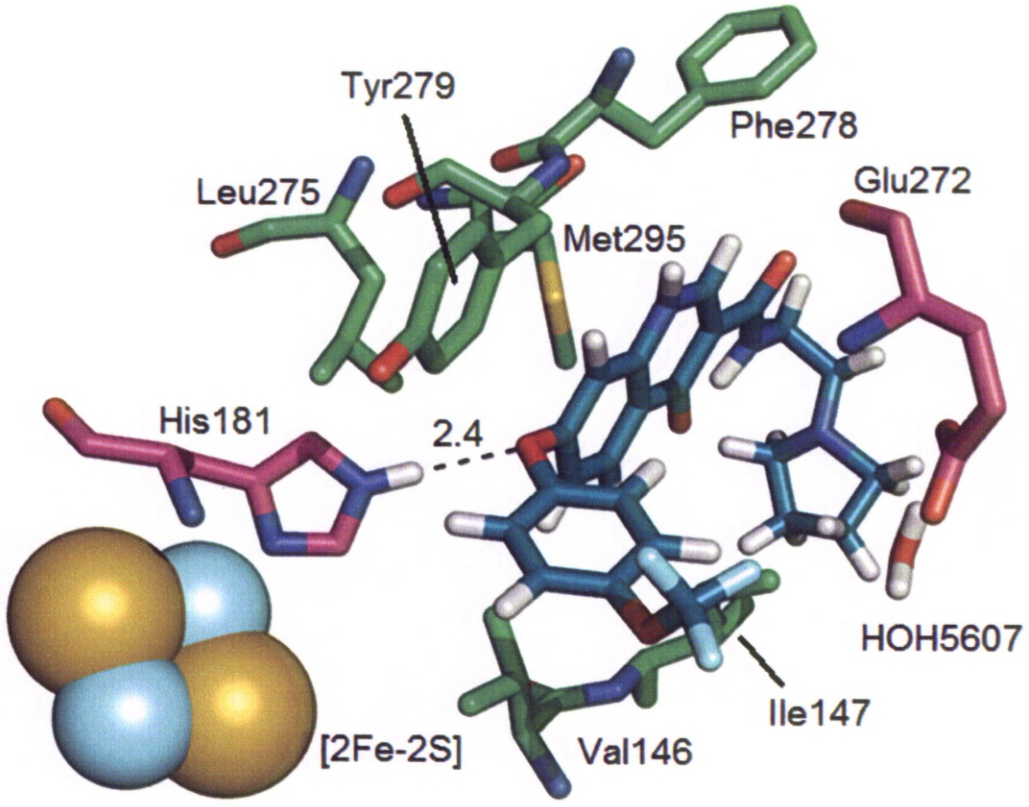

*Figure 3.19: Amide analogue **10** (teal) docked in the Q_o active site in its highest scoring pose with the potential hydrogen bond interaction between His181 and the phenoxy linker highlighted in black and labeled in Å. The key protein residues are highlighted and the [2Fe-2S] cluster is shown as blue and yellow spacefilling atoms.*

3.6.7 The Decarboxylated, Nitrile and Pyrazolo Analogues

The functionality of these three analogues, **12**, **15** and **16**, is very different, both to each other and the rest of the synthesised library. However, the results in terms of biological activity are similar.

In the docking simulation the decarboxylated compound **12** docks in a manner completely different to any of the poses observed for the rest of the library, as the lack of functionality at C3 allows the molecule to sit much deeper in the active site than any of the other analogues (Figure 3.20).

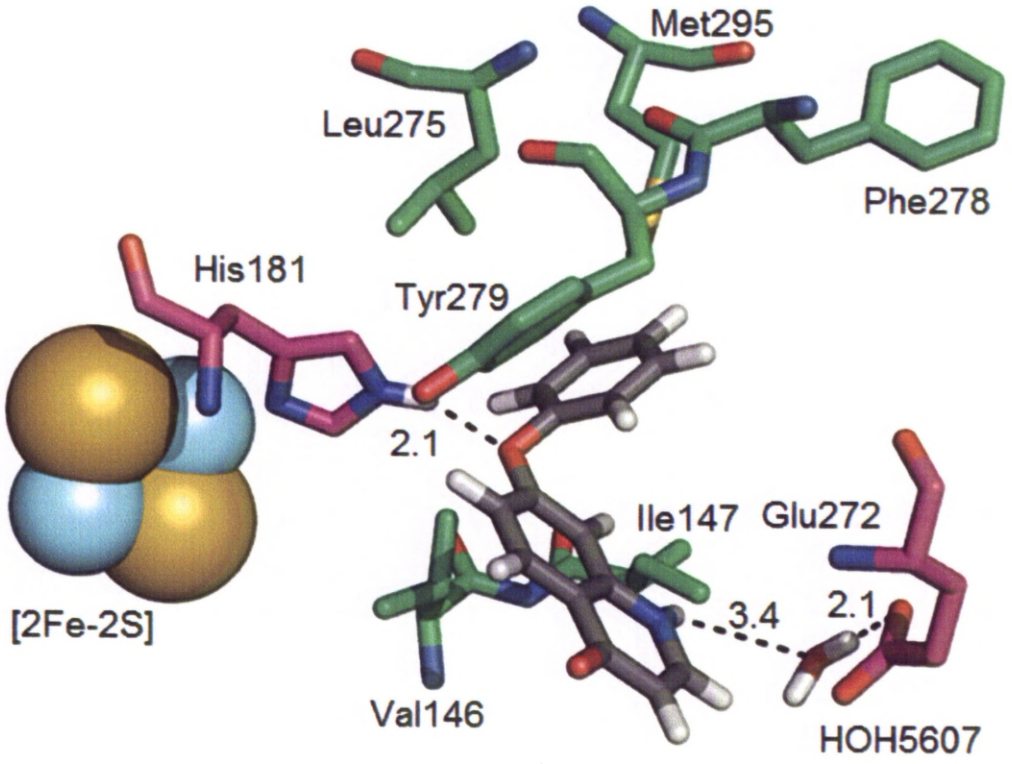

*Figure 3.20: The highest scoring docking pose for decarboxylated compound **12** in the Q_o active site with the postulated hydrogen bonding interactions with His181 and Glu272 indicated in black and labeled in Å. The key protein residues are highlighted and the [2Fe-2S] cluster is shown as blue and yellow spacefilling atoms.*

As a result of this increased penetration into the Q_o active site the compound appears to form a hydrogen bond interaction with His181 through the phenoxy linker oxygen while simultaneously interacting with Glu272 through the quinolone NH. The reduced activity observed for this species is probably a result of these hydrogen bonds being relatively weak interactions.

The 3-nitrile analogue **15** is predicted to dock in broadly the same manner as the more active ester species (Figure 3.21). In order for a hydrogen bond to form between the nitrile nitrogen and His181 however the quinolone head is moved away from Glu272 (4.4 Å) such that a strong water mediated bond from the quinolone NH is no longer predicted.

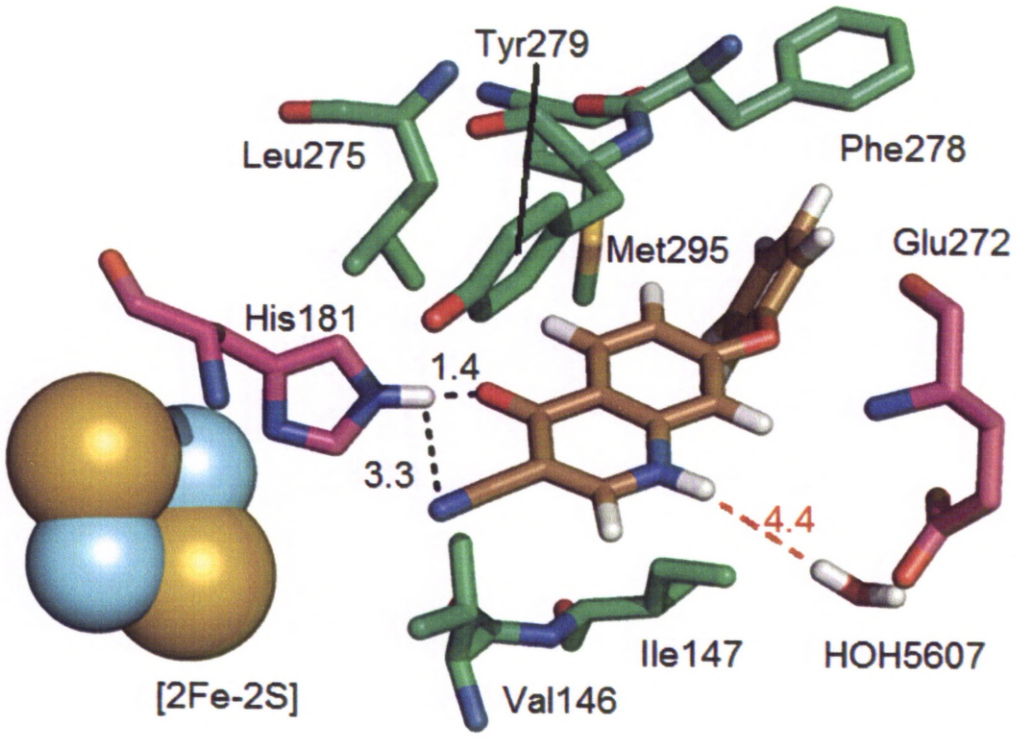

*Figure 3.21: 3-Nitrile compound **15** in the Q_o active site with the postulated hydrogen bonding interactions with His181 indicated in black and labeled in Å. The key protein residues are highlighted and the [2Fe-2S] cluster is shown as blue and yellow spacefilling atoms. The possible weak interaction with HOH5607 is indicated in red.*

The pyrazolo compound **16** also binds in a manner completely different to the docking poses observed for the rest of the synthesised compounds. The addition of the third ring in the head group appears to result in inversion of the quinolone head relative to the most active configurations (Figure 3.22).

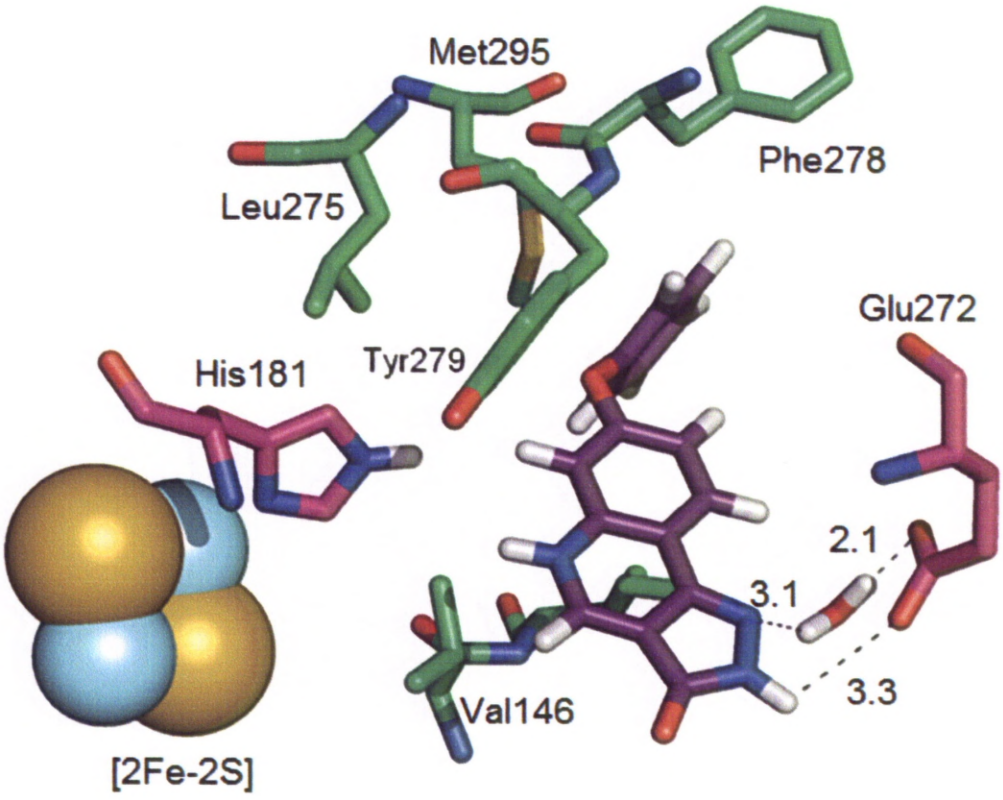

*Figure 3.22: Tricyclic derivative **16** in the Q_o active site with the postulated hydrogen bond interactions indicated in black and labeled in Å. The key protein residues are highlighted and the [2Fe-2S] cluster is shown as blue and yellow spacefilling atoms.*

This inversion appears to promote the formation of two hydrogen bonds to Glu272, a water mediated bong from the imine type nitrogen of the ring and a direct interaction between the amine nitrogen and the amino acid. This position results in the phenoxy linker being brought into close proximity to a hydrophobic tyrosine residue (Tyr279) however, and is unlikely to be well tolerated.

The reduced biological activity for all three of these compounds therefore appears to be the result of weakened interactions with the key residues in the active site in turn resulting in increased turnover of the compounds reducing their inhibitory affect.

3.7 Modelling Related Series

In parallel to the discussed library of compounds, two additional libraries were synthesised by other members of the O'Neill research group for comparison with the synthesised 7-quinolones.[129]

3.7.1 Modelling of 6-Substituted Analogues

A library of ten compounds corresponding to ten of the previously discussed inhibitors was synthesised with the aromatic substituent and linker moved from the 7-position to the 6-position (Table 3.8). With the exception of the 3-unsubstituted analogue **12**, when tested *in vitro* the 6-substituted compounds were all between 8-fold and 100-fold less active than they're corresponding 7-substituted analogue. In the case of the lead compound **39**, the associated 6-substituted **39-SL** exhibited a greater than 300-fold drop in potency against 3D7 *P.falciparum* parasites.

Table 3.8: In vitro results for the 6-series and the equivalent 7-series compounds.

Compound	Structure	IC_{50} *versus* 3D7 (nM)[a]
4	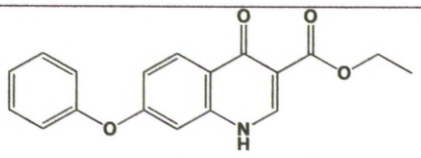	19.3
4-SL	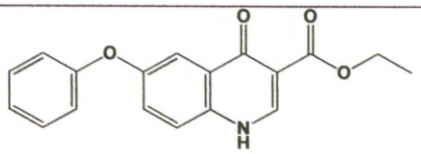	164.0
5	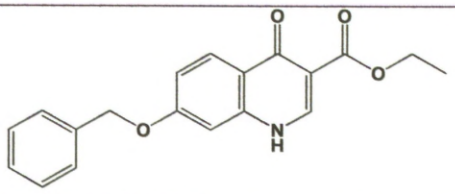	No Data[b]
5-SL	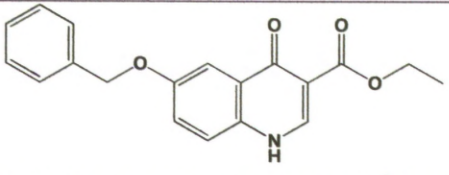	No Data[b]

[a] *Average value from at least 3 independent experiments.* [b] *Insufficient solubility for testing.*

Table 3.8 continued: In vitro results for the 6-series and the equivalent 7-series compounds.

Compound	Structure	IC_{50} *versus* 3D7 (nM)[a]
6	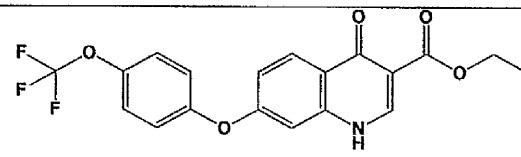	5.30
6-SL	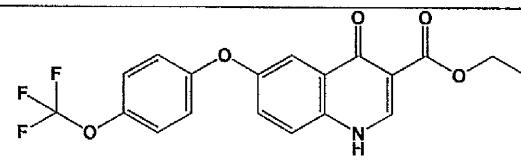	229.8
12	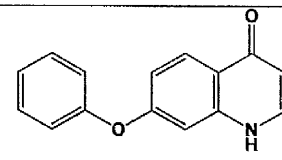	6725.0
12-SL	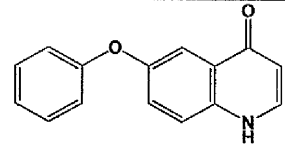	4698.0
15	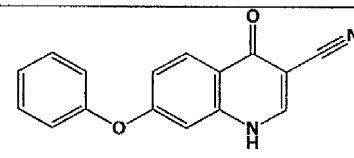	8102.5
15-SL	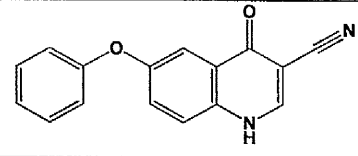	> 10 µM
18	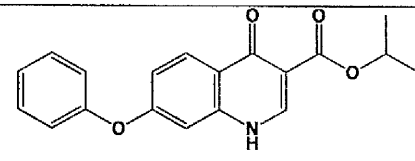	8.45
18-SL	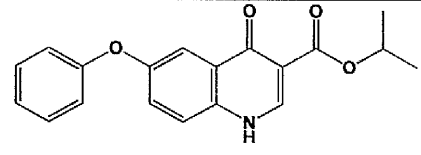	183.9
20	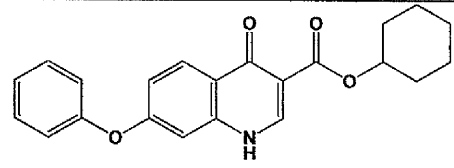	29.6
20-SL	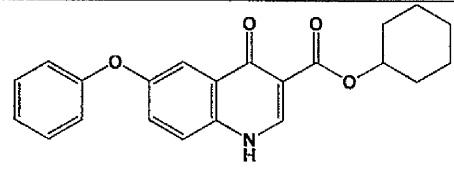	1820.4

[a] *Average value from at least 3 independent experiments.* [b] *Insufficient solubility for testing.*

Table 3.8 continued: In vitro results for the 6-series and the equivalent 7-series compounds.

Compound	Structure	IC_{50} *versus* 3D7 (nM)[a]
22	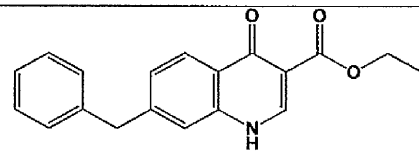	4.57
22-SL	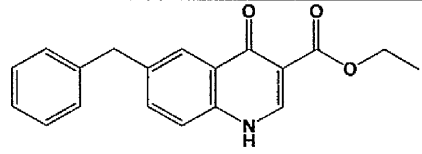	40.4
26	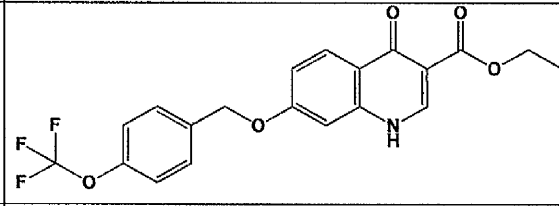	5.00
26-SL	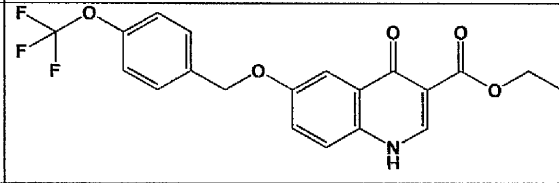	674.8
39	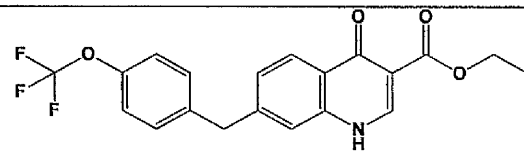	0.46
39-SL	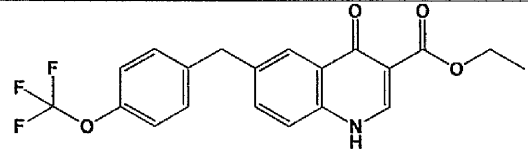	141.5

[a] *Average value from at least 3 independent experiments.*

The 6-series analogues were modelled *in silico* using the same method as previously discussed, using GOLD 5.0[136, 142] to run a docking simulation using the crystal structure of yeast bc_1[43] with flexibility introduced at the Val146, Ile147 and Glu272 residues.[54] Examination of the docking poses in comparison to the 7-series compounds reveals that the observed drop in biological potency is due to an inversion of the quinolone ring in the active site.

For the majority of the 6-substituted compounds the polar quinolone "head" occupies the binding pocket between His 181 and Glu272 and the aromatic "tail" portion extends into the hydrophobic channel as was observed

for the more potent 7-substituted compounds. However due to the curvature of the hydrophobic channel[64, 65] and the relocation of the flexible linker groups, the quinolones of the 6-substituted compounds are now orientated such that the quinolone nitrogen is adjacent to His181 and the 4-carbonyl moiety is pointing towards Glu272 (Figure 3.23).

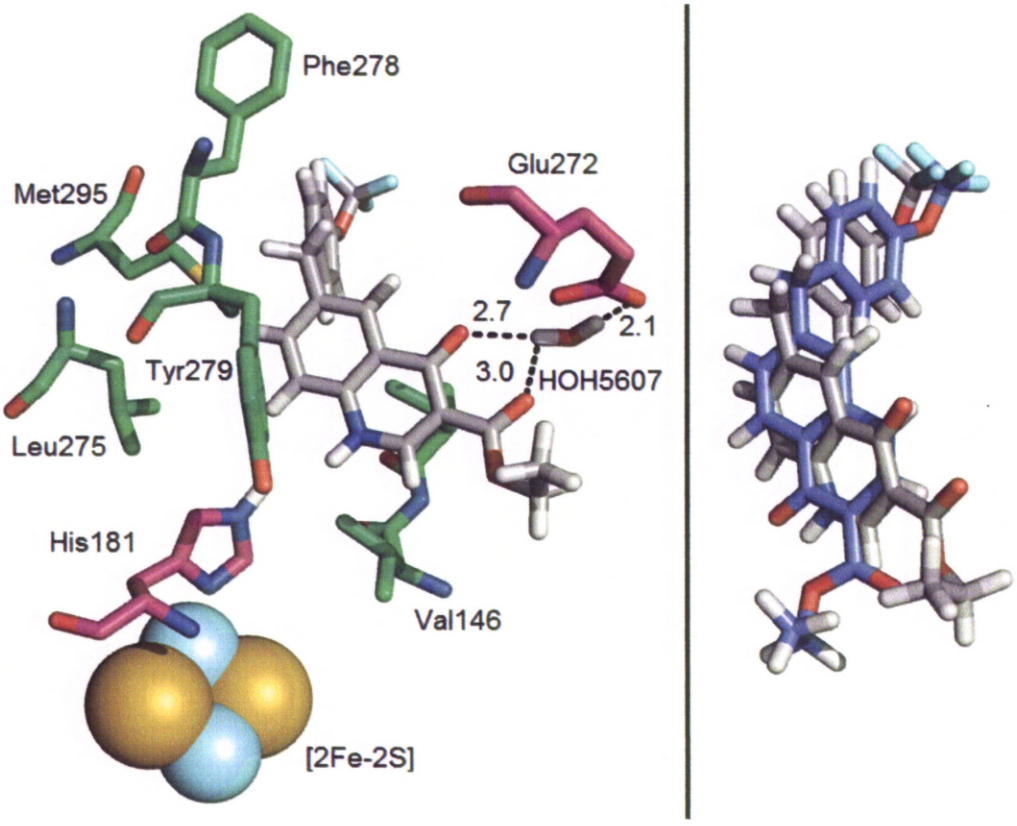

*Figure 3.23: Left; an image of the Q_o site with compound **39-SL** docked. The key protein residues are highlighted and the [2Fe-2S] cluster is shown as blue and yellow spacefilling atoms. **39-SL** and water molecule HOH5607 are shown in their highest scoring orientation as silver and red capped sticks respectively. Key hydrogen bonding interactions between **39-SL** and the protein residues are shown in black and labelled in Å. Right; the highest scoring poses for **39** (blue) and **39-SL** (silver) are overlapped showing the relative inversion of the quinolone head group.*

The net result of this rotation within the active site is a reduced ability to hydrogen bond; where as the 7-substituted compounds can form three separate H-bonds to the key protein residues, the 6-substituted analogues can only form two such interactions through the carbonyl oxygens and water molecule HOH5607 (Figure 3.24).

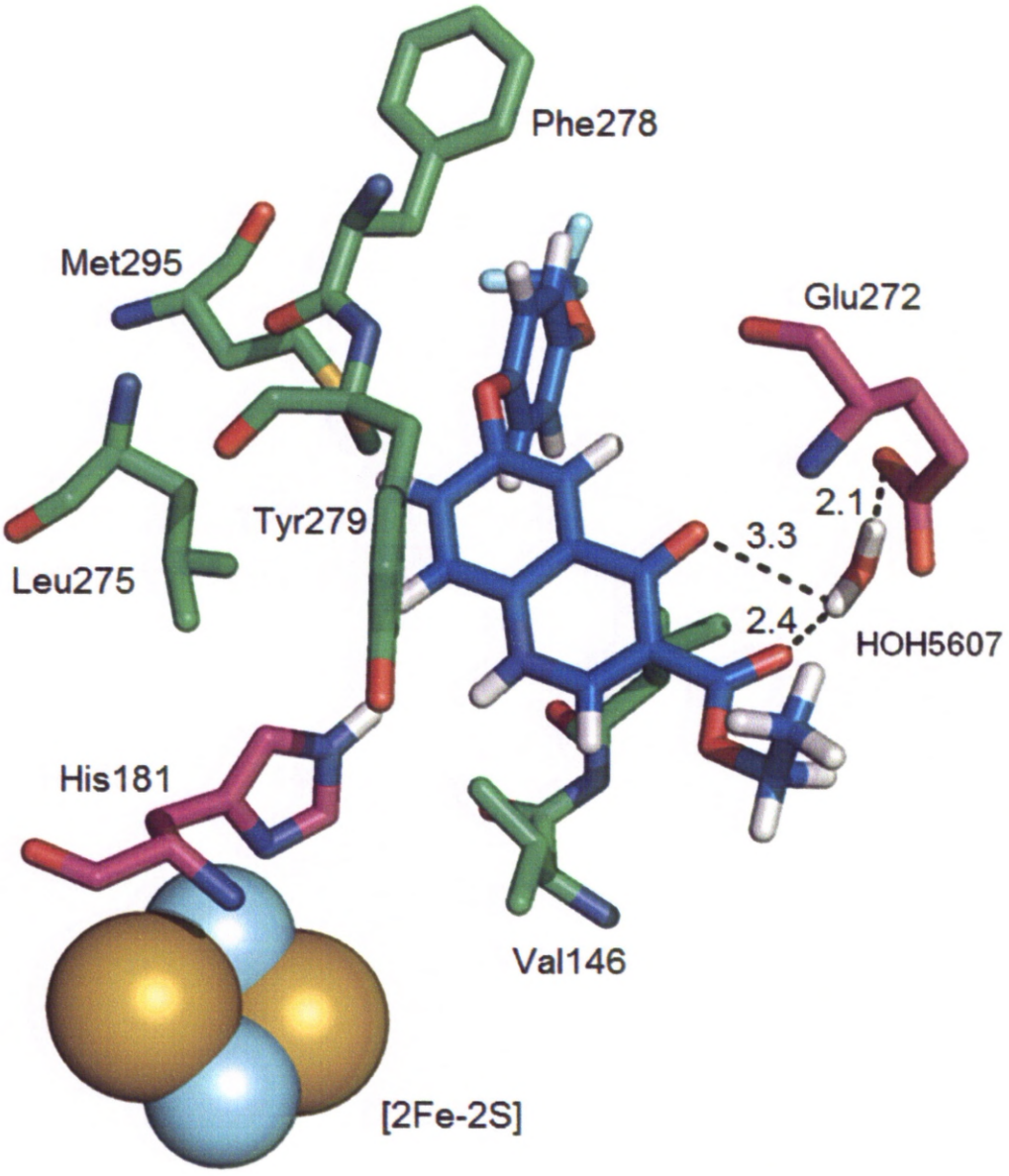

Figure 3.24: ***6-SL*** *in the Q_o active site with the potential, water mediated, hydrogen bonds between the carbonyls and Glu272 indicated in black and labeled in Å. The key protein residues are highlighted and the [2Fe-2S] cluster is shown as blue and yellow spacefilling atoms.* ***6-SL*** *and water molecule HOH5607 are shown in their highest scoring orientation as blue and red capped sticks respectively.*

Interestingly the 6-series inhibitors exhibit a number of relationships that oppose those of the original 7-series library. For example inclusion of a trifluoromethoxy moiety on the aryl ring portion of the compound was observed to cause a significant drop in potency for the 6-series compounds as opposed to the equally significant increase in activity that resulted from the group's inclusion in the 7-series. The analogues lacking the

trifluoromethoxy moiety, compounds **4-SL** and **22-SL** are the only compounds not to exhibit the inverted quinolone head and are consequently the most potent inhibitors in the 6-series (Figure 3.25).

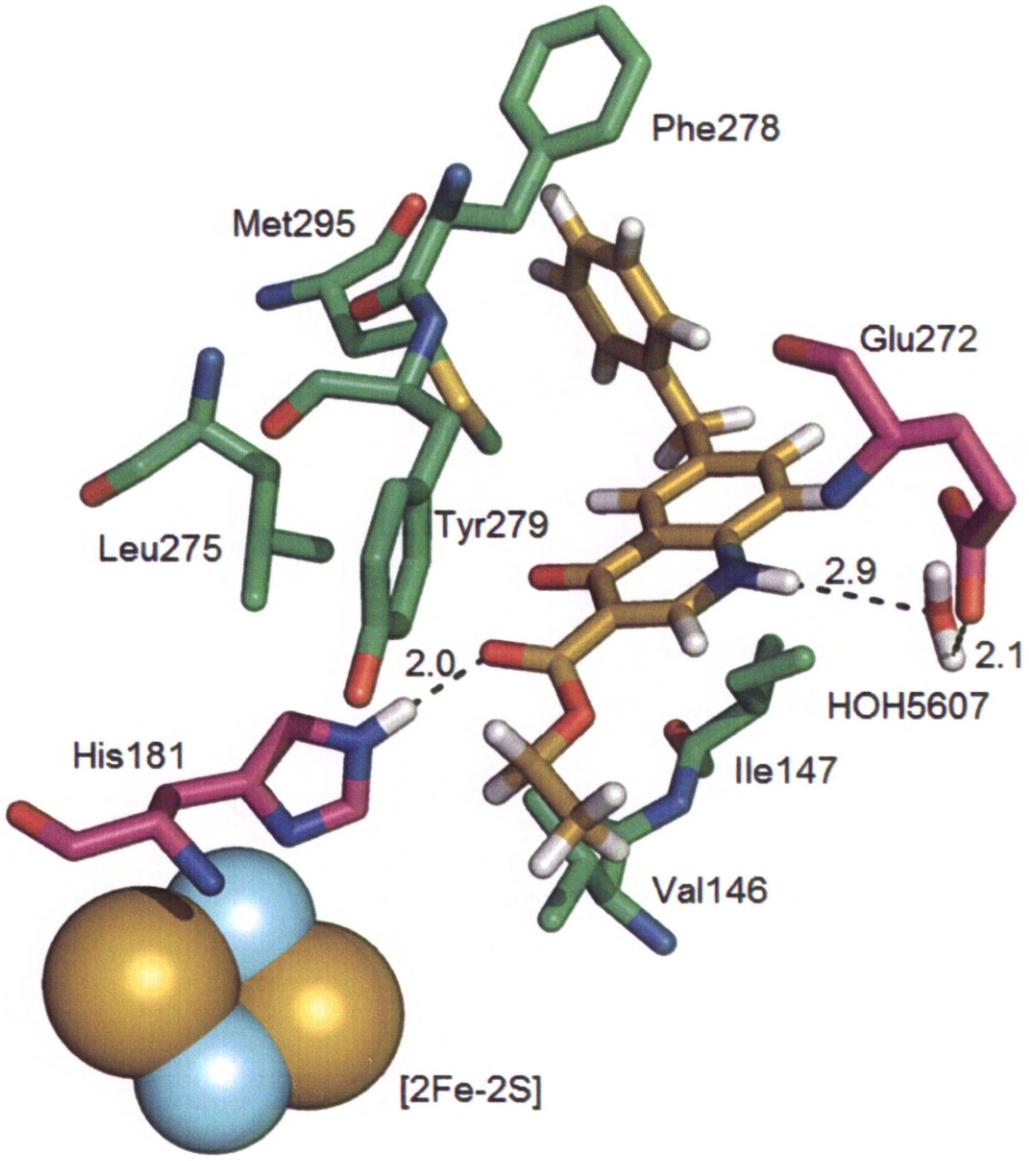

Figure 3.25: ***22-SL*** *docked in the Q_o active site with the potential hydrogen bond interactions with the protein residues indicated in black and labelled in Å. The key protein residues are highlighted and the [2Fe-2S] cluster is shown as blue and yellow spacefilling atoms.* ***22-SL*** *and water molecule HOH5607 are shown in their highest scoring orientation as gold and red capped sticks respectively.*

The reduced size of the "tail" portion allows the compounds to dock such that hydrogen bonds can form between both His181 and Glu272. This stabilises the complex resulting in improved activity. Inclusion of the

trifluoromethoxy group prevents this docking pose however and the result is reduced biological activity.

Similarly, for the 7-substituted compounds the change from ethyl to isopropyl ester resulted in greater potency; however for the 6-substituted analogues the opposite relationship was observed, **18-SL** being around 10% less potent than **4-SL** (183.9 *versus* 164.0 nM) where as **18** is more than 2-fold more active than **4** (8.45 *versus* 19.3 nM). Comparison of the docking poses for **18** and **18-SL** suggests that this is again the result of a change in the orientation of the quinolone ring (Figure 3.26).

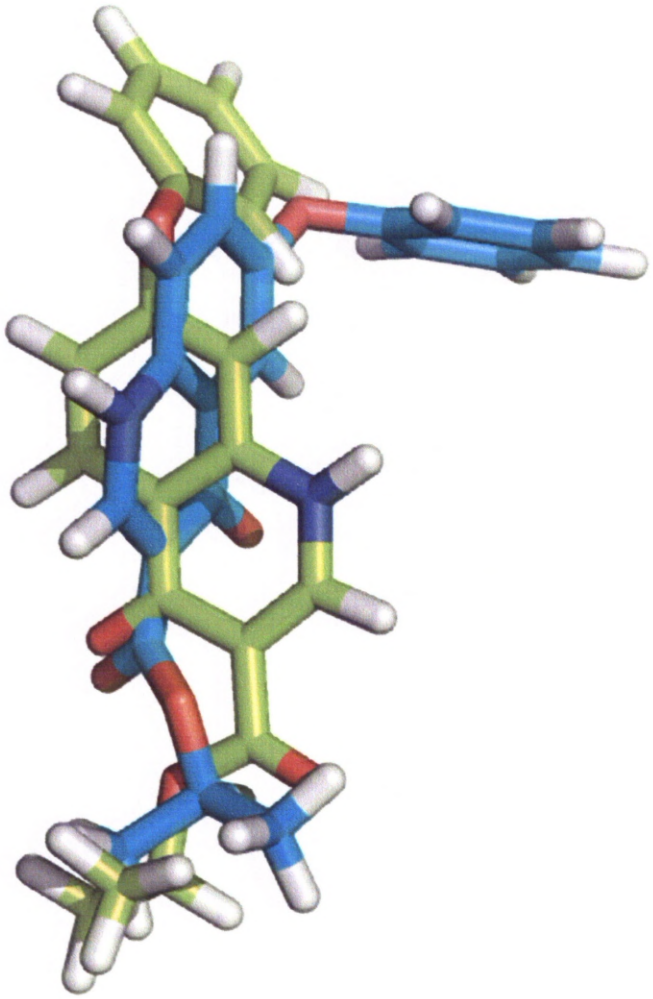

*Figure 3.26: Comparison of the highest scoring docking poses for isopropyl ester compounds **18** (green) and **18-SL** (blue).*

The isopropyl group of both compounds is situated in roughly the same position such that hydrogen bonds can form with His181. However in order to accommodate the phenyl "tail" of **18-SL** in the hydrophobic channel, the

quinolone "head" is rotated along its axis, twisting such that the quinolone NH and ester oxygens are no longer in the appropriate plane for interaction with Glu272 and His181 (Figure 3.26).

3.7.2 Biphenyl type derivatives

At the conclusion of the previous chapter it was noted that the synthetic routes to the compounds were largely linear and consequently relatively inefficient. In an effort to overcome this, some time was spent attempting to develop a route to the compounds that would allow derivitisation towards the end of the synthesis and so allow a number of compounds to be made rapidly from a single intermediate. To this end a route to ethyl 4-chloro-7-iodoquinoline-3-carboxylate **50** was devised (Scheme 3.1) in the hope that Suzuki couplings with a range of boronic acids would result in a more efficient route to the lead compound **39** and swift synthesis of novel compounds for testing. The 4-chloroquinoline was utilised as poor solubility of the analogous quinolone **49** was found to be an issue in subsequent reactions.

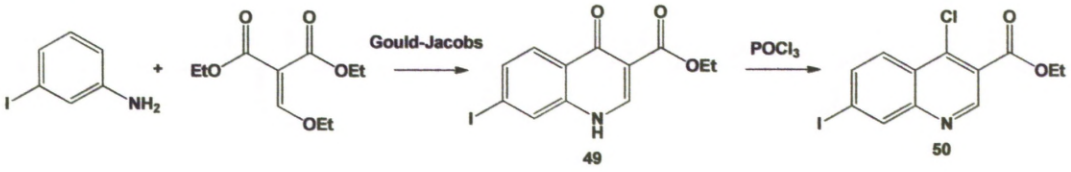

*Scheme 3.1: Synthesis of **50** from 3-iodoaniline **51** and diethyl 2-(ethoxymethylene) malonate **1** via the 7-iodoquinolone intermediate **49**.*

Unfortunately **39** was never successfully synthesised in this manner despite numerous attempts, however, this approach has since been utilised to synthesis a small library of compound with the general structure shown in figure 3.27.

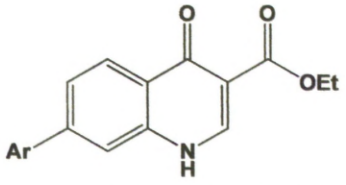

Figure 3.27: General structure of the biphenyl type analogues.

These compounds were tested *in vitro* in the same manner as the original library and the related 6-series quinolones discussed previously and in a

number of cases displayed reasonable activity against 3D7 *P.falciparum* (Table 3.9). *In silico* docking of the WM compounds in the yeast Q_o site model then allowed comparison of their docking poses with those of the lead compound **39** in order to rationalise the differences in their activities.

Table 3.9: In vitro test results for biphenyl type compounds.

Code	Structure	IC_{50} *versus* 3D7 parasites (nM)[a]
WM-1	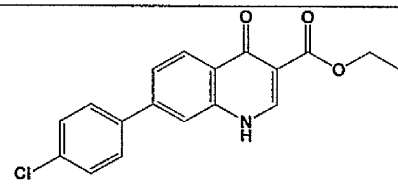	33
WM-2	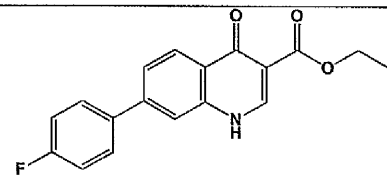	35
WM-3	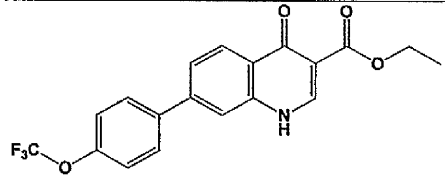	147
WM-4	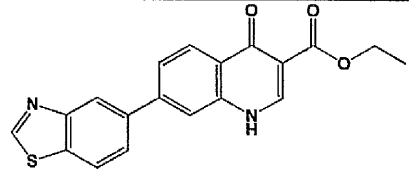	1100
WM-5	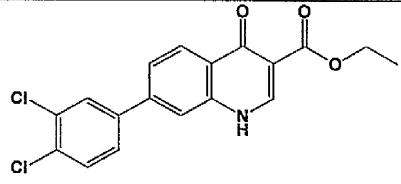	874
WM-6	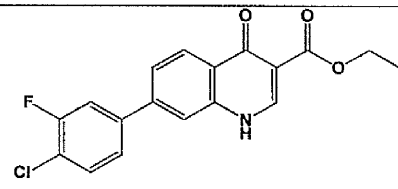	303
WM-7	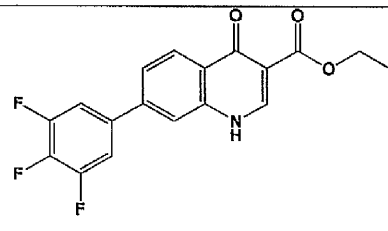	312

[a]*Average value from at least 3 independent experiments.*

It is clear from the predicted docking poses that the rigid, rod-like structure of these compounds is not well tolerated by the bc_1 Q_o site. In order to avoid steric clashes with the curved hydrophobic channel all of the compounds are orientated such that the substituted aromatic portion of the molecules occupies the active site with the quinolone ring lies along the hydrophobic channel (Figure 3.28).

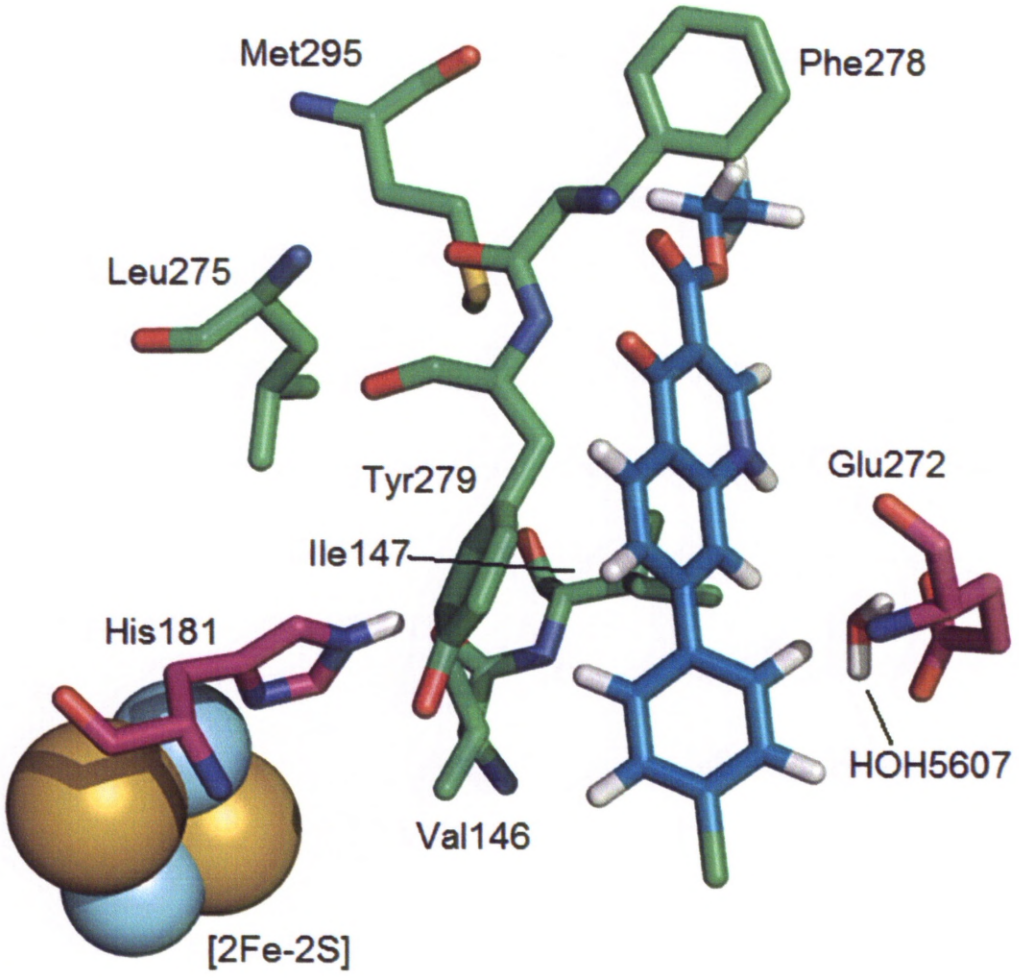

*Figure 3.28: Highest scoring predicted docking pose for **WL-1** in the Q_o active site. The key protein residues are highlighted and the [2Fe-2S] cluster is shown as blue and yellow spacefilling atoms. **WL-1** and water molecule HOH5607 are shown in their highest scoring orientation as teal and red capped sticks respectively.*

This orientation does not allow for the formation of any hydrogen bonds between the inhibitor and the key amino acids of the active site. There also appears to be no relationship between the substitution pattern of the compounds and the observed docking poses and it is likely that the

differences in biological activity are affected significantly by the individual solubility profiles of the compounds.

3.8 Summary

Modelling of the synthesised library has revealed that compounds with structures that maximise hydrogen bonding interactions with His181 and Glu272 exhibit the highest potency with ethyl and isopropyl esters demonstrating the strongest binding. Interaction between the "tail" of the compound and the hydrophobic channel is also an important consideration as demonstrated by the stabilising effect of methylene as opposed to oxygen linkers and the inclusion of a trifluoromethoxy moiety. Comparison of the docking of the compounds against that of related molecule libraries has shown 7-substitution to be superior to 6-substitution and that there is a requirement for a certain amount of flexibility in the molecules to prevent unfavourable interactions with the curved hydrophobic channel.[129] This information can now be used to inform the development of new bc_1 inhibitors with the aim of maintaining high potency while increasing solubility.

3.9 Experimental

Docking simulations were carried out using the GOLD 5.0.1 Protein-ligand docking suite[136] running in Hermes 1.4.1 on an IBM compatible PC running an Intel® Core™ 2 Duo CPU at 2.33 GHz. The protein file used was derived from the crystal structure of yeast bc_1 protein from *Saccharomyces cerevisiae* (Protein Data Bank accession code 3CX5).[43] Using a PDB editor all non-essential water molecules were deleted and amino acid residues greater than 20 Å from the designated Q_o binding region were removed to reduce processing time. The resulting 40 Å ball was used as the protein file for the docking simulation in GOLD.

Docking Protocol Validation – Docking Stigmatellin

Using the GOLD protein docking wizard the prepared protein file described above was loaded into Hermes and implicit hydrogen atoms added to the crystal structure. Water molecule HOH5607 was extracted and reloaded with spin state set to translate and spin. Sidechain flexibility was introduced for residues Val146, Ile147 and Glu272, restricted to their library conformers and the protonation state of residue His181 was checked to ensure that the correct tautomer was present; the proton should extend into the Q_o site away from the Rieske [2Fe-2S] cluster.

The stigmatellin ligand, designation N, was then extracted from the Q_o active site and saved as a separate .mol2 file and selected as the ligand for docking. The binding site was defined as the vacated ligand cavity and all atoms within 6 Å, as defined by the solvent accessible surface according to the default settings. The extracted stigmatellin ligand file was loaded as the reference file for calculation of RMSD. The genetic algorithm was set to 200% search efficiency and early termination was not allowed. All other options were maintained as their default settings.

Average RMSD 1.56 Å (standard deviation = 0.92).

Docking Atovaquone and the Quinolone Ligands

Energy minimised (MMFF94) 3-dimensional representations of each of the inhibitors were constructed using Spartan '08 V1 and saved as Sybyl Mol2 files.[143] The gold.conf configuration file generated during the validation with stigmatellin was reloaded and the appropriate ligand files selected in place of stigmatellin. No reference file was loaded. The number of genetic algorithm runs was increased to 20 per ligand file and the options to allow ligand flexibility by flipping of amide bonds and pyramidal nitrogen atoms were selected. All other settings were maintained as in the validated protocol. The resulting docking poses were visualised and evaluated using PyMol.[146]

*Synthesis of ethyl 4-chloro-7-iodoquinoline-3-carboxylate (**50**)*

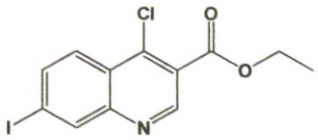

3-Iodoaniline (1 eq.) was combined with diethyl ethoxymethylenemalonate (1 eq.) and heated to 100 °C, under a nitrogen atmosphere, for 24 hours. The volatile components were evaporated under reduced pressure and the resulting solid washed with cold petroleum ether. The dried solid was suspended in Dowtherm A (5 mL/g) and heated to 240 °C for 1 hour, cooled to room temperature and precipitated from solution using n-hexane. The precipitated ethyl 7-iodo-4-oxo-1,4-dihydroquinoline-3-carboxylate **49** was washed with petroleum ether, dried and suspended in phosphoryl chloride (10 mL/g). The suspension was heated to reflux for 1 hour. The hot yellow solution was poured onto ice (15 g/mL) and stirred overnight. The resulting aqueous solution was extracted with chloroform and the combined organic extracts dried over magnesium sulphate and evaporated. Purified by column chromatography (Silica gel, 5% ethyl acetate/petroleum ether) to yield **50** as a pale brown solid.

(0.47 g, 63.2%)

^{1}H NMR ($CDCl_3$) δ 9.19 (s, 1H), 8.58 (s, 1H), 8.12 – 8.09 (d, 1H, J = 8.9), 7.98 – 7.95 (d, 1H, J = 8.9), 4.53 – 4.48 (q, $OC\underline{H}_2CH_3$, J = 7.1), 1.49 – 1.45 (t, $OCH_2C\underline{H}_3$, J = 7.1);

^{13}C NMR δ 164.6 (C=O), 151.4, 150.3, 144.2, 139.2, 137.6, 127.0, 125.9, 123.7, 99.5, 62.7, 14.7;

HRMS: $[M+H]^+$ $C_{12}H_{10}NO_2{}^{35}Cl^{127}I$ requires 361.9445, found 361.9434;

CHN for $C_{12}H_9ClINO_2$ requires C 39.86 H 2.51 N 3.87, found C 39.59 H 2.55 N 3.91.

Chapter 4

Results and Discussion 3: Computer Lead Design of a New Chemotype

4. Results and Discussion 3: Computer Lead Design of a New Chemotype

4.1 Attempts to Predict Activity Using *in silico* Docking Results

As covered in the previous section, *in silico* protein-ligand docking studies were carried out on three related libraries of quinolone compounds developed in the group. The data from these docking studies allowed us to rationalise the observed biological activity of these compounds with their structural features. For example, it had been established by the biological results that small ester groups (ethyl or isopropyl) at the 3-position of the quinolone core demonstrated the highest activity. Modelling studies revealed that this was due to a restrictive active site domain, requiring a specific configuration of hydrogen bond donors and acceptors to optimise binding. We hoped to use the docking models to predict the biological activity of new analogue designs before synthesising them.

The analysis of the previous libraries had made two aspects of the structure-activity relationship apparent; at the "head" of the compound in the 3-position, a small polar group such as an ethyl ester was optimal. For the "tail" region, flexible, hydrophobic groups performed best, while substitution at the 7-position gave better results than at the 6-position. As a result of these observations, a number of proposed structures were docked in the model system developed using the previously synthesised compounds. The structures which scored highest in these docking runs had the general structure shown below (Figure 4.1). In terms of their binding interactions (GoldScore), the structures scored higher than any of the earlier compounds, scoring similarly to the natural bc_1 inhibitor stigmatellin.

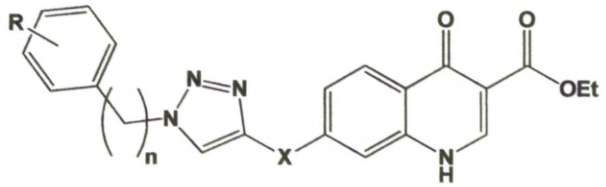

X = direct, -CH_2- or -OCH_2- n = 0 - 2
R = -OCF_3, -F, -Cl etc.

Figure 4.1: The general structure of the highest scoring proposed compounds in the in silico screening.

These structures were attractive targets when docked in the bc_1 Q_o site. The quinolone "head" adopted the same position as previously observed for the most potent analogues (Figure 4.2a), whereas the curvature of the triazole containing "tail" appeared to match the shape of the hydrophobic channel to the active site very closely (Figure 4.2b). The incorporation of the triazole itself also allowed us to reduce the CLogP of the compounds without introducing any particularly polar functionality into the hydrophobic region, suggesting that we could expect to improve on the poor solubility encountered with the current lead compounds. The structures also represented a completely novel chemotype, as no triazole containing quinolone based compounds of this particular substitution pattern exist in the literature.

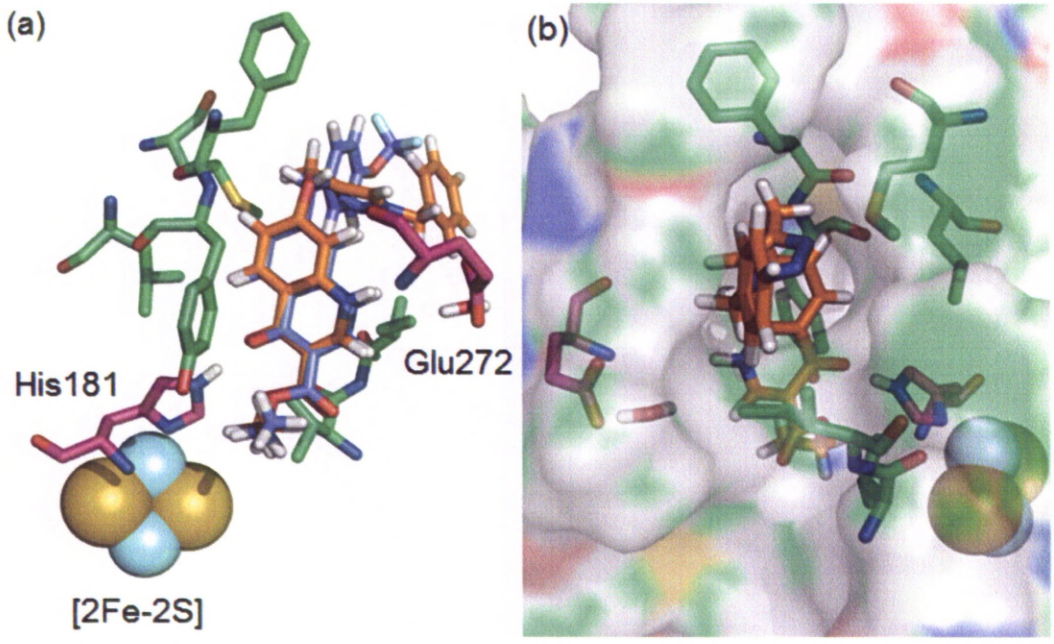

Figure 4.2: (a) Comparing the proposed compounds with the docking of lead compound ***39*** *and (b) with the solvent accessible surface of the protein displayed, revealing how the predicted pose fits the curvature of the hydrophobic channel extending the terminal group out towards the cytosol.*

4.2 Retrosynthesis

Having determined that the compounds of the chosen design (Figure 4.1) were viable targets, we devised a synthetic route. A frustrating aspect of the previously developed library was the linear synthetic routes taken to each compound. This did not allow for any common intermediates to be

synthesised. Consequently, the development of each analogue was very time consuming, and if a particular synthetic step failed to progress as expected, the result was often a return to the very beginning of the total synthesis. Therefore, when considering the route to the new targets, a divergent synthesis that would allow for a single key intermediate to be synthesised in bulk and quickly differentiated, was desirable.

The formation of 1,4-triazoles by the copper catalysed Huisgen 1,3-dipolar cycloaddition of azides and alkynes (Scheme 4.1) is well documented and is the classic example of "click-chemistry", as termed by K. B. Sharpless in 2001.[147] As such, the triazole ring formation provided an ideal point on which to centre our divergent synthesis strategy. Using this reaction as the final derivatising step in the synthesis would allow the rapid development of a library by synthesis of a single quinolone intermediate with a terminal acetylene group at the 7-position. Reaction of this intermediate with a selection of azides would then provide our new library (Scheme 4.2).

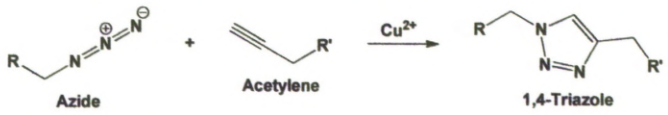

Scheme 4.1: A general example of the Huisgen 1,3-dipolar cycloaddition "click" formation of a 1,4-triazole from an azide and an acetylene.

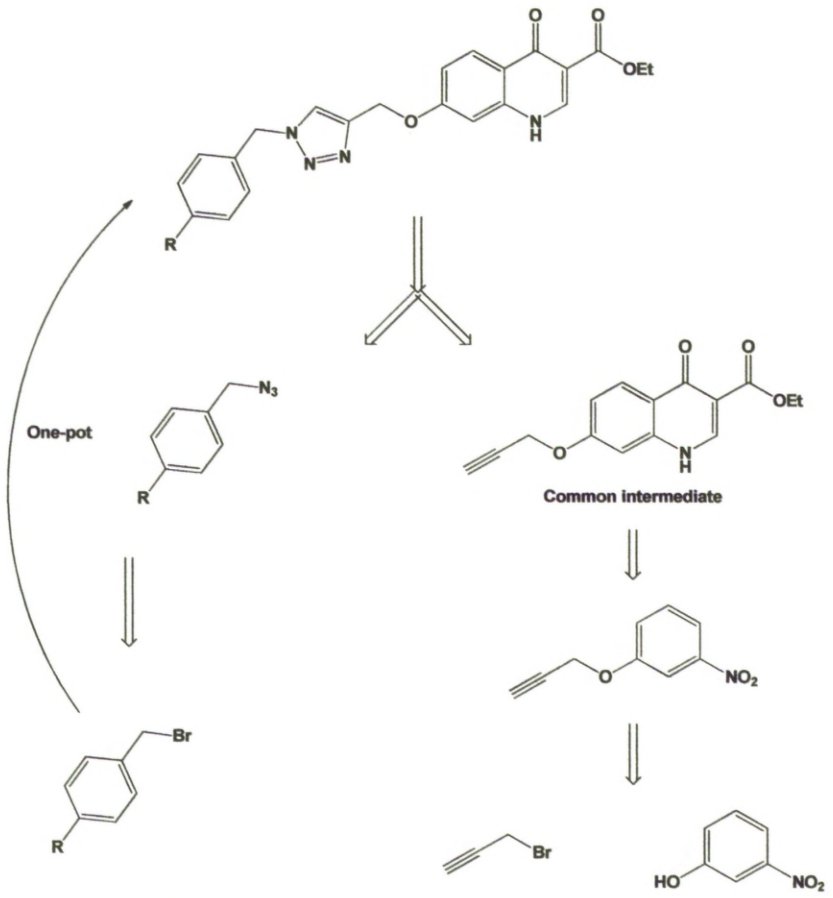

Scheme 4.2: Retrosynthetic design of the route to the proposed targets.

4.3 Synthesis of the Common Intermediate

To begin, benzyloxy linked analogues were selected. This subset of compounds was chosen for a number of reasons: they had scored highest in the predictive model, the benzyloxy compounds synthesised in the earlier 3,7-substituted quinolone library had demonstrated reasonable potency (**26** = 5 nM *versus* 3D7), and the intermediates were simple to synthesise at multigram scales from affordable starting materials.

4.3.1 Synthesis of the Required Aniline

As our intention was to synthesise the common intermediate compound by the Gould-Jacobs method with which we had already become familiar, it was necessary to first synthesise 3-(prop-2-yn-1-yloxy)aniline **51**. This was achieved in two simple steps. The first of which was the reaction of propargyl bromide **52** with 3-nitrophenol **7**. Initially, the conditions from Issei Iwai's 1963 study on napthyl propargyl ethers were employed to good effect,

achieving quantitative yields (Scheme 4.3a).[148] However while investigating conditions for the reduction step, we came across a patent filed by Avila Therapeutics Inc., in which the synthesis of our aniline target was covered.[149] The patent conditions (Figure 4.3b), whilst similar to those already utilised, allowed reaction times to be reduced from 24 hours to 2 < 4 hours (depending on scale) with no observed reduction in product yield.

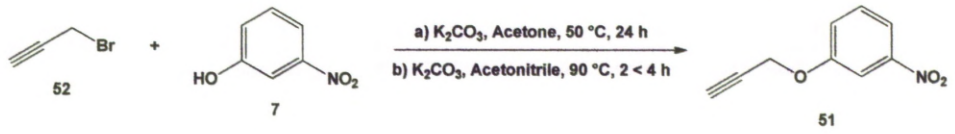

*Scheme 4.3: Synthesis of **51**; a) by Issei Iwai's conditions[148] and b) by the conditions used in the Avila Therapeutics patent.[149]*

The Avila patent also provided the conditions for the reduction of nitro compound **51** to the desired aniline **53**, employing an iron-mediated procedure (Scheme 4.4).[149] This was particularly useful, as there was concern over the lability of the triple bond under reducing conditions following a small scale test run of the previously utilised zinc mediated conditions, which resulted in the generation of multiple by-products.

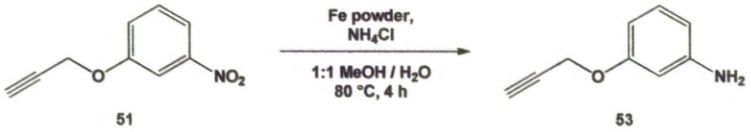

*Scheme 4.4: Conditions for the iron-mediated reduction of nitro compound **51** to aniline 53.[149]*

For unknown reasons, the 91% yield claimed in the original patent was never achieved, with our yields being consistently more modest at 43 - 56%, despite following the patent procedure as closely as possible. TLC analysis indicated no residual nitro compound in the reaction mixture and no significant quantity of any by-products. Our only explanation is that the aniline was not fully extracted from the aqueous residue.

4.3.2 Synthesis of Ethyl 4-oxo-7-(prop-2-yn-1-yloxy)-1,4-dihydroquinoline-3-carboxylate by the Gould-Jacobs Procedure

Aniline **53** was reacted with diethyl ethoxymethylenemalonate **1** *via* the original, solvent free conditions used previously, to give the enamine product in > 99% yield (Scheme 4.5).

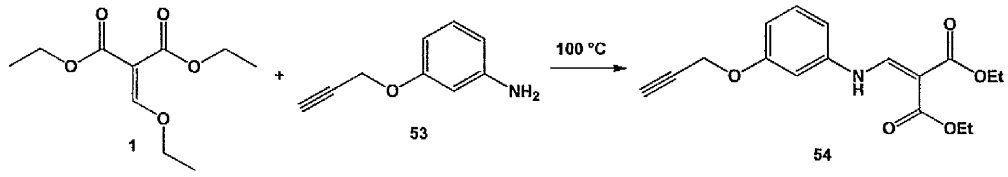

*Scheme 4.5: Reaction of aniline **53** with deiethyl ethoxymethyelenmalonate **1** to give enamine intermediate **54**.*

Attempts to cyclise enamine **54** by the Gould-Jacobs method (Scheme 4.6) proved less successful. A small quantity of the desired product **55** was obtained, but the reaction produced a number of by-products which were only removed by a sequence of recrystallisations.

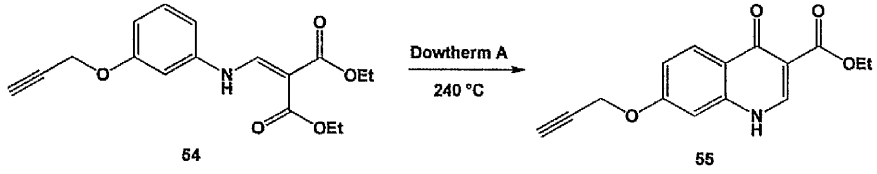

*Scheme 4.6: Gould-Jacobs cyclisation to give the target common intermediate quinolone **55**.*

Of greater concern was the poor solubility of the quinolone product, which suggested that it was likely to be a poor choice as a common intermediate for further reactions.

4.3.3 Redesigning the Common Intermediate to Improve Solubility

During the synthesis of the pyrazolo tricyclic compound **16** for the original library, the 4-chloroquinoline intermediate (compound **17**) had been synthesised by reaction of the parent quinolone **4** with phosphoryl chloride (Scheme 4.7).

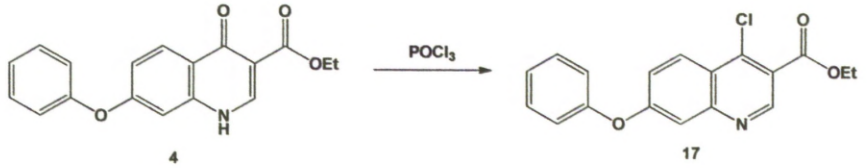

4 17

*Scheme 4.7: Chlorination of **4** with phosphoryl chloride to give ethyl 4-chloro-7-phenoxy-1,4-dihydroquinoline-3-carboxylate **17**.*

Due to poor yields and difficulty purifying the quinolone **55**, avoiding the cyclisation step prior to chlorination was desirable. A literature source provided the means to combine both steps into a single reaction (Scheme 4.8).[150] It was possible to simultaneously cyclise the enamine and chlorinate the 4-position by heating a solution of the enamine precursor **54** in phosphoryl chloride just below reflux temperature, under a nitrogen atmosphere, giving the 4-chloroquinoline target **56** in good levels of purity with consistent yields of around 84%.

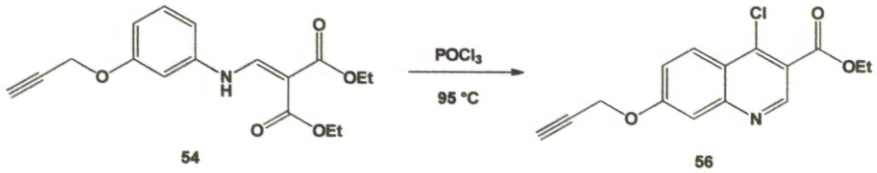

54 56

*Scheme 4.8: Simultaneous cyclisation and chlorination of enamine intermediate **54** to give the 4-chloroquinoline intermediate **56**.*

As expected, the 4-chloroquinoline **56** demonstrated much improved solubility over the corresponding quinolone **55**. It could be synthesised in multi-gram quantities with relative ease, making it an ideal candidate for a common intermediate in a divergent synthesis.

4.4 Building the Series: Huisgen 1,3-dipolar Cycloaddition

The original Huisgen 1,3-dipolar cycloaddition, first published in 1963, was a thermally driven process between any alkene or alkyne and a suitable 1,3-dipolar compound, such as a diazoalkane or, classically, an azide.[151] As there was no catalyst present to influence regioselectivity, and alkynes are

relatively poor dipole acceptors, the reaction frequently required sustained high temperatures that would generally result in a mixture of 1,4 and 1,5 substituted heterocyclic products (Figure 4.3).

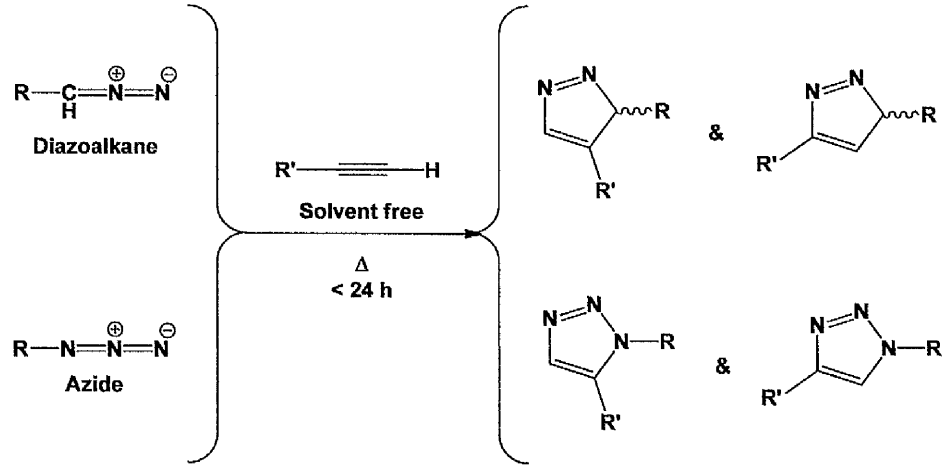

Figure 4.3: The original Huisgen 1,3-dipolar addition shown for the reaction of either a diazomethane or an azide, with a terminal alkyne, to give diazole or triazole products respectively.

In 2002, it was independently discovered by the groups of Meldal[152] and Sharpless[153] that the presence of copper (I) in the reaction between azides and terminal alkynes allowed temperatures to be considerably reduced, and that only the 1,4-substituted regioisomers were obtained. The mechanism for this transformation is not fully understood, but DFT studies by Sharpless *et al.* have gone some way to explaining a viable route, involving an unusual copper (III) metallocycle intermediate (Figure 4.4).[154]

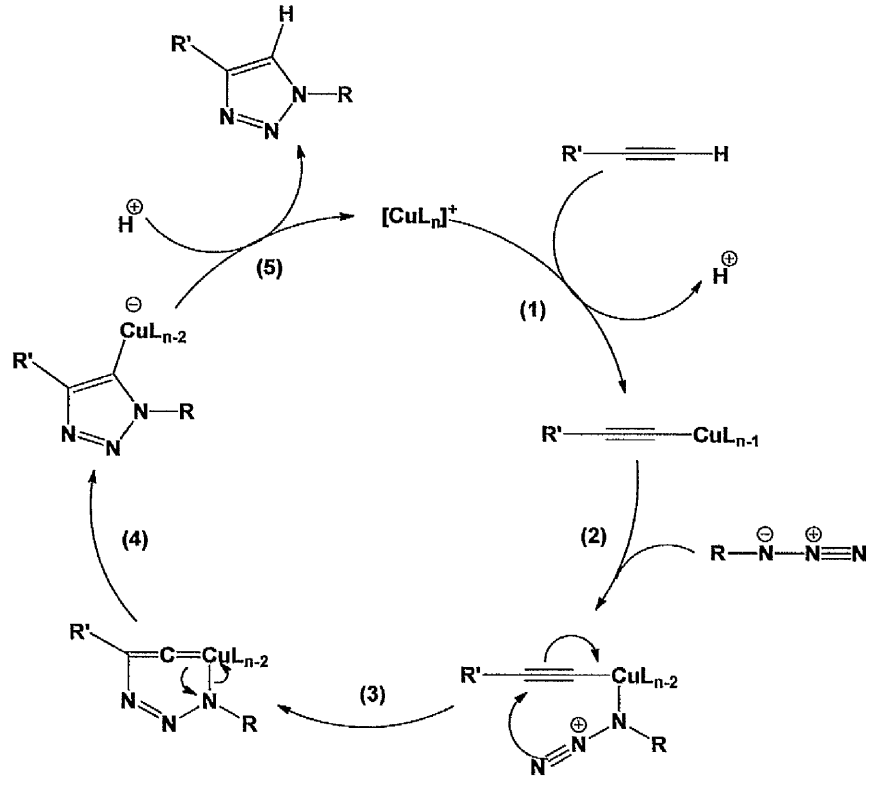

Figure 4.4: The proposed mechanism for the copper catalysed Huisgen 1,3-dipolar addition of an azide to a terminal alkyne; (1) Displacement of a ligand from copper gives the copper acetylide; (2) Displacement of a second ligand by the azide gives the reactive copper complex, with the groups orientated such that the acetylene and azide groups are in close proximity; (3) Attack of the azide terminal nitrogen on acetylide C-2 gives the unusual 6-membered Cu(III) complex; (4) Rearrangement of the intermediate gives the more stable Cu(II) species and forms the triazole; (5) Acidic cleavage of the copper carbon bond realeases the triazole product and allows the original Cu(I) catalyst to reform.[154]

4.4.1 Problems Clicking

Numerous conditions exist for carrying out the eponymous "click" reaction in a variety of different solvents. For the first attempt we selected a method that had been used in the group previously with great success. This method had the advantage of generating the required benzyl azide reactant *in situ* using sodium azide and the corresponding benzyl bromide (Scheme 4.9).[155] This method was beneficial in that the potentially explosive organic azide intermediate would not require isolation, avoiding a potential safety issue.

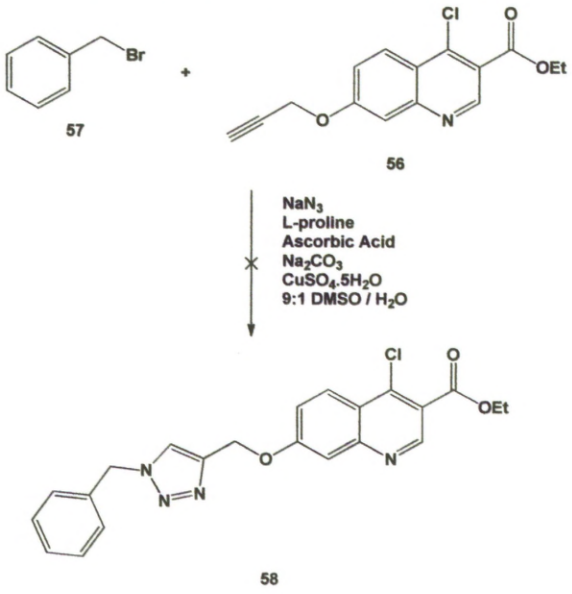

Scheme 4.9: The conditions trialled for the unsuccessful one-pot "click" synthesis.

Although this procedure had worked well for us in previous projects, the added complexity of the quinoline appeared to be a problem, as no reaction was observed beyond the gradual hydrolysis of the 4-chloroquinoline **56**. Therefore, the desired benzyl azides **59a-f** were synthesised and isolated by direct displacement of the appropriate benzyl bromide **57a-f** with sodium azide in dimethylformamide (Scheme 4.10).[156]

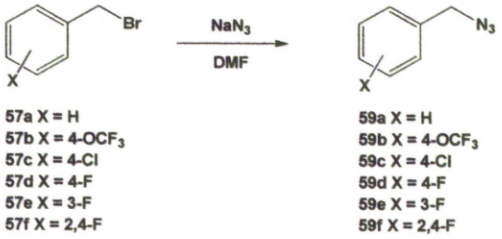

*Scheme 4.10: Synthesis of the benzyl azides **59a-f** for reaction with **56**.*

Once the azides **59a-f** had been synthesised, they were subjected to the same "click" conditions used previously. This time a successful reaction was observed. It had been assumed that the product of the "click" reaction would be the 4-chloroquinoline precursor to the targeted quinolone, which would then require hydrolysis in an additional step. This did not appear to be the case, however, as the isolated product showed no trace of chlorine when analysed by mass spectrometry (a quinolone N-H was also visible in the proton NMR spectrum). Unfortunately, the hydrolysis of the 4-chloroacetylene starting material appeared to be a competing process, with the isolated solid consisting of an approximate 1:1 mix of hydrolysed product and hydrolysed starting material (Scheme 4.11).

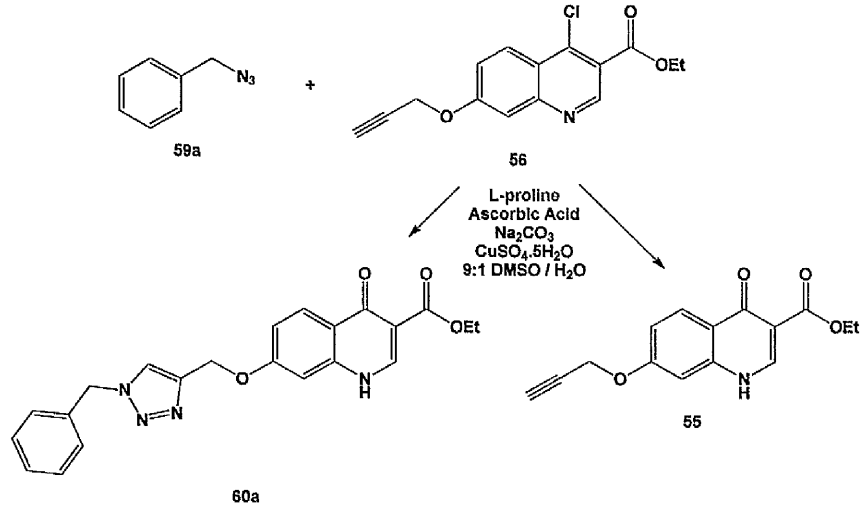

*Scheme 4.11: The two reaction pathways observed when **56** was subjected to the displayed "click" conditions with **60a**.*

It appears that even in the 9:1 dimethylsulphoxide / water solvent system used for the reaction, the quinolone acetylide is not sufficiently soluble to react once formed.

To avoid the necessity of a difficult column chromatography purification of the hydrolysed compound mixture it was decided to determine whether the hydrolysis could be prevented in the first place. The reaction to hydrolyse the 4-chloroquinoline "click" products once formed was going to use mild acid. On that basis it was suggested that the ascorbic acid present in the reaction mixture may be sufficient to induce the hydrolytic cleavage of the carbon chlorine bond. Consequently, the reaction conditions were altered to use sodium ascorbate as opposed to ascorbic acid. It was indeed observed that

the reaction now gave the desired 4-chloroquinoline product precursors in modest but acceptable yields (Scheme 4.12).

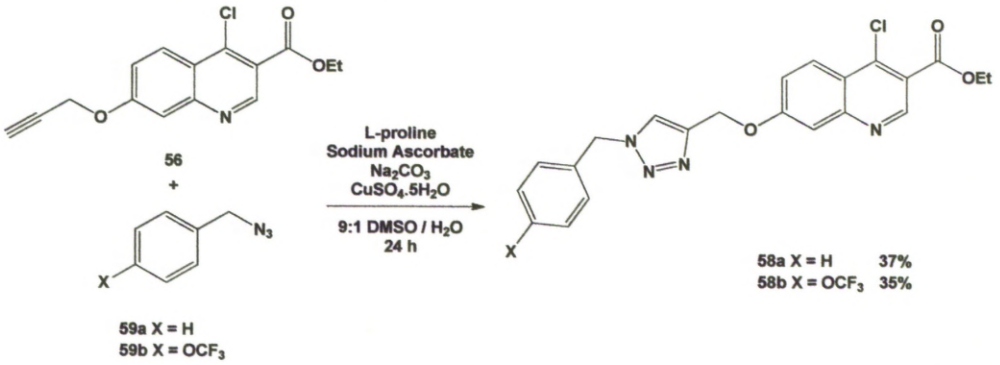

Scheme 4.12: Successful "click" coupling of ***56*** *with a variety of azides under basic conditions.*

Further research in the literature led to the discovery of a set of superior reaction conditions. A review of the effects of different bases on the outcome of Huisgen reactions by Burgess *et al.* found that the use of ammonium carbonate as the base promoted faster reaction and a reduction in unwanted by-product formation (Scheme 4.13).[157]

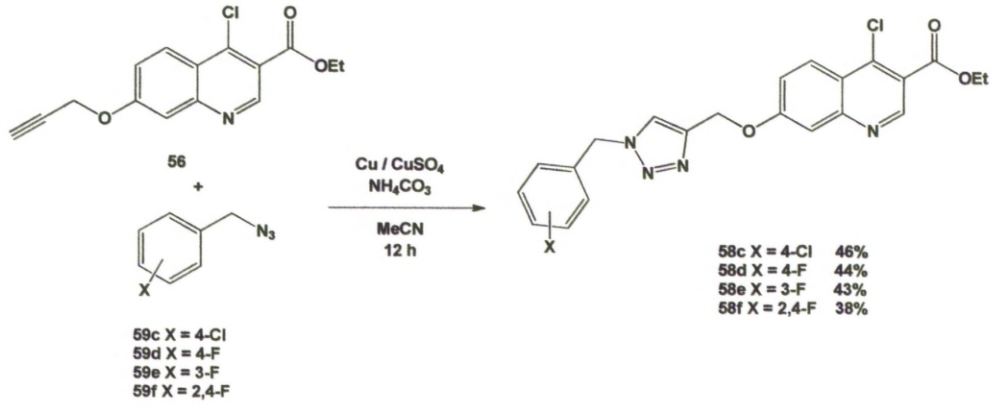

Scheme 4.13: "Click" coupling of ***56*** *with benzyl azides according to the improved conditions.*[157]

4.5 Synthesis of the "Click" Series

Having established a viable route to convert the 4-chloroquinoline precursors to the desired quinolone products, the final step was to establish a reliable method of hydrolysing the 4-chloro bond without hydrolysing the ester group. It was found that simply refluxing the compounds in ethanol for 2 – 3 hours, followed by extracting with chloroform to remove any remaining 4-

chloroquinoline gave the target compounds in high yields, 75 - 90% (Scheme 4.14).

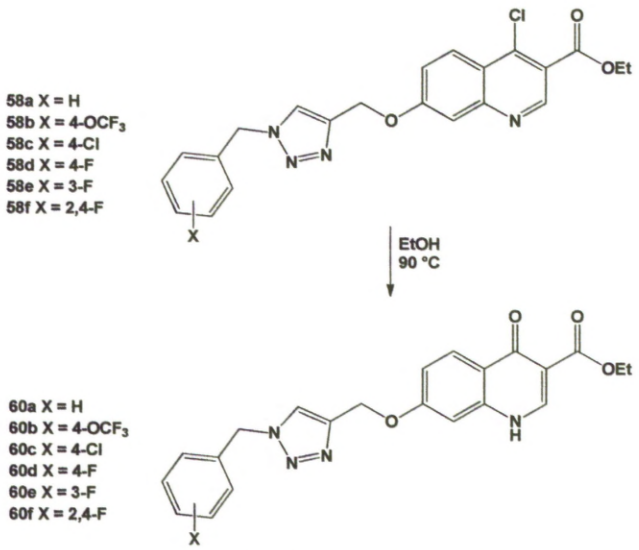

*Scheme 4.14: Thermal hydrolysis of the 4-chloroquinolines **58a-f** to the quinolone targets **60a-f** using ethanol.*

Seven compounds were synthesised by this method in total. Six were generated using benzyl azides (synthesised as described), and a seventh using an *N*-ethylphthalimido azide (synthesised by a literature method) (Scheme 4.15).[158]

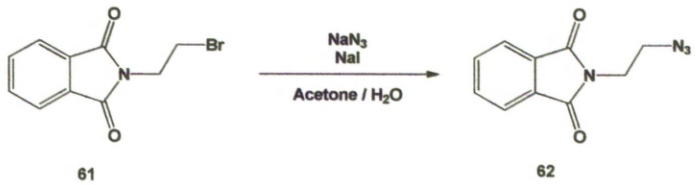

*Scheme 4.15: Synthesis of 2-(2-azidoethyl)isoindoline-1,3-dione **62**.*

In addition to the seven benzyloxy type quinolone triazoles synthesised, a single, directly linked quinolone-triazole compound was prepared by MChem student Walid Abd El Magid using a similar synthetic route (Scheme 4.16).

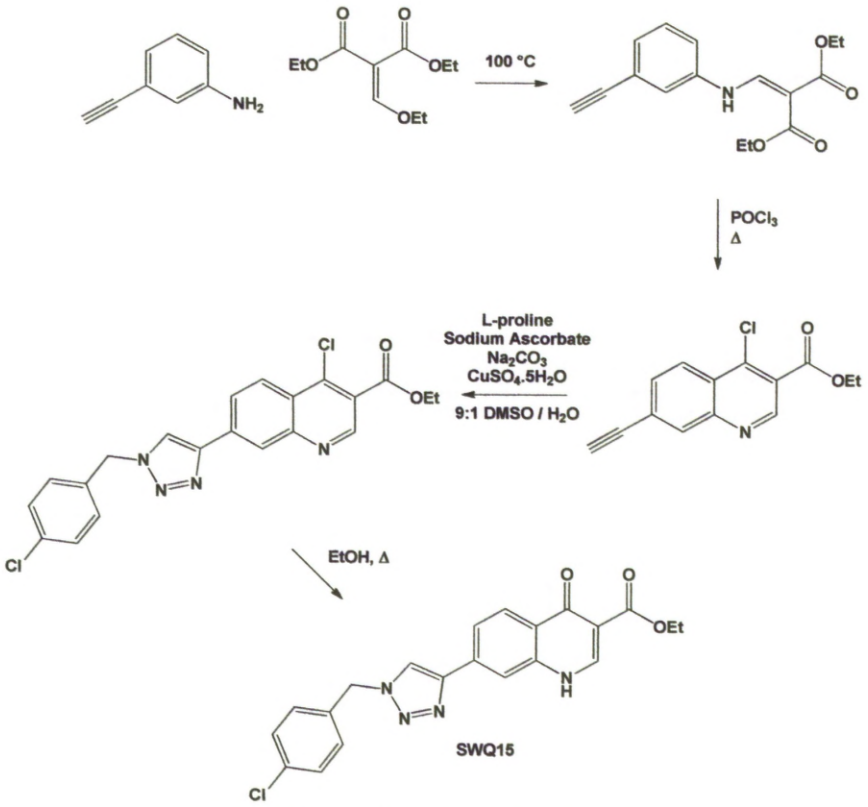

*Scheme 4.16: Synthetic route taken to **SWQ15**.*

4.6 Biological Evaluation of Quinolone-Triazole Compounds

Compared to the majority of previously synthesised library targets, the triazole compounds did exhibit improved solubility, although they were still relatively insoluble (requiring the use of DMSO-*d6* for NMR analysis).. Once purified, the eight compounds were evaluated for biological activity against cultured 3D7 *P.falciparum* parasites *in vitro* (Table 4.1).

Table 4.1: Biological results for the quinolone-triazole series.

Code	Structure	IC_{50} *versus* 3D7 parasites (nM)[a]	CLogP by ALog PS2.1[b]
60a	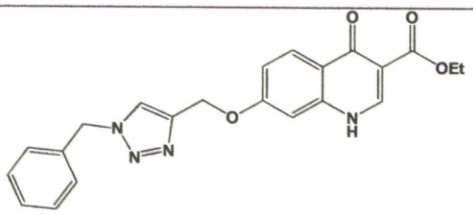	N/A[c]	2.95 ± 0.73
60b	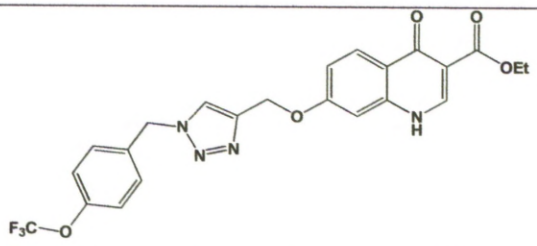	800	4.06 ± 0.59
60c	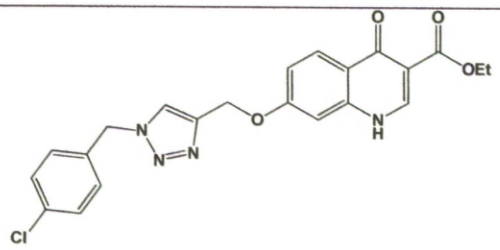	N/A[c]	3.63 ± 0.66
60d	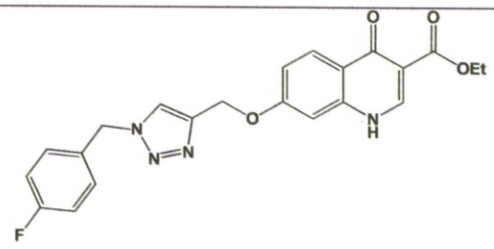	N/A[c]	3.12 ± 0.72

[a] *Average value from at least 3 independent experiments.*

[b] *http://www.vcclab.org/lab/alogps/* [c] *No activity at 1 μM.*

Table 4.1 continued: Biological results for the quinolone-triazole series.

Code	Structure	IC_{50} *versus* 3D7 parasites (nM)[a]	CLogP by ALog PS2.1[b]
60e	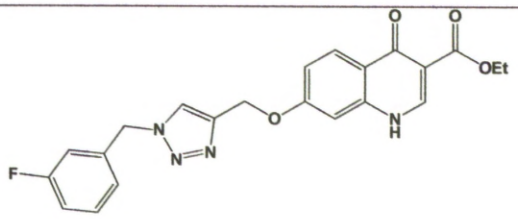	N/A[c]	3.11 ± 0.75
60f	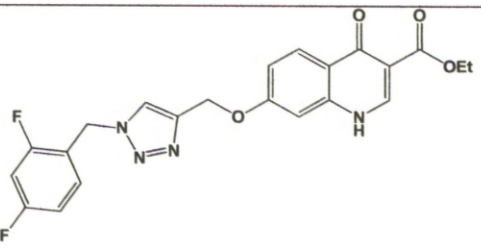	N/A[c]	3.22 ± 0.69
64	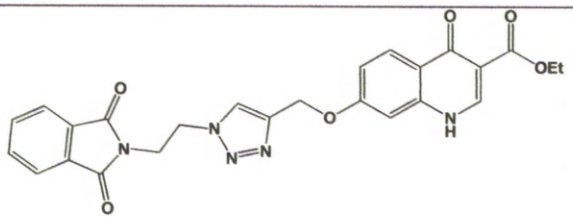	N/A[c]	1.88 ± 0.76
SWQ 15	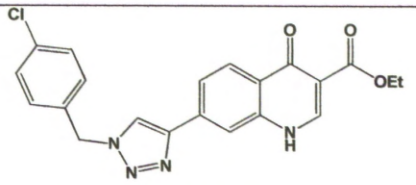	N/A[c]	3.55 ± 0.69

[a] *Average value from at least 3 independent experiments.*

[b] *http://www.vcclab.org/lab/alogps/* [c] *No activity at 1 μM.*

4.7 Summary

After the encouraging modelling results that identified these compounds as viable targets, the lack of activity *in vitro* was puzzling. We surmise that this is a result of the computer model being unable to account for several factors that contribute to a compounds biological activity. The docking simulation only models the interaction of the compound with the target protein, regardless of whether the compound would actually reach that point.

The *in vitro* testing of the compounds is carried out in whole cell infected erythrocytes. Consequently, before the compounds reach their intended

target, they must pass through several cell membranes (belonging both to the parasite and the infected red blood cell). It is possible that having lowered the CLogP of the compounds (in an attempt to increase aqueous solubility), we have reduced the lipophilicity of the compounds to the extent that it has been detrimental to their ability to pass through biological membranes. This could prevent them from reaching therapeutic concentrations at their intended site of action. This theory is in part supported by the observation that only the trifluoromethoxy compound **60b**, with the highest CLogP of the compound set, exhibits any measurable activity.

4.8 Experimental

Commercially available starting materials were sourced from Sigma-Aldrich, Alfa Aesar, Acros Organics or Apollo Scientific Ltd. and used without additional purification. Solvents were obtained from either Fisher Scientific or VWR and used without purification unless otherwise stated.

Flash column chromatography purification was carried out using silica gel (particle size 40-63 μm) sourced from Sigma-Aldrich and thin layer chromatography (TLC) was carried out using Merck aluminium backed sheets 20 x 20 cm Silica gel 60 F_{254}. TLC plates were visualised using an ultraviolet lamp (254 nm).

Analysis

^{1}H NMR spectra were recorded using a Bruker Avance 400 (400 MHz) machine; ^{13}C spectra were recorded on the same machine (100 MHz). Chemical shifts (δ) are recorded in ppm relative to an internal tetramethylsilane standard. Deuterated solvents were supplied by Sigma-Aldrich and Cambridge Isotope Laboratories and were used without additional purification. ^{1}H spectra multiplicities are recorded as singlet (s), broad singlet (bs), doublet (d), triplet (t), quartet (q), doublet of doublets (dd), doublet of triplets (dt) or multiplet (m), coupling constant *J* values are given in Hz where appropriate.

High resolution mass spectroscopy (HRMS) was carried out by Miss M. McCarron via electrospray ionisation (EI) using a Micromass LCT Mass Spectrometer. Samples were injected as methanol or tetrahydrofuran

solutions, as appropriate, using a direct infusion syringe pump. Compound **53** was analysed at the EPSRC National Mass Spectroscopy Centre in Swansea using a LTQ Orbitrap XL system.

Melting points and decomposition temperatures, where reported, were identified using a Gallenkamp melting point apparatus and are reported uncorrected in °C.

*Synthesis of 3-(prop-2-yn-1-yloxy)aniline (**53**)*

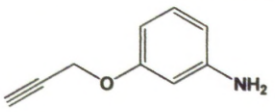

To a suspension of 3-nitrophenol **2** (8.0 g, 57.5 mmol) and potassium carbonate (11.2 g, 81.0 mmol) in acetonitrile (30 mL) was added propargyl bromide solution (80% in toluene, 7.6 mL, 68.4 mmol). The reaction mixture was heated to reflux (~ 90 °C) and progress monitored by thin layer chromatography. Upon full consumption of the starting material (~ 2½ hours) the solution was diluted with water (50 mL) and the resulting biphasic mixture extracted with ethyl acetate (3 x 75 mL). Combined organics extracts were dried over magnesium sulphate and evaporated to give crude 1-nitro-3-(prop-2-yn-1-yloxy)benzene as a brown solid.

The crude nitro compound was dissolved in a mixture of methanol and water (1:1, 120 mL). Ammonium chloride (20.6 g, 388 mmol) was added followed by iron powder (13.6 g, 242 mmol) and the resulting mixture was stirred vigorously and heated to 80 °C for 4 hours. The reaction mixture was then cooled and diluted with methanol (200 mL) before the inorganic solids were removed by filtering through a layer of celite. The filtrate was concentrated by evaporation under reduced pressure and the aqueous residue extracted with ethyl acetate (3 x 250 mL). The combined organic extracts were washed with water (250 mL) and brine (100 mL) respectively, before drying over magnesium sulphate and evaporation to give the crude product as a cloudy brown oil. Purification by column chromatography (4% methanol/chloroform) gave the pure product as a clear brown oil.

(4.76 g, 56.3%)

^{1}H NMR ($CDCl_3$) δ 7.09 – 7.05 (t, 1H, *J* = 7.9 Hz), 6.40 – 6.37 (ddd, 1H, *J* = 8.2, 2.4, 0.8 Hz), 6.35 – 6.32 (ddd, 1H, *J* = 7.8, 2.2, 0.8 Hz), 6.32 – 6.30 (t, 1H, *J* = 2.2), 4.65 – 4.64 (d, 2H, *J* = 2.4 Hz), 3.68 (s, NH_2), 2.52 – 2.51 (t, 1H, *J* = 2.4 Hz);

^{13}C δ 159, 148, 130, 109, 105, 102, 79, 75, 56;

HRMS: $[M+H]^+$ $C_9H_{10}NO$ requires 148.0757, found 148.0756.

*Synthesis of diethyl 2-(((3-(prop-2-yn-1-yloxy)phenyl)amino)methylene)malonate (**54**)*

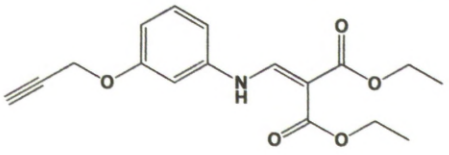

53 (4.76 g, 32.4 mmol) was combined with diethyl ethoxymethylenemalonate **1** (6.5 mL, 32.4 mmol) and heated to 100 °C overnight. On cooling the reaction mixture solidified. Washed with *n*-hexane and dried under vacuum to yield an off-white solid.

(10.27 g, 99.9 %)

Melting point: 76 – 78 °C

^{1}H NMR ($CDCl_3$) δ 11.00 – 10.97 (d, NH, *J* = 12.4), 8.52 – 8.49 (d, 1H, *J* = 13.5), 7.31 – 7.27 (^{app}t, 1H), 6.79 – 6.76 (m, 3H), 4.71 (s, Ar$C\underline{H}_2$C≡), 4.34 – 4.22 (m, 4H), 2.56 (s, C≡C$\underline{H}$), 1.40 – 1.31 (m, 6H);

^{13}C NMR δ 169.4, 165.9, 159.1, 152.1, 140.9, 131.1, 111.3, 110.8, 104.7, 94.1, 78.4, 76.4, 60.8, 60.5, 56.3, 14.8, 14.7;

HRMS: $[M+Na]^+$ $C_{17}H_{19}NO_5Na$ requires 340.1161 found 340.1172.

*Synthesis of ethyl 4-chloro-7-(prop-2-yn-1-yloxy)quinoline-3-carboxylate (**56**)*

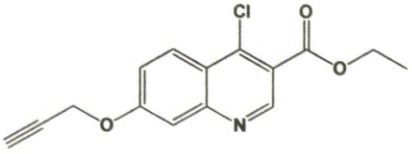

54 (10.26 g, 32.3 mmol) was suspended in phosphoryl chloride (45 mL) and heated to 95 °C overnight, under nitrogen. Evaporation of the phosphoryl chloride under reduced pressure followed by co-evaporation with xylene (2 x 50 mL) gave a bright red wax. The residue was dissolved in dichloromethane (100 mL) and washed with NaOH solution (1 M, 100 mL). The organic layer

was then concentrated and the residue redissolved in ethyl acetate (400 mL). The organic solution was then washed with water (100 mL) and brine (75 mL) respectively, before drying over magnesium sulphate and evaporation to give the product as a pale yellow solid.

(7.82 g, 83.5%)

Melting point: 133 – 135 °C (decomposition)

^{1}H NMR ($CDCl_3$) δ 9.18 (s, 1H), 8.35 – 8.32 (d, 1H, *J* = 9.3), 7.56 (d, 1H, *J* = 2.5), 7.39 – 7.36 (dd, 1H, *J* = 9.3, 2.6), 4.89 – 4.88 (dd, 2H, *J* = 3.9, 2.5), 4.52 – 4.46 (q, $OC\underline{H}_2CH_3$, *J* = 7.1) 2.60 (s, C≡C$\underline{H}$), 1.48 – 1.45 (t, $OCH_2C\underline{H}_3$, *J* = 7.1);

^{13}C δ 165.0, 160.8, 151.5, 149.5, 131.7, 127.5, 124.1, 121.9, 110.9, 109.5, 77.0, 76.7, 62.3, 56.6, 14.7;

HRMS: $[M+Na]^+$ $C_{15}H_{12}{}^{35}ClNO_3Na$ requires 312.0403 found 312.0405.

General Method E for the Synthesis of benzyl azides

Substituted benzyl bromide (1 eq.) was added to stirring dimethylformamide (10 mL) under a nitrogen atmosphere. Sodium azide (2 eq.) was added carefully and the resulting solution stirred at room temperature for 3 hours. The solution was diluted with water (20 mL) and extracted with ethyl acetate (3 x 25 mL). Organic extracts were washed with water (25 mL) and brine (25 mL). Organic solution was concentrated to a crude oil which was suspended in water (10 mL) and extracted with n-pentane (3 x 10 mL). Dried over magnesium sulphate and evaporated to give the products as clear oils.

*Benzyl azide (**59a**)*

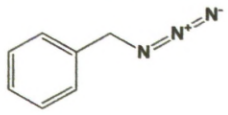

Synthesised from benzyl bromide **57a** according to general method E.

(0.59 g, 75.7%)

^{1}H NMR ($CDCl_3$) δ 7.39 – 7.29 (m, 5H), 4.31 (s, 2H);

^{13}C NMR δ 135.8, 129.3 (2C), 128.8, 128.7 (2C), 55.2.

*4-(Trifluoromethoxy)benzyl azide (**59b**)*

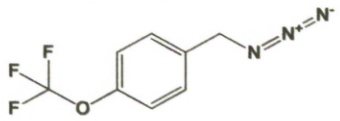

Synthesised from 4-(trifluoromethoxy)benzyl bromide **57b** according to general method E.

(0.47 g, 69.9%)

^{1}H NMR ($CDCl_3$) δ 7.37 – 7.34 (dt, 2H, *J* =9.3, 2.7), 7.25 – 7.23 (d, 2H, *J* = 7.9), 4.37 (s, 2H);

^{13}C NMR δ 134.5, 129.9 (3C), 121.7 (2C), 99.9, 54.3.

*4-Chlorobenzyl azide (**59c**)*

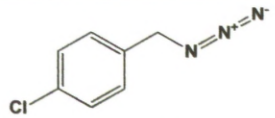

Synthesised from 4-chlorobenzyl bromide **57c** according to general method E.

(1.36 g, 81.9%)

^{1}H NMR ($CDCl_3$) δ 7.55 – 7.07 (m, 4H), 4.32 (s, 2H);

^{13}C NMR δ 137.0, 131.3, 130.4 (2C), 128.7 (2C), 55.0.

*4-Fluorobenzyl azide (**59d**)*

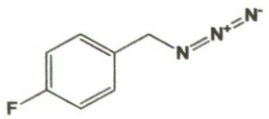

Synthesised from 4-fluorobenzyl bromide **57d** according to general method E.

(1.17 g, 80.9%)

^{1}H NMR ($CDCl_3$) δ 7.31 – 7.28 (m, 2H), 7.10 – 7.05 (m, 2H), 4.31 (s, 2H);

^{13}C NMR δ 164.3, 161.8, 131.6, 130.4 (2C), 116.2 (2C), 54.5.

*3-Fluorobenzyl azide (**59e**)*

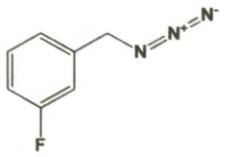

Synthesised from 3-fluorobenzyl bromide **57e** according to general method E.

(1.20 g, 83.3 %)

^{1}H NMR ($CDCl_3$) δ 7.38 – 7.32 (m, 1H), 7.11 – 7.02 (m, 3H), 4.35 (s, 2H);

^{13}C NMR δ 164.6, 138.3, 130.8, 124.1, 115.7, 115.3, 54.6.

*2,4-Difluorobenzyl azide (**59f**)*

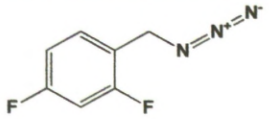

Synthesised from 2,4-difluorobenzyl bromide **57f** according to general method E.

(1.15 g, 73.3%)

^{1}H NMR ($CDCl_3$) δ 7.35 – 7.29 (m, 1H), 6.93 – 6.84 (m, 2H), 4.37 (s, 2H);

^{13}C NMR δ 164.7, 164.6, 162.6, 162.2, 162.1, 160.3, 160.1, 131.8 – 131.6, 112.1 – 111.9, 104.7, 104.4, 48.4.

*General Method F for Click Coupling (**58a** and **58b**)*

56 (0.28 g, 1 mmol) was dissolved in dimethylsulphoxide and water (9:1, 10 mL). To the stirring solution was added sodium carbonate (0.02 g, 0.2 mmol), *L*-proline (0.02 g, 0.2 mmol), sodium ascorbate (0.02 g, 0.1 mmol) and copper (II) sulphate pentahydrate (0.01 g, 0.05 mmol). The resulting blue solution was heated to 65 °C before addition of the desired benzyl azide (2.2 mmol). After 24 hours the reaction was diluted with water (25 mL) and extracted with ethyl acetate (3 x 25 mL). Combined organic extracts were washed with brine (25 mL) and dried over magnesium sulphate before evaporation to give crude product as yellow solids which were purified by flash column chromatography (ethyl acetate/*n*-hexane).

*Ethyl 7-((1-benzyl-1H-1,2,3-triazol-4-yl)methoxy)-4-chloroquinoline-3-carboxylate (**58a**)*

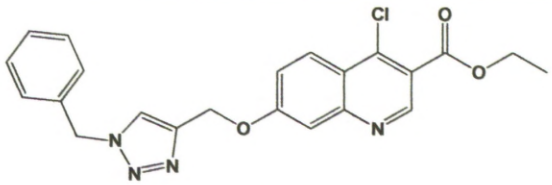

Synthesised from **56** and **59a** according to general method F to yield a pale yellow powder.

(0.16 g, 37.3 %)

Melting point: > 250 °C

^{1}H NMR ($CDCl_3$) δ 9.18 (s, 1H), 8.32 – 8.30 (d, 1H, *J* = 9.3), 7.61 (s, 1H), 7.55 (d, 1H, *J* = 2.4), 7.40 – 7.34 (m, 4H), 7.32 – 7.29 (m, 2H), 5.57 (s, 2H), 5.34 (s, 2H), 4.51 – 4.46 (q, $OC\underline{H}_2CH_3$, *J* = 7.1), 1.48 – 1.44 (t, $OCH_2C\underline{H}_3$, *J* = 7.1);

^{13}C NMR δ 165.0, 161.8, 161.6, 151.4, 145.5, 141.4, 136.3, 129.6 (2C), 129.3, 128.6 (2C), 127.4, 123.3, 121.9, 115.7, 109.1, 62.7, 62.3, 54.8, 14.7;

HRMS: $[M+Na]^+$ $C_{22}H_{19}{}^{35}ClN_4O_3Na$ requires 445.1043 found 445.1043.

*Ethyl 4-chloro-7-((1-(4-(trifluoromethoxy)benzyl)-1H-1,2,3-triazol-4-yl)methoxy)quinoline-3-carboxylate (**58b**)*

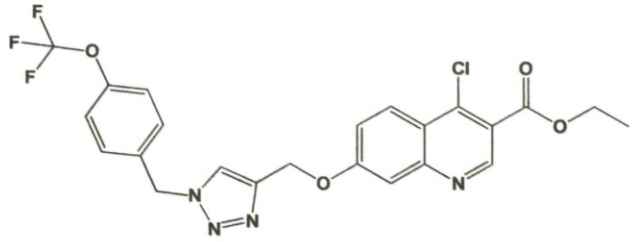

Synthesised from **56** and **59b** according to general method F to yield a white solid.

(0.18 g, 35.1%)

Melting point: 184 – 187 °C (decomp.)

^{1}H NMR ($CDCl_3$) δ 9.17 (s, 1H), 8.31 – 8.28 (d, 1H, *J* = 9.3), 7.67 (s, 1H), 7.54 (d, 1H, *J* = 2.2), 7.36 – 7.33 (m, 3H), 7.24 – 7.22 (m, 2H), 5.57 (s, 2H), 5.35 (s, 2H), 4.51 – 4.46 (q, $OC\underline{H}_2CH_3$, *J* = 7.1), 1.48 – 1.44 (t, $OCH_2C\underline{H}_3$, *J* = 7.1);

^{13}C NMR δ 164.9, 161.4, 151.8, 151.4, 149.8, 148.9, 143.9, 143.8, 133.4, 130.0 (2C), 127.4, 123.4, 122.0 (2C), 121.8, 121.4, 119.4, 109.1, 62.6, 62.3, 53.8, 14.6;

HRMS: $[M+Na]^+$ $C_{23}H_{18}{}^{35}ClF_3N_4O_4Na$ requires 529.0866 found 529.0850.

*General Method G for Click Coupling (**58c-f**)*

The appropriate azide (1.3 mmol) was mixed with ammonium carbonate solution (2 $M_{(aq)}$, 1.5 mL) and acetonitrile (1.5 mL). **56** (0.28 g, 1.0 mmol) was suspended in the mixture followed by copper (II) sulphate solution (1 $M_{(aq)}$, 0.1 mL) and copper (0) powder (64 mg, 1.0 mmol). The mixture was stirred at room temperature and reaction progress monitored by thin layer chromatography. Upon completion the mixture was suspended in water (10 mL) and extracted with ethyl acetate (3 x 10 mL). Combined extracts were washed with water (15 mL) and brine (15 mL) respectively, dried over magnesium sulphate and evaporated to give the crude products. Purification by flash column chromatography (ethyl acetate/*n*-hexane) gave the pure products as off-white to yellow powders.

*Ethyl 4-chloro-7-((1-(4-chlorobenzyl)-1H-1,2,3-triazol-4-yl)methoxy)quinoline-3-carboxylate (**58c**)*

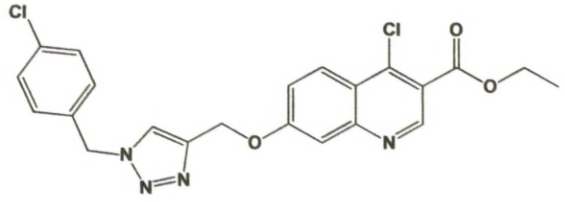

Synthesised from **56** and **59c** according to general method G to give a yellow solid.

(0.21 g, 46.1%)

Melting point: 134 – 138 °C

^{1}H NMR ($CDCl_3$) δ 9.17 (s, 1H), 8.32 – 8.30 (d, 1H, *J* = 9.3), 7.61 (s, 1H), 7.55 – 7.54 (d, 1H, *J* = 2.5), 7.38 – 7.34 (m, 3H), 7.25 – 7.23 (m, 2H), 5.54 (s, 2H), 5.35 (s, 2H), 4.51 – 4.46 (q, $OC\underline{H}_2CH_3$, *J* = 7.1), 1.48 – 1.44 (t, $OCH_2C\underline{H}_3$, *J* = 7.1);

^{13}C NMR δ 164.9, 161.4, 151.9, 151.4, 143.9, 143.8, 135.4, 133.2, 129.9 (2C), 129.8 (2C), 127.4, 123.2, 121.9, 121.8, 121.4, 109.1, 62.6, 62.3, 53.9, 14.6;

HRMS: $[M+H]^+$ $C_{22}H_{19}{}^{35}Cl_2N_4O_3$ requires 457.0834 found 457.0830.

*Ethyl 4-chloro-7-((1-(4-fluorobenzyl)-1H-1,2,3-triazol-4-yl)methoxy)quinoline-3-carboxylate (**58d**)*

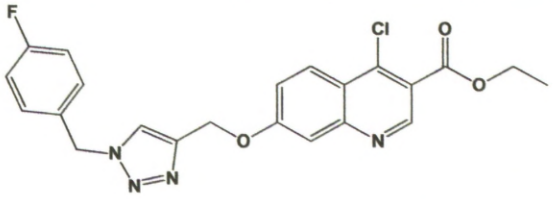

Synthesised from **56** and **59d** according to general method G to give a cream solid.

(0.19 g, 43.6%)

Melting point: 110 – 112 °C

^{1}H NMR ($CDCl_3$) δ 9.17 (s, 1H), 8.32 – 8.30 (d, 1H, *J* = 9.3), 7.61 (s, 1H), 7.55 – 7.54 (d, 1H, *J* = 2.5), 7.37 – 7.34 (dd, 1H, *J* = 9.3, 2.6), 7.31 – 7.28 (m, 2H), 7.11 – 7.05 (tt, 2H, *J* = 8.6, 3.0), 5.53 (s, 2H), 5.34 (s, 2H), 4.51 – 4.46 (q, $OC\underline{H}_2CH_3$, *J* = 7.1), 1.48 – 1.44 (t, $OCH_2C\underline{H}_3$, *J* = 7.1);

^{13}C NMR δ 164.9, 161.5, 151.9, 151.4, 143.9, 143.8, 130.6, 130.5 (2C), 130.4, 127.4, 123.1, 121.9, 121.8, 121.4, 116.7, 116.5, 109.1, 62.6, 62.3, 53.9, 14.6;

HRMS: $[M+H]^+$ $C_{22}H_{19}{}^{35}ClFN_4O_3$ requires 441.1130 found 441.1124.

*Ethyl 4-chloro-7-((1-(3-fluorobenzyl)-1H-1,2,3-triazol-4-yl)methoxy)quinoline-3-carboxylate (**58e**)*

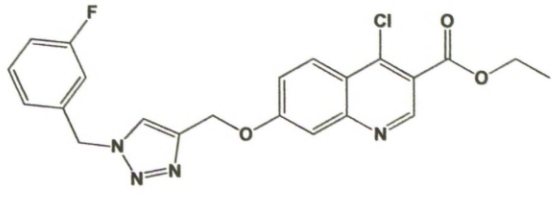

Synthesised from **56** and **59e** according to general method G to give a cream solid.

(0.19 g, 43.4%)

Melting point: 108 – 111 °C

^{1}H NMR ($CDCl_3$) δ 9.17 (s, 1H), 8.32 – 8.30 (d, 1H, *J* = 9.3), 7.64 (s, 1H), 7.56 – 7.55 (d, 1H, *J* = 2.5), 7.39 – 7.33 (m, 2H), 7.08 – 7.04 (m, 2H), 7.00 – 6.98 (d, 1H, *J* = 9.2), 5.56 (s, 2H), 5.36 (s, 2H), 4.51 – 4.46 (q, $OC\underline{H}_2CH_3$, *J* = 7.1), 1.48 – 1.44 (t, $OCH_2C\underline{H}_3$, *J* = 7.1);

^{13}C NMR δ 164.9, 161.5, 151.9, 151.4, 144.0, 143.8, 137.0, 131.3, 131.2, 127.4, 124.1, 124.0, 123.3, 121.9, 121.8, 121.4, 116.4, 116.2, 115.6, 115.3, 109.2, 62.6, 62.3, 54.0, 14.6;

HRMS: $[M+H]^+$ $C_{22}H_{19}{}^{35}ClFN_4O_3$ requires 441.1130 found 441.1121.

*Ethyl 4-chloro-7-((1-(2,4-difluorobenzyl)-1H-1,2,3-triazol-4-yl)methoxy)quinoline-3-carboxylate (**58f**)*

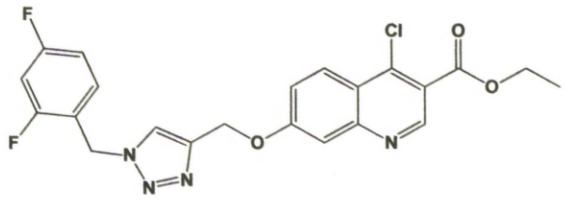

Synthesised from **56** and **59f** according to general method G to give a white solid.

(0.17 g, 38.1%)

Melting point: 138 – 141 °C

^{1}H NMR ($CDCl_3$) δ 9.14 (s, 1H), 8.28 – 8.26 (d, 1H, *J* = 9.3), 7.71 (s, 1H), 7.53 – 7.52 (d, 1H, *J* = 2.5), 7.34 – 7.29 (m, 2H), 6.91 – 6.84 (m, 2H), 5.56 (s, 2H), 5.32 (s, 2H), 4.49 – 4.42 (q, $OC\underline{H}_2CH_3$, *J* = 7.1), 1.46 – 1.42 (t, $OCH_2C\underline{H}_3$, *J* = 7.1);

^{13}C NMR δ 164.9, 161.5, 151.9, 151.4, 143.9, 143.8, 132.3 – 132.1, 127.4, 123.5, 121.9, 121.8, 121.4, 118.3, 118.1, 112.8 – 112.5, 109.1, 105.1 – 104.6, 62.6, 62.3, 47.7, 14.7;

HRMS: $[M+Na]^+$ $C_{22}H_{17}{}^{35}ClF_2N_4O_3Na$ requires 481.0855 found 481.0842.

General Method H for Hydrolysis of 4-chloroquinolines to quinolones

4-chloroquinoline (approx. 0.2 mmol) was suspended in ethanol (5 mL) and heated to reflux for 24 hours. The resulting precipitate was recovered by vacuum filtration of the still hot solution. The recovered solid was then washed with diethyl ether and chloroform and dried in a vacuum desiccator to yield the product as a white powder.

*Ethyl 7-((1-benzyl-1H-1,2,3-triazol-4-yl)methoxy)-4-oxo-1,4-dihydroquinoline-3-carboxylate (**60a**)*

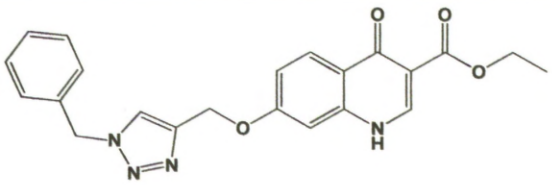

Synthesised from **58a** according to general method H to give a white solid.

(53.9 mg, 74.0%)

Melting point: > 250 °C

^{1}H NMR (DMSO-d6) δ 12.51 – 12.13 (d, NH, *J* = 6.6), 8.49 – 8.47 (d, 1H, *J* = 6.6), 8.33 (s, 1H), 8.06 – 8.04 (d, 1H, *J* = 8.9), 7.39 – 7.31 (m, 4H), 7.15 (d, 1H, *J* = 2.2), 7.08 – 7.05 (dd, 1H, *J* = 8.9, 2.2), 5.62 (s, 2H), 5.27 (s, 2H), 4.23 – 4.17 (q, $OC\underline{H}_2CH_3$, *J* = 7.1), 1.29 – 1.25 (t, $OCH_2C\underline{H}_3$, *J* = 7.1);

^{13}C NMR not obtained due to poor solubility;

HRMS: $[M+Na]^+$ $C_{22}H_{20}N_4O_4Na$ requires 427.1382, found 427.1401.

*Ethyl 4-oxo-7-((1-(4-(trifluoromethoxy)benzyl)-1H-1,2,3-triazol-4-yl)methoxy)-1,4-dihydroquinoline-3-carboxylate (**60b**)*

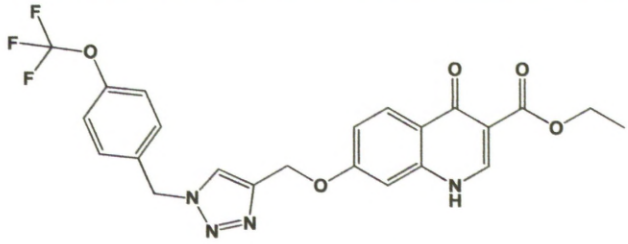

Synthesised from **58b** according to general method H to give a white solid.

(66.9 g, 76.1%)

Melting point: > 250 °C

^{1}H NMR (DMSO-d6) δ 12.16 – 12.15 (d, NH, *J* = 6.3), 8.50 – 8.48 (d, 1H, *J* = 6.4), 8.36 (s, 1H), 8.07 – 8.05 (d, 1H, *J* = 8.9), 7.47 – 7.37 (d, 2H, *J* = 8.7), 7.39 – 7.37 (d, 2H, *J* = 8.3), 7.16 – 7.15 (d, 1H, *J* = 2.3), 7.08 – 7.06 (dd, 1H, *J* = 8.9, 2.4), 5.68 (s, 2H), 5.28 (s, 2H), 4.23 – 4.18 (q, $OC\underline{H}_2CH_3$, *J* = 7.1), 1.29 – 1.26 (t, $OCH_2C\underline{H}_3$, *J* = 7.1);

^{13}C NMR not obtained due to poor solubility;

HRMS: $[M+Na]^+$ $C_{23}H_{19}F_3N_4O_5Na$ requires 511.1205, found 511.1198.

*Ethyl 7-((1-(4-chlorobenzyl)-1H-1,2,3-triazol-4-yl)methoxy)-4-oxo-1,4-dihydroquinoline-3-carboxylate (**60c**)*

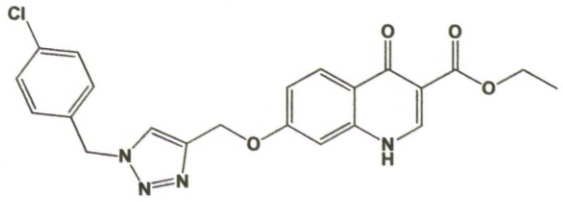

Synthesised from **58c** according to general method H to give a cream solid.

(87.3 mg, 90.9%)

Melting point: > 250 °C

^{1}H NMR (DMSO-d6) δ 12.16 – 12.14 (d, NH, *J* = 6.7 Hz), 8.49 – 8.47 (d, 1H, *J* = 6.6 Hz), 8.34 (s, 1H), 8.06 – 8.04 (d, 1H, *J* = 8.9 Hz), 7.46 – 7.44 (d, 2H, *J* = 8.5 Hz), 7.36 – 7.34 (d, 2H, *J* = 8.6 Hz), 7.15 – 7.14 (d, 1H, *J* = 2.4 Hz), 7.08 – 7.05 (dd, 1H, *J* = 8.9, 2.4 Hz), 5.63 (s, 2H), 5.27 (s, 2H), 4.23 – 4.17 (q, $OC\underline{H}_2CH_3$, *J* = 7.1 Hz) 1.29 – 1.25 (t, $OCH_2C\underline{H}_3$, *J* = 7.1 Hz);

^{13}C NMR not obtained due to poor solubility;

HRMS: $[M+Na]^+$ $C_{22}H_{19}{}^{35}ClN_4O_4Na$ requires 461.0993, found 461.0977.

*Ethyl 7-((1-(4-fluorobenzyl)-1H-1,2,3-triazol-4-yl)methoxy)-4-oxo-1,4-dihydroquinoline-3-carboxylate (**60d**)*

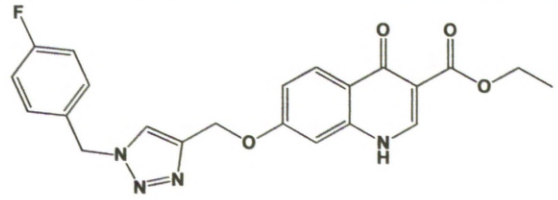

Synthesised from **58d** according to general method H to give a cream solid.

(76.6 mg, 80.5%)

Melting point: > 250 °C

^{1}H NMR (DMSO-d6) δ 12.14 – 12.12 (d, NH, *J* = 6.4), 8.48 – 8.47 (d, 1H, *J* = 6.8), 8.32 (s, 1H), 8.06 – 8.04 (d, 1H, *J* = 8.9), 7.42 – 7.38 (dd, 2H, *J* = 8.2, 5.6), 7.23 – 7.19 (t, 2H, *J* = 8.8), 7.15 – 7.14 (d, 1H, *J* = 2.2), 7.07 – 7.05 (dd,

1H, *J* = 9.0, 2.2), 5.61 (s, 2H), 5.26 (s, 2H), 4.23 – 4.17 (q, $OC\underline{H}_2CH_3$, *J* = 7.1), 1.29 – 1.25 (t, $OCH_2C\underline{H}_3$, *J* = 7.0);

^{13}C NMR not obtained due to poor solubility;

HRMS: $[M+H]^+$ $C_{22}H_{20}FN_4O_4$ requires 423.1469, found 423.1476.

*Ethyl 7-((1-(3-fluorobenzyl)-1H-1,2,3-triazol-4-yl)methoxy)-4-oxo-1,4-dihydroquinoline-3-carboxylate (**60e**)*

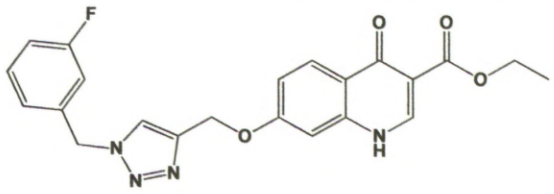

Synthesised from **58e** according to general method H to give a white solid.

(90.3 mg, 92.9%)

Melting point: > 250 °C

^1H NMR (DMSO-d6) δ 12.15 – 12.13 (d, NH, *J* = 6.4), 8.49 – 8.47 (d, 1H, *J* = 6.6), 8.36 (s, 1H), 8.06 – 8.04 (d, 1H, *J* = 8.9), 7.46 – 7.39 (m, 1H), 7.19 – 7.14 (m, 4H), 7.08 – 7.05 (dd, 1H, *J* = 8.9, 2.4), 5.66 (s, 2H), 5.28 (s, 2H), 4.23 – 4.17 (q, $OC\underline{H}_2CH_3$, *J* = 7.1), 1.29 – 1.25 (t, $OCH_2C\underline{H}_3$, *J* = 7.1);

^{13}C NMR not obtained due to poor solubility;

HRMS: $[M+H]^+$ $C_{22}H_{20}FN_4O_4$ requires 423.1469, found 423.1483.

*Ethyl 7-((1-(2,4-difluorobenzyl)-1H-1,2,3-triazol-4-yl)methoxy)-4-oxo-1,4-dihydroquinoline-3-carboxylate (**60f**)*

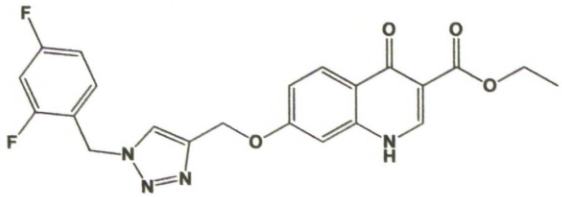

Synthesised from **58f** according to general method H to give a white solid.

(86.8 mg, 98.5%)

Melting point: > 250 °C

^1H NMR (DMSO-d6) δ 12.15 – 12.13 (d, NH, *J* = 6.6), 8.49 – 8.47 (d, 1H, *J* = 6.6), 8.31 (s, 1H), 8.06 – 8.04 (d, 1H, *J* = 8.9), 7.52 – 7.46 (m, 1H), 7.36 –

7.30 (td, 1H, *J* = 10.4, 2.5), 7.16 – 7.11 (m, 2H), 7.08 – 7.05 (dd, 1H, *J* = 8.9, 2.4), 5.67 (s, 2H), 5.26 (s, 2H), 4.23 – 4.17 (q, $OC\underline{H}_2CH_3$, *J* = 7.1), 1.29 – 1.25 (t, $OCH_2C\underline{H}_3$, *J* = 7.1);

^{13}C NMR not obtained due to poor solubility;

HRMS: $[M+H]^+$ $C_{22}H_{19}F_2N_4O_4$ requires 441.1374, found 441.1385.

*Synthesis of 2-(2-azidoethyl)isoindoline-1,3-dione (**62**)*

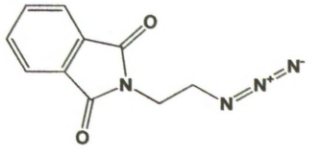

(2-Bromoethyl)phthalimide **61** (6.01 g, 23.7 mmol), sodium azide (3.94 g, 60.6 mmol), and sodium iodide (0.53 g, 3.5 mmol) were dissolved in acetone/water (5:1, 100 mL). The solution was refluxed for 24 h, diluted with water (50 mL), and extracted with ethyl acetate (3 x 75 mL). The organic phase was dried over magnesium sulphate and evaporated to yield the product as a sticky crystalline solid.

(4.10 g, 80.0%)

^1H NMR ($CDCl_3$) δ 7.91 – 7.72 (m, 4H), 3.92 – 3.89 (t, $NC\underline{H}_2CH_2N_3$, *J* = 6.0), 3.62 – 3.59 (t, $NCH_2C\underline{H}_2N_3$,, *J* = 6.1);

^{13}C NMR δ 168.5 (2 C=O), 134.6 (2C), 132.3 (2C), 123.9 (2C), 49.4, 37.3.

*Synthesis of ethyl 4-chloro-7-((1-(2-(1,3-dioxoisoindolin-2-yl)ethyl)-1H-1,2,3-triazol-4-yl)methoxy)quinoline-3-carboxylate (**63**)*

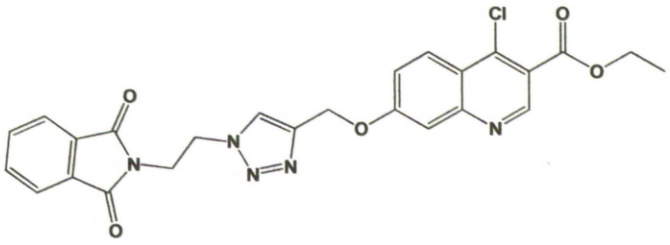

Synthesised from **56** and **62** according to general method G to give a pale yellow solid.

(0.23 g, 44.7%)

Melting point: 162 – 165 °C

^1H NMR ($CDCl_3$) δ 9.16 (s, 1H), 8.30 – 8.28 (d, 1H, *J* = 9.3), 7.80 – 7.77 (m, 3H), 7.72 – 7.67 (m, 2H), 7.53 – 7.52 (d, 1H, *J* = 2.5), 7.35 – 7.32 (dd, 1H, *J*

= 9.3, 2.5), 5.35 (s, CCH_2O), 4.75 – 7.72 (t, $NC\underline{H_2}CH_2N$, J = 5.9), 4.52 – 4.46 (q, $OC\underline{H_2}CH_3$, J = 7.1), 4.21 – 4.18 (t, $NCH_2C\underline{H_2}N$, J = 6.2), 1.48 – 1.45 (t, $OCH_2C\underline{H_3}$, J = 7.1);

^{13}C NMR δ 168.0 (2 C=O), 165.0 (C=O), 161.5 (C-Cl), 151.9, 151.4, 143.8, 143.7, 134.7 (2C), 132.0, 127.4, 124.0 (2C), 123.8, 121.9 (2C), 121.3, 109.2, 62.6, 62.3, 48.5, 38.1, 14.7;

HRMS: $[M+Na]^+$ $C_{25}H_{20}{}^{35}ClN_5O_5Na$ requires 528.1051 found 528.1039.

*Synthesis of ethyl 7-((1-(2-(1,3-dioxoisoindolin-2-yl)ethyl)-1H-1,2,3-triazol-4-yl)methoxy)-4-oxo-1,4-dihydroquinoline-3-carboxylate (**64**)*

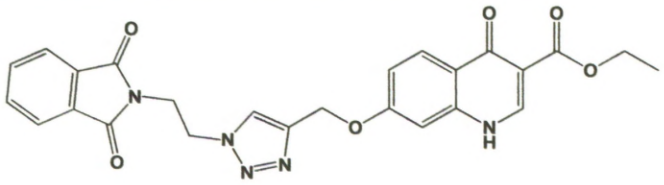

Synthesised from **63** according to general method H to give a white powder.

(67.4 mg, 65.2%)

Melting point: > 250 °C

^1H NMR (DMSO-d6) δ 12.12 – 12.10 (d, NH, J = 6.7), 8.47 – 8.46 (d, 1H, J = 6.6), 8.32 (s, 1H), 8.05 – 8.03 (d, 1H, J = 8.9), 7.81 (s, 3H), 7.12 – 7.11 (d, 1H, J = 2.3), 7.04 – 7.02 (dd, 1H, J = 8.9, 2.4), 5.23 (s, 2H), 4.68 – 4.65 (t, $NC\underline{H_2}CH_2N$, J = 5.0), 4.23 – 4.18 (q, $OC\underline{H_2}CH_3$, J = 7.1), 4.03 – 4.00 (t, $NCH_2C\underline{H_2}N$, J = 5.9), 2.09 (s, 1H), 1.29 – 1.26 (t, $OCH_2C\underline{H_3}$, J = 7.1);

^{13}C NMR not obtained due to poor solubility;

HRMS: $[M+H]^+$ $C_{25}H_{22}N_5O_6$ requires 488.1570, found 488.1568.

Chapter 5

Conclusions and Future Work

5. Conclusions and Future Work

We have been successful in our aim to design and synthesise a small library of quinolone-based compounds with high levels of potency against *P.falciparum* with compounds **39** and **48** achieving IC_{50}'s of less than 1 nM *in vitro*.

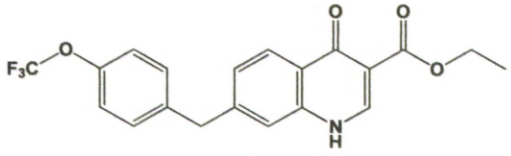

39

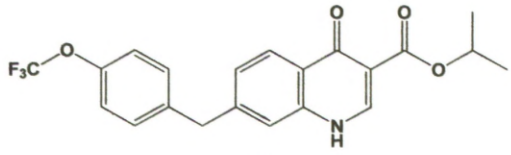

48

Issues with poor solubility have been highlighted and successfully tackled through the development of carbamate prodrugs, **46** and **47**, with the resulting compounds demonstrating rapid parasite clearance at low doses *in vivo* in mouse models.

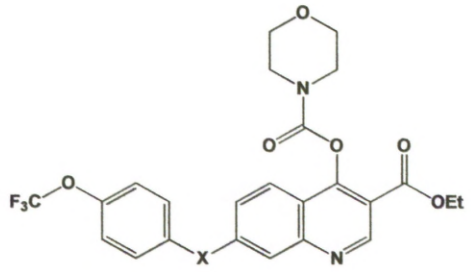

46 X = O
47 X = CH_2

Testing against protein isolates has confirmed that the compounds are active against the parasite bc_1 protein complex target as planned, however only low levels of selectivity for the parasite protein over the corresponding mammalian protein have been observed at present. Some progress has been made towards improving selectivity but further biological testing is required before true conclusions can be drawn from this work. Further improving levels of selectivity needs to be the focus of future work on these compounds along with further improvement of the current resistance profile as cross-resistance with atovaquone is currently evident. The development

of a more efficient synthetic route would also be worthy of future consideration.

Computer modelling has been successfully employed to elucidate the way in which the lead compounds may interact with the protein target. However, as demonstrated by the poor activity of the "click" series compounds, further work is needed before the modelling could be considered capable of predicting active structures.

In addition to these aims it would be of interest to further research the activity of compound **10**; as while significantly less active than the lead compounds *in vitro*, this compound was the only compound tested to maintain similar levels of activity against atovaquone resistant parasites as was demonstrated against wild-type parasites. This may indicate that compound **10** exhibits a different mode of action to the rest of the compounds synthesised in this study.

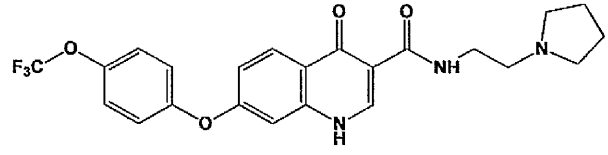

10

1. Joy, D. A.; Feng, X.; Mu, J.; Furuya, T.; Chotivanich, K.; Krettli, A. U.; Ho, M.; Wang, A.; White, N. J.; Suh, E.; Beerli, P.; Su, X.-z., *Science* **2003,** *300* (5617), 318-321.
2. Global Malaria Programme Brochure. In *http://www.who.int/malaria/docs/GMPbrochure.pdf* [Online] 2006.
3. . Fact sheet N°94 - Malaria *http://www.who.int/mediacentre/factsheets/fs094/en/index.html* [Online], 2007.
4. Sachs, J.; Malaney, P., *Nature* **2002,** *415* (6872), 680-685.
5. Snow, R. W.; Trape, J.-F.; Marsh, K., *Trends in Parasitology* **2001,** *17* (12), 593-597.
6. Rang, H. P.; Dale, M. M.; Ritter, J. M.; Moore, P. K., *Pharmacology*. 5th ed.; Churchill Livingstone: 2003.
7. Lee, K.-S.; Divis, P. C. S.; Zakaria, S. K.; Matusop, A.; Julin, R. A.; Conway, D. J.; Cox-Singh, J.; Singh, B., *PLoS Pathogens* **2011,** *7* (4), e1002015.
8. Mendis, K.; Sina, B. J.; Marchesini, P.; Carter, R., *The American Journal of Tropical Medicine and Hygiene* **2001,** *64* (1_suppl), 97-106.
9. Galinski, M.; Barnwell, J., *Malaria Journal* **2008,** *7* (0), 1-18.
10. Snow, R. W.; Guerra, C. A.; Mutheu, J. J.; Hay, S. I., *PLoS Medicine* **2008,** *5* (7), e142.
11. van Agtmael, M. A.; Eggelte, T. A.; van Boxtel, C. J., *Trends in Pharmacological Sciences* **1999,** *20* (5), 199-205.
12. Walgate, R., *Bulletin of the World Health Organization* **2001,** *79* (2), 174.
13. Rodríguez, A.; Mota, M. M.; Pradel, G.; Vanderberg, J. P.; Hafalla, J. C. R.; Frevert, U.; Nussenzweig, R. S.; Nussenzweig, V., *Science* **2001,** *291* (5501), 141-144.
14. Sturm, A.; Amino, R.; van de Sand, C.; Regen, T.; Retzlaff, S.; Rennenberg, A.; Krueger, A.; Pollok, J.-M.; Menard, R.; Heussler, V. T., *Science* **2006,** *313* (5791), 1287-1290.
15. CDC, Morphological comparison and images of Plasmodium species. 2009.
16. Pagola, S.; Stephens, P. W.; Bohle, D. S.; Kosar, A. D.; Madsen, S. K., *Nature* **2000,** *404* (6775), 307-310.
17. Rowe, J. A. http://www.biology.ed.ac.uk/research/groups/arowe/teaching.htm.
18. Rocco, F., *The miraculous fever-tree: the cure that changed the world*. HarperCollins: 2004.
19. Aaron C. Smith, Robert M. W., *Angewandte Chemie International Edition* **2008,** *47* (9), 1736-1740.
20. Ball, P., *Nature* **2008,** *451* (7182), 1065-1066.
21. Slater, A. F. G.; Cerami, A., *Nature* **1992,** *355* (6356), 167-169.
22. Cann, H. M.; Verhulst, H. L., *Pediatrics* **1961,** *27* (1), 95-102.
23. Bray, P. G.; Martin, R. E.; Tilley, L.; Ward, S. A.; Kirk, K.; Fidock, D. A., *Molecular Microbiology* **2005,** *56* (2), 323-333.
24. Greenwood, B., *Nature* **2004,** *430* (7002), 926-927.
25. *Chinese Medical Journal* **1979,** *92* (12), 811-816.

26. Klayman, D. L.; Lin, A. J.; Acton, N.; Scovill, J. P.; Hoch, J. M.; Milhous, W. K.; Theoharides, A. D.; Dobek, A. S., *Journal of Natural Products* **1984,** *47* (4), 715-717.
27. White, N. J., *Science* **2008,** *320* (5874), 330-334.
28. Golenser, J.; Waknine, J. H.; Krugliak, M.; Hunt, N. H.; Grau, G. E., *International Journal for Parasitology* **2006,** *36* (14), 1427-1441.
29. O'Neill, P. M.; Barton, V. E.; Ward, S. A., *Molecules* **2010,** *15* (3), 1705-1721.
30. Mercer, A. E.; Copple, I. M.; Maggs, J. L.; O'Neill, P. M.; Park, B. K., *Journal of Biological Chemistry* **2011,** *286* (2), 987-996.
31. O'Neill, P. M.; Amewu, R. K.; Nixon, G. L.; Bousejra ElGarah, F.; Mungthin, M.; Chadwick, J.; Shone, A. E.; Vivas, L.; Lander, H.; Barton, V.; Muangnoicharoen, S.; Bray, P. G.; Davies, J.; Park, B. K.; Wittlin, S.; Brun, R.; Preschel, M.; Zhang, K.; Ward, S. A., *Angewandte Chemie* **2010,** *122* (33), 5829-5833.
32. Fugi, M. A.; Wittlin, S.; Dong, Y.; Vennerstrom, J. L., *Antimicrobial Agents and Chemotherapy* **2010,** *54* (3), 1042-1046.
33. Cai, H.-H.; Yang, P.-H.; Chen, J.; Liang, Z.-H.; Chen, Q.; Cai, J., *Electrochimica Acta* **2009,** *54* (13), 3651-3656.
34. Charman, S. A.; Arbe-Barnes, S.; Bathurst, I. C.; Brun, R.; Campbell, M.; Charman, W. N.; Chiu, F. C. K.; Chollet, J.; Craft, J. C.; Creek, D. J.; Dong, Y.; Matile, H.; Maurer, M.; Morizzi, J.; Nguyen, T.; Papastogiannidis, P.; Scheurer, C.; Shackleford, D. M.; Sriraghavan, K.; Stingelin, L.; Tang, Y.; Urwyler, H.; Wang, X.; White, K. L.; Wittlin, S.; Zhou, L.; Vennerstrom, J. L., *Proceedings of the National Academy of Sciences* **2011,** *108* (11), 4400-4405.
35. Mather, M. W.; Darrouzet, E.; Valkova-Valchanova, M.; Cooley, J. W.; McIntosh, M. T.; Daldal, F.; Vaidya, A. B., *Journal of Biological Chemistry* **2005,** *280* (29), 27458-27465.
36. GlaxoSmithKline MALARONE®. www.malarone.com.
37. Patel, S. N.; Kain, K. C., *Expert Review of Anti-infective Therapy* **2005,** *3* (6), 849-861.
38. Berman, J. D.; Nielsen, R.; Chulay, J. D.; Dowler, M.; Kain, K. C.; Kester, K. E.; Williams, J.; Whelen, A. C.; Shmuklarsky, M. J., *Transactions of the Royal Society of Tropical Medicine and Hygiene* **2001,** *95* (4), 429-432.
39. Yeates, C. L.; Batchelor, J. F.; Capon, E. C.; Cheesman, N. J.; Fry, M.; Hudson, A. T.; Pudney, M.; Trimming, H.; Woolven, J.; Bueno, J. M.; Chicharro, J.; Fernandez, E.; Fiandor, J. M.; Gargallo-Viola, D.; Gomez de las Heras, F.; Herreros, E.; Leon, M. L., *Journal of Medicinal Chemistry* **2008,** *51* (9), 2845-2852.
40. Srivastava, I. K.; Morrisey, J. M.; Darrouzet, E.; Daldal, F.; Vaidya, A. B., *Molecular Microbiology* **1999,** *33* (4), 704-711.
41. Sutherland, C.; Laundy, M.; Price, N.; Burke, M.; Fivelman, Q.; Pasvol, G.; Klein, J.; Chiodini, P., *Malaria Journal* **2008,** *7* (1), 240.
42. Barton, V.; Fisher, N.; Biagini, G. A.; Ward, S. A.; O'Neill, P. M., *Current Opinion in Chemical Biology* **2010,** *14* (4), 440-446.
43. Solmaz, S. R. N.; Hunte, C., *Journal of Biological Chemistry* **2008,** *283* (25), 17542-17549.

44. Zara, V.; Conte, L.; Trumpower, B. L., *FEBS Journal* **2009,** *276* (7), 1900-1914.
45. Link, T. A.; Haase, U.; Brandt, U.; Jagow, G., *Journal of Bioenergetics and Biomembranes* **1993,** *25* (3), 221-232.
46. Link, T. A.; Iwata, M.; Bjorkman, J.; van der Spoel, D.; Stocker, A.; Iwata, S., Molecular Modelling of Inhibitors at Q_i and Q_o Sites in Cytochrome bc_1 Complex In *Chemistry of Crop Protection*, Ramos, G. V. a. G., Ed. Wiley-VCH: 2003; pp 110 - 130.
47. Gao, X.; Wen, X.; Esser, L.; Quinn, B.; Yu, L.; Yu, C.; Xia, D., *Biochemistry* **2003,** *42* (30), 9067-9080.
48. Mitchell, P., *FEBS Letters* **1975,** *59* (2), 137-139.
49. Brandt, U.; Trumpower, B., *Critical Reviews in Biochemistry and Molecular Biology* **1994,** *29* (3), 165 - 197.
50. Hunte, C.; Palsdottir, H.; Trumpower, B. L., *FEBS Letters* **2003,** *545* (1), 39-46.
51. Trumpower, B. L., *Journal of Biological Chemistry* **1990,** *265* (20), 11409-11412.
52. Berry, E. A.; Guergova-Kuras, M.; Huang, L.-s.; Crofts, A. R., *Annual Review of Biochemistry* **2000,** *69* (1), 1005-1075.
53. Crofts, A. R., *Annual Review of Physiology* **2004,** *66* (1), 689-733.
54. Esser, L.; Quinn, B.; Li, Y.-F.; Zhang, M.; Elberry, M.; Yu, L.; Yu, C.-A.; Xia, D., *Journal of Molecular Biology* **2004,** *341* (1), 281-302.
55. Alzeer, J.; Chollet, J.; Heinze-Krauss, I.; Hubschwerlen, C.; Matile, H.; Ridley, R. G., *Journal of Medicinal Chemistry* **2000,** *43* (4), 560-568.
56. Brasseur, G.; Saribas, A. S.; Daldal, F., *Biochimica et Biophysica Acta (BBA) - Bioenergetics* **1996,** *1275* (1-2), 61-69.
57. Kessl, J. J.; Ha, K. H.; Merritt, A. K.; Lange, B. B.; Hill, P.; Meunier, B.; Meshnick, S. R.; Trumpower, B. L., *Journal of Biological Chemistry* **2005,** *280* (17), 17142-17148.
58. Kessl, J. J.; Meshnick, S. R.; Trumpower, B. L., *Trends in Parasitology* **2007,** *23* (10), 494-501.
59. Palsdottir, H.; Lojero, C. G.; Trumpower, B. L.; Hunte, C., *Journal of Biological Chemistry* **2003,** *278* (33), 31303-31311.
60. Korsinczky, M.; Chen, N.; Kotecka, B.; Saul, A.; Rieckmann, K.; Cheng, Q., *Antimicrobial Agents and Chemotherapy* **2000,** *44* (8), 2100-2108.
61. Wichmann, O.; Muehlberger, N.; Jelinek, T.; Alifrangis, M.; Hoffmann, G. P.; hlen, M. M.; Grobusch, M. P.; Gascon, J.; Matteelli, A.; Laferl, H.; Bisoffi, Z.; Ehrhardt, S.; Cuadros, J.; Hatz, C.; Gjorup, I.; McWhinney, P.; Beran, J.; Cunha, S. d.; Schulze, M.; Kollaritsch, H.; Kern, P.; Fry, G.; Richter, J.; Diseases, E. N. o. S. o. I. I., *Journal of Infectious Diseases* **2004,** *190* (9), 1541-1546.
62. Musset, L.; Bouchaud, O.; Matheron, S.; Massias, L.; Le Bras, J., *Microbes and Infection* **2006,** *8* (11), 2599-2604.
63. Berry, A.; Senescau, A.; Lelièvre, J.; Benoit-Vical, F.; Fabre, R.; Marchou, B.; Magnaval, J. F., *Transactions of the Royal Society of Tropical Medicine and Hygiene* **2006,** *100* (10), 986-988.
64. Fisher, N.; Meunier, B., *FEMS Yeast Research* **2008,** *8* (2), 183-192.
65. Fisher, N.; Meunier, B., *Pest Management Science* **2005,** *61* (10), 973-978.

66. Srivastava, I. K.; Rottenberg, H.; Vaidya, A. B., *Journal of Biological Chemistry* **1997,** *272* (7), 3961-3966.
67. Kapadia, G. J.; Azuine, M. A.; Balasubramanian, V.; Sridhar, R., *Pharmacological Research* **2001,** *43* (4), 363-367.
68. Fieser, L. F.; Berliner, E.; Bondhus, F. J.; Chang, F. C.; Dauben, W. G.; Ettlinger, M. G.; Fawaz, G.; Fields, M.; Fieser, M.; Heidelberger, C.; Heymann, H.; Seligman, A. M.; Vaughan, W. R.; Wilson, A. G.; Wilson, E.; Wu, M.-i.; Leffler, M. T.; Hamlin, K. E.; Hathaway, R. J.; Matson, E. J.; Moore, E. E.; Moore, M. B.; Rapala, R. T.; Zaugg, H. E., *Journal of the American Chemical Society* **1948,** *70* (10), 3151-3155.
69. Fieser, L. F.; Heymann, H.; Seligman, A. M., *Journal of Pharmacology and Experimental Therapeutics* **1948,** *94* (2), 112-124.
70. Kessl, J. J.; Moskalev, N. V.; Gribble, G. W.; Nasr, M.; Meshnick, S. R.; Trumpower, B. L., *Biochimica et Biophysica Acta (BBA) - Bioenergetics* **2007,** *1767* (4), 319-326.
71. Hughes, L. M.; Covian, R.; Gribble, G. W.; Trumpower, B. L., *Biochimica et Biophysica Acta (BBA) - Bioenergetics* **2010,** *1797* (1), 38-43.
72. Hughes, L. M.; Lanteri, C. A.; O'Neil, M. T.; Johnson, J. D.; Gribble, G. W.; Trumpower, B. L., *Molecular and Biochemical Parasitology* **2011,** *177* (1), 12-19.
73. Bueno, C. J. M.; Chicharro, G. J.; Lorenzo, G. M.; Manzano, C. M. P. 4-Pyridinone derivatives as antimalarial agents, their preparation, pharmaceutical compositions, and their use in therapy. WO2007138048A1, 2007.
74. Bueno-Calderon, J. M.; Fiandor-Roman, J. M.; Puente-Felipe, M.; Chicharro-Gonzalo, J.; Kusalakumari, S. S. K.; Maleki, M. Phosphate ester of a 4-pyridone derivative and its use in the chemotherapy of parasitic infections. WO2010094738A1, 2010.
75. GlaxoSmithKline, Protocol Summary 111319: A Single-Blind, Placebo-Controlled, Randomized First Time in Human Study to Evaluate the Safety, Tolerability, and Pharmacokinetics of Single and Repeat Dose Escalation of GSK932121 in Healthy Adult Subjects. 2009.
76. Dorn, A.; Scovill, J. P.; Ellis, W. Y.; Matile, H.; Ridley, R. G.; Vennerstrom, J. L., *The American Journal of Tropical Medicine and Hygiene* **2001,** *65* (1), 19-20.
77. Suswam, E.; Kyle, D.; Lang-Unnasch, N., *Experimental Parasitology* **2001,** *98* (4), 180-187.
78. Biagini, G. A.; Fisher, N.; Berry, N.; Stocks, P. A.; Meunier, B.; Williams, D. P.; Bonar-Law, R.; Bray, P. G.; Owen, A.; O'Neill, P. M.; Ward, S. A., *Molecular Pharmacology* **2008,** *73* (5), 1347-1355.
79. Winter, R. W.; Kelly, J. X.; Smilkstein, M. J.; Dodean, R.; Bagby, G. C.; Rathbun, R. K.; Levin, J. I.; Hinrichs, D.; Riscoe, M. K., *Experimental Parasitology* **2006,** *114* (1), 47-56.
80. Winter, R. W.; Kelly, J. X.; Smilkstein, M. J.; Dodean, R.; Hinrichs, D.; Riscoe, M. K., *Experimental Parasitology* **2008,** *118* (4), 487-497.
81. Kelly, J. X.; Smilkstein, M. J.; Cooper, R. A.; Lane, K. D.; Johnson, R. A.; Janowsky, A.; Dodean, R. A.; Hinrichs, D. J.; Winter, R.; Riscoe, M., *Antimicrobial Agents and Chemotherapy* **2007,** *51* (11), 4133-4140.

82. Kelly, J. X.; Smilkstein, M. J.; Brun, R.; Wittlin, S.; Cooper, R. A.; Lane, K. D.; Janowsky, A.; Johnson, R. A.; Dodean, R. A.; Winter, R.; Hinrichs, D. J.; Riscoe, M. K., *Nature* **2009,** *459* (7244), 270-273.
83. Salzer, W.; Timmler, H.; Andersag, H., *Chemische Berichte* **1948,** *81*, 12-19.
84. Ryley, J. F.; Peters, W., *Annals of Tropical Medicine and Parasitology* **1970,** *64* (2), 209 - 222.
85. Divo, A. A.; Sartorelli, A. C.; Patton, C. L.; Bia, F. J., *Antimicrobial Agents and Chemotherapy* **1988,** *32* (8), 1182-1186.
86. Teja-Isavadharm, P.; Keeratithakul, D.; Watt, G.; Webster, H. K.; Edstein, M. D., *Therapeutic Drug Monitoring* **1991,** *13* (3), 263-267.
87. Watt, G.; Shanks, G. D.; Edstein, M. D.; Pavanand, K.; Webster, H. K.; Wechgritaya, S., *Journal of Infectious Diseases* **1991,** *164* (3), 602-4.
88. McClean, K. L.; Hitchman, D.; Shafran, S. D., *Journal of Infectious Diseases* **1992,** *165* (5), 904-7.
89. Strömberg, A.; Björkman, A., *Transactions of the Royal Society of Tropical Medicine and Hygiene* **1992,** *86* (4), 373-373.
90. Tripathi, K. D.; Sharma, A. K.; Valecha, N.; Kulpati, D. D., *The Indian Journal of Medical Research* **1993,** *97*, 176-8.
91. Tripathi, K. D.; Sharma, A. K.; Valecha, N.; Biswas, S., *Indian Journal of Malariology* **1993,** *30* (2), 67-73.
92. Yeo, A. E. T.; Rieckmann, K. H., *The Journal of Parasitology* **1994,** *80* (1), 158-160.
93. Hamzah, J.; Skinner-Adams, T.; Davis, T. M. E., *Acta Tropica* **2000,** *74* (1), 39-42.
94. O'Donnell, J. A.; Gelone, S. P., *Infectious Disease Clinics of North America* **2000,** *14* (2), 489-513.
95. Norrby, S. R.; Lietman, P. S., *Drugs* **1993,** *45 Suppl 3*, 59-64.
96. Satoh, Y.; Sugiyama, A.; Chiba, K.; Tamura, K.; Hashimoto, K., *Journal of Cardiovascular Pharmacology* **2000,** *36* (4), 510-515.
97. Shimada, J.; Hori, S., *Progress in Drug Research* **1992,** *38*, 133-43.
98. Mahmoudi, N.; Ciceron, L.; Franetich, J.-F.; Farhati, K.; Silvie, O.; Eling, W.; Sauerwein, R.; Danis, M.; Mazier, D.; Derouin, F., *Antimicrobial Agents and Chemotherapy* **2003,** *47* (8), 2636-2639.
99. Anquetin, G.; Rouquayrol, M.; Mahmoudi, N.; Santillana-Hayat, M.; Gozalbes, R.; Greiner, J.; Farhati, K.; Derouin, F.; Guedj, R.; Vierling, P., *Bioorganic & Medicinal Chemistry Letters* **2004,** *14* (11), 2773-2776.
100. Kurasawa, Y.; Yoshida, K.; Yamazaki, N.; Kaji, E.; Sasaki, K.; Hiwasa, Y.; Tsukamoto, A.; Ito, H., *Journal of Heterocyclic Chemistry* **2010,** *47* (3), 657-663.
101. Zhang, Y.; Guiguemde, W. A.; Sigal, M.; Zhu, F.; Connelly, M. C.; Nwaka, S.; Guy, R. K., *Bioorganic & Medicinal Chemistry* **2010,** *18* (7), 2756-2766.
102. Cross, R. M.; Monastyrskyi, A.; Mutka, T. S.; Burrows, J. N.; Kyle, D. E.; Manetsch, R., *Journal of Medicinal Chemistry* **2010,** *53* (19), 7076-7094.
103. Winter, R.; Kelly, J. X.; Smilkstein, M. J.; Hinrichs, D.; Koop, D. R.; Riscoe, M. K., *Experimental Parasitology* **2011,** *127* (2), 545-551.
104. Jones, C. P.; Anderson, K. W.; Buchwald, S. L., *The Journal of Organic Chemistry* **2007,** *72* (21), 7968-7973.

105. Conrad, M.; Limpach, L., *Berichte der deutschen chemischen Gesellschaft* **1887,** *20* (1), 944-948.
106. Camps, R., *Berichte der deutschen chemischen Gesellschaft* **1899,** *32* (3), 3228-3234.
107. Niementowski, S., *Berichte der deutschen chemischen Gesellschaft* **1894,** *27* (2), 1394-1403.
108. Gould, R. G.; Jacobs, W. A., *Journal of the American Chemical Society* **1939,** *61* (10), 2890-2895.
109. Crofts, A. R., *Biochimica et Biophysica Acta (BBA)* **2004,** *1655* (1-3), 77-92.
110. Stern, E.; Muccioli, G. G.; Millet, R.; Goossens, J. F.; Farce, A.; Chavatte, P.; Poupaert, J. H.; Lambert, D. M.; Depreux, P.; Henichart, J. P., *Journal of Medicinal Chemistry* **2006,** *49* (1), 70-79.
111. Boschelli, D. H.; Wang, Y. D.; Ye, F.; Wu, B.; Zhang, N.; Dutia, M.; Powell, D. W.; Wissner, A.; Arndt, K.; Weber, J. M.; Boschelli, F., *Journal of Medicinal Chemistry* **2001,** *44* (5), 822-833.
112. Boschelli, D. H.; Wang, Y. D.; Johnson, S.; Wu, B.; Ye, F.; BarriosSosa, A. C.; Golas, J. M.; Boschelli, F., *Journal of Medicinal Chemistry* **2004,** *47* (7), 1599-1601.
113. Wang, C. G.; Langer, T.; Kamath, P. G.; Gu, Z. Q.; Skolnick, P.; Fryer, R. I., *Journal of Medicinal Chemistry* **1995,** *38* (6), 950-957.
114. Furuta, T.; Sakai, T.; Senga, T.; Osawa, T.; Kubo, K.; Shimizu, T.; Suzuki, R.; Yoshino, T.; Endo, M.; Miwa, A., *Journal of Medicinal Chemistry* **2006,** *49* (7), 2186-2192.
115. Mann, G.; Hartwig, J. F., *Tetrahedron Letters* **1997,** *38* (46), 8005-8008.
116. Ma, D.; Cai, Q., *Organic Letters* **2003,** *5* (21), 3799-3802.
117. Chandrasekhar, S.; Sultana, S. S.; Yaragorla, S. R.; Reddy, N. R., *Synthesis* **2006,** (5), 839-842.
118. Kuhn, W. E., *Organic Syntheses* **1933,** *13*, 74.
119. Wells, T., New Medicines for Malaria Control and Eradication Target Product Profiles for 2010 2010.
120. Clayden, J.; Greeves, N.; Warren, S.; Wothers, P., *Organic Chemistry.* Oxford University Press: 2000; p 1568 pp.
121. Savini, L.; Massarelli, P.; Nencini, C.; Pellerano, C.; Biggio, G.; Maciocco, A.; Tuligi, G.; Carrieri, A.; Cinone, N.; Carotti, A., *Bioorganic & Medicinal Chemistry* **1998,** *6* (4), 389-399.
122. Lima, L. M.; Barreiro, E. J., *Current Medicinal Chemistry* **2005,** *12* (1), 23-49.
123. Lager, E.; Andersson, P.; Nilsson, J.; Pettersson, I.; Nielsen, E. O.; Nielsen, M.; Sterner, O.; Liljefors, T., *Journal of Medicinal Chemistry* **2006,** *49* (8), 2526-2533.
124. Somfai, E. Process for N-cyclopropylation of aromatic amines, particularly quinolones and naphthyridines. WO9502573A2, 1995.
125. Tangallapally, R. P.; Yendapally, R.; Lee, R. E.; Lenaerts, A. J. M.; Lee, R. E., *Journal of Medicinal Chemistry* **2005,** *48* (26), 8261-8269.
126. Tao, B.; Boykin, D. W., *Journal of Organic Chemistry* **2004,** *69* (13), 4330-4335.
127. Press, J. B., *Synthetic Communications* **1979,** *9* (5), 407-10.

128. Woschek, A.; Mahout, M.; Mereiter, K.; Hammerschmidt, F., *Synthesis* **2007,** *2007* (10), 1517,1522.
129. Cowley, R.; Leung, S.; Fisher, N.; Al-Helal, M.; Berry, N. G.; Lawrenson, A. S.; Sharma, R.; Shone, A. E.; Ward, S. A.; Biagini, G. A.; O'Neill, P. M., *MedChemComm* **2011,** *Advance Article.*
130. Friesner, R. A.; Banks, J. L.; Murphy, R. B.; Halgren, T. A.; Klicic, J. J.; Mainz, D. T.; Repasky, M. P.; Knoll, E. H.; Shelley, M.; Perry, J. K.; Shaw, D. E.; Francis, P.; Shenkin, P. S., *Journal of Medicinal Chemistry* **2004,** *47* (7), 1739-1749.
131. Halgren, T. A.; Murphy, R. B.; Friesner, R. A.; Beard, H. S.; Frye, L. L.; Pollard, W. T.; Banks, J. L., *Journal of Medicinal Chemistry* **2004,** *47* (7), 1750-1759.
132. Huey, R.; Morris, G. M.; Olson, A. J.; Goodsell, D. S., *Journal of Computational Chemistry* **2007,** *28* (6), 1145-1152.
133. Cole, J. C.; Nissink, J. W. M.; Taylor, R., *Drug Discovery Series* **2005,** *1*, 379-415.
134. Verdonk, M. L.; Cole, J. C.; Hartshorn, M. J.; Murray, C. W.; Taylor, R. D., *Proteins: Structure, Function and Genetics* **2003,** *52* (4), 609-623.
135. Verdonk, M. L.; Chessari, G.; Cole, J. C.; Hartshorn, M. J.; Murray, C. W.; Nissink, J. W. M.; Taylor, R. D.; Taylor, R., *Journal of Medicinal Chemistry* **2005,** *48* (20), 6504-6515.
136. ***GOLD 5.0.1***, The Cambridge Crystallographic Data Centre: Cambridge, UK.
137. Perola, E.; Walters, W. P.; Charifson, P. S., *Proteins: Structure, Function, and Bioinformatics* **2004,** *56* (2), 235-249.
138. Kellenberger, E.; Rodrigo, J.; Muller, P.; Rognan, D., *Proteins: Structure, Function, and Bioinformatics* **2004,** *57* (2), 225-242.
139. Jones, G.; Willett, P.; Glen, R. C., *Journal of Molecular Biology* **1995,** *245* (1), 43-53.
140. Rich, P. R., *Biochimica et Biophysica Acta (BBA) - Bioenergetics* **2004,** *1658* (1-2), 165-171.
141. Jhansi, R. G.; Vinoth, M.; Anitha, P., *Journal of Bioinformatics and Sequence Analysis* **2011,** *3* (3), 31-36.
142. Verdonk, M. L.; Chessari, G.; Cole, J. C.; Hartshorn, M. J.; Murray, C. W.; Nissink, J. W. M.; Taylor, R. D.; Taylor, R., *Journal of Medicinal Chemistry* **2005,** *48* (20), 6504-6515.
143. ***Spartan'08***, Wavefunction Inc.: Irvine, CA.
144. Shao, Y.; Molnar, L. F.; Jung, Y.; Kussmann, J.; Ochsenfeld, C.; Brown, S. T.; Gilbert, A. T. B.; Slipchenko, L. V.; Levchenko, S. V.; O'Neill, D. P.; DiStasio Jr, R. A.; Lochan, R. C.; Wang, T.; Beran, G. J. O.; Besley, N. A.; Herbert, J. M.; Yeh Lin, C.; Van Voorhis, T.; Hung Chien, S.; Sodt, A.; Steele, R. P.; Rassolov, V. A.; Maslen, P. E.; Korambath, P. P.; Adamson, R. D.; Austin, B.; Baker, J.; Byrd, E. F. C.; Dachsel, H.; Doerksen, R. J.; Dreuw, A.; Dunietz, B. D.; Dutoi, A. D.; Furlani, T. R.; Gwaltney, S. R.; Heyden, A.; Hirata, S.; Hsu, C.-P.; Kedziora, G.; Khalliulin, R. Z.; Klunzinger, P.; Lee, A. M.; Lee, M. S.; Liang, W.; Lotan, I.; Nair, N.; Peters, B.; Proynov, E. I.; Pieniazek, P. A.; Min Rhee, Y.; Ritchie, J.; Rosta, E.; David Sherrill, C.; Simmonett, A. C.; Subotnik, J. E.; Lee Woodcock Iii, H.; Zhang, W.; Bell, A. T.; Chakraborty, A. K.; Chipman, D. M.; Keil, F. J.; Warshel, A.; Hehre, W. J.;

Schaefer Iii, H. F.; Kong, J.; Krylov, A. I.; Gill, P. M. W.; Head-Gordon, M., *Physical Chemistry Chemical Physics* **2006,** *8* (27), 3172-3191.
145. Cape, J. L.; Bowman, M. K.; Kramer, D. M., *Trends in Plant Science* **2006,** *11* (1), 46-55.
146. ***The PyMOL Molecular Graphics System, Version 1.3***, Schrödinger, LLC.
147. Kolb, H. C.; Finn, M. G.; Sharpless, K. B., *Angewandte Chemie International Edition* **2001,** *40* (11), 2004-2021.
148. Iwai, I.; Ide, J., *Chemical & Pharmaceutical Bulletin* **1963,** *11* (8), 1042-9.
149. Kluge, A. F.; Petter, R. C.; Tester, R. W.; Qiao, L.; Niu, D.; Westlin, W. F.; Singh, J.; Mazdiyasni, H. Preparation of heteroaryl compounds protein kinase inhibitors. WO2009158571A1, 2009.
150. Willard, A. K.; Smith, R. L.; Cragoe, E. J., Jr., *Journal of Organic Chemistry* **1981,** *46* (19), 3846-52.
151. Huisgen, R., *Angewandte Chemie* **1963,** *75* (13), 604-37.
152. Tornoe, C. W.; Christensen, C.; Meldal, M., *Journal of Organic Chemistry* **2002,** *67* (9), 3057-3064.
153. Rostovtsev, V. V.; Green, L. G.; Fokin, V. V.; Sharpless, K. B., *Angewandte Chemie International Edition* **2002,** *41* (14), 2596-2599.
154. Himo, F.; Lovell, T.; Hilgraf, R.; Rostovtsev, V. V.; Noodleman, L.; Sharpless, K. B.; Fokin, V. V., *Journal of the American Chemical Society* **2004,** *127* (1), 210-216.
155. Feldman, A. K.; Colasson, B.; Fokin, V. V., *Organic Letters* **2004,** *6* (22), 3897-3899.
156. Luehr, G. W.; Sundaram, A.; Jaishankar, P.; Bhakta, C.; Druzgala, P. Preparation of pyrazole and triazole based compounds as therapeutic agonists of peroxisome proliferator activated receptor-α. WO2010071813A1, 2010.
157. Angell, Y.; Burgess, K., *Angewandte Chemie International Edition* **2007,** *46* (20), 3649-3651.
158. Cantrell, A. S.; Engelhardt, P.; Hoegberg, M.; Jaskunas, S. R.; Johansson, N. G.; Jordan, C. L.; Kangasmetsae, J.; Kinnick, M. D.; Lind, P.; et, a., *Journal of Medicinal Chemistry* **1996,** *39* (21), 4261-4274.

This thesis is dedicated to my parents and my fiancée Michelle; I can honestly say that it wouldn't have happened without you.

Thanks for reading...